



**THERMOCHEMICAL CONVERSION OF
NON-WOODY BIOMASS:
UPGRADING COTTON GIN WASTE INTO SOLID FUEL**

A Thesis submitted by

Elita Rahmarestia Widjaya, B.Sc., M.Eng.Sc.

For the award of

Doctor of Philosophy

2018

Abstract

Non-woody biomass is a common waste material found in agriculture. Despite its abundance, the waste is not widely utilised due to unfavorable physical properties (bulkiness, irregular size and varied composition) and low energy content.

The aim of this research is to study the solid fuel properties of a non-woody biomass in order to improve their qualities. Cotton gin waste (CGW), a source of non-woody biomass from the processing of cotton, was selected. Methods of densification and blending of biochar were proposed and evaluated for transforming CGW into pellets in order to create a fuel with high density and energy content, as well as uniform physical properties. The development of CGW pellets was achieved by using a small scale pellet mill. CGW was blended with 5 to 20 percent weights of biochar. The developed CGW pellets were accordingly defined as CGW100, CGW95, CGW90, CGW85 and CGW80 pellets, implying the weight percentages of CGW as much as 100%, 95%, 90%, 85% and 80% in pellets, respectively.

It has been found that pelleting the CGW increases the bulk density from 112 kg/m³ to 600 kg/m³. The biochar blends upgraded the heating values of CGW pellets from 14 MJ/kg of CGW100 to 18 MJ/kg of CGW80. In the process of stabilisation, the blended pellets slightly shrank, while the pure CGW pellet marginally expanded. In contrast to the pellet durability, the hardness was significantly influenced by the biochar addition. The biochar in the pellets diminished the rancid smell of raw CGW.

It has also been found that CGW95 and CGW90 behaviours in the thermogravimetric (TGA) combustion were almost identical with CGW100 combustion. In addition, CGW95 pellets had the highest conversion rate and resulted in the least residual ash. On the contrary, CGW85 and CGW80 pellets were slow in conversion and burn out at closer to the biochar ignition temperature. From the examination of ash content and activation of energies, all the blended pellets show a synergism in co-combustion.

Similar to combustion, the TGA pyrolysis using inert gas also resulted in a slightly higher conversion for CGW95. Other biochar blended pellets show a lower and more linear conversion as a function of biochar content.

A CFD model has been developed using ANSYS Fluent 17.2 software. The approaches are the discrete phase and non-premix combustion models. The model shows an accurate prediction of the gasifier temperature and resulting gas composition. The simulation also predicts that CGW95 will have a higher CO yield than CGW90. The gasification of CGW95 pellets with air to fuel ratio of 1.3 v/w results in a gas composition of CO, CO₂, H₂ and CH₄ gas of 19.8%, 11.6%, 14.2% and 0.2%, v/v respectively. The estimated gas heating values are in the range of 3.9-5.1 MJ/m³.

It has been found that 30% energy produced from CGW pellet gasification is sufficient to cover the energy need for pellet production. The costs of energy in the ginning house can be reduced by 20-40% from the use of produced gas. The GHG emission is also lowered. Overall, it can be concluded that upgrading the non-woody biomass into pellets and applying it in a co-gasification could potentially provide an effective alternative fuel source to achieve agricultural energy self-sufficiency and off-grid operation.

Certification of Thesis

This Thesis is entirely the work of **Elita Rahmarestia Widjaya** except where otherwise acknowledged. The work is original and has not previously been submitted for any other award, except where acknowledged.

Principal Supervisor : *Assoc. Professor Guangnan Chen*

Associate Supervisor : *Dr Les Bowtell*

Student and supervisors signatures of endorsement are held at the University.

Acknowledgments

First of all, I would like to express my deepest gratitude to the Indonesian Agency for Agricultural Research and Development (IAARD), Ministry of Agriculture, Republic of Indonesia, for providing the scholarship to perform this study. I also appreciate the Indonesian Center for Agricultural Engineering Research and Development (ICAERD) for my award nomination.

I would like to thank to my supervisor, Associate Professor Guangnan Chen, for his continuous guidance, encouragement, comments and advices. His patience in supporting my study journey is highly appreciated. Thanks is also extended to my associate supervisor, Dr Les Bowtell, for his advice and support. Their efforts for the completion of this study are highly appreciated.

Thanks to Dr Andrew Wandel for his suggestion in the model development using the fluid dynamic software. I also express my special gratitude to Dr Pavel Faigl for his valuable effort in editing this thesis. Thanks to the staff members of technical laboratories, Dr F. Susette Eberhard and Dr Venkata S. Chevali, Faculty of Health, Engineering and Sciences, for their patience in supporting and assisting the laboratory works. I also express my gratitude to Namoi cotton for providing me the samples of cotton gin waste.

Finally, my sincere gratitude is due to my beloved family, my husband Muharam and children (Teuku Reza and Cut Elma) for their patience and support. My sincere gratitude is also due to my parents for their continuous support. Many thanks are also extended to my housemates in the student village and other Indonesian friends for cheering me up during the study. Thanks are also due to those who are directly or indirectly related to this study.

List of Publications

The following articles have been submitted or published from the research contained within this thesis

1. Refereed international journal articles

Widjaya, E.R., Chen, G., Bowtell, L., Hills, C (2018). Gasification of non-woody biomass: a literature review. *Renewable & Sustainable Energy Reviews*, 89. pp. 184-193.

Widjaya, E.R., Bowtell, L., Chen, G., Hills, C., Jagatapu, G.S and Sutcliffe, J (2018). Cotton gin waste pellets: effect of biochar blending on physical and element properties. *'Biomass and Bioenergy'*, resubmission

2. Refereed full-length conference article

Widjaya, E R., Chen, G., Bowtell, L and Hills, C (2015) A preliminary assessment of cotton gin waste-mixture co-gasification performance. In: *2nd International Conference on Agriculture, Environment and Biological Sciences (ICAEBS'15)*, 1617 August 2015, Bali, Indonesia.

Table of Contents

ABSTRACT	II
CERTIFICATION OF THESIS	IV
ACKNOWLEDGMENTS	V
LIST OF PUBLICATIONS.....	VI
TABLE OF CONTENTS.....	VII
LIST OF FIGURES	XI
LIST OF TABLES	XIII
GLOSSARY TERMS	XIV
CHAPTER 1: INTRODUCTION.....	1
1.1. Background.....	1
1.2. Research goal and objectives.....	4
1.3. Organisation of Chapters	6
CHAPTER 2: LITERATURE REVIEW.....	7
2.1. Potential of solid fuel development from cotton gin waste.....	8
2.1.1. <i>Australian cotton industry</i>	8
2.1.2. <i>Methods of converting cotton gin waste for energy production</i>	10
2.1.3. <i>Upgrading non-woody biomass into solid fuel</i>	12
2.1.4. <i>Standard quality of the non-woody fuel pellet</i>	20
2.2. Thermochemical conversion of solid fuel	20
2.3. Design and performance of gasifier plant/reactor	23
2.4. Single fuel non-woody biomass thermochemical conversion	25
2.5. Co-blended fuel and synergy in thermochemical conversion	27
2.5.1. <i>Synergistic effect in co-conversion</i>	28
2.5.2. <i>Factors influencing synergistic effect in co-conversion</i>	33
2.6. Modelling & simulation in the gasification	36
2.6.1. <i>Equilibrium model</i>	38
2.6.2. <i>Kinetic model</i>	39
2.6.3. <i>Computational fluid dynamics</i>	40

2.7. Summary of the literature review	41
CHAPTER 3: DEVELOPMENT OF COTTON GIN WASTE FUEL PELLETS - UPGRADING THE PHYSICAL AND ELEMENTAL PROPERTIES.....	43
3.1. Introduction	43
3.2. Development of CGW pellets.....	44
3.2.1. <i>Properties of raw materials</i>	44
3.2.2. <i>Materials and pelleting equipment</i>	46
3.2.3. <i>Pre-treatment</i>	47
3.2.4. <i>Pellet productions</i>	49
3.3. Methods of measurement and analyses	51
3.3.1. <i>Physical properties</i>	52
3.3.2. <i>Proximate and ultimate analyses of the developed pellets</i>	54
3.4. Results and discussions	54
3.4.1. <i>Pellets dimensional stability</i>	54
3.4.2. <i>The effect of biochar blends in CGW pellet size and density</i>	58
3.4.3. <i>The effect of biochar blends in pellet durability</i>	59
3.4.4. <i>The effect of biochar blends in pellet hardness</i>	61
3.4.5. <i>The effect of biochar blends on elemental composition, ash content and calorific values of the developed pellets</i>	62
3.5. Summary and conclusion	64
CHAPTER 4: THERMO-KINETICS BEHAVIOUR OF CGW PELLETS IN COMBUSTION.....	66
4.1. Introduction	66
4.2. Theoretical models of thermal analyses.....	68
4.2.1. <i>Forced fitting equation model</i>	69
4.2.2. <i>Free methods</i>	71
4.3. Experimental materials and methods.....	74
4.3.1. <i>Materials and equipment</i>	74
4.3.2. <i>Method</i>	75
4.3.3. <i>Data treatments</i>	75
4.4. Results and discussions	76
4.4.1. <i>Thermal combustion behaviour of CGW100 pellet and coconut shell biochar</i>	76
4.4.2. <i>Effect of biochar addition in thermal combustion of CGW pellets</i>	78
4.4.3. <i>Effect of heating rates in thermal decomposition of CGW pellets combustion</i>	84
4.4.4. <i>Thermo-kinetics combustion of CGW pellets</i>	88
4.4.5. <i>Synergistic in co-combustion</i>	90
4.5. Summary and conclusion.....	93

CHAPTER 5: THERMO-KINETIC BEHAVIOUR OF CGW PELLETS IN PYROLYSIS.....95

5.1. Introduction95

5.2. Material and methods97

5.3. Results and discussions97

 5.3.1. *Thermal pyrolysis behaviour of pure CGW pellet and biochar*.....97

 5.3.2. *Effect of biochar addition in the thermal pyrolysis of CGW-biochar blend pellets*100

 5.3.3. *Effect of heating rates to the pyrolysis of CGW pellets*102

 5.3.4. *Thermo-kinetics pyrolysis of CGW pellets*105

 5.3.5. *Synergistic effect in co-pyrolysis*108

5.4. Summary and conclusion.....109

CHAPTER 6: COMPUTATIONAL FLUID DYNAMICS MODELING OF COTTON GIN WASTE PELLETS GASIFICATION111

6.1. Introduction111

6.2. Theoretical biomass thermochemical conversion116

6.3. Modeling of thermochemical conversion of solid fuel117

6.3. Gasification modeling118

 6.4.1. *Governing equations for fluid flow*120

 6.4.2. *Radiation model*121

 6.4.3. *Turbulence model*123

 6.4.4. *Turbulence and chemistry interaction*124

 6.4.5. *Particle combustion model*127

 6.4.6. *Input data and boundary condition*.....130

 6.4.7. *Numerical calculation*.....133

6.5. Results and discussions134

 6.5.1. *Model validation through the previous experimental data on macadamia shell gasification*.....134

 6.5.2. *Predicted profiles of temperature, velocity, mass of carbon fraction, particle density and species fraction*.....137

 6.5.3. *Impact of different CGW pellets on gasification performance*.....144

6.6. Summary and conclusion147

CHAPTER 7: INDUSTRY IMPACT OF CONVERTING COTTON GIN WASTE INTO THERMOCHEMICAL ENERGY149

7.1. Introduction149

7.2. Methods.....150

7.3. Results and discussions154

7.3.1. Net energy analyses	154
7.3.2. Economic analyses.....	157
7.3.3. Greenhouse gas emission reduction	160
7.4 Summary and conclusion	161
CHAPTER 8: CONCLUSIONS AND RECOMMENDATIONS.....	163
8.1. General summary and conclusions.....	163
8.2. Recommendations for further research	166
References	167
APPENDIX A: LITERATURE.....	180
APPENDIX B: PELLET SIZE	193
B.1. Raw data of pellet size before and after storage.....	193
B.2. Independent T-Test of pellet size before and after storage (stabilization)	206
B.3. One way ANOVA TEST and POSTHOC test of effect biochar blends treatment in pellet size	216
APPENDIX C: DROP TEST	225
C.1. Raw data of Drop Test.....	225
C.2. One-way ANOVA TEST and POSTHOC Test of effect biochar blends treatment in the drop test (durability)	232
APPENDIX D: HARDNESS TEST	234
D.1. Raw data of Hardness Test.....	234
D.2. One way ANOVA TEST and POSTHOC Test of effect biochar blends treatment in the hardness test.....	237
APPENDIX E: ISO-SURFACE OF TEMPERATURE PROFILES FOR CGW PELLETS GASIFICATION A/F=1.3.....	240

List of Figures

Figure 1.1: Scope of Study	5
Figure 2.1: Cotton plants with fibre in its fruit (Cotton-Australia, 2014).....	8
Figure 2.2: A pile of compost made from cotton gin waste	10
Figure 2.3: Phase diagram of solid thermochemical conversion (Bain, 2004)	21
Figure 2.4: Downdraft gasifier types (a) throated (b) un-throated (Mendiburu, Andrés Z. et al., 2014)	25
Figure 2.5: Residual mass versus temperature for biomass pyrolysis and coal/biomass co-pyrolysis (Onay et al., 2007).....	35
Figure 3.1: Cotton gin waste sample	45
Figure 3.2: Pellet mill	47
Figure 3.3: Pellet Production Process	47
Figure 3.4: Cotton gin waste before and after size reduction	48
Figure 3.5: Materials (chopped CGW, gelatinised cassava starch, biochar).....	48
Figure 3.6: SEM images before and after fermentation using starch.....	49
Figure 3.7: CGW and CGW-biochar blended of pellet fuels.....	50
Figure 3.8: Instrumentation for measurement of the pellet size, weight and apparent density.....	52
Figure 3.9: Single drop pellet test	53
Figure 3.10: Load Testing Machine for pellet hardness	54
Figure 4.1: Time plot of typical reaction models applied in kinetic analyses (Vyazovkin, 2006)	71
Figure 4.2: Thermogravimetric Analyzer	74
Figure 4.3 Determination of ignition (T_i) and burnout (T_b) temperatures method (Lu & Chen, 2015)	76
Figure 4.4: Thermogravimetric (TG) and derivatives thermogravimetric (DTG) curves of CGW100 pellet combustion at heating rate 20°C/min	77
Figure 4.5: Thermogravimetric (TG) and derivatives thermogravimetric (DTG) curves of coconut shell biochar combustion at heating rate 20°C/min	78
Figure 4.6: Thermogravimetric (TGA) of CGW pellets and biochar curves during combustion at heating rate 20°C/min	80
Figure 4.7: Comparisons of weight reductions of CGW100, CGW95, CGW90 pellets during combustion at constant heating rate 20°C/min	81
Figure 4.8: Comparison of weight reductions of CGW100, CGW85, CGW80 pellets and biochar during combustion at heating rate 20°C/min.....	83
Figure 4.9: Thermogravimetric (TG) curves of CGW100 pellet and CGW-biochar pellets combustion at different heating rates.....	85
Figure 4.10: Derivative thermogravimetric (DTG) curves of CGW100 Pellet and CGW-biochar pellets combustion at different heating rates	86
Figure 4.11: Comparison of activation energy values of pellets combustion from empirical kinetic and calculation	91
Figure 4.12: Comparison of ash yield of CGW pellets combustion from experimental and predicted based on individual weight proportion	93

Figure 5.1: Thermogravimetric (TG) and derivatives thermogravimetric (DTG) curves of CGW100 pyrolysis at heating rate 15°C/min	98
Figure 5.2: : Thermogravimetric (TG) and derivatives thermogravimetric (DTG) curves of biochar pyrolysis at heating rate 15°C/min	99
Figure 5.3: Thermogravimetric (TGA) curves of CGW pellets pyrolysis at heating rate 10°C/min, 15°C/min, 20°C/min	101
Figure 5.4: Derivative thermogravimetric (DTG) curves of CGW pellets pyrolysis at devolatilization stage	102
Figure 5.5: Char production from TG pyrolysis of CGW pellets	109
Figure 6.1: Thermochemical conversion of solid fuel (NIEMELÄ, 2015)	116
Figure 6.2: Modeling scheme of fuel in the fixed bed gasifier ((Souza-Santos, 2010)	118
Figure 6.3: the 2D gasifier model (Source: http://www.allpowerlabs.com)	119
Figure 6.4: Chemistry models calculation based on Probability Density Function (PDF) ANSYS Theory Guide (ANSYS-Inc, 2016)	127
Figure 6.5: Experiment of macadamia shell gasification	135
Figure 6.6: Iso-surface of the temperature of CFD model result for macadamia shell gasification.....	136
Figure 6.7: Model interpretation of temperature contours	137
Figure 6.8: Baseline of temperature analyses and surface zone of product gasses analyses	138
Figure 6.9: Temperature and velocity magnitude (right side) profiles	139
Figure 6.10: Mass fraction of C(s) and density distribution	140
Figure 6.11: CO and CO ₂ mole fraction profile.....	142
Figure 6.12: CH ₄ and H ₂ mole fraction profile.....	143
Figure 6.13: Model interpretation of reactions in each stage of gasification.....	143
Figure 6.14: Iso-surface of the temperature profiles for CGW100 and CGW80 gasification	144
Figure 7.1: Scenarios constructed for re-utilizing CGW pellets as an energy source	151

List of Tables

Table 2.1: Proximate and ultimate analysis of woody, non-woody biomass and other carbonaceous materials (Higman & van der Burgt, 2008; Lapuerta et al., 2008; Mohammed et al., 2012; Samy, 2013).....	12
Table 2.2: Thermochemical conversion technologies (Wang & Yan, 2008)	21
Table 2.3: Single non-woody biomass stock gasification and combustion.....	26
Table 2.4: Biomass co-gasification	28
Table 2.5: Mineral content in ashes of CGW, EFB, Oakwood and bituminous coal (%weight,dB).....	31
Table 2.6: Modelling in gasification	37
Table 3.1: Physical composition of cotton gin waste.....	45
Table 3.2: Proximate (ASTM D3173, D3174, D3175) and ultimate analysis (ASTM D5373) of raw materials of mixture fuels.....	46
Table 3.3: Pellet size before and after 14 days storage.....	57
Table 3.4: Mean size expansion and density changes after 14 days storage	57
Table 3.5: Pellet sizes (measured after 14 days stabilisation)	58
Table 3.6: Durability measured from Single Drop Test.....	60
Table 4.1: Typical models of reaction for fitting equations in kinetic analyses (Vyazovkin, 2006)	70
Table 4.2: CGW pellets combustion properties at heating rate 20°C/min.	87
Table 4.3: Activation energy and pre-exponential factor of combustion CGW pellets.....	89
Table 5.1: Maximum conversion rates and corresponding temperatures	105
Table 5.2: Activation energy and pre-exponential factor of pyrolysis CGW Pellets.....	107
Table 6.1: Developed CFD models for batch type of gasifiers	113
Table 6.2: Input data of CGW properties in the model simulations.....	131
Table 6.3: Summary of model development parameters and assumptions for CGW pellets gasification.....	132
Table 6.4 Gasification of macadamia shell: modeling and experimental results	137
Table 6.5 CFD model generated results of combustion and reduction temperatures of gasification CGW Pellets at A/F=1.3.....	145
Table 6.6: Prediction of species gas fraction (% volume)	146
Table 7.1: Assumptions for economic calculations.....	153
Table 7.2: Energy input-output analyses from pellet processing energy	157
Table 7.3: Costs of CGW pellets production (in AU\$)	158
Table 7.4: Sensitivity analyses of production costs of CGW95 and CGW80 pellets based on the biochar price in the market (AU\$).....	159
Table 7.5: Energy cost (AU\$) of current business-as-usual (BAU) at gin capacity 35000 bales/year	159
Table 7.6: Scenarios constructed for energy replacement at gin using CGW pellets.....	160
Table 7.7: GHG emission reduction (% of BAU)	161
Table 8.1: Summary of properties CGW pellets.....	164

Glossary Terms

Ash:	the operationally defined fraction of biomass/coal and typically includes inorganic oxides and carbonates
Activation of energy (E_a):	in chemical kinetics, activation of energy in the Arrhenius equation, a minimum amount of energy for reactants to transform into products
Apparent density	the ratio between the weight of a single particle and its volume
Axisymmetric:	the analyses symmetrical to an axis
Biochar:	charcoal used for ranges of applications such as soil amendment, improved resource use efficiency, remediation and/or protection against particular environmental pollution and as an avenue for greenhouse gas mitigation
Bulk density:	the ratio of the mass of a bed of particles to its volume; the sum volume of individual particles and void spaces between them
Charcoal:	produced by thermochemical conversion from biomass mainly for energy generation.
Cotton gin waste (CGW):	the by-product of cotton ginning; the biomass waste contains of pods, seed, fibre, dirt (leafy and trunk crumb) and fine dust.
Constant rate reaction model:	in devolatilization, the rate of reaction is independent of the concentration of the reactants
Diffusion limited rate model:	in combustion, the surface reaction in a particle is assumed to proceed a rate of reaction determined by the diffusion of the gaseous oxidant to the surface of particle
Discrete phase:	a Lagrangian trajectory calculations for dispersed phases (particles, droplets or bubbles)
Eddy dissipation model:	a turbulent chemistry reaction model. Most fuels are fast burning and the overall reaction is controlled by turbulence mixing

Eddy dissipation concept:	an extension of eddy dissipation model to include detailed chemical mechanism in turbulent flows
Ginning:	a post-harvest processing of cotton, separating the fibre and seeds from other contaminated harvesting parts
Hydrochar:	the solid product of hydrothermal carbonization or liquefaction
Higher heating value (HHV):	the energy released as heat of the products of combustion and considering the heat of vaporization
Intrinsic model:	in combustion, the surface reaction rate includes the effects of both bulk diffusion and chemical reaction. The chemical rate is explicitly expressed in term of the intrinsic chemical and pore diffusion rates
Kinetic/diffusion limited rate model:	in combustion, the surface rate reaction is determined either by kinetics or a diffusion rate. The diffusion rate coefficient and a kinetic rate are weighted to yield a char combustion rate
Laminar finite rate model:	the model which ignores the turbulence
Low heating value (LHV):	the energy released as heat of the products of combustion and subtracting the heat of vaporization
Multiphase:	a simultaneous flow of materials with different states/phases or with different chemical properties but in the same state or phase
Pre-exponential factor (A):	in chemical kinetics, the pre-exponential constant in the Arrhenius equation, an empirical relationship between temperature and reactivity
Proximate analysis:	characterisation of solid fuel; the proximate provides moisture content, volatile content, the fixed carbon and ash
Reactivity:	the rate at which chemical substance tends to undergo chemical reaction
Relaxed density:	the ratio of the expansion in the apparent density of a particle after storage to its initial apparent density. The negative expansion shows that the shrinkage occurs in the particle after storage

Single kinetic rate model:	in devolatilization, the rate of reaction is assumed to follow first order reaction
Synergistic:	the effect of two chemicals taken together is greater than the sum of their individual effect
Syngas:	a product of gasification, a fuel gas mixture consisting primarily of hydrogen, carbon monoxide, very often some amount of carbon dioxide and small amount of methane or other hydrocarbon gasses
Thermochemical conversion:	the conversion of solid fuel into liquid, gas and or heat by thermal and chemical reactions. The process conversions included in this term are combustion, pyrolysis and gasification
Thermogravimetric analyses (TGA):	a method in thermal analyses in which the mass of sample is measured over time as the temperature changes
Thermo-kinetics:	the thermogravimetric analyses explored for the insight into the reaction mechanism of thermal (e.g. catalytic or non-catalytic) decomposition involves in thermochemical conversion of materials. A constant heating rate or a constant mass loss rate is usually applied for the analyses
Two competing rates model:	in devolatilization, the rate of reactions are controlled by two kinetic rates over different temperature ranges
Ultimate analysis:	characterisation of solid fuel; the ultimate provides the composition by weight percentage of carbon, hydrogen, oxygen as well as sulphur and nitrogen

CHAPTER 1: Introduction

1.1. Background

Agricultural production and processing often generate a considerable amount of biomass by-products and wastes. Paddy husks, straw, grasses, crop stubble and trash are typical biomass wastes from agricultural field. On the other hand, sawdust, cotton gin waste (CGW), palm oil waste, cane bagasse and animal excreta are biomass wastes from processing plants. In general, these wastes can be categorised as either woody or non-woody biomass. Having a lower lignin content, non-woody type is a common waste found in agricultural processing plants. This non-woody are sourced from a wide range of agricultural processes, animal solid excretion and herbaceous plants. The non-woody waste from agricultural processing plants may be low in density and calorific value, but typically abundant and readily available based on production schedule and capacity.

Cotton, a non woody produced from a herbaceous type plant, is one of Australia's top commodities. Currently, Australia produces 2-5 million bales of cotton per year (1 bale = 227 kg). The cotton yield in Australia is on average 9.7 bales/ha, twice of the world average (Hamawand *et al.*, 2016). This industry also generates income of \$1-3 billion/year. Most (98-99%) of the cotton produced is exported as the high quality lint. New South Wales (NSW) and Queensland are the two main cotton producing states in Australia (Cotton-Australia, 2014).

The current disposal of cotton waste in Australia represents significant environmental problem and associated plant diseases issues. Currently, cotton stalk wastes are usually returned to the field in situ to increase the soil organic matter. Gins, the next places of post-harvest stage separating the lint from the seed, discharge a total average of 100,000 tonnes of cotton gin waste (CGW) per year in Australia with a typical moisture content of about 8-10% (Chen, 2014). A common practice of managing this large amount of CGW is by composting. However, this option often faces the problem of low market demand. A concern of possible pathogen presence within the composted product adds to low market appeal (Hamawand *et al.*, 2016)

Recycling the waste to generate energy is another and perhaps more preferable option. The cotton gin waste can be recycled into energy source to meet the energy demand in ginning plants. This option may not require any extra cost of transportation. A similar practice has also been used in other industries such as sugarcane and palm fruit processing plants. There, cane bagasse and oil palm kernel shells have been recycled as fuel in the combined heat and power systems. The potential energy conversion from combusting the CGW in Australia would be about 3.6 million GJ/year (Hamawand *et al.*, 2016).

The non-woody biomass has typically low density, low quality as solid fuel. Hence, upgrading it to a higher quality of fuel is a first step towards improving the energy conversion efficiency. The processes of energy conversion can be roughly divided into the biological and thermochemical. Biological processes including fermentation into ethanol and methane gas face the challenge of low lignocellulosic conversion. The thermochemical process is more widely used in the conversion of biomass into energy. It refers to the conversion of solid fuel into gas or higher energy solid fuel utilising heat for chemical reactions with or without oxidiser.

The thermochemical conversion technology comprises of the processes of combustion for heat generation, fast pyrolysis for liquid bio-oil, slow pyrolysis for solid carbon and gasification for gas production. Pyrolysis technology, besides char production, can also produce chemicals. Combustion technology which generates heat and power is an established technology and has been applied widely in the energy supply for processing industries. However, gasification is often considered as a more efficient way of converting the lignocellulose materials into energy via gaseous intermediates, with the typical energy conversion efficiency of higher than 50% (Puig-Arnau *et al.*, 2010). In gasification, the biomass is converted through partial oxidation into a mixture products of gas, a small quantity of char and a condensate.

Thermochemical conversion has been studied for a wide range of biomass feedstock. Compared to woody biomass, non-woody biomass conversions face additional technical difficulties. This is because the non-woody gasification often meets the problem of ash sintering and tar bed bridging (Gai & Dong, 2012; Guo *et al.*, 2014). A sticky melting material can block the part of gasifier such as grate, gas pipes, and air duct etc (Natarajan *et al.*, 1998; Chandrasekaran *et al.*, 2016). In combustion application, high ash content can often lead to high particulates emission and low particulate matters melting point. Furthermore, the problem of low density

generally results in an unstable process of thermochemical conversions. Appropriate treatments are therefore crucial for upgrading the non-woody into a good quality of solid fuel.

Densification has been investigated as a possible method to improve the drawback of low density. For example, pelleting the CGW has previously been studied by Holt *et al.* (2006). The function of pelleting is predominantly to densify the biomass. This in turn shall also increase the efficiency of thermochemical conversion. In the pellet form, non-woody biomass combustion can produce higher conversion efficiency compared to raw material. Holt *et al.* (2006) reported that combusting CGW pellets in a household wood pellet stove resulted in two to three-fold lower ash residue compared to combusting the raw CGW.

Upgrading the biomass feedstock into a pelleted form may also be desirable for residential and industrial heating systems, particularly in regards to the infeed system operation. This is because the pellet feeding system can be easier to control than with comparable raw biomass system. Currently, pellet fuels are available on the market for utilisation in both residential/commercial and industrial applications. Eventhough pellets from wood wastes have been available commercially for some time, the wide variation of non-woody biomass properties requires specific studies (e.g. binder application, treatment prior pelleting) for the development of appropriate pelleting process of feedstocks. This study uses a modified CGW pelleting method reported by Holt *et al.* (2006).

It is known that blending the biomass with coal could reduce the tar problems in gasifiers and combustors (Xu *et al.*, 2011; Tchapda & Pisupati, 2014). The additional heat due to higher carbon content of the coal will assist in cracking of tar components into combustible gasses. Particularly, for the non-woody biomass blends, the elevated mineral content of K, Ca, Mg and Na may act as natural catalysts during the thermochemical conversion. Improved tar cracking by coal heat and catalytic activities of non-woody biomass are known as synergistic effects of co-conversion.

The available reports on synergistic aspect of co-conversion are generally inconsistent and can be divided into three groups. The first group of researchers (Sjöström *et al.*, 1999; Lapuerta *et al.*, 2008; Xu, 2013; Bai *et al.*, 2014; Howaniec & Smoliński, 2014) found synergistic occurrences. Another group reported no such synergistic results (Pan, Y. G. *et al.*, 2000; Kumabe *et al.*, 2007; Collot *et al.*, 2009). A third group even found a negative synergy. They reported that depending on the

feedstock compositions, some chemical reactions during the process of the thermochemical conversion could be inhibited (Pinto *et al.*, 2003; Habibi, 2013). Thus, there appears to be still a significant knowledge gap in the co-conversion process of biomass-coal blend and how to optimise it.

Currently, most studies apply coal as the preferred blending materials due to low cost and reliable supply. However, the high carbon blended material can be in the form of biochar. A biochar application may be more effective from the combined environmental and economic aspects if it originates from the char of woody biomass pyrolysis or gasification. At this moment, there are very few studies applying the biochar as the blended material for the co-conversion process (Sahu *et al.*, 2010; Yi *et al.*, 2013). In this study, a renewably sourced biochar as the blending material for CGW pellets has been proposed.

1.2. Research goal and objectives

This study aimed to develop and assess the methods to convert non-woody biomass into a valuable source of fuel. The scope of this study covered both the technical development and the cost estimation. This included the characterisation of its physical, chemical and thermo-kinetic properties and the application of the developed material in a small scale plant.

An industrially generated by-product biomass, cotton gin waste (CGW), was blended with different percentages of biochar and formed into pellets. The physical, chemical and thermo-kinetic behaviour of pellets was examined both on the laboratory scale as well as in a small pilot plant.

A model of gasification for a small scale plant capacity was further developed. The developed model was then utilised to simulate and compare the gasification characteristics of different blends of CGW pellets. The cost estimation of CGW pellets production and utilisation for an alternative energy generation in a gin house was also evaluated. The following figure (Fig 1.1) shows the scope of this study.

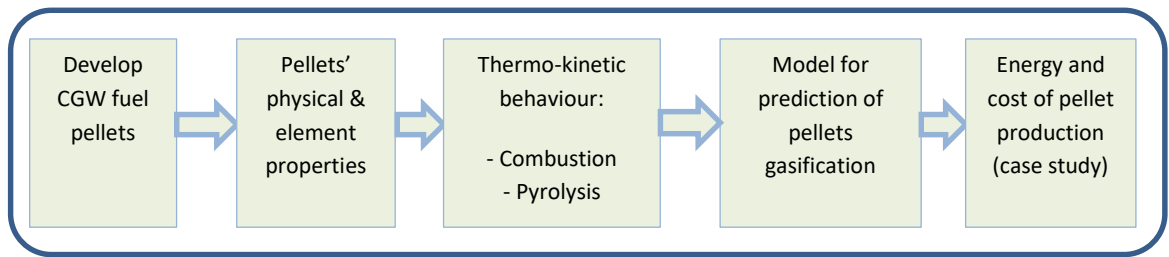


Figure 1.1: Scope of Study

The specific objectives of this project are as follows:

1. *Development a good quality CGW fuel pellets*

Development of CGW fuel by upgrading the raw CGW into a good quality of solid fuel was investigated in this study. The effects of the biochar blended in the CGW pellets were studied to investigate whether the blends could improve the physical and element properties of the fuel.

2. *Investigation the kinetic characteristics of thermal conversion of the developed CGW fuel pellets*

This covered the thermochemical conversion of the developed CGW fuel pellets as well as any interactions of the composition with the thermo-kinetics. The thermo-kinetic properties of the developed fuels were obtained through experiments and the possible synergistic effect in co-conversion of the blended fuel was studied.

3. *Development a CFD model for simulation the developed CGW fuels gasification performances.*

A Computational fluid dynamics (CFD) model was developed to simulate the gasification performance of the developed CGW fuel pellets. The gasification was modelled in a fixed bed downdraft gasifier type.

4. *Evaluation the potential of cotton gin waste conversion into fuel pellets in a gin and the impact of the energy generation.*

The impact of CGW pellets production and utilisation for an alternative energy generation in a gin house was evaluated. This evaluation included both technical, cost estimation and greenhouse gas emission compared with current energy used in a gin.

1.3. Organisation of Chapters

The organisation of this dissertation is as follows:

- Chapter 1. Introduction: this chapter presents the research background driving this work. This chapter also defines the research objectives and broad methodology of this study.
- Chapter 2. Literature Review: this chapter reviews the resources of material used in this study, state-of-the-art of the blend fuels in the thermochemical conversions, and the factors influencing co-conversion and modelling in gasification.
- Chapter 3. Development CGW Fuel Pellets: this chapter investigates properties of materials used in this study and also the processing steps. The physical and chemical properties of the developed pellets are discussed.
- Chapter 4. Thermo-kinetic Behaviour of CGW Pellets Combustion: this chapter describes the combustion behaviour of the developed CGW pellets, the effect of fuel blends in the combustion performance including any synergistic effect of the co-combustion.
- Chapter 5. Thermo-kinetic Behaviour of CGW Pellets Pyrolysis: this chapter investigates the pyrolytic behaviour of the developed CGW pellets, the effect of fuel blends in the pyrolysis process including the potential synergistic effect of the co-pyrolysis.
- Chapter 6. CFD Modelling and Simulation: this chapter develops a detailed CFD model to study the gasification of fuels at the plant scale of downdraft gasifier. The developed model is then used for simulation and comparison of the gasification performance of developed CGW fuels.
- Chapter 7. Industrial Impact of Converting CGW into Thermochemical Energy: this chapter explores the technical, economic and environmental implications of CGW conversion into fuel pellet and potential re-utilisation of the pellet for an alternative energy production in the gin.
- Chapter 8. Conclusions and Recommendation: this chapter summarise the main findings from this work and recommend applications and future research.

CHAPTER 2: Literature Review

In this chapter, the resources of material used in this study, state of the art of the blended fuels in the thermochemical conversions, and the factors influencing co-conversion and modelling in gasification are reviewed.

Firstly, the potential of cotton gin waste (CGW) as a non-woody biomass feedstock is discussed (Section 2.1). The properties of CGW are investigated and compared with other solid fuels. By knowing the properties, possible approaches of upgrading the raw material into a good quality of fuel are then identified and selected.

Secondly, Section 2.2 reviews the current thermochemical conversion methods of the biomass fuel. Thermal condition required in each method and general chemical reactions identified from these thermal conversions are discussed. Considered the highest conversion efficiency among others, the gasification is selected for the next method of CGW fuel conversion. Hence, the designs and performances of available gasifiers are discussed in more detail in the following section (2.3).

Sections 2.4 and 2.5 further review the available literatures of biomass thermochemical conversions (combustion, gasification and pyrolysis). In general, the non-woody can be used as a fuel either in a single mode application (section 2.4) or co-blended with other high quality fuels (Section 2.5). These sections also highlight the potential benefits and drawbacks of converting the single fuel and co-blended biomass fuel. This enables the current research gaps be identified and the suitable methods for upgrading the CGW fuel be selected.

An objective of this study, as stated previously, is also to apply the developed CGW fuel in a gasifier. Thus, Section 2.6 reviews the different computational models of biomass gasification. This section assesses and compares several models in respect to a variety of requirements and computing complexities for further consideration in the development of a suitable model for this study.

2.1. Potential of solid fuel development from cotton gin waste

2.1.1. Australian cotton industry

The cotton industry is one of Australia's major agricultural sectors. Australia is also the world's third largest cotton exporter behind the US and India. The exported product is a high-quality lint as a textile raw material. The Australian cotton crop is worth \$1-3 billion annually, sustaining 152 rural communities. In Australia, cotton is mainly produced in the states of New South Wales and Queensland. The most (95%) common species grown for commercial purposes in Australia is *Gossypium hirsutum* L. (Cotton-Australia, 2014)

The planting season calendar for cotton in Australia is in September-November and the harvest season followed by ginning activity is in March-May. The off season is usually in May-August. At this time, growers may plant winter crops or use their land for grazing (Cotton-Australia, 2014). Cotton is a leafy shrub, with cream and pink flower. After pollination, it is replaced by the fruit containing cotton fibre (Figure 2.1).



Figure 2.1: Cotton plants with fibre in its fruit (Cotton-Australia, 2014)

The harvest product containing the mix of lint, seed, pods, stems and leafy fragments is transported into the gin houses. This is in the form of round or cubical

modules. The content of modules is then processed and separated into lint (the fibre for textile industries), seeds (the feedstock for seed oil industries) and the remaining plant biomass often referred to as cotton gin waste (CGW). The lint is pressed in form of bales. The bale weight is approximately about 227 kg. In Australia, one hectare of cotton farm typically produces approximately 1.6 tonne of lint, 2.5 tonne cotton seed, 2 tonne of stalk, and 0.4 tonne cotton gin waste. At present, these stalk wastes are usually returned to the field as soil amendment (Chen, 2014).

The ginning process is fully mechanised in Australia and is energy intensive. At this moment, the sources of energy for ginning operation are usually gas and electricity. The process often requires a drying operation for preparing a uniform moisture content of materials. Most of the dryers are still fuelled by natural gas or LPG at this time. Ismail (2009) has reported that the ginning process consumed about 0.74 – 3.90 m³ of natural gas or 2.27 – 5.61 litres of liquefied petroleum gas (LPG) per bale (227 kg) production. The electricity for running the machinery is mainly sourced from the national electricity grid. The gas and electricity usage comprises approximately 39% and 61% respectively of the total energy required for producing a bale.

From an average 250,000 ha of cotton growing area each year, a total of 100,000 tonnes (about 10% w.b. moisture content) of cotton gin waste may be produced in Australia. This can cause considerable disposal and storage problems for cotton ginners. The current practice of waste management is usually by composting (Figure 2.2). If this CGW is sold as feed material for composting, the economic value of this by-product may be at around 0.4 t/ha*\$10/t or \$4/ha. On the total, it will make \$1 million for the whole cotton industry (Chen, 2014). However, this option may not be available for most ginners. A concern of possible presence of pathogen contamination in this compost product has resulted in only a small market demand.



Figure 2.2: A pile of compost made from cotton gin waste

2.1.2. Methods of converting cotton gin waste for energy production

Another option to utilise the cotton gin waste is by converting it into bio-energy. The potential of Australian cotton gin waste to bio-energy has been reviewed by Hamawand *et al.* (2016). They assessed four methods of conversion, including combustion for fuelling the boiler, biological fermentation for ethanol production, anaerobic digestion for methane generation, and gasification for gas production. Their analyses showed that the combustion would produce the highest revenue, while the fermentation into ethanol would be the lowest one. The ethanol generation from CGW still involves some challenging steps. Furthermore, they also highlighted that the CGW conversion through anaerobic digestion and gasification requires further research in the technical improvement for application in the plant stage.

More widely applied commercially in the plants, the thermochemical conversion is the method focused on this non-woody biomass fuel study. In general, there are two possible approaches of converting the non-woody biomass into energy. Firstly, it is by improving or selecting the optimal design of converter and secondly, by upgrading the fuel to be compatible with the available reactors. Considering the widely varying properties of non-woody biomass, it is often suggested to focus first on the improvement of non-woody to a high quality solid fuel so that it can be fed into the existing thermochemical energy converters without extensive modification. Thus, this research starts with studying the CGW properties, upgrading CGW into the solid

fuel and studying the performance of upgraded fuel for the application in the thermochemical converters.

Solid fuel properties are typically characterised by proximate and ultimate analyses. Proximate analysis characterises the fuel in terms of fixed carbon, moisture, ash and volatile matter. Ultimate analysis identifies composition of the main chemical (C, H, O, N, S) and relevant minor elements (Na, K, Ca, Mg etc) which enter directly or indirectly into the thermochemical reactions. During these thermochemical processes, the minerals are converted into ash, which is a generally an inert material that reduces the effective energy value of a feedstock.

Tables 2.1 and Table A.1 in Appendix A show the fuel properties of CGW in comparison with other non-woody biomass, woody biomass and carbonaceous stock (coal & biochar). The higher carbon content in solid fuel leads to higher energy content. In contrast, higher moisture and ash in non-woody biomass decreases the energy content. However, the carbon component is not the only factor influencing the thermochemical conversion. The elements of hydrogen and oxygen from the moisture and oxidants entering the process will also react to produce gas with main components hydrogen, methane, CO and CO₂.

The mineral materials found in biomass mainly comprise of alkali (potassium, sodium), alkaline earth (calcium, magnesium) and other minerals such as Fe, Si, Al, together with Cl and P. These materials form ash during the thermochemical conversion process. Some alkali and alkaline earths may also help as the reactions catalysts of the conversion. However, these mineral materials can react at high temperature with silica to form silicates, which are significantly high in non-woody materials. The problem with high ash content of non-woody biomass can also cause agglomeration in the gasifier or combustor bed (Fryda *et al.*, 2008; Lahijani & Zainal, 2011).

Table 2.1: Proximate and ultimate analysis of woody, non-woody biomass and other carbonaceous materials (Higman & van der Burgt, 2008; Lapuerta et al., 2008; Mohammed et al., 2012; Samy, 2013)

Analyses	Woody			Non-woody			Others		
	Sawdust	Pinus pruning	Olive pruning	Cotton gin waste***	Cane baggase ***	Empty fruit bunch ***	Lignite ***	Bituminous***	Wood charcoal
Proximate (% weight, db)									
- Moisture				11.80	9.4	5.18	25-75	3-10	
- Ash	1.28	2.67	3.67	10.5	3.6	3.45	10	5	2-5
- Volatiles	1.28	82.10	82.35	68.7	65	82.58	> 45	14-45	8-25
- Fixed carbon	1.28	15.13	13.98	20.8	31	8.97	< 69	69-86	70-89
- Heating value,(MJ/kg)	1.28	19.99**	19.99**	16.6*	18.9*	17.02*	6.7-25**	25-36**	18-19*
Ultimate (% weight, db)									
Carbon	50.26	50.55	47.5	45.14	49.4	46.62	40-52	59-81	70-90
Hydrogen	6.14	6.12	6	4.93	6.3	6.45	6.2-6.9	5-5.8	1.7 -3
Nitrogen	0.07	0.45	1.06	1.16	0.3	1.21	0.7-1.0	1.1-1.4	0.5-1.3
Sulfur	0.05	<0.01	0.04	0.29	0.07	0.035	1	1.5-3.5	0
Oxygen (by diff)	42.2	40.20	43.66	34.82	43.9	45.66	29.5-44	5-20.6	4-18
Ash							7.3-9.8	6-9.4	
Geometric mean diameter (mm)				0.6	0.09-4	0.3-0.5			
Bulk density (kg/m ³)				390	68	1422			300-500
* : High Heating Value		*** : as received							
** : Lower Heating Value									

An additional issue with non-woody biomasses is that they generally have low densities, particularly for sources originating from herbaceous plants. This can cause difficulties in handling during the conversion, particularly in controlling the fuel flow rate. Upgrading the material into a good quality fuel, thus, becomes a critical factor.

2.1.3. Upgrading non-woody biomass into solid fuel

The objective of the treatment is to create a biomass formula suitable as a feedstock for the thermochemical conversions, a treatment which could minimize failure in the thermochemical conversion process. The treatment of feedstock includes one or a combination of processes of size reduction, drying, blending and densification.

2.1.3.1. *Size reduction*

The irregular shape and size along with the varied composition found in non-woody biomass often requires size reduction. This is to provide a uniform size for the conversion or for the next treatment steps such as pelleting. In general, smaller particles have larger surface areas, allowing faster reactions and better heat transfer.

The common particle size range in feedstocks is 1 μm to 1 cm (Souza-Santos, 2010). The required size of feedstock for gasification is dependent upon the type of converter. For example, the fluidized bed gasifier/combustor usually requires the feedstock to be sized for easy fluidization to maximize the contact of the feedstock particle surface with the oxidant. The entrained bed type requires finer particles. On contrary, fixed bed gasifiers would require larger particle sizes, of the cm order, as a slower reduction is required. This is for the purpose of delaying the process of combustion while allowing effective devolatilization.

Equipment for size reduction can include hammer mills, rotary knife cutters or grinders. Energy consumption for these machines depends on moisture content, required size reduction ratio and biomass properties such as fiber content. For fibrous materials, Souza-Santos (2010) suggested using knife cutters instead of grinders. The grinding processes dramatically increase the fraction of particles having broom-like ends. This kind of feedstock can become entangled, leading to agglomeration in the feeding system.

2.1.3.2. *Drying*

Non-woody biomass from a processing plant or from the field often has a high moisture content. Drying is typically required for reducing moisture content to 10-15% (Basu, 2010). Low moisture content biomass, such as cotton gin waste, does not require drying. However, solid waste having the moisture content higher than 20% would require drying in its pre-processing stage. Drying can be an energy intensive task which would negatively reduce the overall efficiency of energy production. Each kilogram of moisture requires about 2,300 kJ for vaporization (Basu, 2010). The energy for drying can, however, be recovered from the heat generated during the process of thermal conversion. Assuming the typical heating energy conversion efficiency of biomass heating energy conversion is about 50% (Puig-Arnavat *et al.*, 2010), the energy consumption for drying can be as much as 4,600 MJ/kg of moisture

vaporized. Drying can also be achieved with other renewable means including solar heating.

2.1.3.3. *Blending and mixing with additives*

To overcome the problem of high ash and tar problems in the thermochemical conversion, the non-woody biomass can be mixed or blended with materials which would dilute the ash or reduce bind formation of tar (*i.e.* converting the tar into volatile). It can also be mixed with a catalyst or blended with other high grade fuel. The mix with commercial catalysts such as dolomite, NaOH, NaCl, CaO, ZnO, NiO have been investigated by Mohammed *et al.* (2012) in order to reduce the tar and increase the gasification efficiency. Li *et al.* (2009) reported using dolomite to crack the tar from the product of biomass combustion.

Alternatively, this ash issue can be altered by blending the non-woody materials with other higher quality solid fuels of low ash. By blending with the solid fuel, not only the fuel quality is upgraded, but this also can reduce other technical problems related to the thermochemical conversion of non-woody biomass (Pan, Y.G. *et al.*, 2000; Lapuerta, M. *et al.*, 2008; Zhu *et al.*, 2008; Collot *et al.*, 2009; Ataei *et al.*, 2012; Habibi, 2013; Xu, 2013; Jeong *et al.*, 2014; Nemanova *et al.*, 2014; Rizkiana *et al.*, 2014). Researches have shown that the co-conversion (be it co-gasification, co-combustion or co-pyrolysis) could bring about two other “synergistic” beneficial effects, namely tar cracking and catalytic conversion. These synergistic effects may be particularly significant for the blend fuel in pelleted form due to the more uniform mixture and close proximity of components in pelleted form when compared to the loose mixture (Xu *et al.*, 2011).

Most of the blend fuel studies have utilised coal as the blended material for the biomass (both woody and non-woody) or vice versa. Overall, biomass and coal are quite different in terms of their relative chemical compositions. Biomass has higher volatile content whereas coal has more fixed carbon. Under thermal stress, biomass breaks easily into volatiles, water, fixed carbon and finally into ash. In contrast, coal requires a much higher temperature for breakdown and decomposition. The increased heat from the coal can crack the tars produced from the biomass conversion, resulting in more combustible gases and less tar production. On other hand, the catalytic activity is expected from some mineral components in biomass. Table A.2 of Appendix A lists

recent literatures related to the addition of catalysts to biomass and also mixture of the biomass to coals for providing catalytic reactions in the thermochemical conversion.

Sources of blending materials for non-woody biomass

Charcoal is defined as a porous black solid consisting of an amorphous form of carbon, obtained as a residue when wood, bone, or other organic matter is heated in the absence or under a limited access of air. Coal has a similar composition with charcoal in the term of high fixed carbon. In coal, the fix carbon resulted from organic matter decomposed naturally in the absence of air and at high temperatures below the earth surface for periods of millions of years. Occasionally, coal is also defined as mineral charcoal.

- *Coal*

Coal is mainly composed of carbon (50 to 98%), oxygen (3 to 25%) and hydrogen (3-15%), with lesser amounts of nitrogen, sulphur and other elements (Table 2.1 and Table A.1 of Appendix A). It originates from organic matter which metamorphoses over long period of time, making up from fossil rocks (coal) that are combustible. Australia is the world's fifth largest coal producer, after China, USA, India and Indonesia. Coal from Australia is more than 70% exported, mostly to East Asia. There are two forms of coal mined in Australia: high-quality black coal (from Queensland and New South Wales) and low quality brown coal (from Victoria and South Australia). The Australia's high-quality black coal shares 9% of the world available black coal (Mineral-Council-of-Australia, 2015).

Coal is considerably less expensive than other energy sources. The use of coal accounts for about 37% of the shared total primary energy supply in the world (IEA, 2012). Coal in Australia is mainly used for power generation. While the utilization of coal as the blending material in biomass conversion may lead to an economically more flexible and reliable operation for an energy plant at the moment, the use of the mixed char by-product should be treated carefully in order not to contaminate the soil.

Providing a secure, affordable and uninterrupted supply of energy, as a non-renewable source of energy, coal is also a major source of problematic greenhouse gas emissions. Coal contributes up to 37% of total emissions in Australia (<http://www.newgencoal.com.au/coal-in-australia.aspx>). Due to this aspect of

pollution and emissions, this study has chosen not to use coal as the blending material for non-woody biomass upgrading.

- *Biochar*

Biochar is made by heating the wood-or other biomass-in a reactor without or with limited input of air. Thus, the carbon content is maximised, while the water and volatiles are released. This increases the energy density of the biomass as a fuel, as water content and other volatiles rather lower the energy content. Biochar is a stable, carbon rich charcoal that results from pyrolysis of biomass materials. Before coal was found, the biochar had been used in iron production. The current utilisation is now also for barbeque fuel and as a soil amendment.

The material for biochar production can be wood or other biomass. As the process fixes the carbon by releasing the volatiles and water, the higher lignin content in the biomass corresponds to the higher chemically bound carbon content. Thus, a higher char conversion should result. The presence of cellulose at an optimum temperature in carbonisation also influences the polymerisation into a stable char structure (Strezov *et al.*, 2006).

The utilisation of wood as a material for biochar production may lead to the deforestation. Hence, applying woody waste such as timber waste, nut shells, coconut husk and shells may reduce this impact. The properties of referred woody biomass, non-woody biomass, coals and biochar as solid fuels are provided in Table A.1 of Appendix A.

The biochar may have characteristics close to coals (such as high fixed carbon) but would have higher volatile content than high-rank coals. The biochar has also lower ash and sulphur content than low-rank coals. This might become an advantage if the blended substance is compared with coal. To date, the literature of co-conversion biomass and biochar is very limited (Sahu *et al.*, 2010; Yi *et al.*, 2013). Thus, this study focuses on the use of biochar.

2.1.3.4. *Densification*

Non-woody biomass has often a low bulk density, irregular shape and size. This is one of the main difficulties of handling, storing and applying non-woody biomass in its' original form. Densification can be a solution as a pre-treatment of non-woody biomass for use as a solid fuel. Densification not only increases the density but

can also improve the efficiency of the thermochemical conversion process. There are generally two methods of feedstock densification: torrefaction and pelleting (Samy, 2013; Tchapda & Pisupati, 2014).

- *Torrefaction*

Torrefaction is achieved by heating biomass at moderate temperatures (200-300°C) in an inert atmosphere. It can increase the mass density and energy density of the fuel (Sarkar *et al.*, 2014). It can also reduce moisture content and volatiles. Studies on biomass torrefaction as the treatment for upgrading the fuel have been applied to cotton gin trash (Samy, 2013). The comparison of raw and the torrefied cotton gin trash gasification showed that the torrefied products generally achieve higher carbon conversion and gasification efficiency. The reaction rate of raw cotton gin trash gasification was already greatly improved by simply increasing the temperature of the reactor from 850 to 950°C (Samy, 2013) without any pelleting. By increasing the reactor temperature, the carbon conversion and cold gas efficiency of the raw material was close to that achieved with the torrefied process. At 950°C, the carbon conversion of both raw and torrefied processes reached 55%.

Torrefaction and pelleting can increase the devolatilisation rates. Sarkar *et al.* (2014) compared the devolatilisation kinetics of switchgrass that was torrefied, torrefied and pelleted or raw-pelleted as pre-treatment processes. In both inert and oxidising atmospheres, the highest devolatilisation rates were achieved with post-torrefied pellets, followed by raw-pelleted and finally raw-torrefied biomass. The research showed that it was hence pelleting that would be a process preferred over torrefaction. The pelleting increased devolatilisation for both raw and torrefied materials.

Torrefied pellets show promise as a pre-treatment technology for solid fuel applications. Uslu *et al.* (2008) studied solid fuel production by the three processes mentioned above and found that energy densities of the torrefied, torrefied & pelleted and raw-pelleted biomass are 4.6 GJ/m³, 14.9-18.4 GJ/m³ and 7.8-10.5 GJ/m³ respectively. Thus, pelleting has a clear-cut beneficial effect on energy density. This research reported that other studies have promoted the raw torrefied as the highest energy production efficiency. However, it was also noted that the data were not taken from any commercial plant. Uslu *et al.* (2008) thus recommended that the torrefied pellet could be the best option in the international bioenergy supply chain.

- *Pelleting*

Pelleting or briquetting is another method of densification. The initial objective of pelleting or briquetting the non-woody biomass is to increase the density. Of about 1-2 cm size in the form of pellet material is often best option for simple biomass gasifiers of fixed bed design. The biomass pellet, particularly the wood pellet from wood waste, has been available commercially for many years.

While the main function of pelleting is predominantly to densify the biomass, it can also increase the efficiency of thermochemical conversion in the process that follow. In the pellet form, non-woody biomass combustion can produce lower ash compared to raw material. Holt *et al.* (2006) reported that the ash produced from combusting cotton gin waste pellets in a household wood stove was decreased two to three fold compared to that of the unpelleted material. Using the same stove, the conversion efficiency of CGW pellet combustion was higher than that of the raw material one.

Upgrading the biomass feedstock into a pelleted form may also be desirable for industrial heating systems, particularly in regards to the infeed system operation. This is because the pellet feed can be easier to control than raw biomass one. The irregular shape and size of raw non-woody biomass are often the cause of entangled 'clumps' in the feeding system. This can cause unstable combustion or gasification with ensuing increased emissions and lower overall efficiency. In a pelleted form, controls are of a comparable level to that of a liquid/gas fuelled system. The virtually same constant size, water content and particle density can also make it easier for automated operation (Vinterbäck, 2004).

A summary of recent studies on biomass pelleting is presented in Table A.3 of Appendix A. Although wood pellets from waste has been available commercially for some time, the wide variation of biomass properties requires specific steps for the development of appropriate pelleting processes for each different feedstock.

- *Pelleting techniques*

Essentially, the biomass pelleting process is a method of compressing the raw materials. The standard equipment used for this process is a screw extruder or a roller-plate, die pellet-mill. The efficiency of the equipment depends on the die temperature, die and roller configuration, pressure, feed rate and moisture content and properties of the feedstock (Holt *et al.*, 2006; Uslu *et al.*, 2008). Recent studies have looked into the

effect of binder addition or additive materials along with the treatment effects of extrusion temperature, pressure and moisture content. These studies focus primarily onto the quality of the developed fuel pellet and associated biomass properties.

In general, natural lignin, protein, starch and water soluble carbohydrate may act as a pellet binder (Lu *et al.*, 2014). Lignocellulosic materials have lignin bonded in the form of a lignocellulosic matrix. The softening, flow and subsequent hardening of lignin in the process of pelleting are similar in nature to a bonding process. The applied pressure combined with elevated temperature at which the polymer softens and passes from a glassy into a plastic form are the key factors of pelleting biomass.

As each non-woody biomass has its own particular lignocellulosic composition and bonding structure, sometimes a pre-treatment with loosening the lignin bonds, cellulose and hemicellulose is required prior to pressing. This modification is for the purpose to generating a uniform durability and stability of the produced pellet.

The bonds modification method can be either one or combination of steam, acid/alkali and biological fermentation processes (Agbor *et al.*, 2011). At the industrial scale, the established technology of steam treatment is often applied. It applies steam at the temperatures of 180-240°C to rupture the cellular structure (Shahrukh *et al.*, 2016). The biological fermentation is also promising but still challenging in reaching the efficiency of colder process application in the large scale industries (Agbor *et al.*, 2011). Occasionally this bonds modification may be inadequate for the non-woody biomass pelleting (Sultana *et al.*, 2010). Binder or other additives would need to be added to improve the strength, the durability and the thermochemical properties of the pellet. Additional starch, bentonite, lignosulfonate may further improve the mechanical structure of the pellet (Table A.3 of Appendix A).

The idea of upgrading pellet fuel heating value and thermochemical properties by addition of some substances –apart for charcoal/coal blends- during the pelleting process has also been investigated (Holt *et al.*, 2006; Jordan & Akay, 2013; Lu *et al.*, 2014). It was found that presence of calcium based catalysts, oils and glycerol in the pelleting process could increase the fuel properties and overall efficiency of thermochemical process. However, addition of these substances can sometimes cause negative effects in pellet durability and lowering the density, e.g. addition of oil to cotton gin trash (Holt *et al.*, 2006). Studies in this area are still on-going.

A method of pelleting cotton gin waste has been developed under the patent name COBY (cotton by products) system (Holt *et al.*, 2006). The process of pelleting

treated the ground CGW using gelatinised starch with or without cotton seed oil and then pressurized in a commercial pellet mill (Holt 2014).

Originating from its raw material of having low energy content, the produced CGW pellet had also low energy. This research therefore aims to upgrade the pellet properties by blending CGW with charcoal already during the pelleting step. This presumably intends to increase the pellet quality by having higher energy content, higher durability and possibly promoting the synergistic during the process of co-conversion.

2.1.4. Standard quality of the non-woody fuel pellet

As mentioned earlier, wood pellets have been successfully used in domestic heating applications in the USA and European countries. The standard quality attributes of the wood pellets for both regions have been based generally on the total ash content and durability (Holt *et al.*, 2006; Toscano *et al.*, 2013; Duca *et al.*, 2014).

Ensuing in particular for the flow of non-woody pellets in the market, the ISO 17225-6-2014: Part 6 Graded non-woody pellet, the standard for solid biofuels specifications and classes (Table A.4 of Appendix A), has been issued for commercial and household applications (ISO, 2014). It should be noted that this non-woody pellet standard is not tailored for specific industrial purposes. The industries may have varied and adjustable equipment and emission control systems, so that even the lower grade pellet fuel quality may be acceptable. Such a grade of the pellet fuel can be sourced from the typical non-woody biomass and Refuse-Derived Fuel (RDF).

2.2. Thermochemical conversion of solid fuel

Thermochemical conversion of solid fuel refers to the process of solid fuel changes utilising heat for the purpose of obtaining chemical reactions among the components with or without oxidizer. The relevant technology comprises of processes such as gasification for gas production, fast pyrolysis for liquid bio-oil, slow pyrolysis for solid carbon and combustion for heat energy (Figure 2.3). The differences between them are often characterised by operation conditions (temperature, residence time, amount of oxidant) and the desired product of the conversion (Table 2.2).

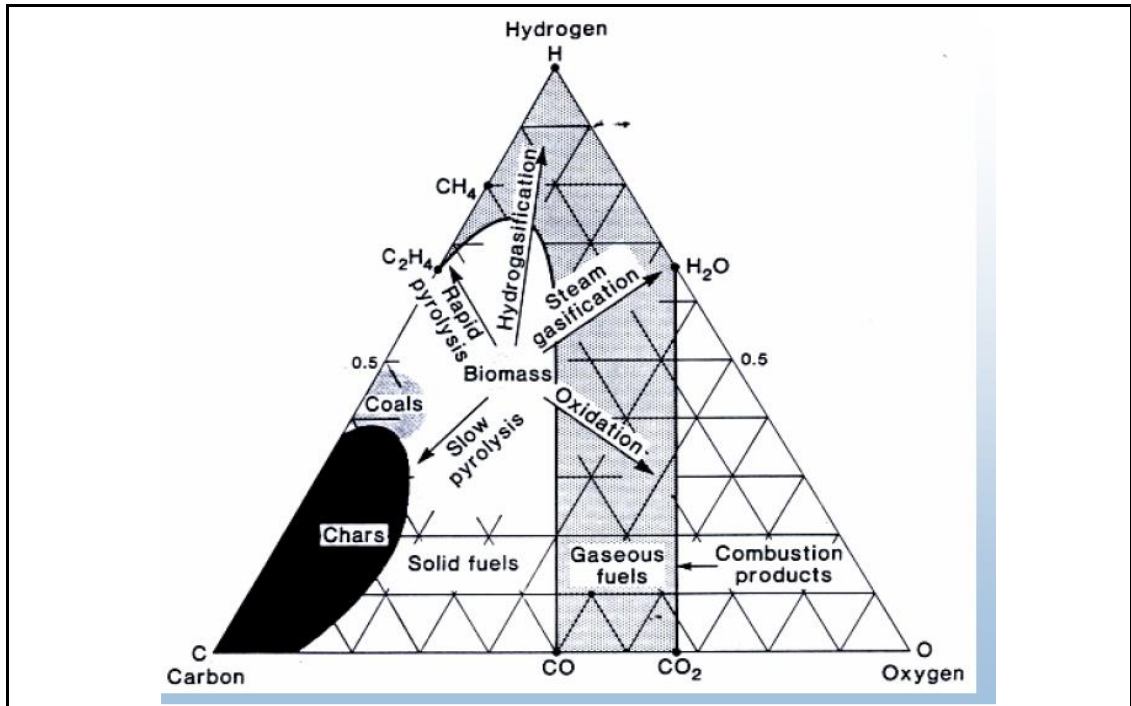


Figure 2.3: Phase diagram of solid thermochemical conversion (Bain, 2004)

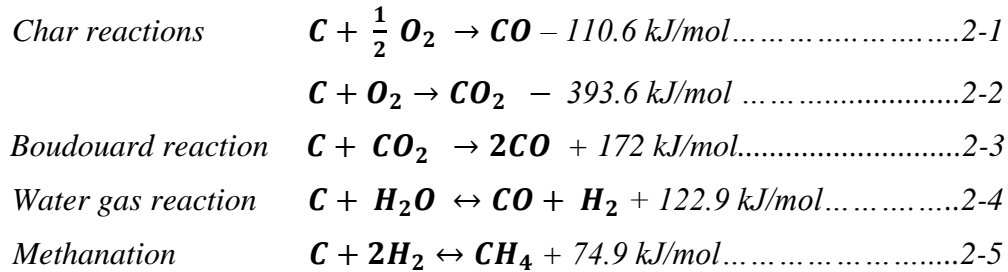
Table 2.2: Thermochemical conversion technologies (Wang & Yan, 2008)

Technology	Temperature	Residence time	Oxidant	Aim /Products
Slow pyrolysis	low (~ 400 °C)	very long	absent	charcoal
Fast pyrolysis	medium (~ 500 °C)	short	limited	bio oils, chemicals
Gasification	high (~800 °C)	long	limited	gas, chemicals
Combustion	High	long	sufficient/excess	heat

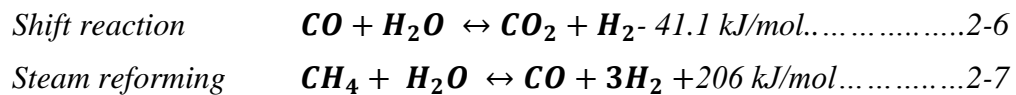
Thermochemical conversion of solid fuel is a complex chemical and physical process which can be summarized as follows:

- Vaporization: the early stage of heating being applied; the water content will vaporize.
- Devolatilization/pyrolysis: the devolatilization process begins when the biomass temperature reaches a critical level. The products are char and volatiles. The volatiles condense into a dense liquid (Natarajan *et al.*, 1998) while a small amount gasses escape.
- Secondary cracking tar: tar is a mixture of condensable hydrocarbons. The heat may crack the tar. The cracking causes some homogenous reactions in the gas phase and heterogeneous ones at surface of solid fuel or char particles

- Reactions/reduction/gasification: char as the residue after devolatilization will react with the gas species in heterogeneous reactions (Sharma, 2008; Souza-Santos, 2010; Mendiburu, Andres Z. *et al.*, 2014).



- The devolatilisation gas and cracking gas species will be also reacted with the oxidant and among other species as homogenous reactions. The heat generated is used for the release of volatiles and char ignition (Sharma, 2008; Souza-Santos, 2010; Mendiburu, Andres Z. *et al.*, 2014).



Dependent on the aim of conversion, pyrolysis process is set at the best conditions for achieving high devolatilization but low heterogeneous reactions, so the conversion efficiency of char generation or bio oil production is high. Because gasification aims to create combustible gasses (CO, CH₄, H₂, and amounts of hydrocarbons), the process is often conditioned for a high conversion of combustible gasses, including tar cracking. On other hand, the combustion (with a very rich oxidant/fuel mix) converts fuel preferably into only carbon dioxide and water vapour; the heat energy is the main intention. All oxidative processes above are controlled by the amounts of oxidant and heat.

The heat originates from the self-generation as to the product of chemical reaction of the fuel and/or addition of an external heat. The amount of oxidant applied is related to the stoichiometric amount of oxidation for the thermochemical conversion. This is often defined as stoichiometric air to fuel ratio (AFR) or stoichiometric fuel to air ratio (FAR) which is defined as the mass of air to fuel or mass of fuel to air for the stoichiometric proportion of complete combustion. In a common situation, the fuel to air equivalence ratio (ϕ) is often conveniently defined the ratio of actual FAR to the stoichiometric FAR. The advantage using equivalence

ratio rather than mass ratio is that the definition can easily determine the condition of the mixture. If the ϕ is less than 1, then it means there is more fuel than the oxidiser. On contrary, the ϕ more than 1 represents an excess oxidiser in the mixture (Souza-Santos, 2010; ANSYS_INC, 2013).

$$\phi = \frac{(fuel/air)_{actual}}{(fuel/air)_{stoichiometric}} \dots\dots\dots 2-8$$

For gasification process, the lean mixture is applied in contrast to rich mixture of combustion. In gasification, the ϕ is renamed as ER, equivalence ratio. The typical range of ER for dry biomass gasification is 0.25-0.33. Applying a higher value can lead to more gasification but lower the heating value of producer gas and liquid mass. In actual condition, the biomass has water content that has to be vaporized at the early stage. A heat energy is required to vaporize it. In an auto-thermal gasification, the heat is sourced from exothermic energy. Therefore, the oxidant requirement may be slightly higher than it used to dry the feed biomass.

The gaseous product from gasification is sometimes called syngas. This is, however, strictly speaking not correct. The definition of syngas is a pure mixture of equivalent molar of CO and H₂. The name of syngas came into a wide use in early twentieth century as the epimolar of high CO and H₂. It was used in catalytic synthesis of hydrocarbon fuels with steam (H₂O as by product) or partial oxidation. An appropriate name in the context of biomass pyrolysis and gasification is a producer gas, which is preferably (but interchangeably) often used with syngas.

Producer gas comprises of combustible gasses of CO, H₂ and CH₄ and a significant amount of the inert gas of CO₂ and nitrogen, a component from the air if air is used as an oxidant. The typical calorific value of the gas produced from biomass gasification using air as the oxidant is about 4-6 MJ/m³ with the carbon conversion efficiency about 50-70% (Reed & Das, 1988).

2.3. Design and performance of gasifier plant/reactor

The gasifier is a reactor for the gasification process. The type of gasifier is often classified by the design for flows of fuel and gas. The fixed bed has intimate contact of fuel particles and gasses, while the fluidised bed has less contact between fuel particles but between fuel and oxidiser. The entrained bed type has even lesser fuel particle contact, as the finer fuel particles are feed by atomiser conditioned for

high surface contact with oxidiser. Under these three categories, there are two sub-types both for fixed bed (downdraft and updraft) and fluidised bed (bubbling and circulating). This is summarized in the Table A.5 of Appendix A. Depending upon the source of heating, if the heating originates from external source, the reactor is categorised as allo-thermal, while if the heat is sourced from the partial combustion of the fuel, it is known as an auto-thermal reactor.

The fixed bed is the simplest type, suitable for small to medium scale capacity. The heat for a fixed bed gasifier is sourced from an auto-thermal arrangement which can be economical for small to medium scale capacity. The reactor uses a less external input energy and simpler design, minimising the investment and operational costs. The fuel is expected to have a longer residence time in this reactor, compared to the fluidised and entrained bed types.

In updraft type (Reed & Das, 1988), the fuel flows down through drying, pyrolysis, gasification and combustion, while the generated gas passes up through the interspace of the fuel. The gas can swap some tar, moisture and small particle during passing through the pyrolysis and drying zone. Consequently, the producer gas has high impurities.

Downdraft gasifier is a type of fixed bed gasifier in which the feed flows through the consecutive phases of drying, pyrolysis (devolatilization), combustion and gasification (reduction) (Reed & Das, 1988). In this type, both the feed and the oxidant flow downwards which allows all the pyrolytic products to pass through the hot combustion zone causing the thermal cracking of some tar into non-condensable tar and water. This system will produce a low tar content in the producer gas. There are two types of downdraft looking at its throat shape: the first is throated at the oxidant inlet and the second is un-throated (Figure 2.4). The throat creates more gas turbulence, increasing the temperature in combustion zone for thermally cracking the tar (Reed & Das, 1988).

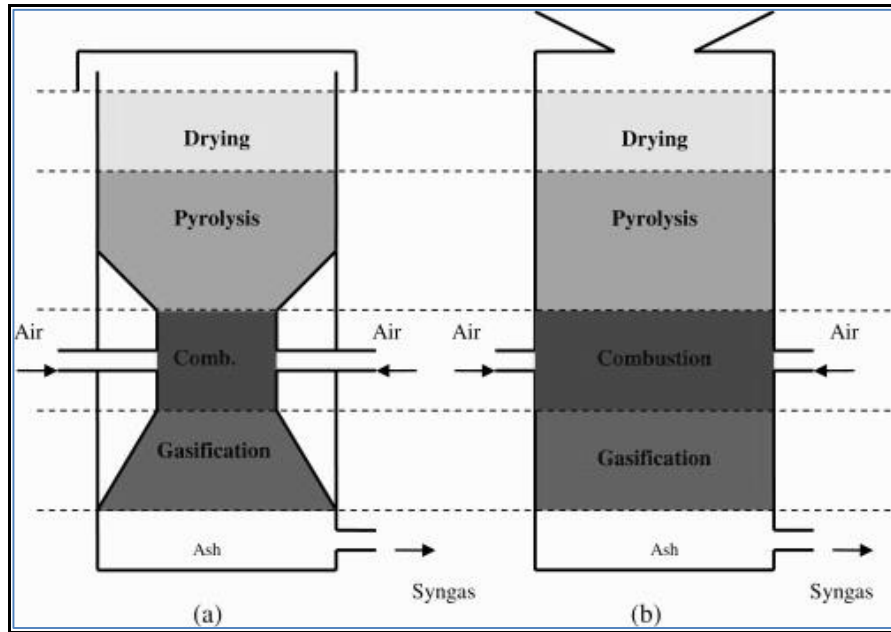


Figure 2.4: Downdraft gasifier types (a) throttled (b) un-throttled (Mendiburu, Andrés Z. *et al.*, 2014)

Studies on co-gasification were mostly conducted at the medium to big scales in fluidized bed and entrained bed reactors (Pan, Y.G. *et al.*, 2000; Pinto *et al.*, 2003; Xu, 2013; Howaniec & Smoliński, 2014). Only a few studies were conducted at small scale (Kumabe *et al.*, 2007) not counting the small laboratory scale.

In terms of fuel contact, the fixed bed allows more intimate contact of particles compared to the fluidised bed. The gasification in the fixed system also takes place at a slow process, allowing longer interaction of fuel particles. This may give more possibility of synergism occurrence. The function of high-grade carbon blended material in this co-gasification would be then to create more stable temperatures in the zones. Hence, the slow process will give more time for chars to react, thus producing more gasses rather than tars.

Nevertheless, other factors such as fuel composition and gasification operating conditions also interrelate to influence the complex process of gasification. Hence, optimisation of the working parameters specific to the design of the gasifier is required for delivering the optimum working parameters. The optimisation would deliver the result of the highest efficiency of fuel to producer gas energy conversion.

2.4. Single fuel non-woody biomass thermochemical conversion

Studies in the non-woody biomass gasification and combustion have been conducted by many researchers. Particularly for the gasification process, the

success/failure of gas production is often controlled by the air/fuel ratio. Technical problems or failures reported in gas production of non-woody biomass, as indicated earlier, were often due to low density of fuel, high ash or tar and also low energy content. The approach of effectively converting the non-woody into thermochemical energy has been addressed from the two sides: firstly, by improving or selecting the appropriate reactor design and secondly, by upgrading the feedstock quality.

From the side of converter design, feedstock can enter either the fluidisation or pressing (Table 2.3). Applying less pre-treatment e.g. only size reduction is suitable for fluidisation, pressurised or entrained flow and cyclone type. However, more complex design of equipment and external energy are often required to control the process of gasification. Samy (2013) could directly compress the raw cotton gin waste but using an auger and external heater for gasification. Other researchers applied specific fluidisation in response to the properties of the definite particles either using cyclone or fluidised gasifier (Gabra *et al.*, 2001; Mohammed *et al.*, 2011; Samy, 2013; Maglinao Jr *et al.*, 2015). It was found, however, that some feedstock faces considerable difficulties in the fluidisation. Because of the high mineral content of the non-woody biomass, the formation of low melting ash (of alkali silicates or carbonates as major component) can create problems in fluidised bed reactors. The formation of sticky glassy melt has caused bed particle agglomeration and this can lead to fluidisation failure and operational shutdown (Fryda *et al.*, 2008).

Table 2.3: Single non-woody biomass stock gasification and combustion

Materials	Type of converter	Reference
Sugarcane bagasse	Cyclone gasifier	Gabra <i>et al.</i> (2001)
Oil palm empty fruit bunch	Bubbling fluidized bed	Lahijani and Zainal (2011)
Sugar cane bagasse pellet, oil palm empty fruit bunch pellet, wood pellet	Downdraft gasifier	Erlich and Fransson (2011)
Cotton gin waste	Fluidized bed gasifier	Groves <i>et al.</i> (1979)
Cane bagasse pellet	Downdraft gasifier	Jordan and Akay (2012)
Oil palm empty fruit bunch	Bubbling fluidized bed	Lahijani and Zainal (2011)
Sugar cane bagasse	Fluidised bed gasifier	Sahoo and Ram (2015)
High tonnage sorghum, cotton gin trash, beef cattle manure	Fluidized bed gasifier	Maglinao Jr <i>et al.</i> (2015)
Raw cotton gin waste, torrefied cotton gin waste	Auger system gasifier	Samy (2013)

Materials	Type of converter	Reference
Switch grass pellets	Commercial furnaces: horizontal feed, dropdown feed, underfeed	Chandrasekaran <i>et al.</i> (2016)

For typical non-woody biomass raw feedstock which has a low density problem, a fixed bed gasifier is rarely directly used. A fixed bed gasifier generally requires the ability of the feedstock to flow continuously, passing smoothly each zone of drying, pyrolysis, combustion and gasification. Each zone is naturally conditioned by the required amount of oxidant to fuel ratio. The low flow ability of raw low-density feedstock may affect the space in the gasifier reactor to be occupied by air instead of the feedstock. This can create a fluctuation of air to fuel ratio, so the expected ratio of gasification reactions cannot be reached. Therefore, to be used in a fixed bed, a pre-treatment of densification is usually required.

Jordan and Akay (2012) studied the sugarcane bagasse pellet gasified in the downdraft type. The amount of tar was low due to tar cracking benefited from the downdraft type and pelleted the raw materials. Nevertheless, the types of tar from sugarcane bagasse were easy to condense even at low temperature of about 90°C. To reduce this effect, the granular CaO were mixed with the pellet for cracking the tar (Jordan & Akay, 2013).

The problems of non-woody due to its low density, high ash and tar problems in gasification and combustion can be resolved by upgrading the non-woody to become a good quality solid fuel feedstock. The densification can resolve the low-density problem. The densification can also reduce the ash build up during the gasification process. Furthermore, to improve the thermochemical conversion efficiency, the stock can be mixed with other substance, blended into the fuel for a co-conversion system.

2.5. Co-blended fuel and synergy in thermochemical conversion

Described previously, utilising the non-woody biomass waste frequently faces the problem associated with lower quality fuel. One of the recent ideas to upgrade the quality is by blending it with other types of fuel. The blending of two or more source components into a feedstock for the thermochemical conversion is known as co-conversion; be it co-pyrolysis, co-combustion or co-gasification.

Compared with charcoal/coal, biomass has the characteristics of having high concentration of volatiles, low carbon and low calorific value. These lead to a high tar and/or a high ash in the by-product of the thermochemical processes leading to a low conversion efficiency or even failure. One of the purposes of blending the biomass with charcoal/coal is to reduce this problem. By blending it with high carbon content, the heat from char induces tar cracking, reducing tar bridging problem and producing more combustible gasses. Another potential gain is the products addition as a result of catalytic activities which increase the conversion and produce more combustible gasses compared to individual material conversion. However, these fuel synergies in cracking the tar and catalysing the reactions are still not clear in details.

2.5.1. Synergistic effect in co-conversion

There are three groups of reported results related to researches on the synergistic effects of co-conversion. The first group found that there were no synergy shown by simply addition of the individual fuel conversion results. The second group revealed a negative synergy in which the results of the blend were even lower than of individual thermochemical conversion. The third group reported a synergistic effect shown by higher results in the co-conversion in contrast to the conversion of singular fuel.

2.5.1.1. Synergistic effect in co-gasification

Most of previous studies applied coal as the carbon source in the co-gasification fuel with the biomass (Table 2.4). Coal can generally be categorized into low-rank coal (lignite), medium rank (sub bituminous and bituminous coal) and high-rank coal (anthracite). The higher rank coal is typically higher in carbon content and calorific value; lower in volatile and reactivity.

Table 2.4: Biomass co-gasification

Materials	Type of gasifier	Reference
Pine chips mixed with black coal, low grade coal & sabero (refuse) coal	Fluidised bed (mixtures of air and steam as oxidant)	Pan, Y. G. <i>et al.</i> (2000)
Coal, pine and polyethylene waste	Fluidised bed type (air and steam as oxidant)	Pinto <i>et al.</i> (2003)
Olive bagasse & coal	Fluidised bed type	André <i>et al.</i> (2005)

Materials	Type of gasifier	Reference
Woody biomass (Japanese Cedar) & brown coal (Mulia coal)	Downdraft (air and steam as oxidant)	Kumabe <i>et al.</i> (2007)
- Forestry waste (pine pruning), agricultural waste (grape & olive pruning) - Industrial waste (sawdust & marc of grape) with coal-coke	Circulating flow gasifier	Lapuerta <i>et al.</i> (2008)
Silver birch wood & coal	Fixed bed and fluidised bed	Collot <i>et al.</i> (2009)
The pellet of mixtures lignite and <i>Eucalyptus nitens</i> wood	Fluidised bed types (bubbling fluidised bed and dual fluidised bed) with steam as oxidant	Xu (2013)
Japanese cedar, rice straw, seaweed with low rank coal	Downdraft gasifier (air and steam as oxidant)	Rizkiana <i>et al.</i> (2014)
Pine pellet and petroleum coke	Bubbling fluidised bed	Nemanova <i>et al.</i> (2014)

Fermoso *et al.* (2010) had co-gasified different rank of coals with the addition of biomass in a high-pressure reactor. It was reported that the higher heating value of the coal combined with higher reactivity of the biomass increased the production of free radicals such as hydrogen. However, another research reported that applying high-rank coal, though having a high energy content, its low reactivity tends to leave the carbon as char in the by-product, thus it could also lower the conversion efficiency (Nemanova *et al.*, 2014).

Pan, Y.G. *et al.* (2000) and Rizkiana *et al.* (2014), thus, promoted the use of low-rank coal such as lignite for biomass-coal co-gasification. It was found that this approach increases the efficiency of conversion, resulting in more significant results of methane and hydrogen in the producer gas composition. However, these gasses would significantly appear in the gas composition when using steam as the reactant. In the gasification using air as the oxidant, more oxidized gaseous carbon species (CO, CO₂) would still be generated than CH₄ and H₂.

It should be noted further, applying lower rank coal which has lower carbon content than the biomass itself would theoretically lower the total carbon of the co-

blended fuel compared to that of singular biomass; this could lead to low carbon conversion in the co-gasification. Thus, the medium rank coal such as sub bituminous type may be better in term of higher carbon content than the low rank coal and with its higher volatiles than high-rank coals. Overall, optimisation of the mixed ratio of the applied particular coal to the biomass species in the co-blended fuel would be the best method to achieve the highest conversion efficiency.

Biochar from woody biomass may then have similar properties as medium rank coal. It has relatively high carbon content and is more reactive than high rank coal. Applying biochar as the supplement source of carbon in biomass co-conversion may induce more carbon reactivity, resulting more carbon based gasses.

Another potential gasification effect of the blend of biomass with high graded carbon feedstock is the catalytic action of minerals available in both feedstocks. The catalytic potential is from alkali (K^+ , Na^+), alkaline earths (Ca^{2+} and Mg) and transition metals (Fe^{2+}). The metal catalyst (M) in form of oxides may increase the production of CO gas. The mechanism of the metal catalyst in converting the CO_2 into CO in gasification is described in the reactions below (Huang *et al.*, 2009):



The significance of catalytic effect may depend on the type of biomass and coal used. Compared to low-rank coal, mineral matters in high-rank coals have little catalytic activity during coal gasification (Tchapda & Pisupati, 2014). In high-rank coal, the calcium is in the form calcite, decreasing the catalytic activity. The K is also transformed into aluminosilicate glass. Thus, the natural mineral catalyst in co-gasification will be preferably resourced from the biomass.

Habibi (2013) found that some mineral catalysts can become inactive in reactions. This occurred when the mineral catalyst bound with silicate and/or aluminium. The potassium in switch grass, instead of becoming a catalyst, is bound to an aluminosilicate frame when the molar ratio of potassium to silicate was less than 1. The mineral properties of some example of wood biomass (oakwood) and non-woody biomass (cotton gin waste & oil palm empty fruit bunch) is presented in Table 2.5. The non-woody biomass may have higher mineral catalyst compared to a woody biomass (Lapuerta *et al.*, 2008).

Table 2.5: Mineral content in ashes of CGW, EFB, Oakwood and bituminous coal (%weight, dB)

Material	Composition (% weight of ash)								References
	SiO ₂	Al ₂ O ₃	P ₂ O ₅	Fe ₂ O ₃	CaO	MgO	K ₂ O	Na ₂ O	
Cotton gin waste	7.2	6.9	4.4	0.4	20.7	10.3	35.6	1.3	(www.westbioenergy.org, 2001)
Oil palm empty fruit bunch (EFB)	10.8	1.2	1.8	3.6	12.5	8.8	53.7	1.5	(Mohammed <i>et al.</i> , 2011)
Oakwood	49.0	9.5	1.8	8.5	17.5	1.1	9.5	0.5	(Mohammed <i>et al.</i> , 2011)
Bituminous coal	59.7	19.8	0.2	8.3	2.1	1.8	2.1	0.8	(Mohammed <i>et al.</i> , 2011)

2.5.1.2. Synergistic effect in co-combustion

The co-firing of biomass and coal blended is also studied for their potential of synergistic effect. Initially, the biomass addition to coal was to lessen the emission of the coal firing, improving the environmental impact. Then, it was found that the biomass could also provide a catalytic effect in the coal co-firing (Ruhul Kabir & Kumar, 2012; Duan *et al.*, 2015). The synergistic possibilities of biomass-coal co-combustion were then investigated (Gil *et al.*, 2010; Muthuraman *et al.*, 2010; Sahu *et al.*, 2010; Idris *et al.*, 2012; Vhathvarothai *et al.*, 2014b). Similar to the co-gasification, they reported either synergy or non-synergy occurrences in co-combustion as well.

The woody biochar and fresh wood as the additive to lignite coal co-combustion have been investigated. The mixing with biochar was reported as being higher in reactivity than the fresh wood addition (Kastanaki & Vamvuka, 2006). The lower ash in biochar than that in the fresh wood resulted in lower residual mass (ash) in the product of co-combustion. It can be further predicted that using biochar as the additive to biomass may have more possibility of synergy than the mix with low or high rank coal. However, the research related to the co-conversion of biomass-biochar blends is still limited.

2.5.1.3. Synergistic effect in co-pyrolysis

The co-pyrolysis of coal with biomass was also studied in relation to the fuel combustion and gasification. As known, the combustion or gasification is preceded by the pyrolysis. When some of the particles reaches the devolatilization stage, the volatiles are liberated. In combustion, the volatiles are oxidised converted into gasses to be burnt out. In gasification, the oxidation is incomplete to provide the matters for the following homogenous and/or heterogeneous reactions to produce combustible gasses. Within this partial oxidation, volatiles conversions may impact to liquid phase (tars) formation as well. The excessive tar production could create a difficulty in the next process of cracking into gasses.

Then, the role of coal to biomass co-pyrolysis is to provide a significant heat to crack the tar. On the other hand, the amount of mineral from the biomass can also act as catalysts to further improve the homogenous/heterogeneous reactions to produce more gasses. The latter case could occur not in the pyrolysis stage, but later in the reduction stage. A study was reported that a synergistic was not found in the pyrolysis stage, but the char resulted from the co-pyrolysis which has optimum amount of catalyst could result in synergy later in the reduction process (Zhu *et al.*, 2008).

It is also known, that the pyrolysis is being used to convert the materials into chemicals. One of them is converting the solid hydrocarbons into bio-oil. The fast pyrolysis is being used to produce the bio oil. This requires high degree of hydrocarbons conversion into liquids which has characteristic of light viscosity and density. This process often requires a catalyst to increase the conversion. Co-pyrolysis of biomass-coal may thus be an attractive method to replace the commercial catalyst.

The results related to the synergy in biomass-co-pyrolysis were also unclear. Some of the researchers found no synergistic effect in co-pyrolysis of biomass-coal (Zhu *et al.*, 2008; Collot *et al.*, 2009; Masnadi *et al.*, 2014). Although Collot *et al.* (2009) did not find the synergy in a fluidized reactor, they however found a slight (not significant) increase of tar cracking in a fixed bed one. On contrary, other researchers (Jones *et al.*, 2005; Onay *et al.*, 2007; Wang *et al.*, 2015) found synergistic effect which occurred in co-pyrolysis resulting higher conversion than addition of individual pyrolysis. Onay *et al.* (2007) conducted co-pyrolysis using two methods of investigation, thermo-gravimetric oven and fixed bed reactor. They found significant synergy only in the fixed bed reactor. Apparently, the occurrence of synergistic effect

requires not only enough temperature but also enough fuel contacts and residence time for interaction, as in the case of fixed bed reactor above.

2.5.2. *Factors influencing synergistic effect in co-conversion*

The inconclusive results in synergistic occurrences might be because of the factors such as the design of reactors, temperature profiles, appropriate mixture and the amount load of sample used. Nonetheless, most of the researchers who found rather inconclusive results on synergy in co-conversion agreed that the co-conversion of biomass and coal may reduce the tar problem in which the coal had stabilized the conversion temperature. Overall, the thermochemical conversion is a complex process and can be influenced by the factors such as:

- Effect of fuel composition
- Effect of reaction temperatures
- Effect of reactants.

These factors which influence the co-conversion performance are reviewed in the following paragraphs.

2.5.2.1. *Effect of fuel composition*

In the co-conversion, blending the biomass and charcoal is intended for reducing the respective weaknesses of each fuel. Biomass, in general, has high hydrogen (H) content. It can compensate the low H content of charcoal. On other hand, biomass which has high volatile and low reaction temperature will release more tar. Blending with charcoal affects to higher reaction temperature than biomass alone reaction temperature. While reaching the temperature of charcoal fast reduction, the heat is transferred to crack the biomass tar (Tchapda & Pisupati, 2014).

As charcoal has a higher carbon content, the carbon based gaseous products (CO₂, CO, CH₄ and other light hydrocarbons) should be higher in charcoal conversion compared to biomass conversion (Reed & Das, 1988). However, researches have shown another evidence that increasing the biomass could also increase the carbon based gasses (Pan, Y.G. *et al.*, 2000; Kumabe *et al.*, 2007; Lapuerta, M. *et al.*, 2008). Kumabe *et al.* (2007) reported that the CO₂ and methane gas production had increased because of the effect of biomass mixture in a coal-biomass co-gasification. Apparently, the hydrogen atoms in methane were delivered from the biomass. Some other factors influenced the increase of carbon dioxide with increasing biomass to coal ratio. Kumabe *et al.* (2007) also applied higher oxidant level and lower temperature

than commonly applied in coal gasification. This resulted in more biomass reactivity producing more carbon-based gaseous compounds compared to coal gasification alone.

In co-gasification, examining the only biomass composition in the mixture cannot certainly affect to the hydrogen production. Many studies report the hydrogen generation was reduced as the biomass content increased (Pan, Y.G. *et al.*, 2000; Kumabe *et al.*, 2007; Song *et al.*, 2013). This is perhaps due to lower temperatures of reactions as the addition of biomass, while the hydrogen is usually produced at high temperature. High content of volatiles in biomass would reduce the reactions temperature leading to the reduction of hydrogen. Furthermore, that biomass blends with high-rank coals (high carbon content) lowered the temperature could induce more methanation reactions, converting the available H₂ into methane gasses (Emami-Taba *et al.*, 2013). An opposite result of the hydrogen was increased as to the addition of biomass to coal co-gasification. The co-gasification was, however, done in a combination of slight higher temperature, applying adequate pressure and lower oxygen amount than the requirement of biomass alone gasification (Rizkiana *et al.*, 2014). This showed that the effect of other operational condition can also significantly influence the results besides the factor of fuel composition alone.

The gas yield is defined as the volume of produced combustible gaseous per weight of the dry and ash free feedstock. Gas yield in co-gasification biomass-coal was reported to have increased with an increase of biomass content (Sjöström *et al.*, 1999; Pinto *et al.*, 2003; Kumabe *et al.*, 2007; Fermoso *et al.*, 2010). The authors also reported that due to high oxygen content in biomass and a high carbon content in coal, the CO production was increased. The increase of methane was also highlighted due to the mix of coal with the biomass which has high volatiles.

2.5.2.2. *Effect of temperature*

In the thermochemical conversion, heat is applied to evaporate water and volatiles. It is also useful for depolymerisation and breaking the chemicals bonds in the solid material decomposition. At first, the water is evaporated; then the polymers are liquefied and volatilised. Next, the homogeneous and heterogeneous reactions occur. Every feedstock has its typical mass of solid conversion to the respective applied temperatures. In general, more solids within the biomass will start to

decompose at a much lower temperature than the decomposition temperature of bulk of coal. This means that the reactivity of biomass is higher than coal (Figure 2.5).

In general, raising temperature will increase the carbon conversion, thus increasing the total gas and lower the function of tar. In steam gasification, increasing temperature will increase the hydrogen and decrease the CO₂ (Howaniec & Smoliński, 2014). Increasing temperature will also reduce methane (Pinto *et al.*, 2003).

A catalytic co-gasification, nevertheless, requires an optimum pyrolysis temperature for increasing the possibility of catalytic reactions. Too high temperature would evaporate the catalyst mineral (Habibi, 2013; Masnadi *et al.*, 2014), while low temperature would not provide the mineral to be catalysing the reactions. Zhu *et al.* (2008) reported that the pyrolysis temperature of 750°C was the best compared to 650°C and 850°C for allowing the potassium to be effectively catalysing the reduction reactions in co-gasification.

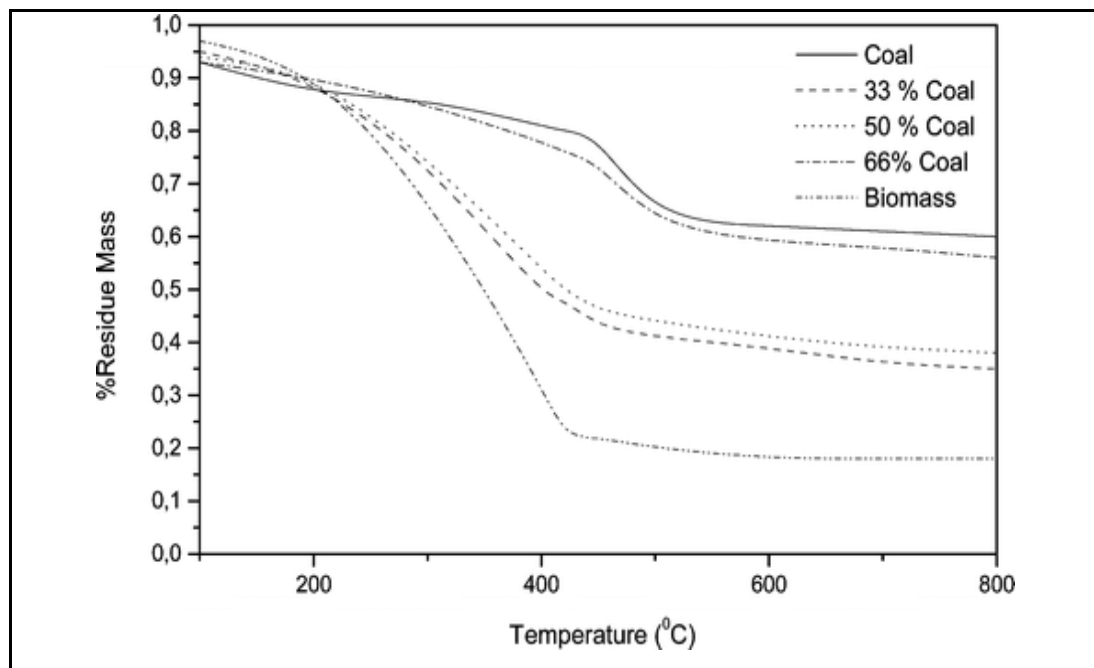


Figure 2.5: Residual mass versus temperature for biomass pyrolysis and coal/biomass co-pyrolysis (Onay *et al.*, 2007)

2.5.2.3. Effect of reactants

Gasification applies oxidants for partial oxidation that is supplying less oxygen than the amount of stoichiometric requirement for the complete combustion. The gasifying agent can be air, steam, oxygen, hydrogen, CO₂. Air is mainly used in the production of gas for power generation or application in a combustion engine, as it is

the simplest method to supply the oxidant. However, it contains nitrogen as an inert gas that will be left in the mixture with all the product gasses. This will dilute the combustible gasses, resulting in a low heating value of the producer gas (Pinto *et al.*, 2003).

In an auto-thermal gasification, reactant to fuel ratio is a key responsible factor controlling the process temperature. Increasing the reactant to the fuel ratio will increase the process temperature. Thus, it will result in more tar reduction and reactivity. In general, applying oxygen or air as reactant will increase temperature and generate more water vapour and CO₂ that in turn lower the heating value (Pinto *et al.*, 2003; Lapuerta, M. *et al.*, 2008). Using steam will increase H₂ and hence heating value. However, energy for steam generation should be considered in the energy production. CO₂ is a promising gasifying agent as it is also produced as the gasification result. In the presence of a catalyst, it will react with char, tar and CH₄ resulting in more H₂ and CO (Kumabe *et al.*, 2007).

Overall, the discussion above highlights that there are effects of fuel composition, temperature, type of reactant and their interaction factors in the conversion system to the gas products and the possibility of synergism in the co-blended fuel. Thermochemical kinetic analyses is therefore necessary in the study. This can be studied by a laboratory scale experiment using the method of either mass decomposition (thermogravimetry analyses, TGA) or converted gas analyses. These studies do not consider the effect of converter design (e.g. household stove, gasifier pilot plant scale, industrial combustor plant) which in some situations can significantly influence the conversion efficiency. Numerical calculations through modelling can also predict the performance of a converter. The following section reviews the modelling activities in particular for gasification.

2.6. Modelling & simulation in the gasification

As described previously, thermochemical conversion of the co-blended fuel would depend on several interacting factors, such as fuel composition, operating condition and the converter design. The laboratory study of the thermo-kinetic behaviour of a fuel is often used to determine the kinetic changes in the material phase. This activity neglects the converter design. For the pyrolysis or combustion, the laboratory kinetic data may be close to the plant application. However, for the more complex process of the gasification, the equipment design also significantly influence

the results. The result of laboratory study can be different with the up-scale situation. On other hand, the plant experiments with several trials and errors could be a hassle. To overcome this problems, a computer model can be initially employed to act as a virtual plant for the prediction of the effect of parameter changes on the performance.

A gasification model can be used to study the process during gasification, evaluate the influence of input parameters and predict the gasification performances. As gasification is a complex process, modelling is also often used with some simplifications. Within the wide properties of the biomass, modelling of biomass gasification is still an emerging field in contrast to coal gasification (Wang & Yan, 2008).

Modelling of biomass gasification has been undertaken by a number of researchers. In general, the approach of gasification modelling can be categorised into the thermodynamic equilibrium, kinetics and computational fluid dynamic models. The general characteristics of these three types of model are summarized in Table 2.6.

Table 2.6: Modelling in gasification

	Equilibrium	Kinetic	Computational fluid dynamics
Main goal	Predict product gas compositions at an infinite period of time	Predict gas yield and composition at a finite time and /or a finite volume in a flowing medium	Predict distribution of temperatures, concentration and other parameters within the reactor
Method	Stoichiometric reactions using Gibbs free energy calculations	Kinetic reactions (char reaction rate) and hydrodynamics of reactors. Char reaction rate applies either: shrinking core model, random pore model or volumetric reaction rates. The dynamic reactor applies either : 0 dimension (Stirred tank), one dimension	Equations of mass, momentum, energy and species of the known dynamic conditions of reactors

	Equilibrium	Kinetic	Computational fluid dynamics
		(plug flow), 2 dimensions or 3D	
Accuracy	Close at prediction performance of high gasification temperatures (~ 750-950°C), particularly for downdraft gasifier working close to equilibrium condition	Accurate and more detailed results for a particular time of reactions and at lower process temperature. Able to predict tar result	Accurate for temperature profile and composition inside the reactors
Limitations	Reactor design not considered. Less accurate for design of reactor working at non- equilibrium stage (e.g. fluidised bed). Cannot predict tar result	Computationally intensive, need more detailed analysis; not enough detailed data, divergent results	The accuracy depends upon the input data of the dynamic parameters of reactor.
References	(Zainal <i>et al.</i> , 2001; Babu & Seth, 2006; Valero & Usón, 2006; Jarunthammachote & Dutta, 2007; Antonopoulos <i>et al.</i> , 2012; Barman <i>et al.</i> , 2012)	(Blasi, 2000; Kaushal <i>et al.</i> , 2010; Xu <i>et al.</i> , 2011; Masmoudi <i>et al.</i> , 2014)	(Gerun <i>et al.</i> , 2008; Murgia <i>et al.</i> , 2012; Xie <i>et al.</i> , 2012; Patel <i>et al.</i> , 2013; Wu <i>et al.</i> , 2013)

2.6.1. Equilibrium model

Thermodynamic equilibrium modelling predicts the gas composition at the equilibrium condition. It more considers the final composition of the gasses. There are two general approaches: stoichiometric and non-stoichiometric. Stoichiometric approach defines chemical reactions and the products using equilibrium constants. Some reactions which are considered unimportant are often omitted for the simplification of calculation. The omissions can sometimes lead to inaccurate results. Non-stoichiometric approach is based on minimisation Gibbs free energy without specifying the feed reactions. The products which were omitted at stoichiometric method may appear here.

Thermodynamic equilibrium predicts the composition of the products in the theoretical value prediction showing by the mole ratios of the defined gas composition. As the calculation is independent of the reactor design, thermodynamic equilibrium model may be more suitable for the prediction of a feedstock gasification performance from the influence of important fuel parameters such as water content, fuel composition and fuel/air ratio. The studies of modelling the gasification using equilibrium model are summarised in Table A.6 of Appendix A.

Thermodynamic equilibrium estimates the gas composition with a rough composition result. Equilibrium models often lead to a disagreement with the experimental results, particularly in respect to hydrogen and methane. The hydrogen is usually lower, while methane is higher than predicted. Nonetheless, some efforts have been made to improve the model, in which it includes the residual chars, tar, equivalence ash in the global gasification reaction and a corrected value for the model (Babu & Seth, 2006; Jarungthammachote & Dutta, 2007; Barman *et al.*, 2012; Simone *et al.*, 2013).

The equilibrium model is able to accurately predict the gas composition of the downdraft gasifier compared to that of the fluidised one. This is because that the gasification temperature is higher in the downdraft type which the combustion zone is in between the pyrolysis and reduction zone. Furthermore, that the fuels in the downdraft type have longer residence time than the fluidised one would lead to the closer condition to the equilibrium state (Baruah & Baruah, 2014).

The equilibrium model has been used for a validation of co-gasification experimental result. Kumabe *et al.* (2007) compared the calculation result of shift gas reaction to their experimental data of biomass-coal co-gasification. In their calculation, the value of theoretical equilibrium analyses was in close agreement to the experimental data of mixed fuel gasification, while the addition of their single fuel gasification experimental data was far below this equilibrium result. They determined that the synergy occurred in the mixture fuel as it could bring the results close to the ideal condition of the gasification reactions.

2.6.2. Kinetic model

Unlike equilibrium model which predicts yields at an infinite time, the kinetic model predicts yields at a finite time or a finite volume (Baruah & Baruah, 2014). It can predict the profiles inside the reactors for a given operating conditions and gasifier

configuration. This model provides more accurate predictions than that of equilibrium results. However, the accuracy is specific to the operation parameters. It needs more empirical data and is also computationally intensive. Simplification of the parameters often results in divergence.

The kinetic model describes the rate of char conversion during gasification using kinetic rate expressions. The expression can be based on either shrinking core model, volumetric model or random pore model (Zhang *et al.*, 2010). The shrinking core considers the surface reaction of solid with oxidant so the structure of char will be changed by the time of reaction. While the volumetric model does not consider the surface structure change, both inside and outside volume will actively react with an oxidant. The random pore model assumes some cylinder pores in a single char structure. The pores will grow and merge during the time of reaction. For the dynamic design of gasifier, parameters are added to the kinetic models. These are zero dimensional (stirred tank), one dimensional (plug flow), two and three dimensional (Baruah & Baruah, 2014). Literature applying kinetic models for the gasification is summarized in Table A.7 of Appendix A.

The kinetic model has been used for several types of gasification. Some models include the dynamic phase change of particles within a time. The inclusion of dynamics aim to find the profiles of reactor temperatures and gas compositions at a specific time for a particular design reactor (Blasi, 2000; Kaushal *et al.*, 2010; Masmoudi *et al.*, 2014). The progress changes of gas composition is described by modelling the char reactions in which empirical data of kinetics are required for the accuracy of the model (Zhang *et al.*, 2010; Xu *et al.*, 2011). These changes in gas composition to the time of reactions could not be described by equilibrium models. Nevertheless, applying only the char reaction kinetics often results in invalid predictions. Moreover, calculations are complex and time-consuming. It also does not consider some important factors of reactor design (e.g. the influence of turbulence as to effect of wall reactor design). These factors could significantly influence the gasification performance. In a CFD model, the respective advantages of gasifier design can be incorporated together with either equilibrium and/or kinetic model.

2.6.3. *Computational fluid dynamics*

The latest development is a computational fluid dynamic(CFD) model. Using a complex computation, it is available already as a commercial software. The CFD

model applies finite mass/volume transport phenomena, mass energy balance and chemical reactions and the mass of phase changes. This model embeds mass, momentum, energy equations in the kinetic model for a known reactor design in which the finite mass/volume is transported within a meshes structure. It also incorporates turbulence which is not included in kinetic models.

The CFD simulations can predict the temperatures profile, gas compositions across the zones and the flow pattern of solid and fluid particles inside the reactor. These analyses are used to examine the quality and the quantity of the gasification process for specific input parameters in a gasifier. Analyses of improvements, modification or optimisation of performance for a particular gasification process can also be conducted. This model can act as a virtual laboratory, serving to analyse the situation in a real plant by simulation. Available commercial software such as ANSYS FLUENT, CFX, PHOENICS etc provides templates and tabs for easier modelling and simulating the input parameters. Table A.8 of Appendix A lists the various models already developed using CFD method.

CFD is successful to model coal or char gasification. It still faces some challenges in modelling the biomass gasification due to complex composition and structure of biomass (Wang & Yan, 2008). Modelling of tar prediction and reduction is the most challenging task for the CFD approach. Some researchers try to develop it using the multiphase model which can simulate the phase changes in each stage (drying, pyrolysis, combustion and gasification). Similar to the kinetic method, the accuracy will also depend upon the empirical data for required inputs. Overall, the more complicated of the model, the more time consuming for solving the equations. An efficient model should consider some simplification in the calculations, recognising the purpose of the modelling activity.

2.7. Summary of the literature review

The cotton industry is one of Australia's major agricultural sector. One hectare of Australian cotton farm can produce approximately 1.6 tonne of lint, 2.5 tonne of cotton seed, 2 tonne of stalk, and 0.4 tonne of cotton gin waste (CGW). The solid waste (CGW) is abundant and readily available in the gin. As a non-woody biomass, CGW has a lower carbon, high ash and lower density. The current utilisation is often by converting the CGW into compost. Due to the pathogen contamination concern in

the compost product, this study proposes to study the alternative approach of CGW gasification into a high quality of solid fuel.

Upgrading the non-woody material into a good quality fuel can incorporate one or a combination of several processes including size reduction, drying, blending and/or densification. The densification of CGW in the form of pellet has been studied by several researchers (Holt *et al.*, 2006). It has been found that densification does not only increase the density but also improve the efficiency of the thermochemical conversion process. Together with pelleting, this study also proposed blending the non-woody with high carbon content materials while pelleting to form a more uniform structure. The blend is expected to significantly increase the physical quality and element properties. The blend can also potentially create a synergy between fuel components to increase the conversion efficiency.

The available literature mostly reported the biomass and coal blending. These studies, however, did not report clear synergistic reactions between the fuels. Having higher reactivity than coal, the biochar blended CGW can potentially achieve higher synergy compared to that of the coal blended CGW. To date, the studies of biomass and biochar co-conversion are limited. This can be further studied by a laboratory scale experiment using a method of either mass decomposition (thermogravimetric analyses, TGA) or converted gas analyses.

Nevertheless, the synergy is not only influenced by the type of the blended fuels, but also other interrelated factors such as fuel compositions, reaction temperatures and the type of oxidant as well as fuel particle contact. The downdraft gasifier may provide a higher possibility in synergistic effect as it has longer residence time and hence higher probability of fuel particle contact than the fluidised type.

Different with pyrolysis and combustion, the gasification performance is also significantly influenced by the reactor design and operating conditions. Computational fluid dynamic model can incorporate these factors. The model can thus act as a virtual laboratory to simulate the fuel properties, operational conditions and the reactor design.

CHAPTER 3: Development of Cotton Gin Waste Fuel Pellets - Upgrading the Physical and Elemental Properties

Abstract

Owing to low density and energy content, the raw cotton gin waste (CGW) was upgraded into five types of CGW fuel pellets, containing of 0 to 20% coconut shell char in the pellets. The biochar blends aimed to improve the calorific value and reduce the ash content. Treatments prior to the densification consisted of homogenising the size, adding the binder of 4% gelatinised cassava starch and modifying the CGW bonds. These pre-treatments were based on the previous COBY system developed by USDA-ARS with some modifications. To soften the lignocellulose bonds, the pre-treatment utilised a natural fermentation of the mixture CGW and binder in an open condition. Pelleting was achieved using a commercial plate die-roller type pellet mill with the optimum barrel temperatures at 60-80°C. The densification resulted in that raw CGW bulk density was increased from 112 kg/m³ to approximately 600 kg/m³ in pellet form. The developed pellets had sizes of 32-40 mm in length, 7.5-76 mm diameter and 1.8-2.4 grams of weight the individual pellet. The statistical analyses of sample mean comparisons showed that biochar incorporation into the CGW pellets significantly increased the mean size and the hardness of pellets. The biochar blends could also diminish the rancid smell of CGW in pellets.

Keywords: non-woody, pellet fuel, agricultural waste, cotton gin waste, biochar

3.1. Introduction

Cotton gin waste (CGW) has low quality of properties as a solid fuel. The CGW, a typical herbaceous non-woody biomass, is bulky and has a high ash content. It was reported that the high ash could cause ash slagging and sintering during the combustion or gasification. The high residual ash could block the equipment such as the grate, and pipes etc. The bulkiness of the material could also cause difficulty in controlling the pre-conditions for the occurrences of some useful thermochemical reactions. This could lead to a lower conversion efficiency or even a failure to convert the biomass into hydrocarbon or combustible gasses. Particularly, in the thermochemical process such as pyrolysis and gasification, oxidant to fuel ratio could critically influence the success of these processes (Erlich & Fransson, 2011; Brar *et al.*, 2012; Tchapda & Pisupati, 2014).

Densification is often necessary as a pre-treatment to increase the conversion efficiency. This was applied for crop straw and stalks (Holt *et al.*, 2006; Sultana *et al.*,

2010; Liu *et al.*, 2014; Nunes *et al.*, 2014). It was found that densification could reduce the sintering in the combustor or gasifier as the denser fuel could reduce the rapid and unstable combustion (Erlich & Fransson, 2011; Brar *et al.*, 2012; Tchapda & Pisupati, 2014).

In this research, densification was achieved by pelleting the CGW. The USDA-ARS has studied the CGW pelleting and patented the method under the name of COBY system (Holt *et al.*, 2006). This study modified the COBY system. In addition, besides pelleting the cotton gin waste alone, the CGW was also blended with different amounts of charcoal. This was to improve the solid fuel quality as well as to assess whether blending can improve the physical properties and the efficiency of the thermal conversion. It is further speculated that blending the CGW with carbon could result in a synergistic effect of the co-conversion. This would be investigated in the next chapters.

The carbon-rich component of blended material can be in form of biochar or coal. At the moment, most studies applied coal as the blending materials due to low cost and wide availability in the market. However, the biochar application may be more effective due to a combination of environmental and economic aspects, particularly if the biochar is obtained from pyrolysis or gasification char of woody biomass. This study applied biochar as the blending material for the CGW pellets.

This chapter specifically discusses the development of CGW as solid fuel by pelleting both the (pure) CGW and also the biochar blended CGW. The blending with biochar aimed to upgrade the CGW to a good quality solid fuel on the basis of its physical and elemental properties. This chapter is divided into three sections: first it looks at the properties of raw material. This is then followed by the discussions of methods for the pellet fuel production. Finally, the fuel properties of developed pellets are investigated.

3.2. Development of CGW pellets

3.2.1. Properties of raw materials

The cotton gin waste used in this research was collected from a local ginning mill (Namoi Cotton gin in Goondiwindi, Queensland). The cotton gin waste is a heterogeneous material and its composition can vary widely in terms of density and appearance (Figure 3.1). As shown in Table 3.1, it is composed of pods, seed, fibre,

dirt (leafy and stem fragments) and fine dust. An orientation test to separate those materials was undertaken in this project. The initial separation was carried out using rotary sieve shaker to separate seeds, dirt and fine dust. Because the pods and fibre were sometimes entangled with each other, a manual separation of these components from the sample was undertaken. The respective weights of all those materials in cotton gin waste samples are shown in Table 3.1.



Figure 3.1: Cotton gin waste sample

Table 3.1: Physical composition of cotton gin waste

No	Component	Typical percentage (% weight)	Typical appearance
1	Fibre	45%	
2	Pods	26%	
3	Seeds	3%	
4	Stems	4%	

No	Component	Typical percentage (% weight)	Typical appearance
5	Coarse dust (0.6-4.75 mm)	12%	
6	Fine dust (< 0.6 mm)	10%	

3.2.2. Materials and pelleting equipment

The proximate and ultimate analyses of the cotton gin waste and the blending material of biochar are shown in Table 3.2. It can be seen that CGW has a significantly higher volatile content in comparison with the coconut shell char which has a high fixed carbon. The cotton gin waste is also very bulky with a bulk density of 112 kg/m³. The coconut shell char was obtained from a Queensland commercial re-seller. The char sample was then analysed with regards to its proximate and ultimate composition as shown in Table 3.2

Table 3.2: Proximate (ASTM D3173, D3174, D3175) and ultimate analysis (ASTM D5373) of raw materials of mixture fuels

No	Analyses	Cotton gin waste	Coconut shell biochar**
1	<i>Proximate (% weight, as received)</i> - Moisture content - Volatile - Fixed carbon* - Ash	8.3 67.5 12.2 12.0	7.4 7.3 81.3 3.9
2	<i>Ultimate (% weight, daf)</i> - Carbon - Hydrogen - Nitrogen - Sulphur - Oxygen*	43.5 7.9 1.5 0.2 46.8	83.9 0.9 0.5 0.1 15.7
3	<i>Typical bulk density (kg/m³)</i>	112	496

* Based on the calculated difference of weight percentage to the sum of other elements

** Iodine number: 500

A flat-die roller type pellet mill was used for developing CGW pellets (Fig. 3.2). The manufacturer specification states that the pellet mill has the capacity of producing 100 kg/hour of wood pellet. In this study, the equipment used for homogenising the CGW was a table top, high speed mixer (Nutri Bullet®, 900 watts).

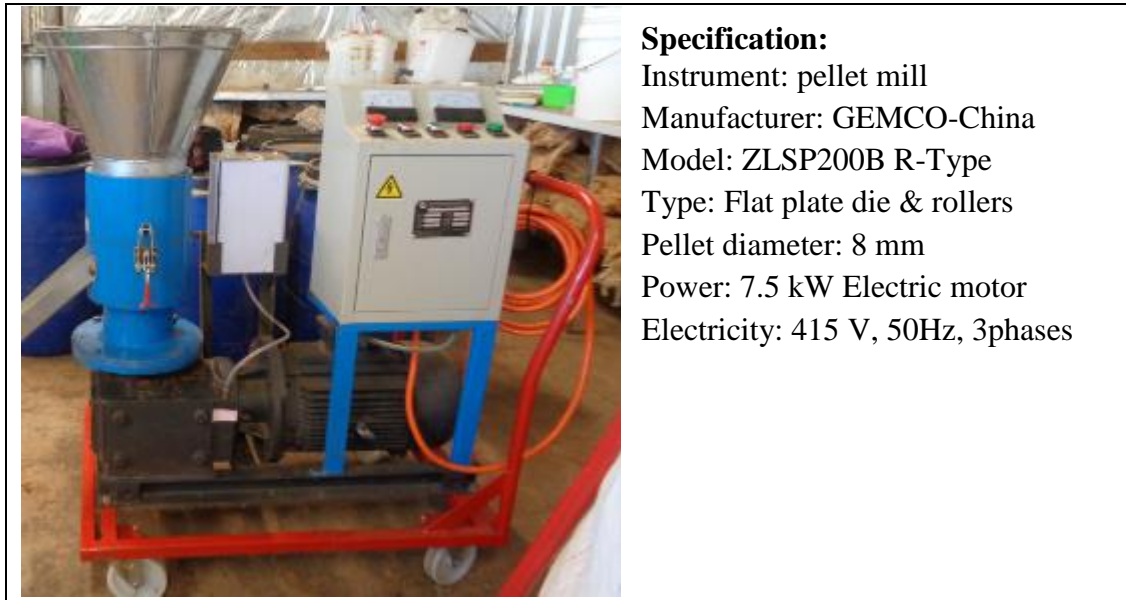


Figure 3.2: Pellet mill

3.2.3. Pre-treatment

This research applied the CGW as it is state, without any separation. This aspect needs to be stressed, as another system (COBY system) developed in the USA applied CGW without notes and other fine components (Holt *et al.*, 2006; Holt, 2014). The processing methods of the raw CGW in this research were size reduction and homogenisation, blending with biochar and or mixing with a binder (gelatinised starch) and withering for at least 3 days before pelleting and drying (Figure 3.3).

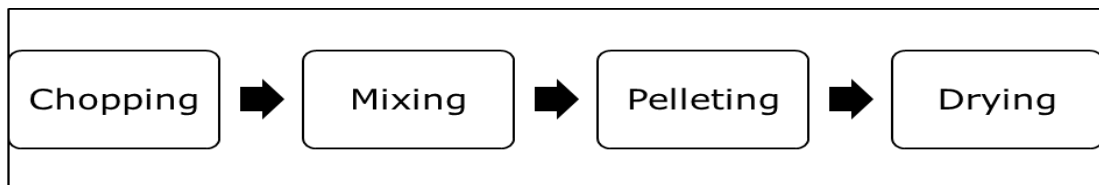


Figure 3.3: Pellet Production Process

The CGW waste was first chopped to reduce the size and homogenise the feedstock. Composing of heterogeneous materials with different sizes (Table 3.1), the raw CGW is difficult to be compacted. Size reduction of the raw CGW was undertaken through chopping (Fig 3.4). This slightly increased the density of the raw CGW from

112 kg/m³ to 148 kg/m³. In this study, the equipment used for homogenising the CGW was a table top, high speed mixer (Trade mark: Nutri Bullet, 900 watts)

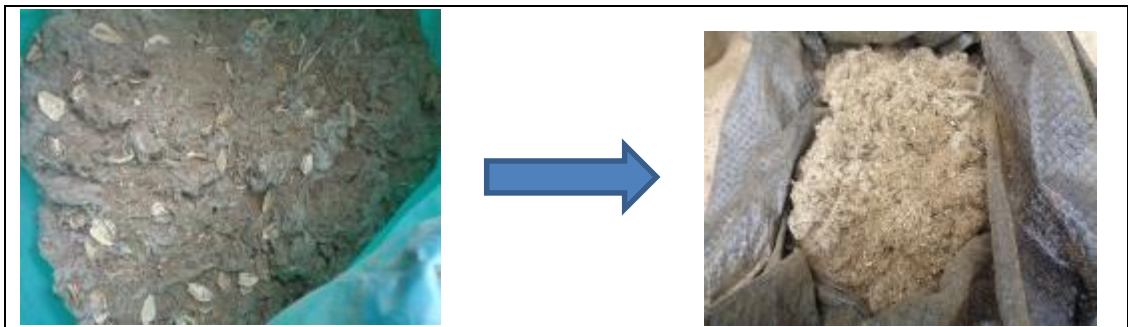


Figure 3.4: Cotton gin waste before and after size reduction

The pelleting process used a flat die-rollers type of pellet mill produced by Gemco, China (Figure 3.2). The treatments of pellets were respectively 100% CGW, and 5%, 10%, 15% and 20% weight of blended charcoal with CGW. The binder additive used was 4% cassava gelatinised starch (Fig 3.5), which was mixed at least 3 days before the pelleting time.



Figure 3.5: Materials (chopped CGW, gelatinised cassava starch, biochar)

As each non-woody biomass has its own particular lignocellulosic composition and bonding structure, sometimes a pre-treatment which modifies the bonds of lignin, cellulose and hemicellulose is required prior to pressing. This is done for the purpose of generating a uniform structure and properties of pellets. The pre-treatment can be done by either one or by a combination of various processes of steam explosion, acid/alkali treatment and biological fermentation (Agbor *et al.*, 2011). At the industrial scale, the established technology of steam explosion is often applied. It utilizes steam at temperatures ranging from 180 to 240°C to rupture the cellular structure (Shahrukh *et al.*, 2016). The USDA-ARS also developed a method of pelleting CGW under the name of COBY system (Holt *et al.*, 2006). The COBY system involved the process of

spraying a pre-cooked gelatinised starch solution into the CGW prior to the hot extrusion into the pellets. It applied 4-5% gelatinised starch slurry as the binder material (Holt *et al.*, 2006).

In this study, the addition of 4% gelatinised starch slurry as the binder was modified based on the COBY system. In addition, this study modified the pre-treatment by adding a stage of softening the CGW bonds. It applied natural fermentation for the purpose of modification of the bonds structure of lignocellulose, lignin and cellulose. Beside as a binder, the starch served also as the media of fermentation to soften the bonds. The wet gelatinised starch was mixed with the CGW at least 3 days prior to the pelleting. The blend was then left to naturally ferment in open. The mixing process served for addition of the binder apart from the softening the lignin by natural fermentation. The comparison of material structures before and after fermentation is shown in Fig 3.6 using scan electron microscope.

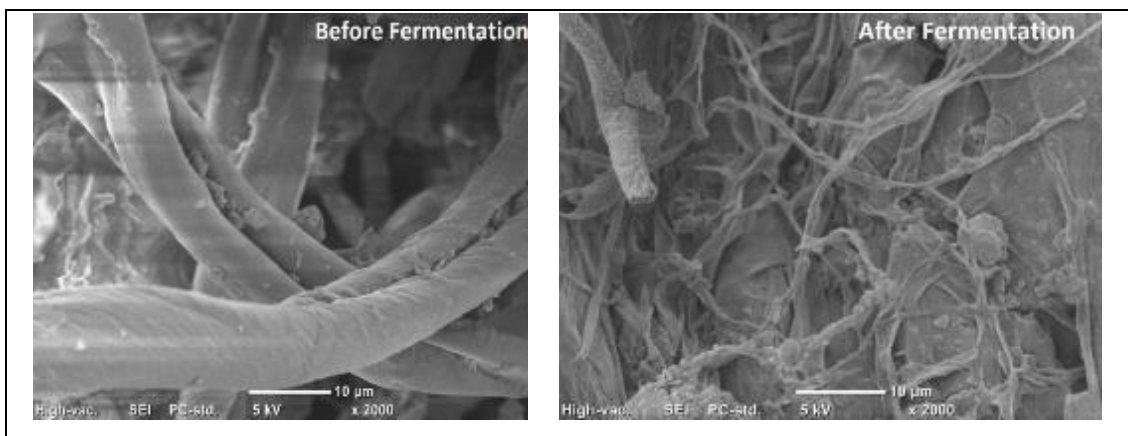


Figure 3.6: SEM images before and after fermentation using starch

3.2.4. Pellet productions

In this study, the plate die-roller pellet mill type was used for the production of 5 types of pellet fuel with the variation of blending composition (Figure 3.7). These 5 types of developed pellets were: CGW100 for the blend weight ratio of 100% CGW-0% biochar, CGW95 for the blend weight ratio of 95% CGW-5% biochar, CGW90 for the blend of 90% CGW-10% biochar, CGW85 for the 85% CGW-15% biochar and CGW80 for the blend of 80% CGW-20% biochar, respectively.



Figure 3.7: CGW and CGW-biochar blended of pellet fuels

In the process of pelleting, the materials were fed into the pellet mill to produce pellets with the size of about 8 mm in diameter and ≤ 45 mm of the length. As the materials were fed into the pellet mill, water was also sprayed more or less continuously to help the material flow through the die to form pellets. The re-feeding of materials into the pellet mill was done 3-5 times until a smooth, non-abrasive and relatively dry pellet product was achieved. This re-feeding resulted in good physical qualities of the pellets but the production capacity was correspondingly reduced. As the barrel temperature reaching 60-80°C, the pellet could be formed directly without re-feeding. However, its moisture content was usually higher than the re-feeding one. In practical situation, at the industrial scale, a mechanical dryer, e.g. a conveyor dryer, is sometimes incorporated with the pellet mill. In this study, the pellets were allowed to cool and dried in an open air after pelleting for a night tempering time. If the moistures were still higher than 10%, then the pellets were sun dried or mechanically dried in a blower-assisted oven, before being packed in a sealed container. The moisture content of the pellet should be $\leq 10\%$ wb for the storage. The reason for having low moisture content was to guarantee good storage quality (mould, fungal growth, hydrolytic breakdown etc.).

Overall, the pelleting process depends upon a variety of factors such as relative humidity, die and ambient temperature, the type of biomass and particle size and content (Holt, 2014). For example, the pellet mill used in this study was originally working without the use of a heater. An increase of the temperature inside of the barrel was expected to arise from the friction of the rotating rollers on the static plate die. However, when the ambient temperature became low, two belt heaters, 30 watts each,

had to be attached to the outer barrel to increase the temperature of the plate die to about 60-80°C.

The plastic phase transition temperatures of a particular biomass, besides the pressure applied on it, are a critical factor in obtaining a good quality of pellet. The temperatures to soften the polymers, or transitioning from a glassy into a plastic phase should be reached (Agbor *et al.*, 2011; Stelte, 2011). On the other hand, too high temperature could result in severe degradation of polymers, reducing the ability to form strong inter particle bonds (Stelte, 2011). Stelte (2011) has reported that wheat straw at 8% moisture content had transition phase at approximately 53-63°C, while spruce lignin was at about 91°C. This CGW pellet study showed that the barrel temperatures should be on the range of 60-80°C for producing a good quality pellet. High temperature above 80°C would, on account of lower moisture content, prevent the extrusion process to proceed smoothly. Lower than 60°C could also cause the materials to block the holes of the plate die.

3.3. Methods of measurement and analyses

Physical parameters and properties of CGW pellets were the size (diameter, length and weight), density, durability and hardness. The aim of this investigation was to find out whether the densification and biochar blends biochar into CGW could improve the fuel quality.

The first measurement and analyses were the effect of biochar blending on the dimensional pellet, its hardness and durability. Within the dimensional topic, two properties were measured, firstly, the pellet dimensional stability; and secondly, pellet sizes determination after the material becomes dimensionally stable. The literature indicates 14 days is a reasonable time after which the pellets do not change anymore (Emami *et al.*, 2014; Lu *et al.*, 2014). The dimensional stability testing examined the possible deformation during the two weeks of storage period after the extrusion. In this study, the apparent density (the density of individual pellet) after the storage was determined as relaxed density (Emami *et al.*, 2014). The dimensional stability was then determined by the size expansion. The negative expansion showed that the size was reduced. The expansion was calculated as the ratio of average change in size before and after storage with its average initial size.

The following analyses would include the effect of biochar blends to the elemental properties, total ash and heating value of the pellets. Another objective of

blending the CGW with biochar in pellet was to increase the heating value and to reduce the ash content. The biochar, in general, has higher heating value than the biomass. Its ash content is also lower. The high carbon elements in biochar will increase the heating value of the blended fuel.

3.3.1. Physical properties

The physical properties of pellets are characterized by following parameters, comprising of size and density, durability and hardness. The results obtained by respective measurements are described below.

- Pellet size and density:

The physical properties comprised of pellet diameter, length, weight and densities. Using 50 pellets, their lengths, diameters and weights were individually determined. The lengths and diameters of pellets were measured by a digital calliper while the weight of the pellet was measured by a digital balance with two decimal points accuracy (Figure 3.8). The first set of measurements on each pellet was taken one day after extrusion, while the second set were done on the day 14th of storage. The first set allowed calculation of *apparent density*, while the second was related to *relaxed density* (Emami *et al.*, 2014; Lu *et al.*, 2014).

In addition to actual material density of a single pellet, it is important to know the bulk density which describes the density of material in bulk. For determination of bulk density, pellets were filled into a 500 ml measurement cup and were weighed on the digital balance. Triplicate measurements were undertaken for each CGW pellet sample.



Figure 3.8: Instrumentation for measurement of the pellet size, weight and apparent density

- *Pellet durability and hardness:*

The durability is defined as the resistance of the pellet to be broken. In this study, the durability of the pellets was measured after 14 days of storage using the single drop test method (Iroba *et al.*, 2014). It was conducted by dropping a single pellet previously weighted from a height of 1.85 m into a stainless pan (Figure 3.9) and taking a weight of the biggest fragment. The durability is calculated by dividing the weight of the biggest broken piece to the weight of original pellet and reported as percentage (Iroba *et al.*, 2014). 50 replicates were made for each sample.

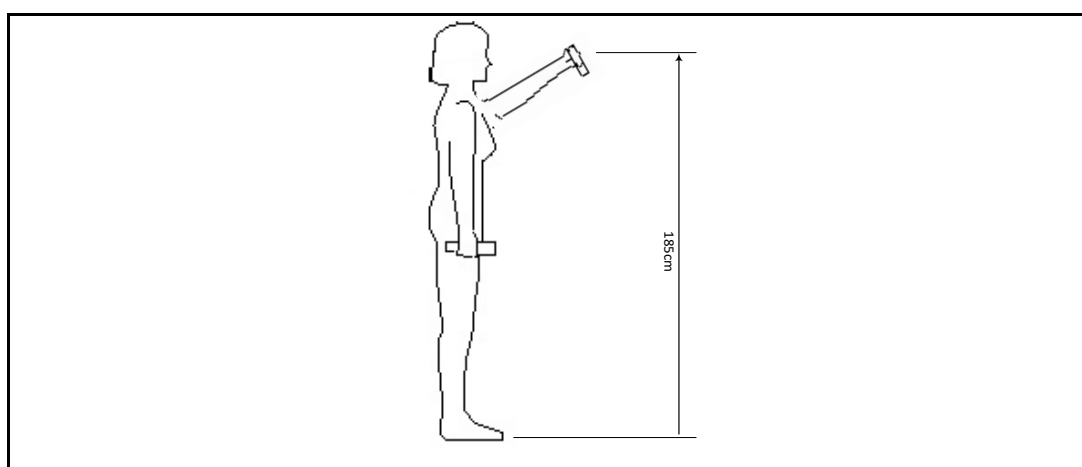


Figure 3.9: Single drop pellet test

The hardness of the pellet was measured by performing the compression test (Mahapatra *et al.*, 2010; Tilay *et al.*, 2015). This test was designed to simulate the effect of the pressure that could be present in pellets of lower layers due to the weight of upper layers during handling and storage. The present test used a universal testing machine (Figure 3.10). A single pellet was placed between two bases. A progressively increasing load was applied until a fracture occurred. The universal testing machine has a maximum load capacity of 2,500 N and the set crosshead speed was 10 mm/min. The maximum load before fracturing was denoted as the pellet hardness. Tests were done for each treatment sample, with 10 replicates for each pellet type.

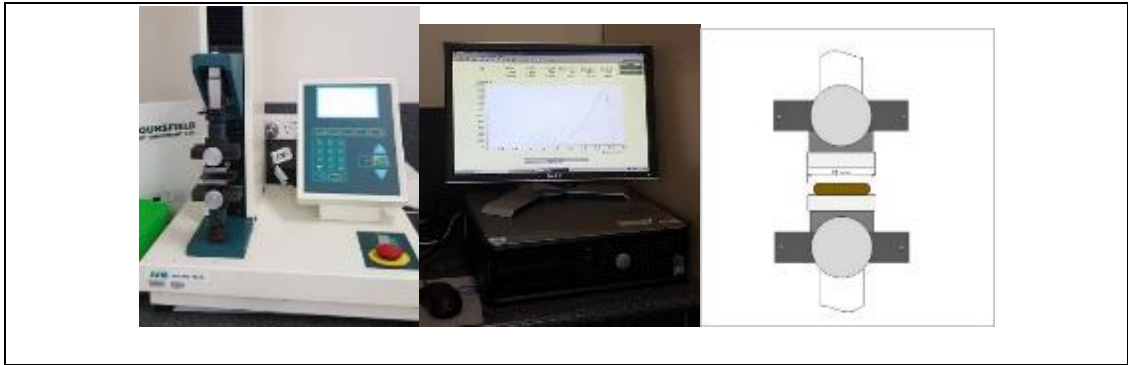


Figure 3.10: Load Testing Machine for pellet hardness

- *Statistical Analyses:*

Independent t-test was used for comparison of the mean size and density of pellets before and after the stabilisation. To evaluate the effect of different levels of biochar addition on size, density, durability and hardness, one-way ANOVA ($P < 0.05$) tests were conducted. The IBM SPSS software version 23 was used for these statistical analyses.

3.3.2. *Proximate and ultimate analyses of the developed pellets*

The proximate and ultimate analyses of the developed fuel pellets were conducted using the ASTM methods D3173, D3174, D3175, and D5373. The sulphur content was measured via ion chromatography (IC), using Dionex ICS-2000 instrument; and the mineral contents of ash were measured using atomic absorption spectrophotometer, Shimadzu AA-7000.

The heating value was predicted from the elemental composition. The heating values of solid fuels were calculated using the formula below (Demirbaş, 1997) :

$$HV \left(\frac{MJ}{kg} \right) = 33.4 m_c + 111.7m_h - 15.6m_o - 14.5m_N \dots \dots \dots 3-1$$

Where m_c is mass fraction of carbon; m_h is mass fraction of hydrogen; m_o is mass fraction of oxygen, and m_N mass fraction of nitrogen, all from the dry basis weight of the ultimate analyses data.

3.4. Results and discussions

3.4.1. *Pellets dimensional stability*

The dimensional stability is concerned with the change in pellet dimension during the process of stabilisation after the densification process. Table 3.3 shows the mean size (length, diameter and weight of pellet) before and after storage. Statistical analyses (t-test) were conducted to compare the mean size of pellets before and after

the stabilisation process (Appendix B.1 and B.2). The results of the t-test indicate insignificant change in the size before and after storage. Though it was relatively significant change for 5% and 20% biochar addition, the standard deviation values were relatively close to each other.

Table 3.4 shows the relaxed density (the mean pellet density from a set of 50 single pellets after 14 days storage) and the percentage of the mean size expansions compared to the initial density. Though statistically insignificant, the results indicate that the pellets tended to expand in length. However, the diameter changes randomly with no clear trend. Overall, effect was a decrease in apparent density during the 14 days of equilibration.

Remarkably, it was found that all pellets show reduction in their relaxed densities, indicating unstable movement within the structure of the pellet during this 14 days storage period. The drop in relaxed density is most likely due to the relaxation of the compressed CGW fibres, mostly noticed from the expansion of all pellet lengths.

It might be also possible that the negative expansion for biochar blended pellets was due to moisture release during the storage. The biochar blended pellets seemed to be less oily and looked drier than the unblended one.

The initial moistures before storage were not measured in detail but they were roughly less than 10%. The average moistures of pellets right after the pressing were found to vary between 8-18%, as measured randomly using a destructive wood moisture tester. Thus, the pellets were sometimes either sun dried or oven dried to reduce the moisture < 10%. For the purpose of this study and for keeping the safe storage, the pellets were oven-blower assisted-dried (40-50°C) for about 12 hours or down to the moisture < 10%. The samples were then placed in an air tight containers. The moistures after the 14 days storage were measured as shown in Table 3.5

After about a month of storage, the unblended (0% biochar) pellet tended to release a rancid oil smell. This might originate from oil in the cotton seed fragments in the CGW. It is known the oil content in the cotton seed is about 30% (Pandey & Thejappa, 1975). Oil released from the broken fragment in the raw CGW is immediately amenable to oxidation by oxygen in the air. Oxidation produces fragmentation of the lipid molecules releasing finally aldehydes and ketones. These are usually summarised as Volatile Organic Compounds (VOC). It was noted, the higher the biochar in the blend, the less the odour. Obviously, the biochar functioned

as an absorbent for the volatile component which were responsible for the smell. The further discussion of oxidative storage behaviour of these CGW pellets is beyond the scope of this study.

Overall, the results of this study confirmed the results of other studies. For both woody and non-woody pellets (Liu *et al.*, 2014; Lu *et al.*, 2014), it was reported that during storage, the pellets expanded longitudinally and either slightly shrank or expanded radially (Lu *et al.*, 2014). However, pellets produced in this study had a higher percentage of longitudinal expansion compared to the study conducted by Lu *et al.* (2014). In this study, the longitudinal expansion was about 5.6%, while the study of wheat straw pelleting (Lu *et al.*, 2014) reported an expansion of only about 2%. The mean length and diameter of the pellets in this study were about 30-40 mm and 7.5 mm respectively. In contrast, the wheat straw pellets (Lu *et al.*, 2014) had lengths of 10-18 mm and diameters of about 6.5 mm. The difference between results in both studies may be because the pellet in this study has both the diameter and length larger than pellets they produced. Obviously, the bulkier the pellet, the more material there was to expand. Overall, the longitudinal expansion of our CGW pellets was in a close agreement with another study conducted by Liu *et al.* (2014). The pellets in Liu *et al.* (2014) study had lengths of 40 mm and diameter of 13 mm. The pellets had longitudinal expansion of about 7 to 10% after storage. The pellets were made from coconut fibre, rice husk, coconut shell and pine sawdust.

Table 3.3: Pellet size before and after 14 days storage

Samples	Length (mm)		Diameter (mm)		Weight (g)	
	Before	After	Before	After	Before	After
CGW100	35.02±3.88	35.99±4.39	7.50±0.13	7.47±0.13	2.00±0.26	2.05±0.28
CGW95	34.60±3.51*	36.01±2.98*	7.61±0.01	7.60±0.10	1.95±0.28*	2.02±0.21*
CGW90	36.47±3.61	36.62±4.13	7.57±0.11	7.59±0.12	2.14±0.22	2.09±0.27
CGW85	36.25±4.44	37.08±3.66	7.53±0.13	7.54±0.10	2.12±0.29	2.15±0.22
CGW80	35.77±5.45*	37.78±3.18*	7.77±0.17*	7.57±0.10*	2.15±0.19	2.10±0.10

* The mean comparison of before and after storage showed a significant difference at P=0.05

Figures following the ± are the standard deviation of samples

Table 3.4: Mean size expansion and density changes after 14 days storage

Samples	Initial apparent density (kg/m ³)	Apparent relax density (kg/m ³)	Average Expansion (%)		
			Relax density	Longitudinal	Diametrical
CGW100	1290.55±78.66	1299.47±70.74	0.69	2.77	-0.40
CGW95	1237.93±41.10	1238.38±36.86	0.04	3.92	-0.13
CGW90	1306.30±53.22	1265.10±30.47	-3.15	0.41	0.26
CGW85	1315.13±63.34	1299.76±47.40	-1.17	2.29	0.13
CGW80	1267.01±41.64	1237.13±41.64	-2.36	5.62	-2.57

Figures following the ± are the standard deviation of samples

3.4.2. The effect of biochar blends in CGW pellet size and density

The determination of pellet size conducted after 14 days of storage is considered as the stable pellet. In this study, the one-way ANOVA test was conducted to compare the effect of blending on the sizes of pellets after the storage followed by DUNCAN Post hoc test (Appendix B.1 and B.3). The comparison was for length, diameter, weight and apparent density (Table 3.5).

Table 3.5: Pellet sizes (measured after 14 days stabilisation)

Samples	Moisture (% wb)	Length* (mm)	Diameter* (mm)	Weight* (gram)	Density (kg/m ³)	
					Apparent*	Bulk
CGW100	7.93	35.99 ±4.39 ^a	7.47 ±0.13 ^a	2.05 ±0.28 ^a	1299.47 ±70.73 ^b	605
CGW95	9.05	36.01 ±2.98 ^a	7.60 ±0.95 ^c	2.02 ±0.17 ^a	1238.38 ±36.86 ^a	602
CGW90	9.18	36.62 ±4.14 ^{ab}	7.59 ±0.12 ^c	2.09 ±0.27 ^{ab}	1265.10 ±30.47 ^a	608
CGW85	7.28	37.08 ±3.66 ^{ab}	7.54 ±0.10 ^b	2.15 ±0.22 ^{ab}	1299.76 ±47.40 ^b	606
CGW80	8.38	37.78 ±3.18 ^b	7.57 ±0.10 ^{bc}	2.10 ±0.19 ^b	1237.13 ±41.64 ^a	606

*superscript letters indicate that means with same letters in the designated rows at the same column are not significantly different at P=0.05.

Figures following the ± are the standard deviation of samples

In general, it was found that blending with the maximum 20% biochar had achieved a significantly longer length, a wider diameter and heavier pellets compared to non-blended ones. This was probably because during the compaction, the biochar particle enhanced the compaction quality of the pellet and was able to maintain a more stable form of pellet exited from the 8 mm holes of the plate die pellet mill. The increase of pellet length by addition of other materials was also reported by Serrano *et al.* (2011), which produced pellets from barley straw blended with pine sawdust to improve the quality. The pine additions were up to 12% by weight. Similar to this study with addition of biochar to a non-woody biomass, Serrano *et al.* (2011) reported that the pellet length increased also with addition of pine meal, a woody biomass. His study reported a more clearly cut linear increase in length.

There were two types of density examined in this study: the apparent density and the bulk density. The apparent density is the ratio between the weight of a single pellet to its volume while the bulk density is the ratio of the mass of a bed of particles to its volume (the sum volume of individual particles and void spaces between them) (Souza-Santos, 2010). The apparent density is essentially calculated from the single pellet mass and pellet dimensional data. Table 3.5 shows lower standard deviations in the apparent density of all blended biochar pellets. This could indicate that the blended biochar pellets were more uniform in apparent density than the unblended one.

In this study, it was found that although the mean weight of single pellets slightly increased with the rate of biochar added, the weight increase was not a simple proportion. Therefore, the mean apparent density values were not linearly related to the increase of biochar composition in the pellet. This study's result was similar to the study reported by (Serrano *et al.*, 2011). They also found that the mean apparent densities were not linearly related to the increase of pine sawdust in the barley pellets.

Furthermore, this study also found that the bulk density of the blended and unblended biochar pellets were very similar, both about 600 kg/m³. Though having greater mass, the longer pellets of the blended pellets might create more void space in the bed of the bulk pellets compared to the shorter ones. Overall, the bulk density of the produced pellets from this study complied with ISO 17225-6 Solid biofuels: Graded non woody pellets (ISO, 2014). This ISO standard states that the bulk density of the pellets for grades A and B should be ≥ 600 kg/m³. Furthermore, this ISO standard also gives in particular a specification for red canary grass pellets, with a lower bulk density allowable (≥ 550 kg/m³). For comparison to this CGW pellets, the EU standard (EN 14961-2) bulk density of commercial wood pellet is ≥ 600 kg/m³ (Toscano *et al.*, 2013; Duca *et al.*, 2014).

3.4.3. *The effect of biochar blends in pellet durability*

The durability is defined as the resistance of the pellet to be broken. It represents the quality of the durable pellet from the agitation, rotating, shear, impact and tumbling during transportation. The single drop test is often be used to represent this (Iroba *et al.*, 2014; Tilay *et al.*, 2015). The durability is as the percentage weight of pellet after dropped.

The durability of pellets may be influenced by several factors such as the pressure and temperature during pelleting, the degree of volume reduction and material

composition (Tilay *et al.*, 2015). This CGW pelleting study used a commercial pellet mill for pelletisation, thus the pressure is assumed relatively constant as the given rotation of rollers and friction between plate die and rollers. As stated previously, the good quality pellet results from the working temperature in the range of 60-80°C of the barrel. Referring to the best CGW pellet result studied by Holt *et al.* (2006), this CGW pelleting study also applied similar 4% wt binder for all of CGW-biochar blending treatments. The moisture content was measured < 10% wb, relatively similar figures for all the samples in each blending treatment category. Thus, the influence on durability mainly originated from the effect of blending treatment, the pellet weight and the possibility of blending treatment covariance with the pellet weight sample.

The drop test results for each treatment are shown in Table 3.6. The sample data of the measurement is provided in Appendix C.1. The ANCOVA test (Appendix C.2) was conducted to study the effect of blending treatment, the pellet weight and their combination to the durability. The ANCOVA test revealed that the samples pellet weight did not significantly affect the pellet durability. In addition, looking from the mean weight and its standard deviation, the sample could be considered homogenous, so the effect of weight of pellet to the durability was negligible. The analyses showed that overall, the blending, the pellet weight and the covariate pellet weight to treatment had insignificant influence on the durability as to the drop test method (sig. > p = 0.05). Either with blending or without blending with biochar, the durability of pellets remained about the same.

Table 3.6: Durability measured from Single Drop Test

Samples	Pellet weight, Mean (%)*	Durability as Single drop test, Mean (%)*
CGW100	2.07 ± 0.38 ^b	97.14 ± 10.15 ^a
CGW95	1.91 ± 0.24 ^b	99.70 ± 0.43 ^a
CGW90	2.23 ± 0.24 ^b	97.02 ± 9.33 ^a
CGW85	2.18 ± 0.23 ^b	97.03 ± 9.58 ^a
CGW80	2.06 ± 0.24 ^b	99.24 ± 2.78 ^a

*superscript letters indicate that means with same letters in the same column are not significantly different at P=0.05.

Figures following the ± are the standard deviation of samples

The durability of this CGW pellets was at about 97-99% with the standard deviation of up to 10%. Comparing this with other non-woody biomass pellets, Iroba

et al. (2014) studied the production of ground barley straw pellets with the pre-treatment radio-frequency and applying temperature variation during the compaction. The durability of the produced pellet tested using the single drop test could also reach up to 99.17%. It was achieved at about 90°C working temperature and biomass: alkali ratio at 1:8.

3.4.4. *The effect of biochar blends in pellet hardness*

The compression tests were conducted by compressing 10 pellet samples from each treatment pellet until its breakage (Appendix D.1). The size of pellets was firstly recorded. The mean average of test results are summarised in Table 3.8. The statistical ANCOVA test (Appendix D.2) was conducted to find the effect of blending treatments to the mean values of hardness. The mean lengths of the pellet samples is also presented in the Table 3.7 to show that the pellet samples length used for this comparisons was relatively uniform. So the effect of pellet length to the hardness was neglected. The summary of this ANCOVA test is presented in Appendix D.2. Overall, it was found that the pellet length and the covariate length with treatment have insignificant influence on the hardness of the pellet, while the blending treatment had a significant influence on the pellet hardness (Sig. < p=0.05).

Table 3.7: Pellet hardness as compression test

Samples	Sample pellet length, mean (mm)*	Hardness as max compressive, mean (N)*
CGW100	32.45 ± 2.83 ^c	1638.8 ± 392.5 ^a
CGW95	32.66 ± 2.87 ^c	1621.4 ± 233.1 ^a
CGW90	33.64 ± 1.92 ^c	1832.7 ± 273.2 ^{ab}
CGW85	32.89 ± 1.38 ^c	1914.2 ± 382.1 ^{ab}
CGW80	31.88 ± 2.33 ^c	1950.0 ± 237.1 ^b

*superscript letters indicate that means with same letters in the same column are not significantly different at P=0.05.

Figures following the ± are the standard deviation of samples

This study also revealed that the produced pellets had mean hardness ranging from 1600-1900N (Table 3.7). The addition of a small portion of biochar into the raw

CGW did improve the hardness of the biomass pellet. In comparison with this results, pellets made from coconut fibre, rice husk and sawdust hydrocar had hardness in the range of 1049 to 1867N (Liu *et al.*, 2014). For a comparison, pellets made from raw materials (i.e. without the pre-treatment of converting them into hydro char) had only maximum compressive of 246-990N, which was significantly lower.

The compressive tests conducted by others (Tilay *et al.*, 2015) reported pellet hardness of less than 100N. The pellet material was from canola meal. The pellets were softer than pellets produced by this study. One of the reasons might be that the oil contained in the canola meal exhibited more lubrication than binding action. The pellets thus produced have virtually no hardness. Holt *et al.* (2006) also reported that addition of cotton seed oil to the CGW pellet affects negatively to the densification process.

3.4.5. *The effect of biochar blends on elemental composition, ash content and calorific values of the developed pellets*

The element properties of the pellet comprise of major and minor elements. The analyses are beneficial for modelling the thermochemical conversion; predicting the solid and gasses phase results and the ratios of reactants required for the thermochemical reactions. Major elements (C, H, N, S, O) were analysed by ultimate analyses. The proximate analyses determined the fixed carbon, moisture, ash and volatile matter. Table 3.8 shows the summary of analytical results of CGW pellets containing various amounts of biochar.

The high ash content in the CGW pellets might come from the mixture of dust in the CGW original material which can reach 20% of the weight (Table 3.1). The ISO 17225-6 Graded non-woody pellets limits the ash content to $\leq 10\%$ for grade B (Table A.4 Appendix A). Table 3.8 shows that without blending, the ash content of CGW pellet was about 15%, while the blending with biochar up to 20%, could lower the ash of the CGW pellets to be only 9% - 11%. This study showed that the blending could upgrade the CGW as a fuel pellet closer to the requirement of the limit of ash content of the commercial non-woody pellet (ISO 17225-6). The varied amount of ash in the blended biochar pellets might be the result of a varied range of ash content from the originated raw CGW material. McIntosh *et al.* (2014) examined some CGW ash contents collected from several gins in Australia. The ash contents were ranging from 8 to 13%. It was found that the ash content in CGW depended upon several factors

such as ginning operation, the amount of seed contamination in the waste and time of cotton harvest. In this study, though the samples were taken from a gin, a varied range of ash content might still be possible considering the samples had different harvest times or originated from different areas of planting.

Table 3.8: Analyses of CGW pellets and biochar

Sample	CGW100	CGW95	CGW90	CGW85	CGW80
<i>Proximate analysis (wt. %, as received)</i>					
Moisture	7.93	9.05	5.69	5.57	8.38
Ash	14.63	9.01	11.87	11.37	11.36
Volatile	62.12	61.92	57.97	52.93	49
Fixed Carbon*	15.32	20.02	24.47	30.13	31.26
<i>Ultimate (wt. % db)</i>					
Carbon	45.18	48.99	51.91	54.31	55.96
Hydrogen	5.58	5.55	5.22	4.89	4.73
Nitrogen	1.97	1.66	1.06	1.24	1.47
Sulfur	0.25	0.21	0.26	0.25	0.17
Oxygen*	47.01	43.59	41.55	39.31	37.67
<i>Ash analyses (wt. % of ash)</i>					
K	3.12	3.20	3.7	2.81	2.07
Ca	12.27	12.60	11.21	10.8	6.24
Mg	1.22	1.13	1.06	0.71	0.21
Na	0.62	0.83	0.76	0.6	0.42
Fe	0.58	0.67	0.68	0.43	0.4
Al	1.44	2.69	1.16	1.63	1.33
Si	2.79	3.33	2.66	3.96	3.540
<i>Calorific value**</i>					
HV, MJ/kg	14.04	15.86	16.85	17.58	18.17

* calculated by difference ** calculated as per formula (Demirbaş, 1997)

The calorific value was predicted from the elemental analyses results based on the equation developed by (Demirbaş, 1997). The calorific values of the produced pellets were thus in range 14.0 – 18.2 MJ/kg. With the increase of biochar in the CGW pellets, the calorific value would increase to values closer to the wood pellets. In comparison to other non-woody biomass pellets, the barley straw pellet had calorific value of 16.23 MJ/kg (Serrano *et al.*, 2011) and wheat straw 17.74 MJ/kg (Lu *et al.*, 2014). The wood pellets in the market are also varied in their heating values ranging from 16-20 MJ/kg (Toscano *et al.*, 2013; Duca *et al.*, 2014).

The nitrogen and sulphur converts to NO_x and SO_x composition in the thermochemical gasses. These elements are included in the commercial pellets

standard for small pellet stove/burner with lack of emission control. By its nature, cotton gin waste may have higher nitrogen and sulphur content compared to wood. The high nitrogen can also be traced to the CGW which already had high nitrogen content (1.5%). Mixing it with biochar can theoretically reduce the nitrogen content. Graded non-woody pellets, i.e. all of pellets produced in this study, however, can comply with the pellet fuel market standard for nitrogen as per ISO 17225-6 (ISO, 2014). This standard sets the $N \leq 1.5\%$ for grade A and $N \leq 2.0\%$ for grade B. The pellets could also meet the criteria for sulphur content, which is set $S \leq 0.2\%$ for Grade A and $S \leq 0.3\%$ for Grade B (Table A.4 Appendix A). For comparison, the nitrogen and sulphur contents in wood pellets are about 0.1-0.3% and 50-150 mg/kg, respectively (Duca *et al.*, 2014).

3.5. Summary and conclusion

This chapter has demonstrated that improving the fuel properties of non-woody material is possible. It has been also demonstrated that by a control over quality of input materials and blending process, pellet may fulfil the quality requirement of standard ISO 17225-6: Graded non-woody pellets.

An initial size reduction process was necessary for homogenization. After mechanical comminution, the pre-treatment by wetting and gentle microbial-assisted hydrolysis, together with gelatinised cassava starch, the material was left to ferment in open for at least three days prior to pelleting. Besides acting as the binder, the wet gelatinised cassava starch also served as a media for enzymatic processes which soften the lignocellulose bonds.

To produce smooth, non-abrasive and dry pellets, it has been found that the barrel temperature of the pellet mill should reach 60-80°C. For good keeping quality, the pellet moisture content should be under 10% w.b. The blended biochar pellets showed a trending to shrink lowering the relax density during the stabilisation time (14 days after pelleting). However, in general, the blend of biochar pellets had more uniform apparent density than the unblended one.

By densification, the raw cotton gin waste bulk density has increased from 112 kg/m³ to about 600 kg/m³ into the pellets. The blends of biochar could create slightly longer and heavier pellet. This study has also found that the biochar blends up to 20% could reduce the ash content from 15% into 9-12%.

The durability of pellets as in the single drop test was found to be about 97-99%. The hardness of pellets as to the compressive test ranged from 1600 -1900N. The single drop tests conducted for the durability indicated an insignificant effect from the blending treatment to the durability of the pellets. However, the hardness of the pellets was significantly increased with the increase of biochar percentage in the pellets.

CHAPTER 4: Thermo-kinetics Behaviour of CGW Pellets in Combustion

Abstract

Cotton gin waste was developed into fuel pellets and its calorific value upgraded by blending the CGW with up to 20% of biochar. The effects of biochar blends on the thermo-kinetic behaviour of the pellets in combustion were studied using thermogravimetric analyses (TGA). Air was used as the carrier gas with the flow rate maintained at 20 mL/min. It was found that originating from a material with low lignin content, the pure CGW was fast in reduction at oxidative pyrolysis zone. Addition of 5-10% of biochar in CGW pellets quickened the combustion reaction by slightly lowering the temperatures of fast mass reduction and burnout, as well as increasing the conversion rate. The addition of 15-20% biochar in CGW shifted the combustion reactions to higher temperatures, lowering the rate of conversion and moving the burnout temperatures closer to the biochar ignition point. The activation energy of the blended fuel was reduced proportionally with the increase of biochar in pellet. The CGW100 had a combustion activation energy of 204 kJ/mol, while the blended CGW-biochar pellets had the activation energy at about 170 kJ/mol. Synergy effect in all blended pellets were confirmed by comparing the activation energies and ashes of experimental results with the theoretical calculations. The synergy was confirmed by having obtained experimental results which were all lower than those expected by theory.

Keywords: thermogravimetric (TGA), combustion, fuel pellet, cotton gin waste, co-blended

4.1. Introduction

Non-woody biomass typically has low quality of solid fuel properties. The non-woody is frequently low in density, ash content and calorific value. However, the non-woody is usually cheaper, particularly when sourced from the agricultural industrial waste. In this study, cotton gin waste, a type of non-woody biomass, was converted into a higher quality solid fuel. The cotton gin waste was pelleted and its calorific value was upgraded by blending with biochar. The development method, physical and element properties of the CGW pellets have been discussed in Chapter 3.

The thermo-kinetic property is an important fuel characteristic. Together with the physical & elemental properties, thermo-kinetics are required as the input data in the design and analyses of a thermochemical conversion process. The thermo-kinetic analyses are basically investigating the kinetic changes of a solid/liquid into products (liquids/gases) which are caused by the application of heat under controlled

atmosphere such as nitrogen, air or other gases. The presence of a medium facilitates the transport of the particles to the chemical reactions. As a result, the conversion rate of the reactants into the product is dependent upon the chemical reaction rate as well as on the reaction medium (Vyazovkin, 2006).

The thermo-kinetic properties of a fuel are often obtained by carrying out laboratory scale studies, applying heat to the fuel. The relevant methods of thermo-kinetic analyses can be categorised into thermogravimetric (TGA/DTG) and calorimetric (DSC/DTA) (Vhathvarothai *et al.*, 2014b; Vhathvarothai *et al.*, 2014a; Zhang *et al.*, 2016). Other methods also include: pyrolysis gas chromatography oven, a lab scale fluidised bed, a lab scale fixed bed reactor and a batch pyrolysis oven (Jeong *et al.*, 2014; Jones *et al.*, 2005; Onay *et al.*, 2007; Wang *et al.*, 2015).

From the obtained empirical data, the thermo-kinetic properties of a particular material can be derived. The results of the empirical kinetic behaviour are then often expressed as a mathematical description of the thermal/thermochemical process for a particular material. Three variables: activation energy, E_a ; pre-exponential factor, A ; and the conversion model, $f(\alpha)$; are used to describe the kinetic properties of a particular fuel.

This study examined the behaviour of CGW pellets conversions by conducting combustion reactions using thermogravimetric analyses (TGA/DTG). The objective was to find the kinetic combustion properties of the developed CGW pellets. These kinetic properties would be used later as the input data in the design and analyses of the pellets conversion into energy (Chapter 6).

Another objective of conducting these laboratory scale studies was to examine the effect of biochar blends in the improvement of CGW combustion behaviour. Several studies also employed this thermo-kinetic approach to examine the synergistic effects of co-blended fuels. Depending on the blend composition, the interaction among its component could lead to an efficiency improvement in the co-conversion reactions compared to one of the individual performance (Brown, R. C. *et al.*, 2000; Jeong *et al.*, 2014; Ren *et al.*, 2011; Zhu *et al.*, 2008). However, some co-conversion studies also found no synergy occurrences (Idris *et al.*, 2010; Vhathvarothai *et al.*, 2014b; Vhathvarothai *et al.*, 2014a). At present, the presence of synergy of the co-blended fuel is still a matter of discussion.

4.2. Theoretical models of thermal analyses

The empirical kinetic behavior data of TGA is often presented as plot of the residual mass portion or mass conversion against a time or a temperature. The mass conversion, α , at a time, t , or temperature, T , can be denoted as

$$\alpha = \frac{m_o - m}{m_o - m_e} \dots\dots\dots 4-1$$

Whereas m_o is initial mass,
 m is the instantaneous mass
 m_e is the end mass

The data of function, α , is then used to model the kinetic decomposition of that particular material. The kinetic rate of thermal decomposition can be expressed as a single step kinetic equation (Vyazovkin, 2006):

$$\frac{d\alpha}{dt} = k(T)f(\alpha) \dots\dots\dots 4-2$$

whereas $f(\alpha)$ is the conversion model of α , the extent of conversion.
 $k(T)$ is the reaction rate constant at temperature T .

This equation expresses the rate of mass conversion as a product of two function $f(\alpha)$ and $k(T)$ which depend on time and temperature. The reaction rate constant almost universally follows the Arrhenius equation (Vyazovkin, 2006):

$$k(T) = Ae^{\frac{-E_a}{RT}} \dots\dots\dots 4-3$$

whereas k is reaction rate constant (s^{-1})
 A is pre-exponential factor (s^{-1})
 E is activation of energy ($J.mol^{-1}$)
 R is gas constant ($J.K^{-1} mol^{-1}$)
 T is temperature (K)

Thus, in the study of thermo-kinetic decomposition, three variables of a particular material are relevant. These variables are activation energy, E_a ; pre-exponential factor, A ; and the conversion model, $f(\alpha)$. These three kinetic parameters are also commonly known as the “kinetic triplet”.

Theoretically, the kinetic triplet represents the physical concept of thermal decomposition (Vyazovkin, 2006). The activation energy (E_a) represents an energy

barrier of a reaction which must be overcome to achieve the product. The pre-exponential factor, (A), means the probability of the reactants get into the right contact to result in a particular reaction. $f(\alpha)$ describes the reaction model (Vyazovkin, 2006). In the empirical data analyses, the activation energy can be calculated from the temperature coefficient of the overall reaction rates, while the value of pre-exponential factor is a scaling factor of the overall reaction rates. This method has been applied and widely used to characterize the thermal properties of variety of material (inorganic, metals, polymers) (Vyazovkin, 2010).

The examination of experimental TGA analyses can be either from isothermal or non-isothermal condition. For both analyses, there exists two approaches to determine the model of reaction (Vyazovkin, 2006). The first is by the forced fitting of the experimental data to the different reaction models and the second one is the free method. The details of theory underlying these two models follows:

4.2.1. Forced fitting equation model

Within this approach, a well-known method is the model of Coats-Redfern (Coats & Redfern, 1964). This method relies on single curve of a constant heating rate treatment. The data plot of conversion from the experiment are fitted to some developed equations (Figure 4.1 and Table 4.1). Combining the equation (4-2) and (4-3) leads to:

$$\frac{d\alpha}{dt} = Ae^{\left(\frac{-Ea}{RT}\right)}f(\alpha). \dots\dots\dots 4-4$$

$$g(\alpha) = Ae^{\frac{-Ea}{RT}t} \dots\dots\dots 4-5$$

Under non-isothermal condition, at a constant heating rate β , the equation 4.4 can be modified as:

$$\frac{d\alpha}{dT} = \frac{A}{\beta} e^{\left(\frac{-Ea}{RT}\right)}f(\alpha) \dots\dots\dots 4-6$$

Integration of the equation 4-6 gives

$$g(\alpha) = \frac{A}{\beta} \int_0^T e^{\left(\frac{-Ea}{RT}\right)}dT \dots\dots\dots 4-7$$

If Ea/RT is replaced by x and the integration limits transformed, Equation 4-7 becomes:

$$g(\alpha) = \frac{AEa}{RT} \int_x^\infty \frac{e^{-x}}{x^2} dx \dots\dots\dots 4-8$$

Equation 4-8 can be written as

$$g(\alpha) = \frac{AE_a}{RT} p(x) \dots\dots\dots 4-9$$

The solution for the $p(x)$ is usually by approximation. The most popular one was developed by Coats-Redfern (Coats & Redfern, 1964). Equation 4-9 becomes:

$$\ln\left(\frac{g(\alpha)}{T^2}\right) = \ln\left[\frac{AR}{\beta E_a}\left(1 - \frac{2RT}{E_a}\right)\right] - \frac{E_a}{RT} \dots\dots\dots 4-10$$

The steps of approximation for the kinetic triplets determination is firstly picking a model description at a certain time or temperature range from the function of $f(\alpha)$ defined as $g(\alpha)$. Secondly, the model of $g(\alpha)$ is fitted into the available pre-defined reactions models as in Figure 4.1. For example, the $g(\alpha)$ is close to the first order equation from Table 4.1. Then, the equation 4.10 becomes

$$\ln\left[\frac{-\ln(1-\alpha)}{T^2}\right] = \ln\left[\frac{AR}{\beta E_a}\left(1 - \frac{2RT}{E_a}\right)\right] - \frac{E_a}{RT} \dots\dots\dots 4-11$$

Plot of $\ln\left[\frac{-\ln(1-\alpha)}{T^2}\right]$ as a function of $1/T$ gives the slope of $-\frac{E_a}{R}$, from which the value of E_a is determined. Fitting of the curve, $g(\alpha)$, should be tried into several pre-defined reaction models (Table 4.1 and Figure 4.1). Finally, the one which gives the highest correlation coefficient (R^2) is determines as the best model for approximating the value of E_a .

Table 4.1: Typical models of reaction for fitting equations in kinetic analyses (Vyazovkin, 2006)

Reaction model	$f(\alpha)$	$g(\alpha)$
1. Power law	$4\alpha^{3/4}$	$\alpha^{1/4}$
2. Power law	$3\alpha^{2/3}$	$\alpha^{1/3}$
3. Power law	$2\alpha^{1/2}$	$\alpha^{1/2}$
4. Power law	$2/3\alpha^{1/2}$	$\alpha^{3/2}$
5. One dimensional diffusion	$1/2\alpha^{-1}$	α^2
6. Mampel (first order)	$1-\alpha$	$-\ln(1-\alpha)$
7. Avrami-Erofeef	$4(1-\alpha)[- \ln(1-\alpha)]^{3/4}$	$[- \ln(1-\alpha)]^{1/4}$
8. Avrami-Erofeef	$3(1-\alpha)[- \ln(1-\alpha)]^{2/3}$	$[- \ln(1-\alpha)]^{1/3}$
9. Avrami-Erofeef	$2(1-\alpha)[- \ln(1-\alpha)]^{1/2}$	$[- \ln(1-\alpha)]^{1/2}$
10. Three dimensional diffusion	$2(1-\alpha)^{2/3}[1-(1-\alpha)^{1/3}]^{-1}$	$[1-(1-\alpha)^{1/3}]^2$

Reaction model	$f(\alpha)$	$g(\alpha)$
11. Contracting sphere	$3(1-\alpha)^{2/3}$	$1-(1-\alpha)^{1/3}$
12. Contracting cylinder	$2(1-\alpha)^{1/2}$	$1-(1-\alpha)^{1/2}$

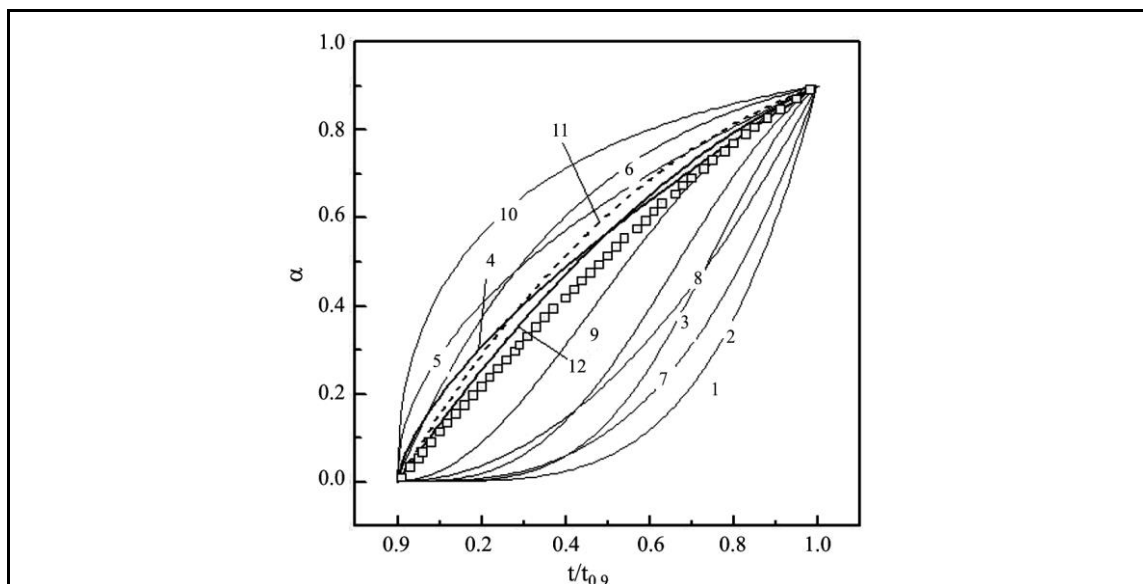


Figure 4.1: Time plot of typical reaction models applied in kinetic analyses (Vyazovkin, 2006)

This method may give a more reliable value for Arrhenius parameter. However, due to complexity of the real data of reaction, many models fail to entirely fit the data (Vyazovkin, 2000). Particularly for non-isothermal, the differences between the temperatures (T), reaction (α) data and their simulation figures could vary simultaneously. Sometimes, a pre-defined model corresponds to the data at only certain range of temperature/time; meanwhile the outer range factually influence the whole process. Thus, it compensates to a variation in kinetic triplets (Vyazovkin, 2000). Nevertheless, some attempts were made to improve the model by increasing the degree of integration or derivation and also trimming into several stages of temperatures which give also several values of activation energy (Urbanovici *et al.*, 1999; Trache *et al.*, 2017).

4.2.2. Free methods

Free method approach utilizes data from the multiple constant heating rates figures or/and temperatures. Instead of observing from a single constant heating rate application, it may be more valid if the analyses employ several treatments (Vyazovkin, 2006). The calculation of the Arrhenius parameters does not require any

assumption of a pre-defined reaction model. Using the multiple data of TG/DTG curves, the kinetic triplets were approximated from the isothermal/iso-conversional condition. Models which follow this approach are: Flynn-Wall, Flynn-Wall-Ozawa (FWO), Kissinger, Kissinger-Akihara-Sunose and Friedman methods (Blaine & Kissinger, 2012) . The Flynn-Wall method was elevated to a standard: ASTM E 1641-04:2014 Standard Test Method for Decomposition Kinetics by Thermogravimetric analyses. The free method requires multiple TG/DTG data of which at least 3-4 curves should be provided for the analyses.

4.2.2.1. Flynn-Wall model

The Flynn-Wall applies the iso-conversional techniques e.g. 5% conversion points (ASTM E1641-2014) or 50% conversion points (half decomposition). The TGA curves at several heating rates are analysed. TGA curve is usually the plot of the portion of remaining mass to the temperature. The linear regression is subsequently made for the iso-conversional points in which it is the plot of $\Delta(\log\beta)/\Delta(1/T)$. The slope can be employed for the calculation of activation of energy.

$$E_a = -\frac{R}{b} * \frac{\Delta \log(\beta)}{\Delta(1/T)} \dots\dots\dots 4-12$$

Whereas E_a is activation energy, R is 8.314 J/mol K, β is constant heating rate, T is temperature at point of isoconversion (K). b is the iterative value, the Doyle's tabulated figures from ($7 \leq E/RT \leq 60$) (provided in ASTM E 1641-04:2014). The conversion of α at temperature T is calculated in the form of integration.

$$\int_0^\alpha \frac{1}{f(\alpha)} d\alpha = g(\alpha) = \frac{A}{\beta} e^{-E_a/RT} dt \dots\dots\dots 4-13$$

This integration is approximated:

$$\int_{T_0}^T e^{-E_a/RT} dT \approx \frac{R}{E_a} T^2 e^{-E_a/RT} \dots\dots\dots 4-14$$

Rearranging this equation in the logarithmic form gives,

$$\frac{\ln\beta}{T_\alpha^2} = \ln \left[\frac{RA}{E_\alpha g(\alpha)} \right] - \left(\frac{E_\alpha}{R_\alpha} \cdot \frac{1}{T_\alpha} \right) \dots\dots\dots 4-15$$

4.2.2.2. Flynn-Wall-Ozawa (FWO) model

The FWO model is also an iso-conversional integral method. It is based on the Doyle's approximation:

$$\ln p \left(\frac{E_a}{RT} \right) \cong -3.315 + \frac{E_a}{RT} \dots\dots\dots 4-16$$

The reaction model can be linearly written as

$$\ln(\beta) = \ln\left(\frac{AE_a}{Rf(\alpha)}\right) - 2.315 - 0.4567 \frac{E_a}{RT} \dots\dots\dots 4-17$$

At α constant value, the plot of heating rate constant ($\ln(\beta)$) versus the inverse temperature ($1/T$) should give a linear line with the slope of $-E_a/R$. The activation energy is then calculated from this slope.

4.2.2.3. Kissinger model

The Kissinger method employs the derivative data curves (DTG) of several constant heating rates. It examines the temperature (T_m) at the point of the maximum rate of reactivity ($r_{max} = \frac{d\alpha}{dt}$). The second derivative of the reactivity at the maximum point is equal to zero.

$$\frac{d^2\alpha}{dt^2} = \left[\left(\frac{E_a\beta}{RT_m^2} \right) + Ae^{-\frac{E_a}{RT}} f'(\alpha) \right] \frac{d\alpha}{dt} = 0 \dots\dots\dots 4-18$$

The approach equation is as in 4-11 and the linear form is as in 4-12

$$\frac{\beta}{T_m^2} = \frac{AR}{E_a} e^{-E_a/RT_m} f'(\alpha) \dots\dots\dots 4-19$$

$$\ln \left(\frac{\beta}{T_m^2} \right) = \left(\frac{-E_a}{RT_m} \right) + \ln \frac{AR}{E_a} + \ln[n(1 - \alpha_m)^{n-1}] \dots\dots 4-20$$

The plot of $\ln \left(\frac{\beta}{T_m^2} \right)$ versus ($1/T_m$) gives the slope which is equal to the value of ($-E_a/R$).

4.2.2.4. Kissinger-Akihara-Sunose (KAS) model

The KAS model also examines the DTG curves. However, it picks data from iso-conversional point, a constant conversion rate value (α), at several heating rate constants in DTG figures. The equation 4.10 is simplified into:

$$\ln \left(\frac{\beta}{T^2} \right) = \left(\frac{-E_a}{RTf(\alpha)} \right) + \ln \frac{AR}{E} \dots\dots\dots 4-21$$

The $\left(\frac{-E}{Rf(\alpha)} \right)$ value is the slope of $\ln \left(\frac{\beta}{T^2} \right)$ to $1/T$.

4.2.2.5. Friedman model

The Friedman method applies iso-thermal data from multiple constant heating rate curves corresponding to the same temperature. The equation 4-2 and 4-3 in its natural logarithmic function becomes

$$\ln\left(\frac{d\alpha(T)}{dT}\right) = \ln(A f(\alpha(T)) - \frac{E_a}{RT} \dots\dots\dots 4-22$$

At a chosen temperature, the plot of $\ln\left(\frac{d\alpha(T)}{dT}\right)$ versus $1/T$ at several constant heating rates data gives the slope of $-\frac{E_a}{R}$.

4.3. Experimental materials and methods

4.3.1. Materials and equipment

Five CGW pellet samples and the coconut shell biochar used for the blend pellets were analysed using a thermogravimetric analyzer, the TGA Q500 (Fig 4.2). The pellet samples were the 100% CGW pellet (CGW100), 95%CGW-5% biochar pellet (CGW95), 90%CGW-10% biochar pellet (CGW90), 85%CGW-15% biochar pellet (CGW85) and 80%CGW-20% biochar pellet (CGW80). Described in the Chapter 3, the elemental properties of the fuel pellet and the biochar material samples are presented in Table 3.8. This TGA combustion testing used a cut piece of pellet sample placed in a platinum pan. Each run required an initial weight of about 50 mg sample.



Figure 4.2: Thermogravimetric Analyzer

4.3.2. Method

Samples were heated to the maximum temperature of 1000°C. The heating rates were 5°C/min, 10°C/min, 15°C/min and 20°C/min. Air was used as the carrier gas with the flow rate at 20 mL/min. The mass changes were recorded in a computer connected to the TG Analyser.

4.3.3. Data treatments

The recorded data were analysed with the universal software V4.5A. The result can be obtained in the form of the remaining masses or processed into the derivatives. To reduce the noise data, the moving average trend lines were used. This method is often applied in the data analyses of TGA studies (Idris *et al.*, 2012; Yi *et al.*, 2013; Vhathvarothai *et al.*, 2014b; Lu & Chen, 2015).

4.3.4. Thermo-kinetic model analyses

Adapted for the thermo-kinetic analyses of CGW100, CGW95 and CGW90 pellets, the approaches were Kissinger-Akihara-Sunose (KAS) model. The equation 4-21 was used for the calculation. This model takes an iso-conversion point of the DTG curves for calculation. In this study, the temperatures at $\alpha = 50\%$ conversion were applied to the model. The Kissinger model were not used here, as the peaks were not in a logarithmic relationship.

For CGW85 and CGW80, as having multistage reactions, the Kissinger model which is based on the reactions peaks was employed (Equation 4-20). Having two peaks of reaction, the results of data analyses would also yield two data sets of activation energies and pre-exponential factors.

4.3.5. Ignition and burnout temperatures

The ignition temperature is the minimum temperature at which a fuel ignites spontaneously without any external source of ignition; while the burnout temperature indicates the maximum temperature of the fuel at which the sample is almost completely consumed during burning (Lu & Chen, 2015). There are several methods of determining ignition and burnout temperatures of the fuel. Those are intersection method, conversion method and deviation method. Further description of those methods has been reviewed by Lu and Chen (2015). In ensuing this study, the intersection method was applied, obtained from the TGA and DTG combustion curves at constant heating rate of 20°C/min. The ignition and the burnout temperatures are

defined in Figure 4.3. The determination of the burnout temperature of a fuel which has only one peak was based on the tangent of that peak to the steady point.

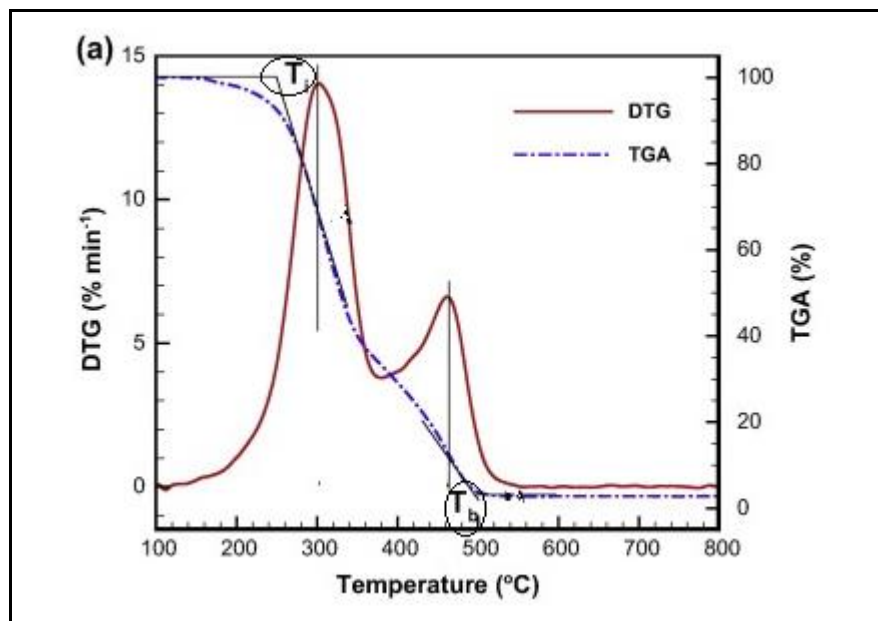


Figure 4.3 Determination of ignition (T_i) and burnout (T_b) temperatures method (Lu & Chen, 2015)

4.4. Results and discussions

4.4.1. Thermal combustion behaviour of CGW100 pellet and coconut shell biochar

In general, there are three phases in the thermal decomposition of biomass during combustion. The first is the release of water or drying stage. This occurs in the temperature up to 150°C. The second is a fastest release of the volatile content, namely oxidative pyrolysis, which can occur at different temperature, specific for each material and its composition. Next stage is a slow volatile release counted with char heterogeneous reaction as indicated by the slow decomposition rate (Idris *et al.*, 2012). The first drying stage will be not discussed here, as the main concern of this study is the combustion process. The decomposition of dry solid happens in the following steps.

Fig 4.4 shows the thermal decomposition (TG) of CGW100 pellet and its derivative (DTG). The TG curve shows the mass losses along the reaction temperatures, while the DTG curve shows the rate of reactivity (da/dt) of the mass change versus the reaction temperatures. The combustion properties that can be derived from this figure are 1) the ignition point (T_i), 2) the maximum rate of reactivity (r_{max}), 3) peak temperature (T_{max}) and 4) burnout temperature (T_b). The ignition point shows how easily a particular fuel can be ignited. It is defined by the starting point of

a sudden change in the weight loss. The maximum rate of reactivity is the peak point as noticed in the DTG curve. The peak temperature is the corresponding temperature at the maximum reactivity. Low peak temperature means that the fuel is easier to combust.

The combustion properties of the CGW100 pellet from the 20°C/min heating rate figure (Fig 4.4) were then found to be: 1) the ignition point was at 287°C; 2) the maximum conversion rate was 92.7%/min at 3) the maximum temperature of 320.2°C as indicated by the peak point of the DTG curve, 4) burnout temperature was at 358°C.

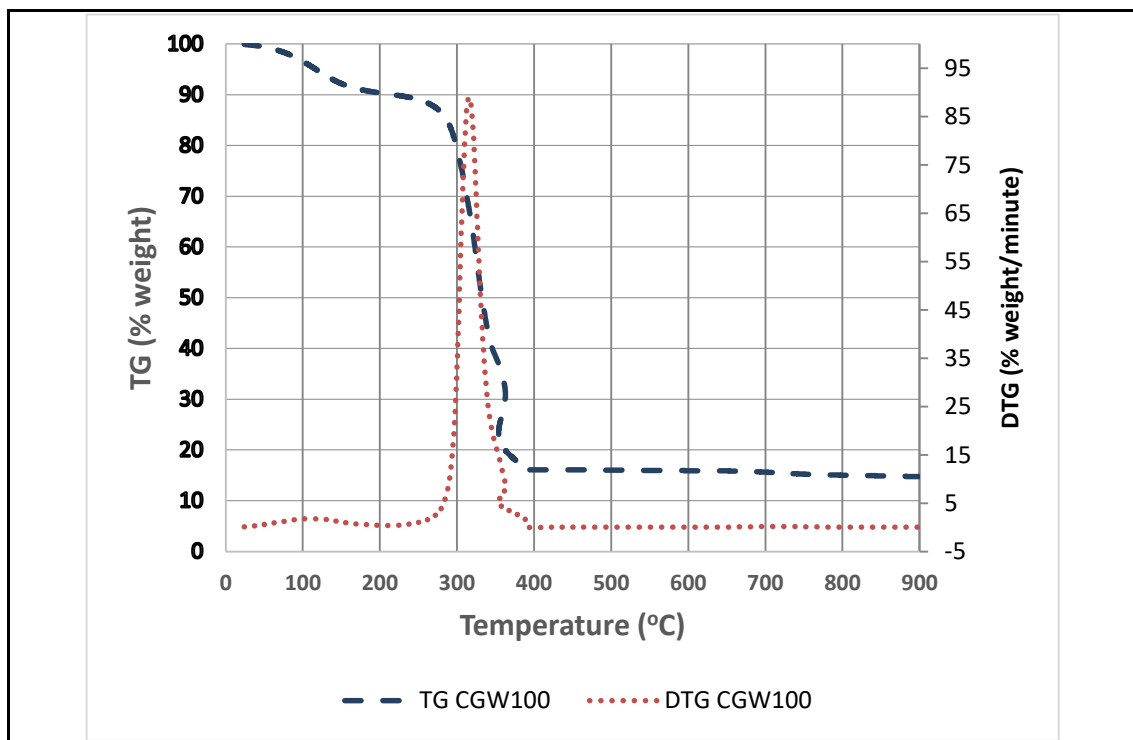


Figure 4.4: Thermogravimetric (TG) and derivatives thermogravimetric (DTG) curves of CGW100 pellet combustion at heating rate 20°C/min

An evidence in literature shows that applying a heat to the non-woody type biomass, such as CGW in our study, results in higher mass loss and a slightly lower temperature than in the case of woody biomass (Rodriguez Alonso *et al.*, 2016). They found that the polysaccharides of wheat straw and miscanthus, the non-woody type, degraded at the same temperature of 260°C and finished at 280 and 300°C, respectively. On the other hand, the polysaccharides of wood still resisted to degrade at 300°C. In addition, woody biomass has higher crystalline cellulose, hence it is less reactive than non-woody.

The thermal decomposition of the individual biochar, used for the blend material, and its derivative curve are shown as in Figure 4.5. From this figure, it can be seen that the ignition point of the biochar was at 500°C, significantly higher than of the CGW pellet. The maximum conversion rate was 20.9%/min at the maximum temperature of 554.4°C. The burnout temperature was at 598°C.

In general, the biochar has higher ignition and burnout temperatures, but lower maximum conversion rate than the biomass thermal properties. This indicates that biochar is much harder to ignite than the cotton gin waste. As a general rule, at a higher temperature, the energy for the reaction is lower than that at the lower temperature. Thus, we expect that the biomass-biochar mixture could impact the extension of the reactions up to the higher temperature, implying some degree of reduction of the reaction energy.

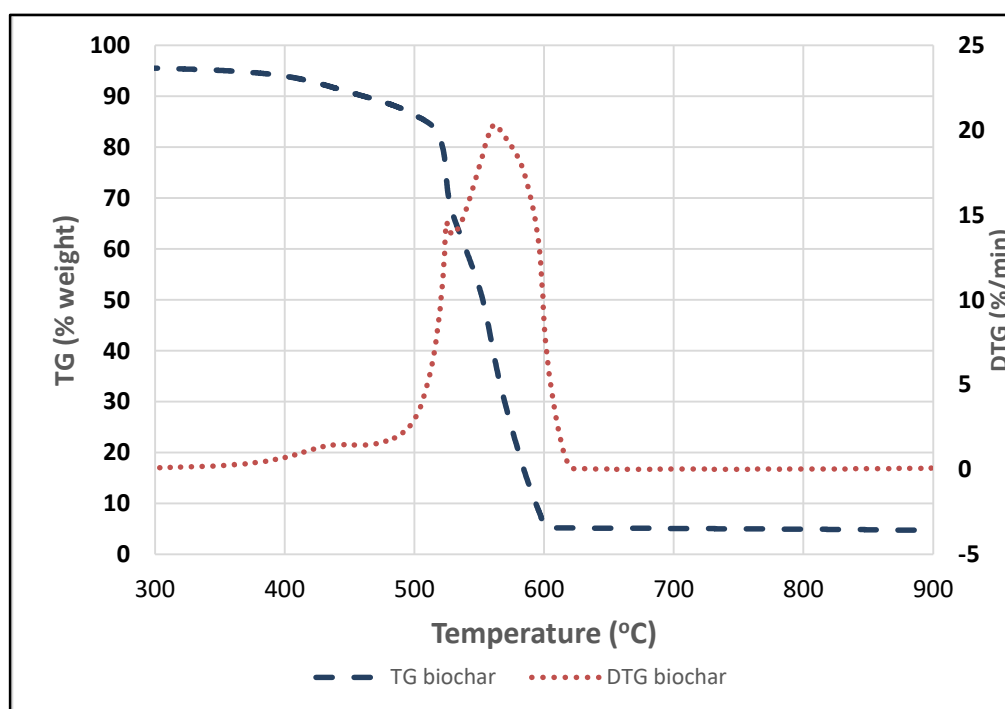


Figure 4.5: Thermogravimetric (TG) and derivatives thermogravimetric (DTG) curves of coconut shell biochar combustion at heating rate 20°C/min

4.4.2. Effect of biochar addition in thermal combustion of CGW pellets

In some recent studies, the biomass was mixed with coal to improve the efficiency of the conversion. Comparing to that of the coal, the biochar might have similar ignition temperature but, generally, biochar has a higher reactivity and low ash content. In this TGA study, the biochar mass loss was up to ~96% (Fig 4.5). Some studies in biomass-coal thermochemical conversion have also suggested applying

middle to low-rank coals as having higher reactivity than high-rank coals (Rizkiana *et al.*, 2014; Tchapda & Pisupati, 2014). By having a high reactivity, the coal/biochar is also expected to react collectively, thus facilitating formation of the products of thermochemical conversion. If synergy occurs, the interaction between coal and biomass could also improve the mixture reactivity resulting in more conversion compared to the conversion of individual components.

As the biochar has higher reactivity than coal, the degree conversion as quantified by gas, liquid and new solid carbon formation would be higher. Then, further extension of the reactions between the products of biomass and biochar is also higher. This can be the result of new heterogeneous reactions (solid carbon, liquid and gasses) as well as homogenous reactions (among gasses). In some cases of biomass-coal conversions, where synergistic effect was not found, the coal and biomass were reacted separately in their individual temperature zones (Idris *et al.*, 2012; Vhathvarothai *et al.*, 2014b). The possibility of interactions between the products of coal and biomass were low due to a wide deference in the rates and/or temperatures of reactions for each biomass and coal.

Figure 4.6 shows the thermogravimetric (TG) combustion of CGW-biochar pellets in comparison to the TG of pure CGW pellet and biochar at a constant heating rate of 20°C/min.

The TG curves of 5% (CGW95) and 10% (CGW90) biochar in CGW pellets are similar to the curve of CGW100 combustion, while the TG curves of 15% (CGW85) and 20% (CGW80) biochar blended pellets are stretched out closer to the biochar decomposition curve. Those two effects of biochar addition to the CGW pellets are described further detail in the following discussions:

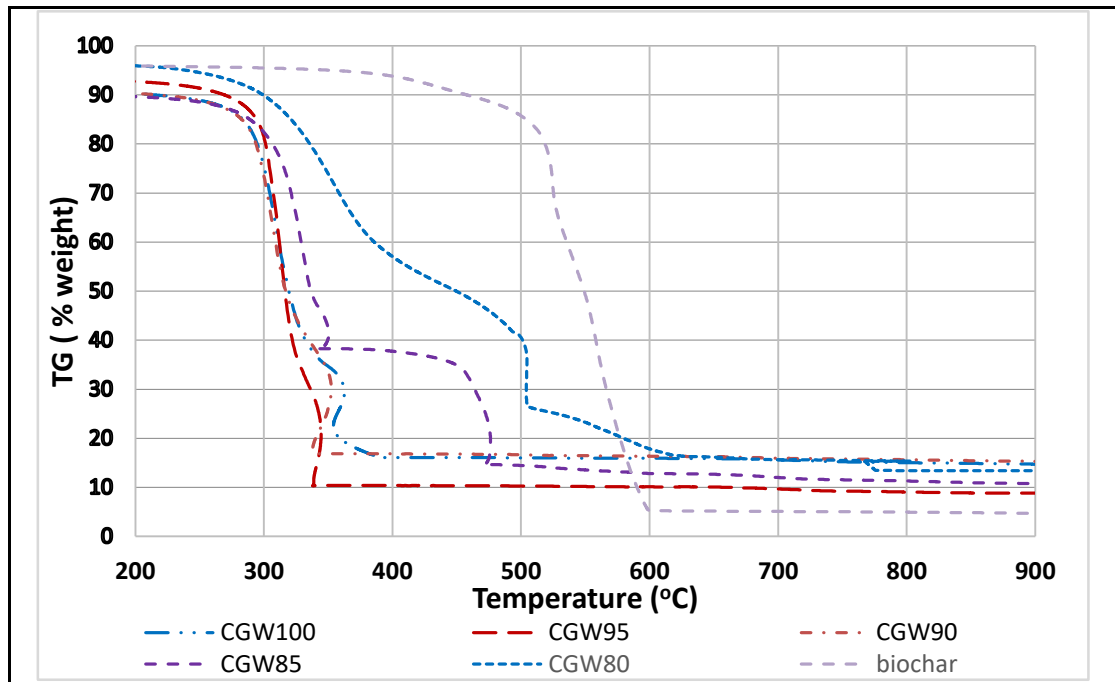


Figure 4.6: Thermogravimetric (TGA) of CGW pellets and biochar curves during combustion at heating rate 20°C/min

- Effect of blending 5% and 10% weight of biochar in CGW pellets

In further tests, the thermal behaviour of 5% biochar (CGW95) and 10% biochar in (CGW90) pellets were compared to the CGW100 pellet and biochar (Figure 4.7). The CGW95 and CGW90 pellets had similar pattern of combustion behaviour with the CGW100 pellet which is faster in burnout at lower temperatures (< 400°C).

In addition to rapid combustion, the maximum conversion rates of CGW95 and CGW90 are faster than CGW 100 (Fig 4.7). Moreover, the burnout points of CGW95 and CGW90 pellets were slightly lower than that of pure CGW pellet. In the blends of biochar up to 10%, then, the biochar could assist in the transfer of the heat to hasten the reaction and hence speed up the burnout. A study in the co-combustion of biomass-low rank coal also shows a slightly low reaction temperature of the low level coal blended with biomass than that of individual biomass combustion; the conversion rate was, however, not increased (Idris *et al.*, 2012)

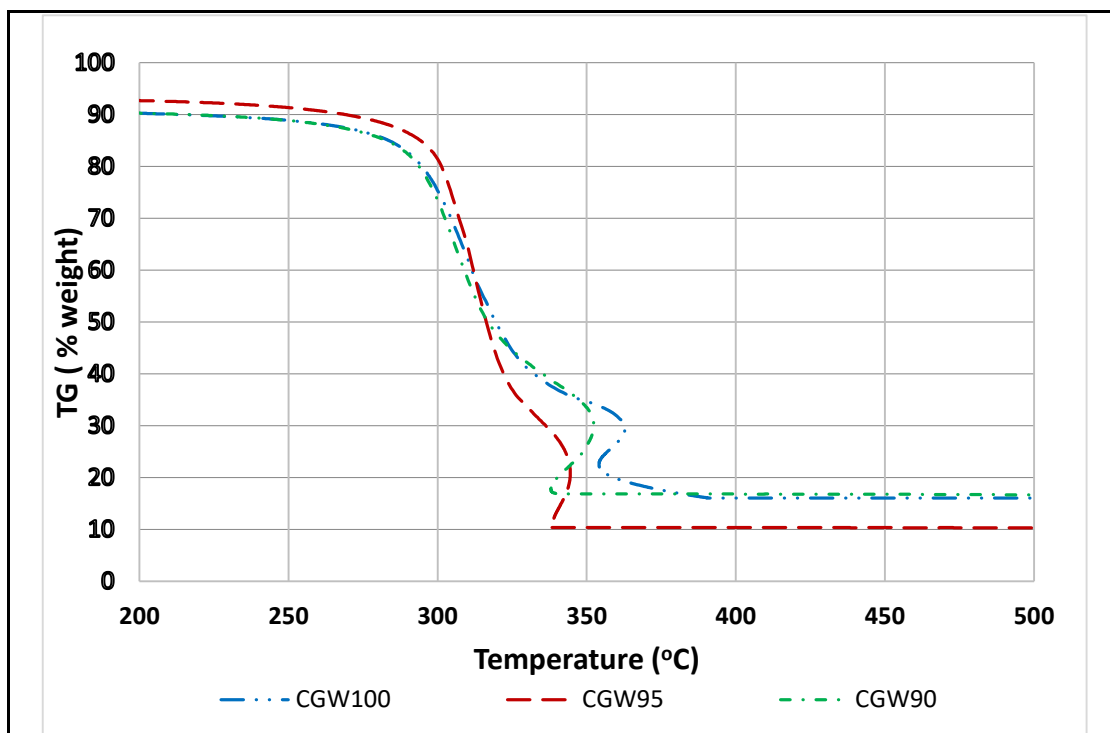


Figure 4.7: Comparisons of weight reductions of CGW100, CGW95, CGW90 pellets during combustion at constant heating rate 20°C/min

A particular observation is noted in TG curves of CGW100, CGW95 and CGW90, a forward wave trend of high increase and reverse back of temperatures occurred here right before the burnout. The samples performed a high heating up and then the cooling before the burnout.

Which air is supplied at constant rate of 20 ml/min, the temperature is also ramped up at a heating rate of 20°C/min. Such a fast heating rate would cause an overlap off all the particle reactions. In other words, a preceding reaction may not be completed yet a new reaction corresponding to immediate reactions take place. These overlapping reactions domains could plausibly be taken as the reason for local temperature reversal, particularly when the heating rate is high. We would expect therefore, a resolution of the overlapping peaks when the heating rate is low. Such fast devolatilization would quickly change of solid biomass into primary low viscosity tar condensate. The behaviour starts when reaching residual mass of about ~30%. The drop in temperatures might be an indication of both the phase change of solid into low density liquid tar as well a consequence of condensation of the primary tars into high density tars.

The phase change of solid sample into some low viscosity tars can be supported by literature. A thermal study of biomass evolution into some acetyl-, methoxyl-,

crystalline and aromatics compounds has been conducted by Rodriguez Alonso *et al.* (2016). In an inert condition and up to temperature of 300°C (heating rate 5°C/min), they investigated the biomass loss using TG analyses coupled with a nuclear magnetic resonance (NMR) to find chemical evolutions during the solid conversion. They reported that the aromatics contained in residual chars at 300°C were more abundant in the wheat straw and miscanthus in comparison to a pine char. The acetyl groups were also faster in release for miscanthus and wheat straw in comparison to the pine's acetyl groups.

Specifically for CGW95 pellet, there was highest mass loss during the conversion. The cooling in sample started at the remaining mass of about 25%. Continuing to reduce, the residual mass of CGW95 is down to about ~10% (Fig 4.7), whilst the remaining masses of CGW100 and CGW90 were about ~18% before the burnout. Beside the effect of heat transfer, blending with the biochar in CGW95 might impact to an extension of chemical reactions and/or more conversions of low density liquid decomposition added to the products of combustion.

The residual mass (ash) at this end of this TGA combustion is also in parallel with the proximate analyses result of ash content (Table 3.10) determined by furnace method. The proximate of CGW95 has the lowest ash as much as 9.2%, whilst the end of TGA combustion (20°C/min heating rate) indicates the mass of ash residue as much as 8.8%.

- *Effect of blending 15% and 20% weight of biochar in CGW pellets*

Different with CGW95 and CGW90 combustion behaviours, the biochar addition of 15% (CGW85) and 20% (CGW80) in CGW pellets shifts the ignition temperature, slightly higher than is CGW100 ignition point. The blends move significantly the burnout temperature closer to the biochar burnout (Fig 4.6). Resulting in slower reduction rates than in the lower level biochar of blended pellets, the TGA figures of CGW85 and CGW80 pellets show a fusion of their fast reaction rates into a multistep decomposition before the burnout (Fig 4.8).

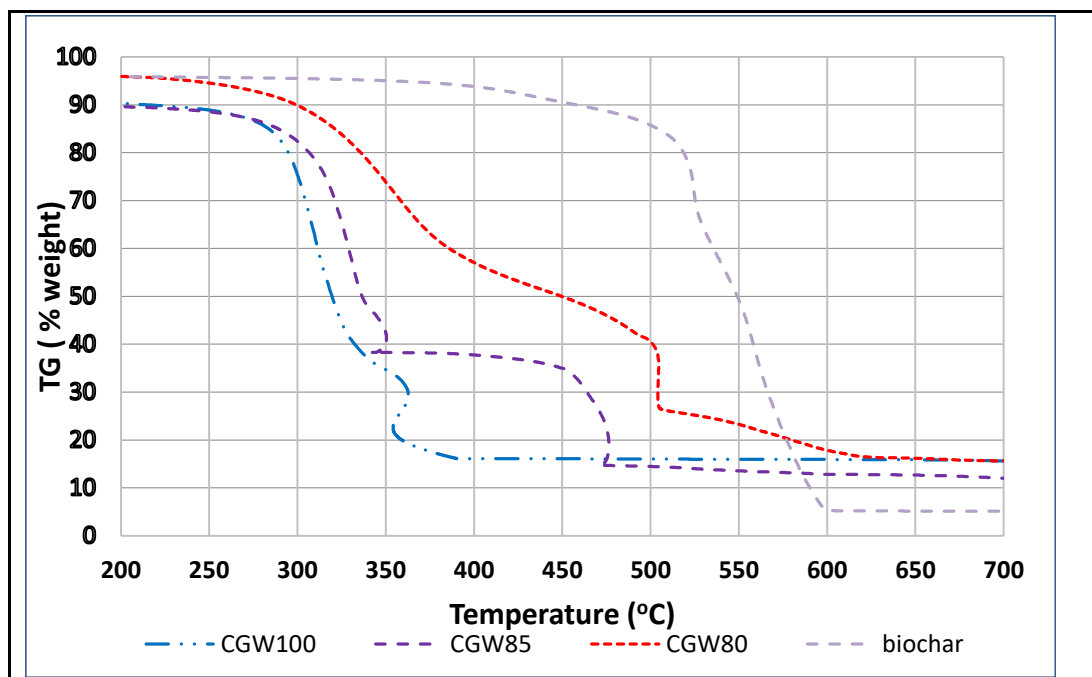


Figure 4.8: Comparison of weight reductions of CGW100, CGW85, CGW80 pellets and biochar during combustion at heating rate 20°C/min

The woody biochar used in our study originates from a raw material with high lignin content. Hence, the resultant form of char has harder walls surrounding a pore structure full of voids. At higher level of biochar content in pellet, this biochar will enter between the essentially fibrous mass structure of the mass of CGW, hindering a fast heat transfer within the structure and hence the slow reduction in mass. These internal pores in biochar might trap the decomposition products (some gasses, primary tars) from the non-woody components and these might be released/liberated later when the biochar was decomposed at higher temperatures.

The TGA CGW85 (Fig 4.8) shows the fast reactions occurred twice, firstly is at a temperature close to CGW100 fast mass reduction zone; and secondly is at a temperature closer to its burning out. The second fast mass reduction started at the remaining mass being about ~ 40% weight. Apparently, in this second fast mass reduction, the high mass conversion of the CGW could initially hold back by the biochar, flared out when the biochar bond ruptures.

The higher biochar content in CGW80 increased the ability to further slow the mass loss (Fig 4.8). Though, once the residual mass reached about ~40%, a fast weight reduction also occurred. The mass of CGW within pellet matrix was slowly converted into light tar which was immediately taken by biochar, and released and burned together with final biochar in burnout.

The phenomenon of having multi-steps of decomposition has also been presented by biomass-coal co-combustion as well. Vhathvarothai *et al.* (2014b) studied the TGA of co-combustion of macadamia nut shell and wood, each of them mixed with 5% to 20% weight of Australian bituminous coal. In all of these degrees of mixing, the DTG curve exhibited two peaks representing ‘individual’ rates of conversion of biomass and coal. In other references, two or three peaks appear TG–DTG analysis of lignocellulosic materials, can be assigned to cellulose, hemicellulose and lignin, indicating that, although there are interactions between fractions, their basic identity is maintained (Ramajo-Escalera *et al.*, 2006; Yu *et al.*, 2017).

In summary, our results found that the biochar addition improved the thermal behavior of CGW pellet fuel combustion. From above results, there were two types of influences of biochar addition to the CGW pellets:

- 1) The first was by addition 5-10% of biochar in CGW pellets. The addition quickened the combustion reaction by slightly lowering the temperatures of fast mass reduction and burnout, as well as increasing the conversion rate.
- 2) The second was that the addition of 15-20% biochar in CGW pellets. The effect slowed the reactions by shifting the combustion reactions to higher temperatures and lowering the rate of conversion.

4.4.3. Effect of heating rates in thermal decomposition of CGW pellets combustion

Figure 4.9 shows the effect of combustion of CGW pellets and the biochar at constant heating rates from 5°C/min to 20°C/min. It can be seen that increasing the heating rates shifts the ignition and burning temperatures higher. This has been described as the effect of ‘thermal lag’ in biomass; that is particles react with delayed response to higher heating rate application (Lu & Chen, 2015).

Of all TG pellets, the cooling before the burnout is more noticeable at low heating rate applications (Fig 4.9). In CGW80, the higher heating rate (15°C/min and 20°C/min) curves do not exhibit this drop in sample temperatures. In particular to the CGW95 decomposition, the extension of mass cooling before the burnout are persistent in all heating rates, hence the residual masses are consistently low.

Figure 4.10, the DTG curves, show the maximum conversion rate of those CGW pellets by examining the peak points. Those maximal conversion rates (r_{max}) and the

corresponding temperatures of the maximum conversion rate (T_{max}) are tabulated in Table 4.2.

In general, increasing the heating rate would increase the rate of conversion. In particular, for the blends of 5% and 10% biochar, the rise of constant heating rate significantly increases of maximal rates of conversion. At lower biochar level (CGW85), the higher constant heating rate application follows the same rule of increasing the maximal conversion rates. However, increasing the biochar level further (CGW80) and applying higher heating rate would shift the higher rate of conversion to a higher temperature (Fig 4.10).

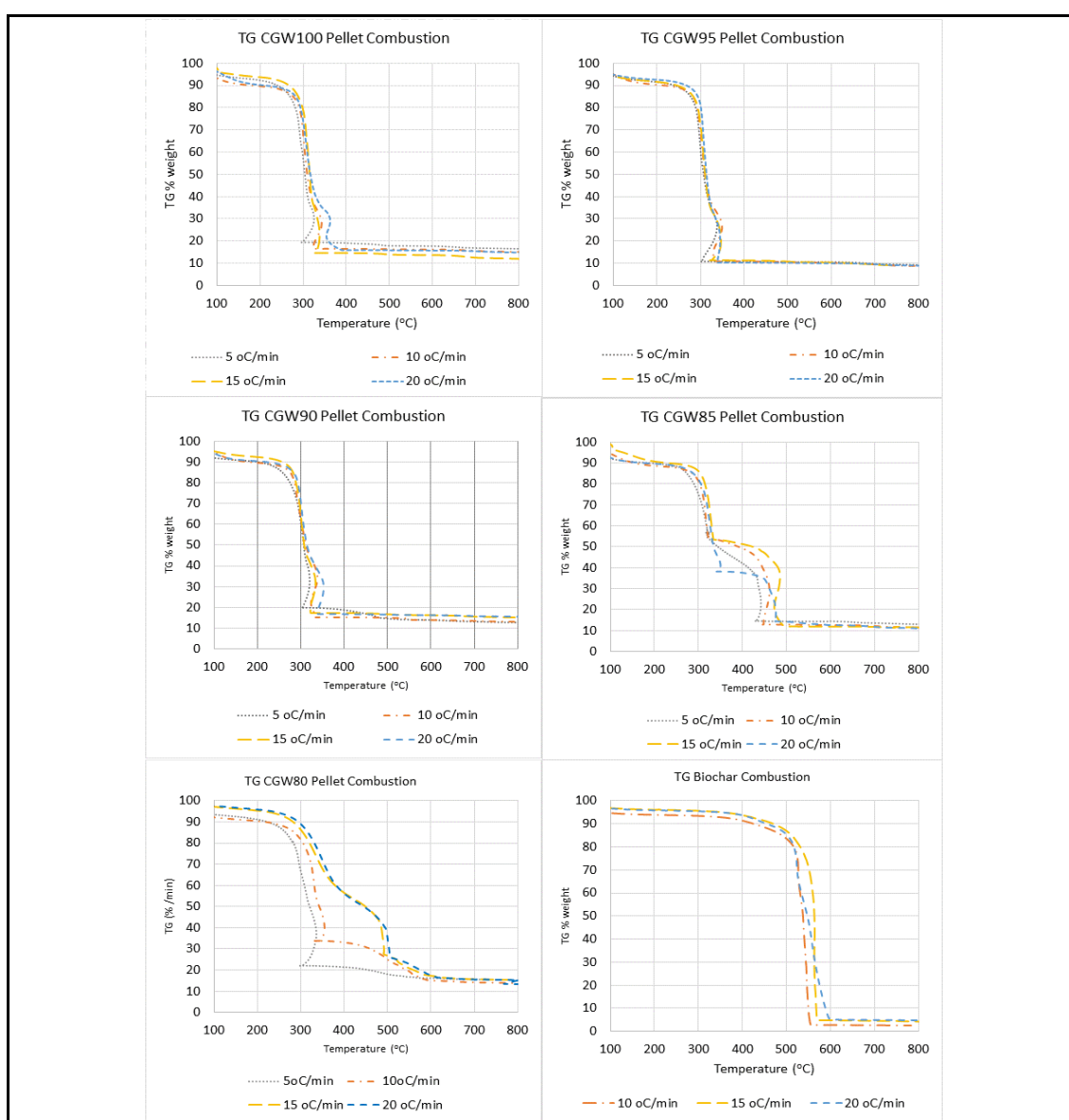


Figure 4.9: Thermogravimetric (TG) curves of CGW100 pellet and CGW-biochar pellets combustion at different heating rates

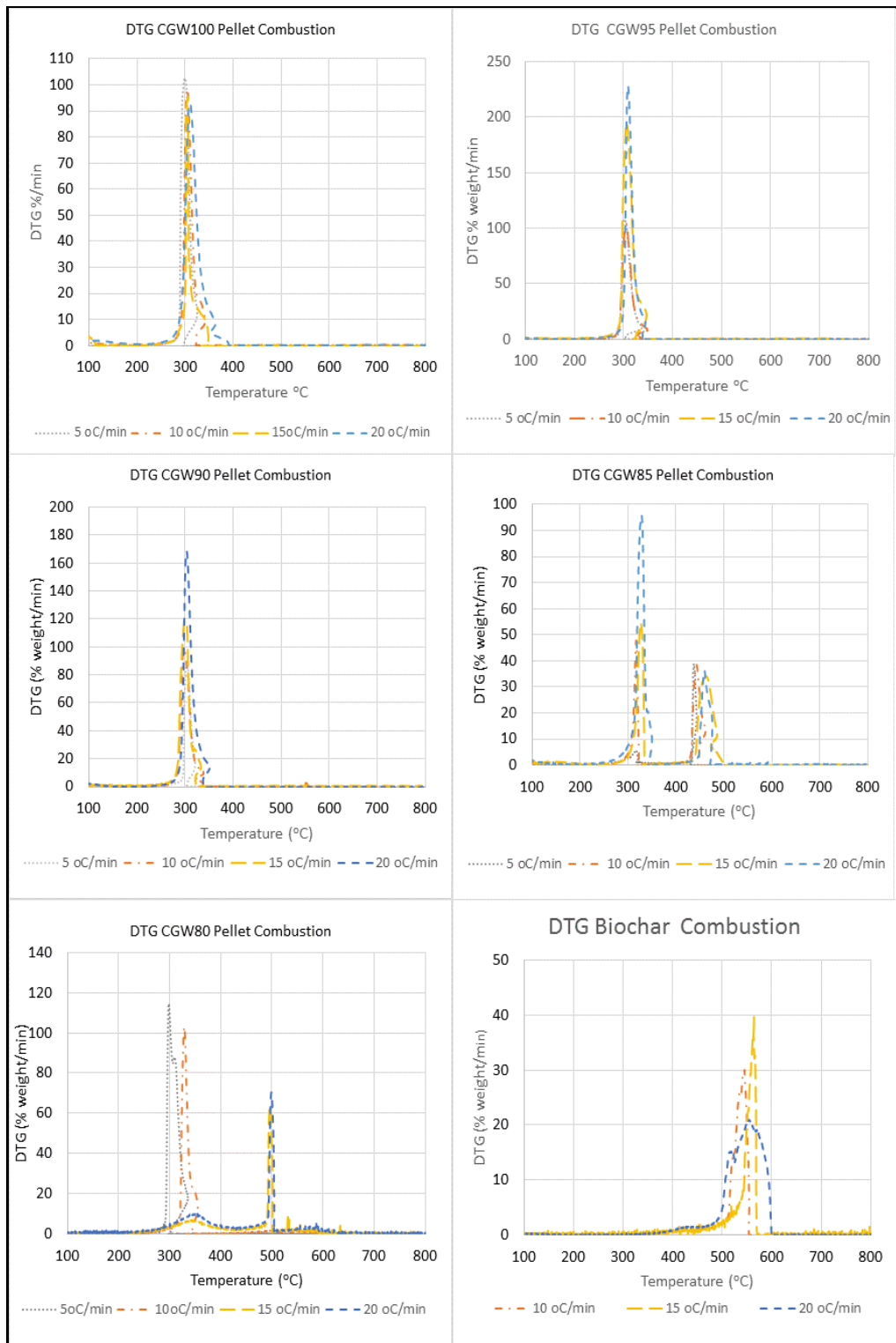


Figure 4.10: Derivative thermogravimetric (DTG) curves of CGW100 Pellet and CGW-biochar pellets combustion at different heating rates

Table 4.2: CGW pellets combustion properties at heating rate 20°C/min.

Sample	Heating rate °C/min	Peak 1		Peak 2		T_i °C	T_b °C
		T_{max} °C	r_{max} % weight/min	T_{max} °C	r_{max} % weight/min		
CGW100	20	310.2	92.7	-	-	287	358
	15	306.3	95.7	-	-		
	10	304.9	98.5	-	-		
	5	299.8	102.8	-	-		
CGW95	20	308.9	228.0	-	-	295	336
	15	306.6	194.6	-	-		
	10	300.5	104.3	-	-		
	5	301.6	108.2	-	-		
CGW90	20	303.8	168.3	-	-	285	338
	15	302.3	118.0	-	-		
	10	298.5	98.3	-	-		
	5	303.6	90.2	-	-		
CGW85	20	328.7	96.0	459.7	36.4	305	480
	15	326.3	54.6	463.2	34.0		
	10	307.0	48.0	433.2	38.6		
	5	306.2	5.7	437.0	39.1		
CGW80	20	354.4	10.3	499.3	70.6	300	510
	15	333.9	6.7	487.0	64.1		
	10	328.8	103.3	489.3	1.4		
	5	298.7	114.7	-	-		
Biochar	20	-	-	554.4	20.9	500	598
	15	-	-	564.7	39.7		
	10	-	-	545.2	30.1		
	5	-	-	517.9	25.9		

r_{max} = Maximum conversion rate

T_i = ignition temperature

T_{max} = temperature at peak point

T_b = burnout temperature

In short, the effect of constant heating rate to the combustion behavior of CGW pellets could be summarized as follow:

- Increasing the constant heating rates shifts the maximum conversion rate to a higher temperature
- In the biochar blended pellets, the increase of heating rate generally increases the maximum conversion rate(r_{max})
- In higher biochar content in pellet, that the effect of higher heating rate increases the maximum conversion will shift to occur only at higher reaction temperatures (second fast reduction zone).

4.4.4. Thermo-kinetics combustion of CGW pellets

Following the Theoretical kinetic analyses (Section 4.2), the reactions models can be assumed to follow the Arrhenius equation (Equation 4-3) which is a formula for the temperature dependence of reaction rates (Laidler, 1987). Arrhenius believed that for reactants to transform into products, they must first acquire a minimum amount of energy, called the activation energy. At an absolute temperature T , at fraction of molecules with their kinetic energy greater than activation energy can change into product of the reaction. Arrhenius provided a physical justification and interpretation for the formula. Currently, it is often seen as an empirical relationship (Laidler, 1987; Vyazovkin, 2006).

The collision theory states that, in order to reactive molecules must first collide. The reactant molecules must get closer than a certain distance (Laidler, 1987). This molecular distances are, however, difficult to measure.

In the Arrhenius theory, the pre-exponential factor, A , can be re-interpreted as the number of collisions per second occurring with the proper orientation to react. Then, it can also be called as a frequency factor. The pre-exponential factor, A , is a constant that can be derived experimentally or numerically from a regression data (Vyazovkin, 2006).

The approximation methods of calculating of the E_a and A from experimental data have been described in Section 4.2. Table 4.3 shows the results of empirical calculation of activation energy, E_a and the pre-exponential factor A based on KAS (equation 4.21) and Kissinger models (Equation 4.20). The Kissinger relates the data of temperatures at the maximum reaction rate points in some heating rate constant curves. Therefore, it approximates the maximum activation energy required for the reactions. The Kissinger model has been extended to the KAS model, in which the calculation based on the iso-conversion.

In combustion, the instantaneous products of reactions often influence the noise data of residual mass in TGA data. Sometimes, the employed data points do not have a good correlation with constant heating rates for calculation the kinetic triplets. Fortunately, the free methods provide several options to approximate the reaction data, $f(\alpha)$ to the constant heating rates (β). The Kissinger model is used to calculate the kinetic triplets of CGW85 and CGW80. This model has been firstly used to calculate the CGW100, CGW95, and CGW90 pellets properties as well. However, the temperature maximal points of reactions were not related in the logarithmic form as

defined in the models. Then, instead of the Kissinger model, the KAS was used for this case, using the data points of 50% conversion ($\alpha=0.5$) as the basis for calculation.

The CGW85 and CGW80 pellets had multi stage reactions. Most of the studies resulted in this case have suggested applying multi step calculations of their activation energy values as well (Vyazovkin, 2006; Idris *et al.*, 2012). Therefore, the analyses are divided based on the number of peaks in the corresponding DTG curve. The Kissinger method was used to relate the peak points for each stage of the reaction. At the end, the one with the highest value of activation energy is determined as the energy required for the overall stages of the combustion reaction.

Table 4.3: Activation energy and pre-exponential factor of combustion CGW pellets

Sample	Empirical				Calculation
	Peak 1		Peak 2		E_{a-indw}
	E_a	A	E_a	A	
	<i>kJ/mol</i>	<i>(1/s)</i>	<i>kJ/mol</i>	<i>(1/s)</i>	<i>kJ/mol</i>
CGW100	203.72	2.4E+16	-	-	203.72
CGW95	173.19	4.9E+13	-	-	200.39
CGW90	173.81	6.0E+13	-	-	197.05
CGW85	117.88	1.4E+19	176.05	3.8E+10	193.72
CGW80	66.17	2.3E+03	169.80	3.3E+09	190.39
Biochar	-	-	137.07	1.1E+05	137.07
	-	-			

E_{a-indw} = Activation energy calculated from weighting factors

E_a and A = Experimental calculation of activation energy and pre-exponential factor

The activation energy of CGW100 is individually higher than biochar (Table 4.3). Without any synergy interaction, the increase of biochar in CGW pellets will reduce theoretical (E_{a-indw}) activation energy of the original CGW. The meaning of it is that, basically, the combination CGW-biochar lowers the energy required for combustion reaction activities (Table 4.3). This can be a benefit of blending the biomass with biochar instead of coal which generally has higher activation energy than the biomass itself.

Investigating the experimental data (Table 4.3), the additions of 5% and 10% biochar, theoretically and experimentally, lower the activation energies. The CGW80 and CGW85 have fast reaction rates in slightly higher temperatures than CGW100 reaction; the conversions were also segmented into two steps in which the second group of reactions occurs at higher temperatures. As to the reactions theory, the activation energy of a multi steps reaction is determined by the highest value of their energy. Then, the values of both CGW85 and CGW80 activation energies are here defined from their second peak values. Overall, Table 4.3 shows that the activation energies of all blended pellets are about the same as much as ~170 kJ/mol, while the pure CGW pellet is higher as much as 204 kJ/mol. As for comparison, the values for activation energy of sugarcane bagasse and cypress wood chip combustion are reported as much as ~ 210 kJ/mol and ~140 kJ/mol, respectively (Ramajo-Escalera *et al.*, 2006; Vhathvarothai *et al.*, 2014b).

4.4.5. Synergistic in co-combustion

The synergistic occurrence in the co-combustion can be interpreted as the interaction between components of the fuels by which the co-combustion has a characteristic of lower energy of the reactions and/or getting increase in the reactivity. In the case of energy reduction in reaction, it acts similar to the “catalyst function”. It only helps to reduce the energy for the combustion reactions, hence, it increases the reactivity compared to the individual fuel combustion. From Table 4.3, it can be seen that higher reactivity is noticeable in the co-blended pellets, particularly at higher constant heating rate application. Therefore, the interaction between the co-blended fuels here is apparently from the heat activity to reduce the energy; hence it facilitates more reactions of combustion.

It has previously referred to the theory that the mineral matters in non-woody fuel can act as natural catalyst to increase the product of co-combustion. The amount of mineral, however, should be sufficient enough to perform the catalytic reactions. Within the natural composition of minerals inside the fuel, the composition of mineral catalyst and the pre-conditions of such catalytic reactions would be difficult to control in contrast to the external addition of catalyst minerals. Thus, this catalytic reactions contribution would be lesser than the heat transfer effect in the co-conversion.

As to effect of heat transfer in the co-blended fuel can reduce the energy for reactions, Vhathvarothai *et al.* (2014b) proposed to compare the activation energy

calculation (E_{a-indw}) with the activation energy from empirical data for the insight whether the co-blended fuel could result in the synergistic occurrence. The E_{a-indw} is calculated based on the portion of activation energies of CGW and biochar in the pellet mixtures:

$$E_{a-indw} = m_b E_b + m_c E_c \dots\dots\dots 4-23$$

- where E_b = Activation energy of biomass (J/mol)
- E_c = Activation energy of biochar (J/mol)
- m_b = Mass fraction of biomass in pellet mixture
- m_c = Mass fraction of biochar in pellet mixture

The calculated E_{a-indw} data are also presented in Table 4.3. The data (Table 4.3 and Fig 4.11) show that the experimental activation energy of all the blended biochar CGW pellets have lower values than those obtained from the proportional calculation one. The coefficient correlation of factual and predicted data is as much as 0.77, higher than 10% of the confidence level of statistical cut off. From these figures, it can be concluded that all biochar blending treatment pellets result in synergy of co-combustion (Fig 4.11).

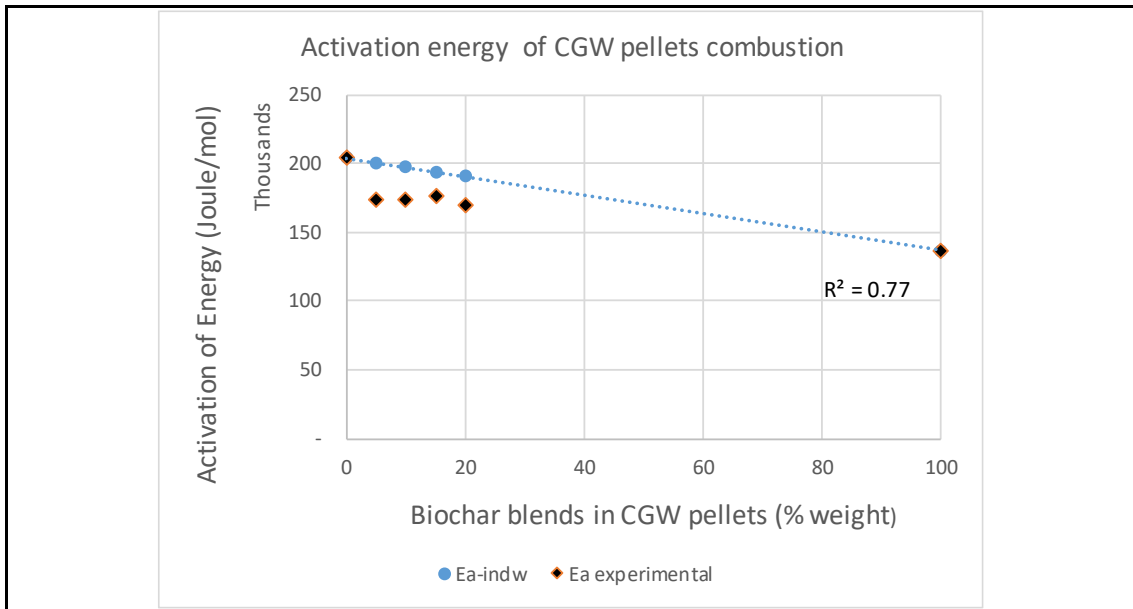


Figure 4.11: Comparison of activation energy values of pellets combustion from empirical kinetic and calculation

The synergy in the CGW95 and CGW90 pellet co-combustion was by higher maximum reactivity, particularly faster demonstrated at the constant heating of 15-20°C/min. Their maximum reactivity could reach a double of the unblended pellet. The synergy in CGW85 and CGW80 pellets could also be detected from the occurrence of two steps reaction in their co-combustion, resulting in the lower activation energies (Fig 4.11).

Idris *et al.* (2012) proposed a method of examining the occurrence of synergistic effect in co-combustion by examining the ash content from the empirical data compared to the predictive data based on the weight proportion as in equation 4-24. The rationale is that the ash is the residue of combustion, then the lower the residue, the higher the conversion.

$$Y_{blend} = m_b Y_b + m_c Y_c \dots\dots\dots 4-24$$

where Y_b = ash content of biomass (%)

Y_c = ash content of biochar (%)

m_b = Mass fraction of biomass in pellet mixture

m_c = Mass fraction of biochar in pellet mixture

Figure 4.12 shows the ash composition of each pellet and the predicted values of ash yield based the weight proportion of each CGW and biochar composition in pellets. The results show that the ash yield is linearly related to the biochar composition in pellets. However, the far lowest experiment ash yield was obtained from CGW95 and its value lays much below the predicted figure. It can be confirmed using this ash yield examination method that though all the blended pellets had lower ash yield than expected calculation, the highest possibility of synergistic occurrence in co-combustion was from the CGW95 pellet.

In contrast to this CGW-biochar co-conversion, other studies resulted in no synergistic with coals of higher ash than biochar ash in our study (Chen & Wu, 2009; Gil *et al.*, 2010; Vhathvarothai *et al.*, 2014b). Idris *et al.* (2012) studied the co-combustion of coal with high volatile content of coal (Mukah Balingian coal) and oil palm waste residues in the blends of 0-100% weight. No synergy effect was found in the co-combustion. This might come from the ash mineral content in the mixture that could inhibit the synergistic effect, such as silicate compound (Masnadi *et al.*, 2014). Alternatively, the amount of coal added was beyond the study scope.

Similar to our study using biochar as the co-blended material, a study of co-combustion biomass (ramie residue) and its biochar had also been conducted by Yi *et al.* (2013) with the blends of biochar ranging from 10-70%. They found that 10-30% mass of biochar had higher reactivity than individual mass conversion, while higher than 30% tended to result in more un-combusted char than individual conversion.

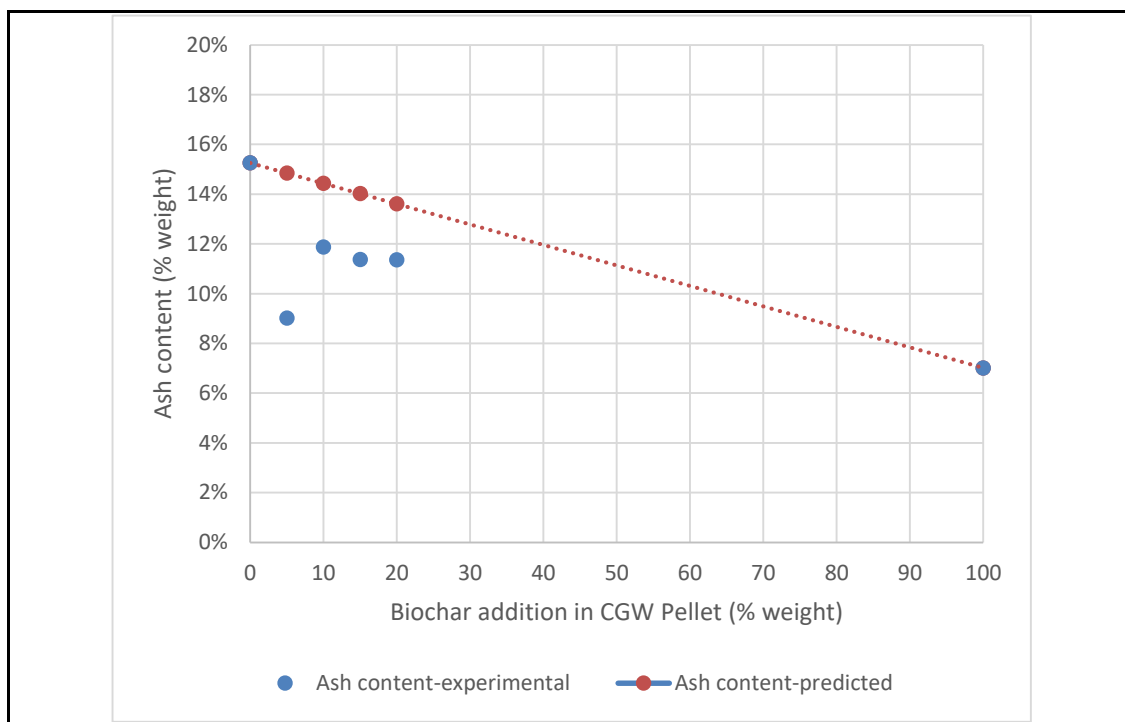


Figure 4.12: Comparison of ash yield of CGW pellets combustion from experimental and predicted based on individual weight proportion

4.5. Summary and conclusion

The behaviour of non-woody CGW pellets was investigated in a TG analyses using air as the media for combustion and gas carrier. Blending the CGW with biochar up to 20% w/w resulted in improvement of combustion behaviour.

Originating from a material with low lignin content, the pure CGW was fast in reduction at oxidative pyrolysis zone. The burnout temperature was about $\sim 350^{\circ}\text{C}$. Addition of 5-10% of biochar in CGW pellet transferred the heat of the biochar to significantly combust the mass faster by slightly lowering the temperatures of fast oxidative pyrolysis reactions and the burnout. On the other hand, addition of 15-20% biochar slowed the rates of combustion delaying the burnout close to the temperature of biochar ignition. The mechanism of slowing the reduction was by having multi-steps of fast reductions; the reactions were distributed to higher temperatures.

Using air at flowrate 20 ml/min as the media of combustion and gas carrier, the TGA of CGW100 presents a cooling phase in the sample right before the burnout. This could be examined as changes of solid into condense tars which have low density and viscosity such as aromatics. Condensation of these low aromatics in primary char into secondary high molecular weight tar requires energy which is consumed as it. In the process of subsequent condensation, water is liberated. This condition occurs in all pellets particularly when applying low constant heating rate combustion. In particular, addition of 5% biochar extended this cooling phase, resulting in the lowest residual mass of solid (ash). This can be interpreted that there was further chemical reactions, beside the heat transfer effect, to result in the highest conversion of CGW95 pellet.

The activation energy and pre-exponential factor for each treatment pellet were approached using Kissinger and Kissinger corrected (KAS) models. The activation energy of the blended fuel was reduced proportionally to the increase of biochar in the composition. The CGW100 had combustion activation energy of 204 kJ/mol, while the blended CGW-biochar pellets had the activation energy at about ~170 kJ/mol. Synergy effect in all pellets were confirmed by methods proposed by other researchers that are comparing the activation energies and ashes of experimental results with the theoretical calculations proportionally based on the individual component. The synergy was further confirmed by having obtained results which were all below those expected by theory.

CHAPTER 5: Thermo-kinetic Behaviour of CGW Pellets in Pyrolysis

Abstract

Cotton gin waste with the blends of 0-20% biochar in pellets was developed. The pellets thermos-kinetics in pyrolysis were studied using thermogravimetric analyses (TGA). The heating rates were respectively 10°C/min, 15°C/min, and 20°C/min; and the gas carrier was nitrogen at a constant flowrate 40 mL/min. This study aimed to determine the kinetics properties of the developed CGW pellets as well as to investigate the effect of biochar blends in the pellets on the pyrolysis behaviour. It was found that all these pellets demonstrated three phases of dehydration, devolatilization and char reduction during the process of pyrolysis. It was also found that the devolatilization of CGW-biochar blends had similar behavior with the unblended CGW pellet. The high rate of conversion in the devolatilization mainly occurred in the temperature zone of 200-350°C. Calculated using Kissinger model, the activation energy of the CGW pellets were found to be between 100 and 132 kJ/mol. The activation energies of empirical data agreed well with the values of the prediction based on the weighting factors with the correlation coefficient of 0.90. It was found that a slight synergism occurred in the co-pyrolysis of CGW95 pellet. This was indicated by higher conversions of CGW95 than the CGW100 in all heating rate treatments.

Keywords: TGA, Pyrolysis, fuel pellet, cotton gin waste, co-blended, biochar

5.1. Introduction

Previous chapter reported on the investigation into the thermo-kinetics of combustion through thermogravimetric analyses of the developed CGW pellets. This chapter discusses the thermo-kinetics of pyrolysis of the developed CGW fuel pellets.

Studies on the biomass and coal pyrolysis have been undertaken by a number of researchers (Idris *et al.*, 2010; Vhathvarothai *et al.*, 2014a; Wei *et al.*, 2017). These studies were conducted mostly on small lab scale equipment and were usually focused on kinetic behavior of a fuel during the thermochemical conversions. Thermogravimetric analyses (TGA) on small equipment, mimicking the plant scale, were often used. Most of the lab scale studies were carried out in order to find the values of reactivity or the thermo-kinetics behavior of a particular matter as to the effect of heat in a given time period. The thermal decomposition of fuel and the products of degradation were examined. Particular to the blending fuels, the studies also reported whether the co-pyrolysis of the blending materials led to an increase in

the conversion activity (synergistic occurrence). The pyrolysis of individual components was carried out for parallel results.

Some studies reported no synergistic occurrences in co-pyrolysis of biomass and coal (Idris *et al.*, 2010; Vhathvarothai *et al.*, 2014a). Other investigations, however, reported the existence of such synergistic effects (Jones *et al.*, 2005; Zhang *et al.*, 2016). Although no synergistic occurrence was found in a treatment application (heating rates, mass of testing, equipment); it may be possible that the synergy may take place in other specification of treatment.

The gasification, which involves pyrolysis in its prior stage, may require a certain co-pyrolysis condition to significantly impact the process of co-gasification. Zhu *et al.* (2008) reported no synergistic occurrence in all their co-pyrolysis treatments of coal-wheat straw blends. However, potassium content in their co-pyrolysis chars were examined and it was found that the highest potassium levels were in the char of pyrolysis temperature at 750°C compared to K content of chars at 650°C and 850°C. When applying gasification at 900°C to each pyrolysis char, they found that this highest potassium content char from the pyrolysis of 750°C had also the highest char reactivity. It was thus concluded that the potentially catalytic gasification had occurred. Another study (Wei *et al.*, 2017) reported that the coal char from co-pyrolysis with rice straw had more enhanced level of active potassium in the char. When that char was further gasified at a higher gasification temperature, the co-pyrolytic char from rice straw mixture had higher reactivity than the pure coal char. This reactivity increase was due to the combination of carbon structure evolution and active AAEM (alkali and alkaline earth minerals) transformation in the co-pyrolytic char.

The objective of this chapter is to investigate the thermo-kinetic behavior of the CGW pellet in pyrolysis and CGW-biochar pellets in co-pyrolysis using thermogravimetric analysis (TGA). The results of the kinetic properties, such as activation energy and reactivity, were analyzed. Furthermore, the synergistic effects in co-pyrolysis blends of CGW-biochar were also examined. The empirical data obtained from physical, combustion and pyrolysis studies from the chapters 3-5 will be utilised for developing the CFD model and simulations in Chapter 6.

5.2. Material and methods

In this study, the CGW five pellet samples were heated to the maximum temperature of 950°C in the TGA instrument type Q500 (Fig 4.2). The heating rates were 10°C/min, 15°C/min, and 20°C/min, respectively. The pyrolysis was conducted using nitrogen as the carrier gas with a flow rate of 40 ml/min. The mass used in this TGA was about 50 mg.

The distribution of the remaining mass and the derivative of mass loss were obtained to find the reaction rate of the samples during the pyrolysis. The data were analysed using the moving average method to reduce the noise as in Section 4.3.3.

Theoretical models and methods of thermo-kinetic performance were already discussed in the previous chapter (Section 4.2). In this study we applied the model developed by Kissinger (Section 4.2.2.3). The reason for the application of this Kissinger model was that the data of DTG peaks show a close fit to the mathematical model developed by Kissinger.

5.3. Results and discussions

5.3.1. Thermal pyrolysis behaviour of pure CGW pellet and biochar

The pyrolysis of the fuels was examined kinetically from the process of pyrolysis using nitrogen as the gas carrier in the TGA. The heating rates applied were 10°C/min, 15°C/min and 20°C/min. The TG and DTG curves of the CGW100 and biochar at heating rate 15°C/min are shown in Figures 5.1 and 5.2 respectively.

In the process of biomass pyrolysis, three processes are usually involved: including dehydration, devolatilization and solid decomposition. The first stage of dehydration process is mainly moisture loss. The devolatilization is the main part of pyrolysis stage, in which the volatiles are released at a high rate. The remaining mass is solid in the form of char. At the last stage, the solid is continually decomposed but at a slow rate. Figure 5.1 shows that CGW100 pellets examined to follow these three phases. The moisture was released at temperatures of 100-150°C, while the volatiles are released between 200°C to 600°C. Similar results were also found by Masnadi *et al.* (2014). The authors studied the pyrolysis behaviour of switchgrass, resulting in three phases of decomposition of up to 600°C. They increased the heating up to a temperature of 1000°C. A small peak was found at temperature 700°C reported as chars converted into gasses which is supported also by Idris *et al.* (2010) experiments as well.

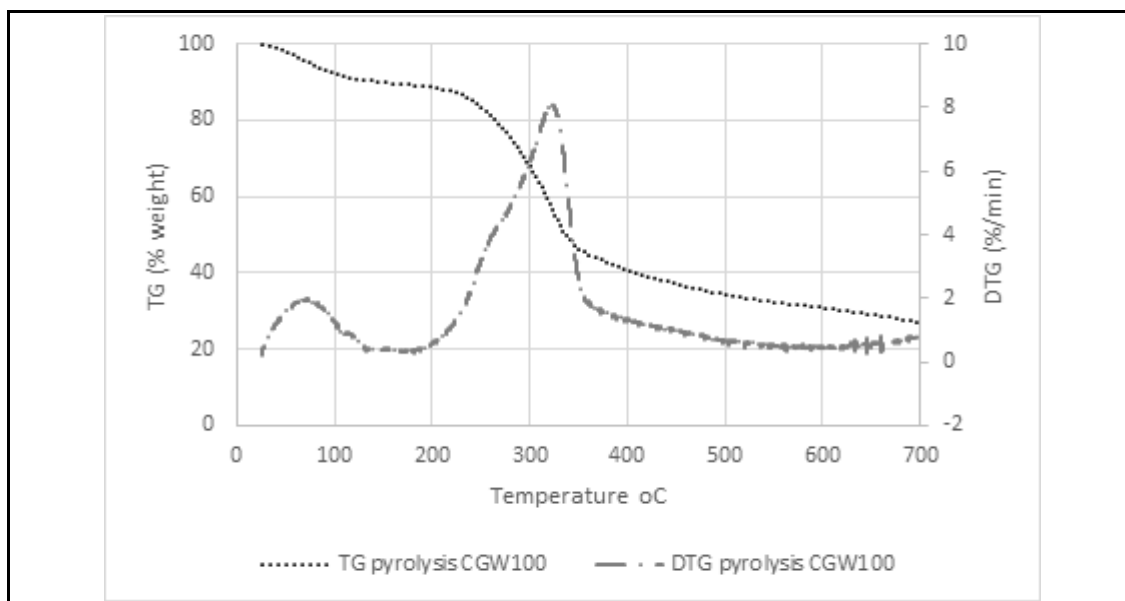


Figure 5.1: Thermogravimetric (TG) and derivatives thermogravimetric (DTG) curves of CGW100 pyrolysis at heating rate 15°C/min

Raveendran *et al.* (1996) conducted TG pyrolysis studies of several biomass types, including cotton gin waste. The behavior of biomass pyrolysis was investigated from their individual component of cellulose, hemicellulose and lignin contents as well as their interactions. They found that the behavior was simply the summative components, without any correlations. According to their general observation, the zonation of biomass contents decomposition could be envisaged, from low to high temperature, as follow: moistures, extractives, hemicellulose, cellulose & lignin and mainly lignin evolutions, respectively. Cotton gin waste with negligible content of lignin, therefore, had only the zonation of fast mass reduction up to the cellulose evolution. The one stage of fast mass reduction in our study (Fig 5.1.) conform to their finding of the only hemicellulose and cellulose evolutions in CGW pyrolysis. The hemicellulose and cellulose are typically devolatilised into condensable group of materials characteristically by a fast mass reduction.

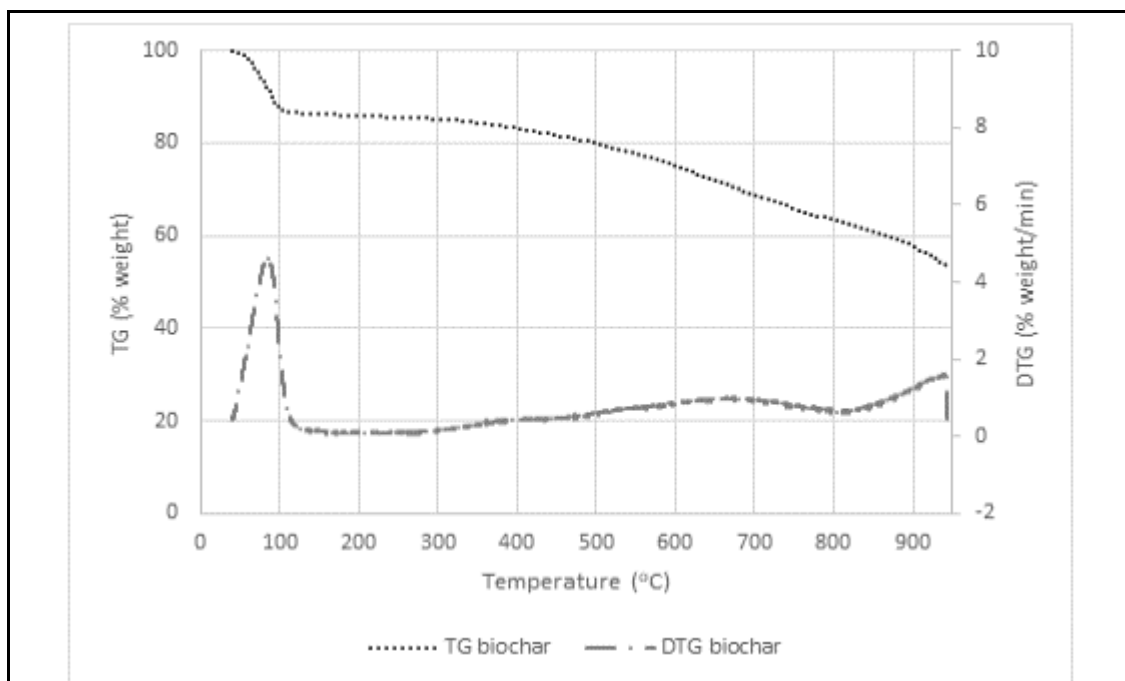


Figure 5.2: : Thermogravimetric (TG) and derivatives thermogravimetric (DTG) curves of biochar pyrolysis at heating rate 15°C/min

It was noted that the TG/DTG curve of coconut biochar used in this study showed a pattern different from the curves of the biomass. The high mass loss was at first stage (dehydration) followed by a slow rate conversion (biochar pyrolysis conversion in Figure 5.2). This result is consistent with the findings in a TGA study of biochar conducted by Nan *et al.* (2016), which showed a quite slowly mass reduction after dehydration. However, their study was only up to 400°C. There was no further information about the behavior past this temperature.

The biochar used in this study originated from woody biomass having higher lignin content than the non-woody type. The second peak of mass reduction for this biochar (Fig 5.2) was laying in temperatures of 500 to 800°C. The maximum conversion rate in this peak is about 1.16 % weight/min. Furthermore, there were a high progress of mass reduction from 800°C upward. This could be the broken of chars walls reduced into gasses.

In other researches, the TG pyrolysis of chars made from torrefied bamboo and pine (Mi *et al.*, 2016), had a maximal conversion rates of about 3.5% weight/min and 5% weight/min, respectively, in the temperature zones of 500-600°C. They found that the volatile was released here before the reductions of chars into gasses. In our study, it was measured as in Table 3.2 that the volatiles and moisture content were 7.3% and 7.4%, respectively. The small content of volatiles in our biochar might also be

liberated in the first zone of dehydration together with moisture release. The evidence was that the mass reduction in this zone was much higher than the amount of moisture content itself. The mass reduction reached about 15%.

As discussed previously, Raveendran *et al.* (1996) reported that the lignin would thermally decompose slowly and at higher temperature than hemicellulose and cellulose. Another pyrolysis study of individual biomass components interpreted that the lignin and xylan are pyrolysed slowly in a longer range of temperature in contrast to cellulose with sharp peak, faster at narrow range temperature (Yu *et al.*, 2017). Our biochar, after the vaporization, shows a low slope of mass reduction. This indicates a mainly char process of reduction having a slow rate of decomposition as the bond structure was originated from lignin.

5.3.2. *Effect of biochar addition in the thermal pyrolysis of CGW-biochar blend pellets*

Figures 5.3 and 5.4 show the TG pyrolysis of CGW-biochar blended pellets in comparison to the pyrolysis of the original materials, CGW100 and the biochar. It can be seen that the blending of biochar up to 20% in the CGW pellets, in general, follows the agreement of less reactivity as to higher biochar composition in pellets. Unlike the behaviour in combustion process, the char blending did not significantly change the pyrolysis performance; it follows the original material behaviour of CGW100.

At first, there was high reactivity from 200-350°C, showing the occurrence of a fast mass reduction of cellulose which mainly contains condensable. According to (Yu *et al.*, 2017), cellulose mainly produces condensable. A gradual reduction was then seen between 350-600°C, indicating the slow phase of pyrolysis. The mass reduction in this zone was mainly detected as xylan and lignin (Yu *et al.*, 2017). Xylan is a group of hemicellulose found in plant cell walls. As this xylan is more ubiquitous than other groups of cellulose, the remaining mass of xylan was mostly decomposed later together with lignin after the degradation of main condensable group of cellulose. As CGW composing a negligible amount of lignin (Raveendran *et al.*, 1996), the slow reduction at this temperature ranges of 350-600°C was mainly the xylan evolution.

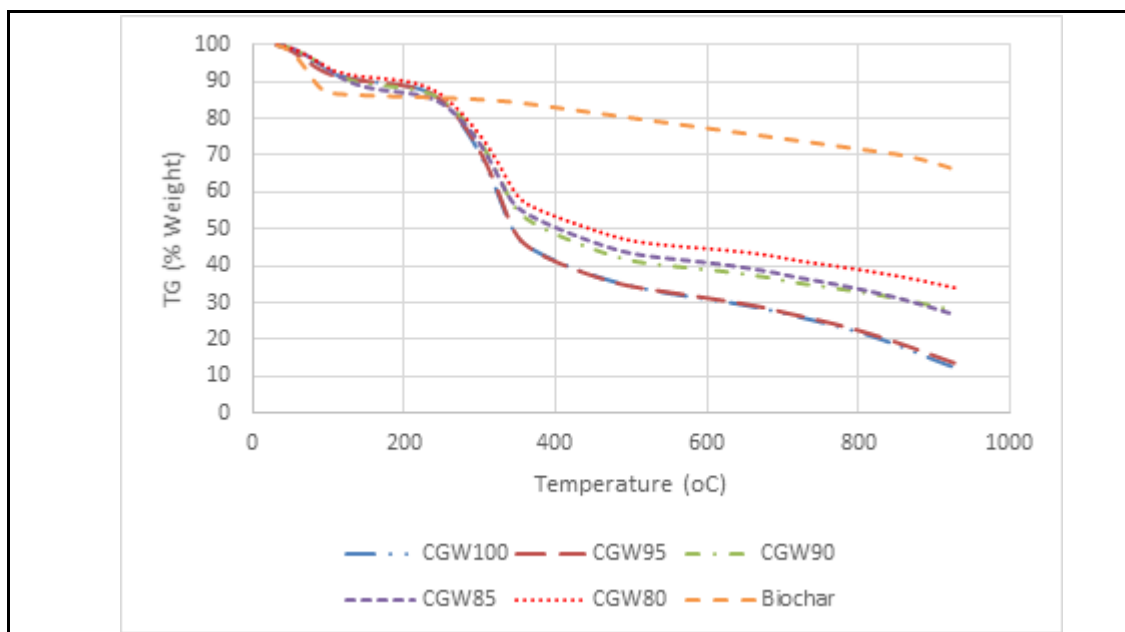


Figure 5.3: Thermogravimetric (TGA) curves of CGW pellets pyrolysis at heating rate 10°C/min, 15°C/min, 20°C/min

Examining further on the pyrolysis stage (200-600°C), the char yields follow general agreement: increase the yields as higher biochar contents in the CGW pellet. However, the TGA curves of the 100% CGW (CGW100) pellet and 95% CGW-5% biochar pellet (CGW95) were nearly overlapped. The peaks of DTG curves for both CGW95 and CGW100 were also nearly coincided (Figure 5.4). Unlike pyrolysis behavior of other blended biochar pellets, the addition of the only 5% biochar in the CGW could increase the rate of conversion. This could be a sign of synergistic occurrence.

Raveendran *et al.* (1995) found that the low ash content significantly influences the higher rate of conversion and lower the initial fast decomposition temperature in pyrolysis. Then, the highest conversion rate in CGW95 was due to the lowest ash content as examined previously in chapters 3 and 4. From the evidence during the combustion tests (Chapter 4), the lowest residual ash in the CGW95 was due to the extension in the cooling stage providing more solid conversion into products. In combustion, this mass reduction occurred at the oxidative pyrolysis zone. Similarly in this inert pyrolysis process, the extension of high mass loss took place also in the similar temperature zone. The high rates of conversion for CGW95 were likely due to the heat transfer from the biochar blended material and/or the presence of chemical interactions.

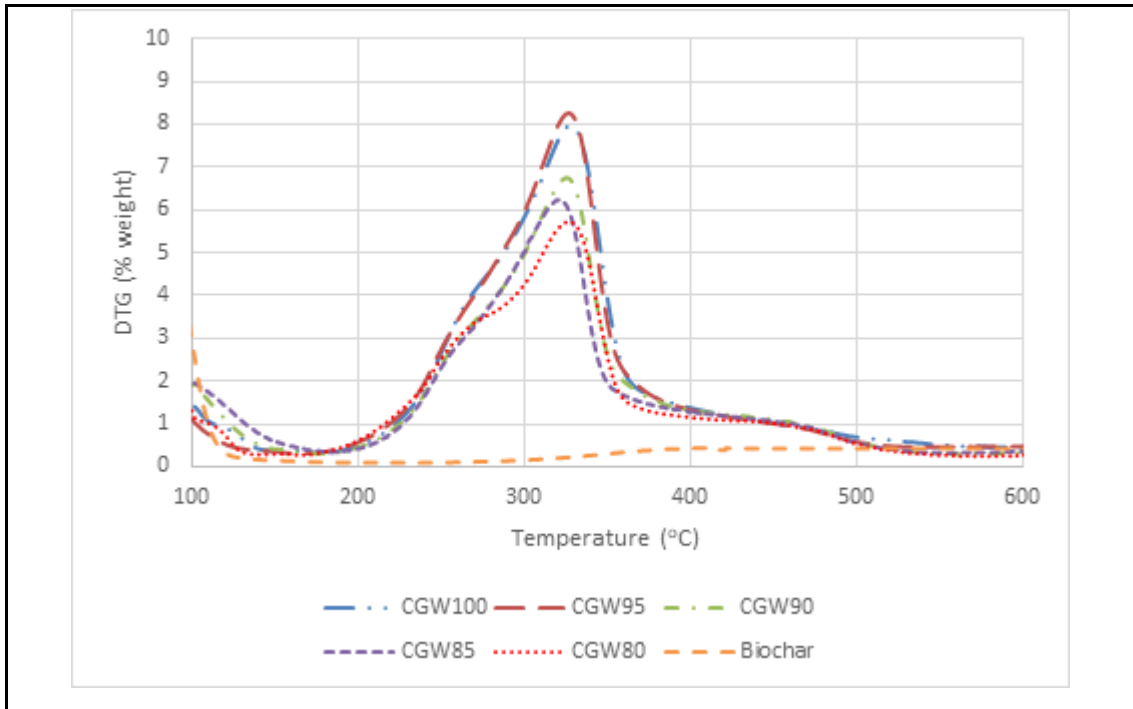


Figure 5.4: Derivative thermogravimetric (DTG) curves of CGW pellets pyrolysis at devolatilization stage

5.3.3. Effect of heating rates to the pyrolysis of CGW pellets

In general, applying higher heating rates will increase the conversion rates. This effect was also confirmed by our results. Figure 5.6 shows that increasing the constant heating rate from 10 to 20°C/min resulted in higher maximum conversions. Figures 5.6 shows that increasing heating rate from 10°C/min, 15°C/min to 20°C/min results in the peaks of conversions of 5% weight/min, 8% weight/min and 14% weight/min, correspondingly. Similar to another non-woody pyrolysis study (Damartzis *et al.*, 2011), the DTG of cardoon leaves shows also the peaks of maximum conversions at 4% weight/min, 8% weight/min and 16% weight/min for the heating rate of 5°C, 10°C and 20°C/min, respectively.

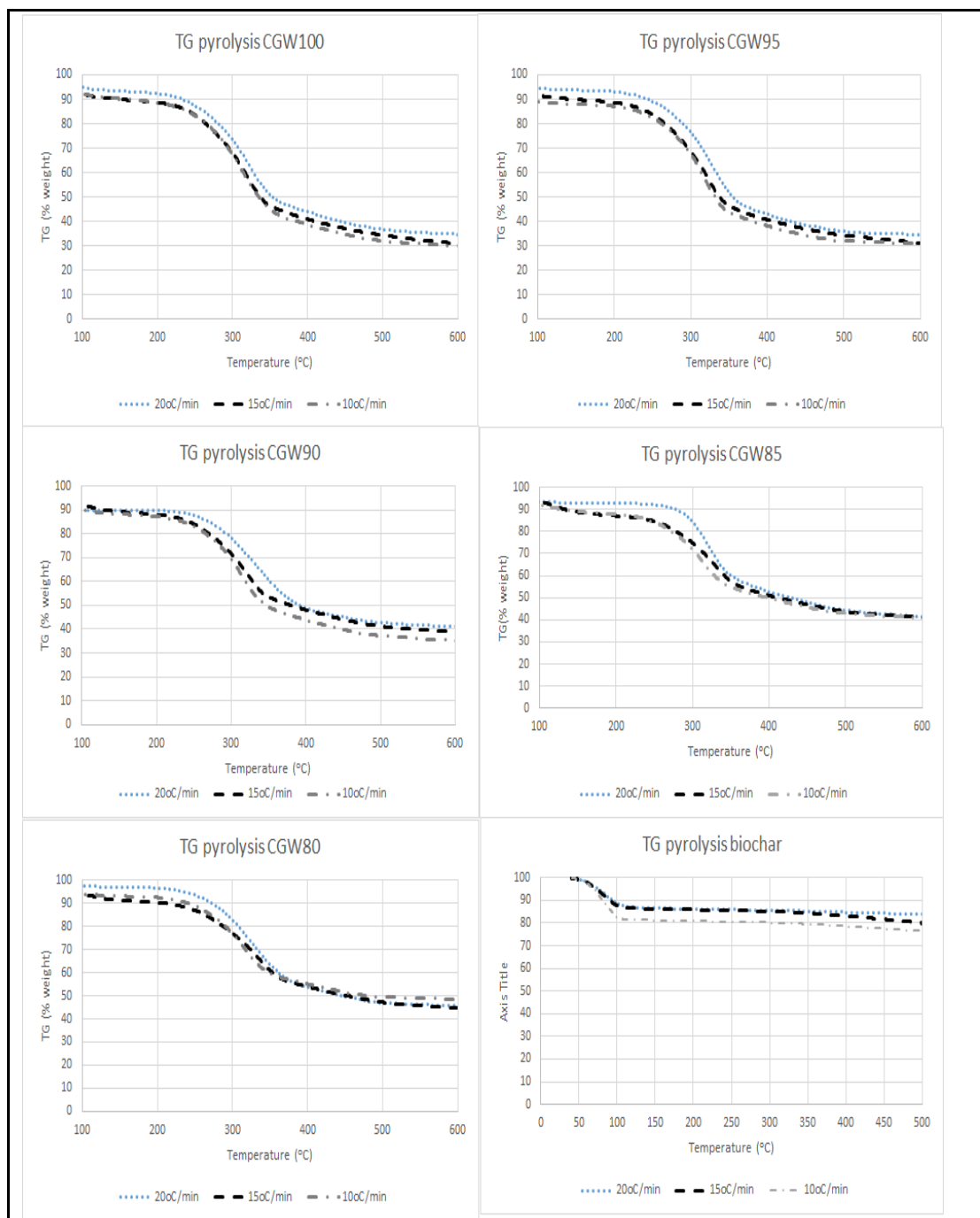


Figure 5.5: Thermogravimetric (TGA) pyrolysis of CGW pellets and biochar at heating rate 20°C/min, 15°C/min and 10°C/min

According to Yu *et al.* (2017), cellulose was less dependent on heating rate, however xylan and lignin were significantly dependent; faster heating rates lead to higher conversion in temperature ranges from 375°C to 600°C, the conversion zone of xylan and lignin. Similar trend with this finding was that the higher conversions at temperatures ranges of ~400°C upwards for the particular faster heating rates of 20°C/min data. Fig 5.5 shows the residual masses at temperature ranges of about ~400°C upward for the 20°C/min curves were overlapped with the masses of 15°C/min

curve. The coincided data were clearer in the pyrolysis profiles of higher blended biochar pellets. Thus, it is interpreted that the higher evolution of xylan and the decomposition of the wall structure from the biochar, -which is originated from a high lignin content material- occurred here in respect to higher heating rate application.

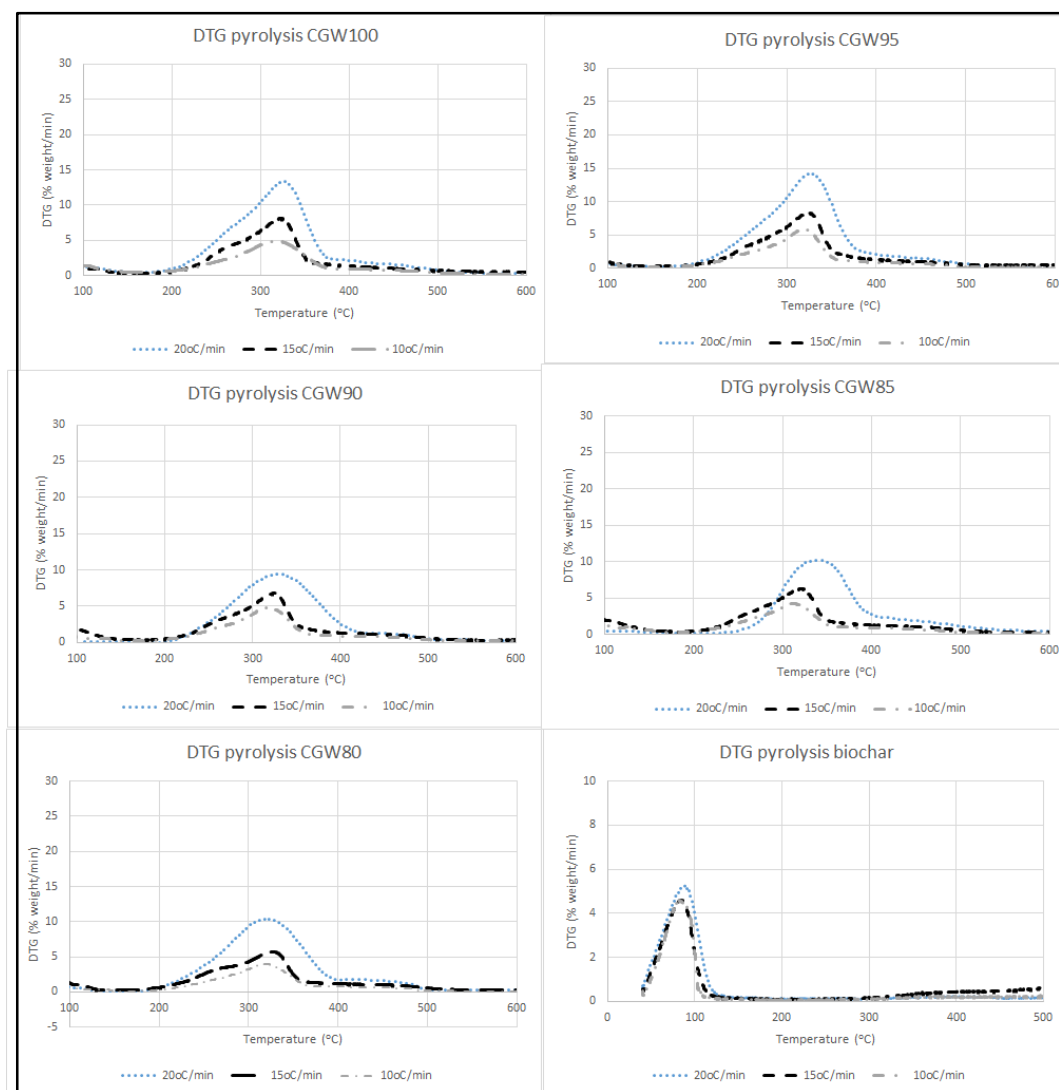


Figure 5.5: Derivative thermogravimetric (DTG) pyrolysis of CGW pellets and biochar at heating rate 20°C/min, 15°C/min and 10°C/min

Table 5.1 presents the maximum conversion rates and the corresponding temperatures at each constant heating rate curves. From the data, it can be seen that the corresponding temperatures of maximum reactions are increased as to the increase of heating rates. The corresponding temperatures of maximum reactivity are relatively similar for all pellets. For each constant heating rate of 20°C/min, 15°C/min and 10°C/min, the peak temperatures of all pellets are laying at 330-333°C, 323-326°C and 315-317°C, respectively.

The higher the biochar content in pellets generally lowers the maximum conversion rates. However, at higher heating rate of 20°C/min, the maximum conversion rate seems to be the same for all blended pellets that are 10% weight/min. Excluded from this group is CGW95 which has the maximum conversion rate nearly the same with that of CGW100.

Table 5.1: Maximum conversion rates and corresponding temperatures

Samples	Constant heating rate (°C/min)	Peak temperature (°C)	Maximum conversion rate (%/min)
CGW 100	20	331.4	13.5
	15	325.5	8.0
	10	316.8	4.9
CGW 95	20	331.5	13.1
	15	326.7	8.2
	10	317.3	5.9
CGW 90	20	330.9	9.9
	15	325.6	6.7
	10	314.7	4.9
CGW 85	20	329.8	10.2
	15	322.5	6.6
	10	312.5	4.2
CGW 80	20	332.8	10.0
	15	326.1	5.7
	10	315.3	4.0
Biochar	20	92.0	5.2
	10	87.4	4.6
	15	81.9	4.6

5.3.4. Thermo-kinetics pyrolysis of CGW pellets

In this section, the pyrolysis kinetic performances of the developed CGW pellets are discussed. This would be examined from the high devolatilization stage at 200-600°C ranges for the pellet fuels. In particular, for the biochar, it was assumed that the devolatilizations were at 25-200°C. In this water vaporization zone, higher masses

were release than the amounts of moisture content of the biochar. The biochar devolatilization might be together with the moisture release. Figure 5.2 shows that the mass released up to temperature of about $\sim 100^{\circ}\text{C}$ was about 15%; the moisture content and the volatile of this biochar from the proximate analysis were 7.4% and 7.3%, respectively (Table 3.2).

The effect of heating rates to the reactivity has been shown in Figures 5.4-5.5 and the main figures were summarized in Table 5.1. The calculations of activation energy (E_a) and the pre-exponential factor (A) were using the free kinetic method (modified Kissinger method). This method calculates the corresponding temperatures of maximum reactivity (T_m) vs their constant heating rates (β). At least three points of constant the heating rates data should be available to find the model relations. The equations 4.20 shows the model relation of temperature at maximum reactivity (T_m) and heating rate constant (β) to activation energy (E_a) and pre-exponential factor (A).

Table 5.2 shows the calculated values of activation energy of the CGW pellets. They are between 100 and 132 kJ/mol. For comparison, the activation energies of the pyrolysis of woody biomasses (wood chips, macadamia nut shell) and bituminous coal were 168 kJ/mol, 165 kJ/mol and 200 kJ/mol, respectively (Vhathvarothai *et al.*, 2014a). The rapeseed straw pyrolysis, a non-woody biomass type, varied between 87-118 kJ/mol (Chen *et al.*, 2003). The evidences show that in general the non-woody has lower activation energy than those of woody and coals.

The biochar pyrolysis studies are very few. However, a research in the thermogravimetric combustion of rice husk biochar and sawdust biochar reported that their activation energy was 74-110 kJ/mol for rice husk biochar and 74-117 kJ/mol for sawdust biochar (Sahu *et al.*, 2010). Obtained from gasification with CO_2 in TG analyser, the activation energies of biochar (from oak) and coke powder were 131 kJ/mol and 56 kJ/mol, respectively (Gan *et al.*, 2017).

Table 5.2 shows that CGW100 had higher activation energy in comparison to the biochar. As to higher mass degraded in CGW100, it required more energy for the pyrolysis in contrast to the biochar. Without any synergy effect, the biochar blends pellets will have lower activation energies ($E_{a\text{-indwp}}$) than that of CGW100. If this pyrolysis results are extended to the gasification, it will provide more chars for further reduction reactions in gasification.

Table 5.2: Activation energy and pre-exponential factor of pyrolysis CGW Pellets

Samples	Experimental		Calculated
	E _a (kJ/mol)	A(1/s)	E _{a-indwp}
CGW 100	130.5	2.73 x 10 ⁹	-
CGW 95	132.2	3.78 x 10 ⁹	127.4
CGW 90	113.7	1.19 x 10 ⁷	124.3
CGW 85	107.9	2.72 x 10 ⁷	121.2
CGW 80	106.7	5.19 x 10 ⁶	118.1
Biochar	68.6	1.35 x 10 ⁸	-

Figure 5.6 shows the comparison of activation energy of the calculated based on the weight proportion to individual data activation energy (E_{a-indwp}) and the experimental data modelling (E_a). Although it shows the empirical activation energies of biochar blended pellets (E_a) are slightly under their predicted values (E_{a-indwp}), the coefficient correlation of this two set data are 0.90. It can be concluded, that empirical data are nearly the same with predicted values, within the standard error of the estimation as much as 10%. The activation energy of CGW 95 is very close to its predicted value.

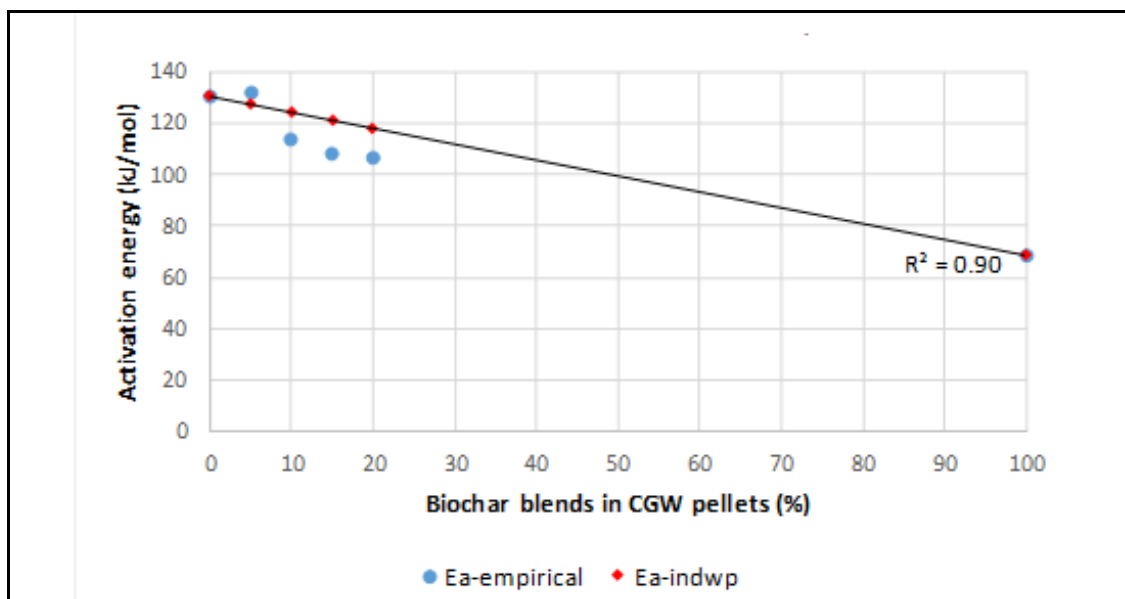


Figure 5.6: Activation energy of pyrolysis CGW pellets

5.3.5. Synergistic effect in co-pyrolysis

The products of pyrolysis are gas, volatile, tar and char. In this thermogravimetric study, the noticeable product was char. The char was determined as the remain mass along the process as seen in the TG curves. Figure 5.7, shows the char yields of the TG pyrolysis pellets at temperature 400°C, 500°C and 600°C for each constant heating rate of 20°C/min, 15°C/min and 10°C/min.

All constant heating rates data shows the same pattern of char yield which is higher char yields at higher biochar composition in pellets and at lower temperatures. However, the CGW95, having higher carbon composition than that of CGW100, resulted in slightly lower or the same char yields than that of the CGW100. This happens consistently in all constant heating rate and all production temperatures. In the co-pyrolysis study, this lower char yield can be used as an indication of synergy between biomass and biochar (Vhathvarothai *et al.*, 2014a). As having lower residual mass than the prediction, higher conversions of CGW95 into products related to the interaction of the co-blended fuels in delivering additional heat leading to more reduction reactions as described previously.

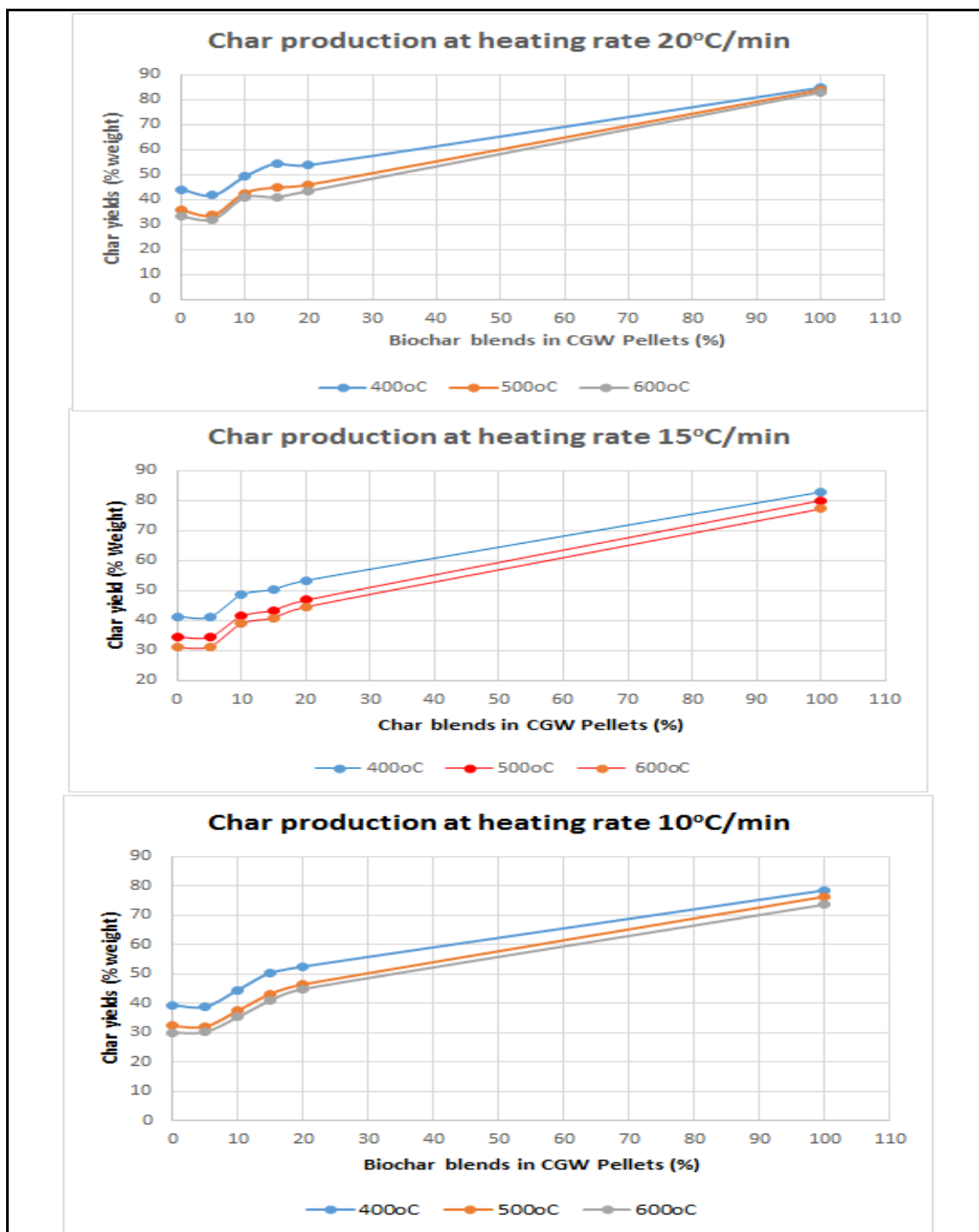


Figure 5.5: Char production from TG pyrolysis of CGW pellets

5.4. Summary and conclusion

In this chapter, the pyrolysis of the developed CGW pellets has been studied using thermogravimetric analyses. The CGW100 pellet, biochar and the CGW biochar blend pellets of CGW95, CGW90, CGW85 and CGW80 were pyrolysed under a nitrogen environment at three different heating rates comprising 10°C, 15°C and 20°C per minute to investigate their pyrolytic behavior and to determine kinetic parameters

of thermal decomposition through Kissinger's corrected kinetic equation using the thermogravimetric analysis results.

It has been found that all these pellets demonstrated three phases during the process of pyrolysis, which included dehydration, devolatilization and char reduction. It has also been found that the devolatilization of CGW-biochar blends had similar behavior with the unblended CGW pellet. The high rate of conversion in the devolatilization mainly occurred in the temperature zone of 200-350°C. This has been reported as the main cellulose decomposition which is typical of non-woody biomass pyrolysis behaviour based on its main composition. The increase of constant heating rates would increase the maximum rate of conversions contributed mainly from the decompositions of xylan and char reduction. Xylan and lignin decompositions have been reported more sensitive to heating rates in contrast to the cellulose decomposition. The maximum rates of conversions of the blended biochar pellets were slightly lower than those of the pure CGW100. However, the CGW95 pellet resulted in similar rates of conversions with those of CGW100, in which this could be an indication of synergism.

It has been found that the coconut biochar used for the blend had two phases of dehydration and char reduction only. Due to a very small amount of volatile materials, the devolatilization of the char might occur with moisture release (dehydration stage). The evidence was high mass decomposition at temperature ranges of below 200°C which is similar to exceeding the amount of moisture and volatile content in the biochar.

The activation energy of the CGW pellets were found to be around 100 – 132 kJ/mol. The increase of biochar blends in pellet reduced the activation energy indicating less mass conversion. It was found that the activation energies of empirical data agreed well with the values of the prediction based on the weighting factors with the correlation coefficient of 0.90.

It has been found that a slight synergism appeared in the co-pyrolysis of CGW95 pellet. This was determined from the analyses of char yields at temperatures of 400, 500 and 600°C. GW95 had a similar or slightly lower char yield than those of CGW100. This indicated that CGW95, though having higher carbon content, has higher conversion than CGW100. As in combustion, the possible heat transfers and/or chemical reactions of the CGW95 pellet resulted in this finding.

CHAPTER 6: Computational Fluid Dynamics Modeling of Cotton Gin Waste Pellets Gasification

Abstract

This chapter developed a CFD model of the 10 kW downdraft gasifier to compare the gasification performance of different CGW pellets. The model was developed using ANSYS FLUENT 17.2 software. It was modeled in a 2D-axisymmetric plant applying a discrete phase particle model, with the reaction of non-premix combustion and the turbulence model of the SST-K ω -Intermittency factors. The developed CFD model was used to predict the profiles within the reactor, particularly the temperature profile. However, a considerable overestimate of the temperature profile inside areas at the bottom grate were detected as the model did not set the mechanism of char and ash removal as in the real situation. The gasification simulation of the CGW pellets with 0-20% biochar composition resulted in an increase of biochar component in the pellet increasing the reduction zone temperature as well as the CO content in the producer gas and heating value. However, the pellet with 5% addition of biochar yielded a gas with higher CO content than those of 0% and 10% biochar in CGW pellets. Despite only having a small synergism, the CGW95 thermo-kinetic properties contributed to this higher gas CO composition in the gasification simulation result.

Keywords: Gasification, modeling, computational fluid dynamic, cotton gin waste, biochar

6.1. Introduction

Previous chapters have discussed the cotton gin waste (CGW) development into fuel pellets and their physical properties and thermo-kinetic performances. Technically, it is desirable to have a dense form of fuel for easier operation in a batch type of gasifier. Otherwise, applying the raw form of CGW into a downdraft gasifier could cause the process of combustion or gasification to be unstable (Jordan & Akay, 2012). Thus, a low conversion efficiency will ensue.

As a solid fuel, the developed CGW pellets can be used in a wide variety of thermochemical energy conversions including combustion, pyrolysis or gasification. The thermo-kinetic behavior of CGW pellets in combustion and pyrolysis was discussed in previous chapters and was supported through lab-scale experimental studies.

This chapter focuses on the performance of CGW pellets gasification. Unlike combustion and pyrolysis, the gasification is more complex because it is a consequence to the pyrolytic step. Lab-scale thermo-kinetic gasification experiments often give inconsistent results. Moreover, there are often even bigger differences when

moving from a lab scale to a small scale or industrial prototype. This is because gasification can be significantly influenced by many factors including the gasifier design and operating condition, as well as in the processes of pyrolysis and combustion which are necessary stages prior to gasification. Although gasification process can achieve the highest gas conversion efficiency compared to combustion and pyrolysis, it is noted that gasification performance is very specific to each fuel characteristic and the equipment design.

In this era, modeling is often employed as a virtual laboratory simulation of a plant design. Computer modeling can be applied for numerical calculations of the complex process variables. In this research, the study of CGW pellets gasification was conducted by developing a numerical model of a downdraft gasifier and then applying it for simulation of the pellets gasification. Besides fuel properties of various CGW pellets, the influence of a given design and operating condition of the gasifier on the pellets gasification performances will be considered. The developed models can be used for future simulations. The results may also be important for many users, particularly for those planning a plant application.

Gasification models can be divided into four categories: 1) Equilibrium model: it predicts the syngas composition at the equilibrium stage. It focuses on the final composition of the gasses. This model ignores the gasifier design. 2) Kinetics model: it predicts yields at a finite time or a finite volume. The model applies char reaction models with empirical data. It ignores some aspects of the equipment design such as turbulence factors. 3) Artificial neural network (ANN) model: ANN computes more complex systems including nonlinear and discrete process. It is described as a non-mechanistic, non-equilibrium and non-analytical model. The limitation of this model is that it requires extensive sets of experimental data and lacks the capacity in dynamic modelling (Patra & Sheth, 2015). 4) Computational Fluid Dynamic model (CFD): The CFD model applies numerical calculations including both the kinetics and the gasifier design. As the purpose of this study stated above, the CFD method would be more appropriate for the current study of the effects of fuel properties, gasifier design and operation conditions.

The CFD model applies finite mass/volume transport phenomena, mass energy balance and chemical reactions of the dynamic mass changes. The model thus embeds mass, momentum, energy equations applied in kinetic models at a known design of reactors in which the finite mass/volume is transported in mesh structure. The

turbulence modelling is also applied. The simulations can predict the temperature profile, syngas compositions along the zones and the flow pattern of solid and fluid inside the reactor. These mathematical analyses can be used to predict the quality and the quantity of the gasses. Based on the results of the computation, improvements, modifications or optimisation of parameters for a particular gasification process can be undertaken. This model can thus act as a virtual laboratory analysis for the first prediction of the performance of a gasifier plant. Available commercial software such as ANSYS FLUENT, CFX, PHOENICS, OpenFOAM etc already exist. For the sake of convenience, this study have chosen ANSYS FLUENT software (ANSYS Inc.). Previous work on CFD models for studying the fixed bed gasification is summarized in Table 6.1.

Table 6.1: Developed CFD models for batch type of gasifiers

Authors	Methods
(Gerun <i>et al.</i> , 2008)	2D-axisymmetric two stage reactions in a downdraft gasifier. The tar was included in the model. The product of pyrolysis was modelled as phenol. The gaseous product of phenol in partial combustion was modeled as benzene which further converted into naphthalene and oxidized into a permanent syngas composition. The model was developed using FLUENT software
(Patel <i>et al.</i> , 2013)	Non-premix combustion for reactions model of lignite downdraft gasification. The model predicts gas composition, reaction temperature, unconverted char and calorific value of gas. The input parameters are coal composition, initial temperature of pyrolysis zone, velocity of air flow and pressure. The model was developed using FLUENT software.
(Janajreh & Al Shrah, 2013)	2D-axisymmetric downdraft gasifier. The reactions were modelled using transport reactions in addition to discrete phase interaction. The input particle size

Authors	Methods
	was smaller (0.1 mm) than in real conditions. The model was developed using FLUENT software
(Wu <i>et al.</i> , 2013)	2D fixed bed downdraft gasifier. The phases of drying, pyrolysis, drying and combustion were modelled. The reactions in each phase were modelled using multiphase model. The model was developed using ANSYS FLUENT 14.5 software
(Ismail & El-Salam, 2015)	2D updraft gasifier. The model used transport reaction model in a multiphase stage. The CFD model was developed using the software of The COMMENT-Code (Combustion Mathematics and Energy Transport).
(Fernando & Narayana, 2016)	2D updraft gasifier. The shrinkage model was used to evaluate the packed bed volume beside the transport reactions. The CFD simulated the movement of interface between solid packed bed and gas free board. The model was developed using OpenFOAM software.

Depending upon the purpose, a complex model may be more accurate in prediction, but be more time-consuming. Previous studies (Table 6.1) have employed either transport reactions (Janajreh & Al Shrah, 2013) or global reaction mechanism (Gerun *et al.*, 2008). These models showed how reactions drive the process of gasification. Gerun *et al.* (2008) developed a model for the purpose of tar reduction in the product gas; where the tar composition was modeled as a phenol. Another model (Murgia *et al.*, 2012) predicted separate reactions in each phase of drying, pyrolysis and combustion using multiphase model for coal gasification in an updraft type.

Patel *et al.* (2013) developed a model of coal downdraft gasification for the purpose of simulating the effect of air velocity on the temperature and species fraction profile. It modeled the gasification as a lean process of combustion. Although this model may be simple, it accurately showed the temperature profiles, which was modeled as the effect of air/fuel velocity and fuel composition. The fuel simulated was

coal. Starting with the properties of the coal, this model was able to predict gasifier performances using the probability density function (PDF) of the reactions. This model has also been selected as being sufficiently suitable for the purpose of this study, of which the main purpose is to compare the gasification performance of different CGW fuel pellets.

Particularly, this study develops a CFD model using ANSYS FLUENT 17.2 software for a 10 kW downdraft gasifier. The downdraft is a type of simple gasifier design. It has less external control of the process. As customary for this type of equipment, the heat for the processes of both pyrolysis and gasification (reduction) are supplied from the partial combustion stage. The control of oxidation is maintained by air to fuel ratio. Therefore, the gasification in the batch type such as the downdraft is typically a lean combustion process. In reality, the process of gasification in the downdraft gasifier cannot be clearly separated from all the processes prior to it. In fact, there is a carryover of the reactions and energy from the combustion area back to the prior stages.

In this study, the reactions are described by the probability density function (PDF). The local mass fraction of burnt and unburnt fuel stream elements (C, H and so on) and all the species (CO_2 , H_2O , O_2 and so on) is conserved to a scalar quantity namely mixture fraction. Combustion is simplified to a mixing problem in which the oxidizer influences the fuel mixture conditions either in a stoichiometric, fuel-rich oxidizer or fuel-lean mixture (ANSYS_INC, 2013).

Furthermore, the developed model is modified from the previous one (Patel *et al.*, 2013). It allows coupling with a discrete phase materials injection. The template allows the utilization of other reactants beside oxygen. The developed model also uses an intermittency factors to cover any turbulence impact inside the batch reactor as to the effect of possible phase changes in the material flow.

This chapter developed a CFD model of a 10 kW downdraft gasifier. The objective of the model was to study and compare the performances of the different CGW-biochar pellets in the gasifier. The developed CFD model is firstly validated using a previous set of experimental data of macadamia shell gasification. The simulation of the CGW pellets gasification is then conducted using this developed model. Five types of CGW pellets gasification performance are compared. They are: the 100% cotton gin waste pellet (CGW100) and the blends of CGW with biochar pellets (CGW95, CGW90, CGW85 and CGW80). The properties of each type of pellet

here are presented in the previous chapters 3, 4 and 5. Based on the previous chapters of TGA studies (Chapter 4 and 5), the synergistic effect occurred in the blended biochar pellets. In this gasification simulation, the model treats each CGW-blended pellet as a unity with specific fuel characteristics. The synergistic aspects of CGW blended pellets are implied by the TGA data entered to the model.

6.2. Theoretical biomass thermochemical conversion

The thermochemical conversion of a biomass solid fuel into ash (Fig 6.1) follows three different stages below:

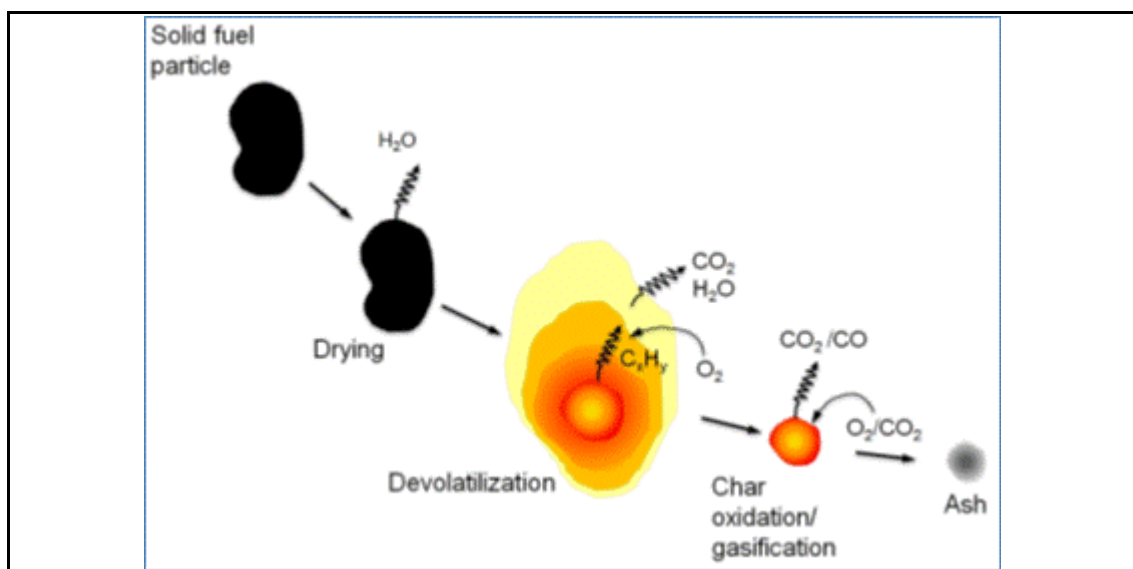


Figure 6.1: Thermochemical conversion of solid fuel (NIEMELÄ, 2015)

- Particle heating up and drying:

The fuel particle starts to heat up mainly by convection from the hot combustion gases and also from the radiation energy of the flame and combustion chamber walls. Water vapor is released.

- Particle devolatilization:

As the particle temperature continues to rise, the chemical structure of the fuel starts to break. During the devolatilization, the particle releases tars, hydrocarbons, various gaseous components and organic vapors. The remaining material is char. It is noted that the devolatilization temperature is specific to each kind of solid fuel.

- *Char burnout:*

The char continues to burn by means of heterogeneous surface reactions, by reactions between the char and gaseous phase. In the combustion system, the expected remaining particles are forming ash, and the complete reactions resulted CO_2 are expected. In the gasification system, however, the char reactions are expected to produce combustible gasses (CO , CH_4 , H_2 and other hydrocarbons). Here, the remaining particles are mostly unburnt chars and a small amount of ash.

6.3. Modeling of thermochemical conversion of solid fuel

Gasification involves complex phenomena such as heat, mass and momentum transfers; chemical reactions of both homogenous gas-gas reactions and heterogeneous solid-gas reactions. For the purpose of modeling, the process would often need to be suitably simplified. The degree of simplification is relative to the needs of model intentions. In the previous text, several models for such purposes have been built.

Overall, the basic feature of gasification modeling is to divide the particle into two streams: gas and solid phases (Souza-Santos, 2010). For a downdraft gasifier, both streams, solid particles and gasses, are flowing in the same direction. The solid and gas would exchange heat and mass in a single continuous surface. The total surface area is equivalent to the summary area of solid and gas surfaces. As the composition of gas and solid vary throughout the bed, the total area of the particles will also vary throughout the bed height. The model is simplified for solid and gas phases flowing through the reactor bed and the particles involved can be modeled here as in the mode of plug-flow regime (Figure 6.2).

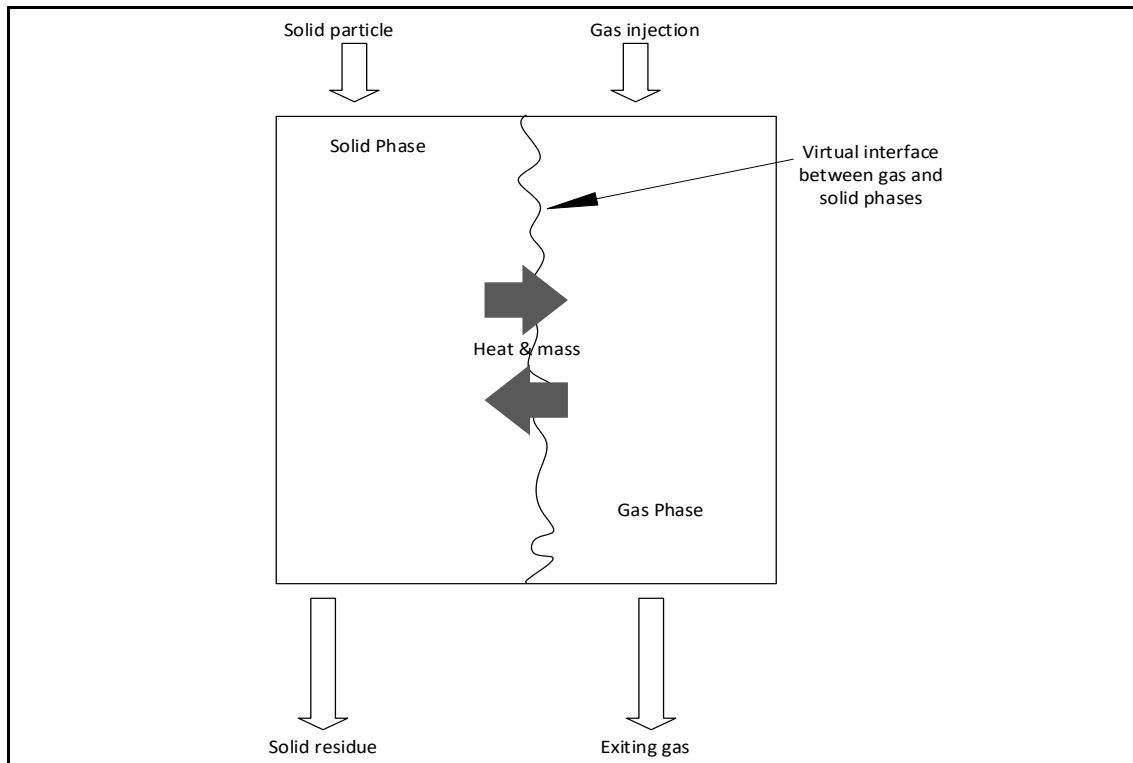


Figure 6.2: Modeling scheme of fuel in the fixed bed gasifier ((Souza-Santos, 2010))

6.3. Gasification modeling

A 10 kW downdraft gasifier (Figure 6.3) was selected for the plant modeling in this study. The gasifier plant was manufactured by ALL POWER LABS, a company in the USA (<http://www.allpowerlabs.com>). This gasifier has an auger to feed the feedstock from a hopper tank to the reactor. The feed and the pyrolysis zones use a heat exchanger (namely *pyrocoil*) utilising the energy from the long outflow pipe of the gas produced while cooling it before entering into a filter tank. Thus, the feed enters the reactor at a lower moisture content, already prepared for devolatilization in the reactor. This gasifier is also equipped with a flaring system and a gas engine gen-set.

For the purpose of CFD modelling, only the part of reactor is simulated in the calculation as shown in Figure 6.3 (boundary of CFD modelling). The model was developed in a 2D axisymmetric arrangement and constructed using ANSYS Fluent 17.2.

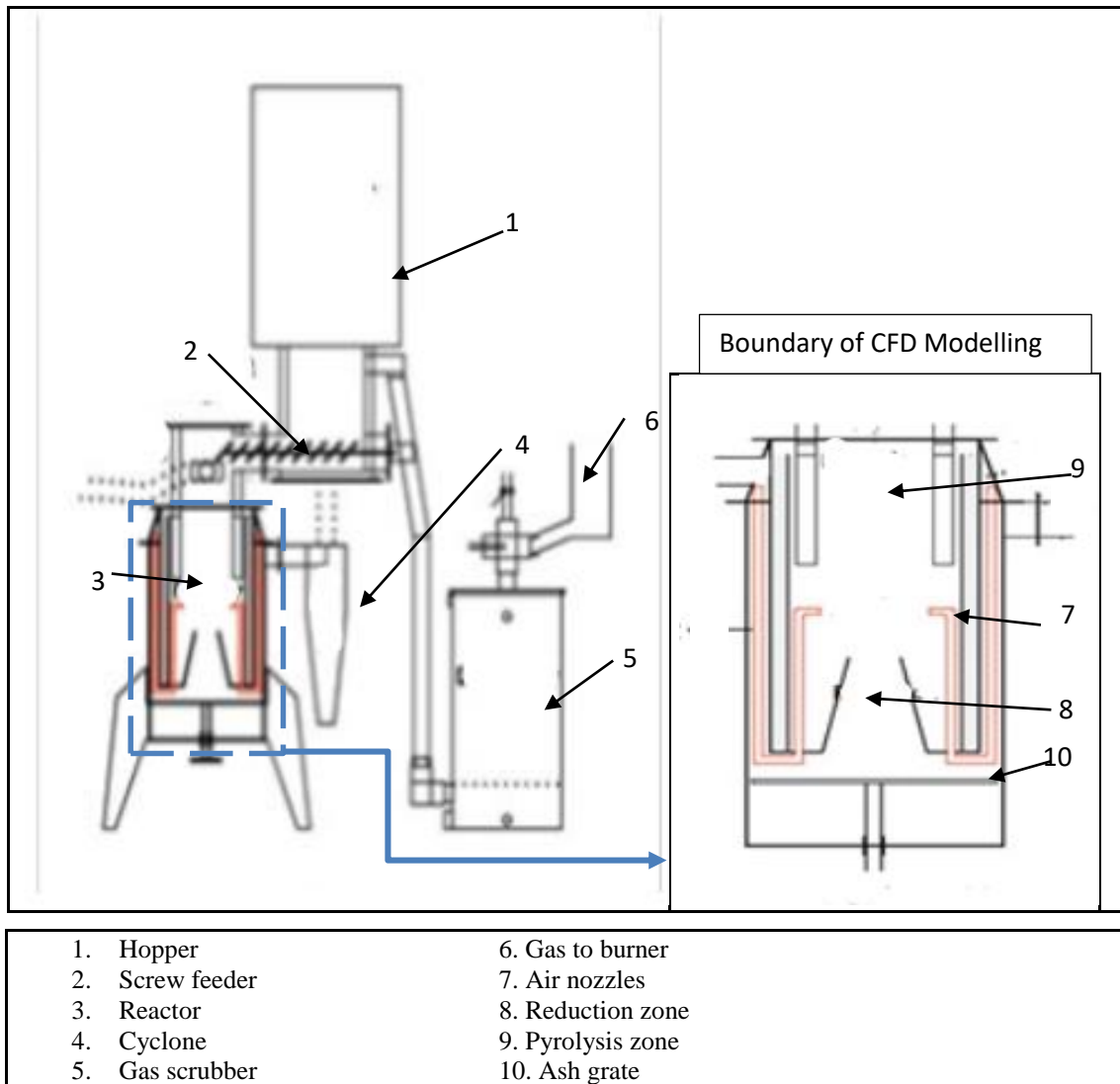


Figure 6.3: the 2D gasifier model (Source: <http://www.allpowerlabs.com>)

Several assumptions were made to simplify the model as follows:

- The operation was assumed to be steady-state. As the downdraft gasifier has longer retention time than other types, the steady-state operation can be reasonably assumed. Additionally, the conditions during starting up and /or shutting down are not included in the calculation, as these would violate the steady-state model.
- It is further assumed that the gas percolates downdraft in a plug flow regime via small channels between particles. At a given cross section of the bed, all variables are uniformly distributed. Using 2D geometry as a start, the software introduces cylindrical rotation of a hypothetical segment around the symmetry axis where the change of laminar flow into turbulence can be calculated. The software allows a modification of the departure from 2D into 2D axisymmetric

model, in which a thickness region to the cylindrical coordinate system is added in order to model the gas in a radial velocity. The solids would be assumed to flow downward laminarly and the gas also flows in the same direction, but through a spiral rotation towards the symmetrical axis (Souza-Santos, 2010).

- The governing equations in numerical calculations are non-linear partial differential equations.

The following sub-sections present the relevant basic equations. However, in reality, these equations are however difficult to solve. Hence, an approximation is usually taken to solve them. CFD converts the partial differential equations into a discrete form and solves the conservation equations in every computational cell. The discretization can be based on Finite Volume Method (FVM), Finite Difference Method (FDM) or Finite Element Method (FEM). ANSYS Fluent uses Finite Volume Method (FVM).

6.4.1. Governing equations for fluid flow

The governing equations of the fluid flow are basically the equations of conservation of mass, momentum and energy. The Navier-Stokes equation can be written in the following form using tensor notation:

$$\frac{\partial(\rho u_i)}{\partial t} + \frac{\partial(u_i u_j)}{\partial x_j} = -\frac{\partial p}{\partial x_i} + \frac{\partial \tau_{ij}}{\partial x_j} + \rho \sum_{k=1}^N Y_k f_{k,j} \dots\dots\dots 6-1$$

Where ρ is the density of the fluid mixture, $u_i u_j$ are the velocity components,
 t is time, $x_i x_j$ are the coordinate axes,
 p is the pressure, τ_{ij} is the viscous stress tensor,
 Y_k is the mass fraction of species k in the fluid mixture,
 $f_{k,j}$ is the volume force acting on species k in j -direction.

This equation is the conversion of momentum equation in which it contains a fluid mixtures of $k = 1 \dots N$ chemical species. The species in the thermochemical conversion reactions are dependent on the thermodynamic state variables such as temperature or pressure. The ideal gas equation is then applied to relate the density of the fluid to the temperature and pressure. Furthermore, an additional equation related to viscous stress

tensor is needed to solve equation 6-1. The mixture can be assumed as a Newtonian fluid and stress tensor can be obtained from equation 6-2:

$$\tau_{ij} = -\frac{2}{3} \mu \frac{\partial u_k}{\partial x_k} \delta_{ij} + \mu \left(\frac{\partial u_i}{\partial x_j} + \frac{\partial u_j}{\partial x_i} \right) \dots\dots\dots 6-2$$

Where μ is the dynamic viscosity of the mixture and δ_{ij} is the tensor unit, the Kronecker delta (Poinsot, 2005)

The law of mass conservation states that no mass can be created nor destroyed. The total mass and elementary compositions therefore follow the equation:

$$\frac{\partial \rho}{\partial t} + \frac{\partial(\rho u_i)}{\partial x_i} = 0 \dots\dots\dots 6-3$$

As many chemical reactions occur in the thermochemical conversion, the mass of species in fluid mixture would depend on the specific chemical reaction occurring at a particular time. Therefore, the mass conservation equation is re-written as follows:

$$\frac{\partial(\rho Y_k)}{\partial t} + \frac{\partial}{\partial x_i} [\rho Y_k (u_i + V_{k,i})] = \dots\dots\dots 6-4$$

whereas $V_{k,i}$ is the i -component of the diffusion velocity of species k .

$\dot{\omega}_k$ is the reaction rate of species k .

The reaction rates can be defined through empirical Arrhenius equation which is calculated from the empirical input data of activation energy and pre-exponential factor.. The conservation of energy equation can be written as follows:

$$\frac{\partial(\rho e_t)}{\partial t} + \frac{\partial}{\partial x_i} (\rho u_i e_t) = -\frac{\partial q_i}{\partial x_i} + \frac{\partial}{\partial x_j} [(\tau_{ij} - p \delta_{ij}) u_i] + \dot{Q} + \rho \sum_{k=1}^N Y_k f_{k,i} (u_i + V_{k,i}) \dots\dots\dots 6-5$$

whereas e_t is the total energy from chemical, potential and kinetic energies.

\dot{Q} is the energy flux from the outer heating source.

q_i is energy flux in the mixture

The energy flux in the mixture can be defined as

$$q_i = -k \frac{\partial T}{\partial x_i} + \rho \sum_{k=1}^N (h_k Y_k V_{k,i}) \dots\dots\dots 6-6$$

The first term in the right hand side is heat conduction through the Fourier's law and the second term is energy flux through species diffusion in the mixture.

6.4.2. Radiation model

The flow of thermal energy from matter occupying one region in space to matter occupying a different region in space is known as heat transfer. Heat transfer can occur in three main modes: conduction, convection, and/or radiation. The inclusion

of radiation heat transfer model is applied when the radiant heat flux is larger compared to the heat transfer rate. The large value of radiant heat flux is due to convection or conduction. Typically, this will occur at high temperatures with the fourth-order dependence of the radiated heat. The Radiative Transfer Equation (RTE) for an absorbing, emitting, and scattering medium at position \vec{r} in the direction \vec{s} is:

$$\frac{dI(\vec{r},\vec{s})}{ds} + (a + \sigma_s)I(\vec{r},\vec{s}) = an^2 \frac{\sigma T^4}{\pi} + \frac{\sigma_s}{4\pi} \int_0^{4\pi} I(\vec{r},\vec{s}')\phi(\vec{s},\vec{s}')d\Omega' \dots\dots\dots 6-7$$

- where
- \vec{r} = position vector
 - \vec{s} = direction vector
 - \vec{s}' = scattering direction vector
 - s = path length
 - a = absorption coefficient
 - n = refractive index
 - σ_s = scattering coefficient
 - σ = Stefan-Boltzmann constant ($5.669 \times 10^{-8} \text{ W/m}^2\text{-K}^4$)
 - I = radiation intensity which depends on position \vec{r} and direction \vec{s}
 - T = local temperature
 - ϕ = phase function
 - Ω' = solid angle

ANSYS Fluent template provides five radiation models:

- Discrete Transfer Radiation Model (DTRM),
- P-1 Radiation Model,
- Rosseland Radiation Model,
- Surface-to-Surface (S2S) Radiation Model,
- Discrete Ordinates (DO) Radiation Model.

Further explanation on the advantages and limitations of those models are provided in ANSYS Theory guide (ANSYS-Inc, 2016) . For combustion applications, where the optical thickness is large, the P-1 model usually works reasonably well. In addition, the P-1 model can be applied easily to the complicated geometries with curvilinear coordinates. The P-1 model assumes that all particles interact through their surfaces and the radiation is controlled by diffusion. This means that the reflection of incident radiation at the surface is isotropic with respect to an incident angle against normal. Only the P-1 and DO models can account for exchange of radiation between gas and particulates (ANSYS-Inc, 2016) .

6.4.3. Turbulence model

Because of the variations of velocity, pressure, energy and mixture composition, turbulence arises. In order to reduce the complexity of the CFD simulations, the *Reynolds-averaging* procedure is applied. Every variable f in the governing equation is divided into a time-averaged value \bar{f} and fluctuating component f' .

$$f = \bar{f} + f' \dots\dots\dots 6-8$$

When the variables in the governing equations are replaced as, for example the velocity, u_i , then the Reynolds decompositions for this becomes:

$$u_i = \bar{u}_i + u'_i \dots\dots\dots 6-9$$

u_i = velocity \bar{u}_i = average velocity u'_i = fluctuating component of velocity

When the variables in the governing equations are replaced with this definition, the so-called Reynolds-Averaged Navier-Stokes equations (RANS) are obtained. Substituting the expression to the Navier-Stokes equation with the Cartesian tensor (equations 6-1), the Reynolds-averaged Navier-Stokes (RANS) equations become equations 6-10.

$$\frac{\partial}{\partial t}(\rho u_i) + \frac{\partial}{\partial x_j}(\rho u_i u_j) = -\frac{\partial p}{\partial x_i} + \frac{\partial}{\partial x_j} \left[\mu \left(\frac{\partial u_i}{\partial x_j} + \frac{\partial u_j}{\partial x_i} - \frac{2}{3} \delta_{ij} \frac{\partial u_l}{\partial x_l} \right) \right] + \frac{\partial}{\partial x_j}(-\rho \overline{u'_i u'_j}) \dots\dots\dots 6-10$$

The Reynolds stress, $-\rho \overline{u'_i u'_j}$, is an impression typical for the turbulence model. ANSYS Fluent provides several approximations for this variable such as k - ϵ models, k - ω models, Spalart-Allmaras model, Reynolds Stress model, Eddy Simulation Models. The standard k - ϵ Model is widely applied in industrial engineering. It is based on model transport equations for turbulence kinetic energy (k) and its dissipation rate (ϵ). This k - ϵ Model can be less accurate than Reynolds Stress Model, but computationally it is more efficient. More details about the equations of those turbulence models can be found in the theoretical guide of ANSYS Fluent (ANSYS-Inc, 2016)

The k - ω model is an empirical model based on transport equations as the ratio of dissipation rate (ϵ) to kinetic energy (k). The effects incorporate a low Reynolds number, compressibility and shear flow spreading. To account for turbulence near the

walls, this model can be coupled with other approximations such as SST (shear stress transport). The SST can account the shear stress transport near the walls. Because this gasifier has concentric wall for the transition of pyrolysis to combustion and reduction, the developed model applies this SST $k-\omega$. The improvement in this model may also include the option to couple with intermittency transition factor. The intermittency transition factor avoids the re-calculation of Reynold-Number as to refer the impact of change in the viscosity (ANSYS-Inc, 2016). The value of intermittency is between the scale 0-1, in which the 0 refers to the laminar flow and 1 refers to turbulence. In this gasifier, it is possible that a change in the viscosity occurs after the flash combustion stage. Our model uses this SST $k-\omega$ approximation coupled with the intermittency factor.

6.4.4. Turbulence and chemistry interaction

The turbulence of gases can cause chemical reactions to impact on each other. While the Reynolds average procedure can be adopted, the Favre average formulation (mass-weighted average) is usually preferred for describing the weighted mass of chemical species:

$$f = \tilde{f} + f'' \dots\dots\dots 6-11$$

Where f is Favre-average value variable,
 \tilde{f} is mass-weighted average and
 f'' the fluctuating component around the mean.

When the mass conservation of chemical series (equation 6.4) is included, the transport equation balance for species k is as follows (Poinsot, 2005):

$$\frac{\partial(\bar{\rho}\tilde{Y}_k)}{\partial t} + \frac{\partial}{\partial x_i}(\bar{\rho}\tilde{u}_i\tilde{Y}_k) = -\frac{\partial}{\partial x_i}(\bar{V}_{k,i}Y_k + \overline{\rho u_i'' Y_k''}) + \bar{\omega}_k \dots\dots\dots 6-12$$

Where \tilde{Y}_k is the average mass fraction of species k . There are 3 main variables of the right hand side of this equations; firstly $\bar{V}_{k,i}Y_k$ reflects the diffusion variable in laminar flows; secondly, $\overline{\rho u_i'' Y_k''}$ is diffusion in the turbulent flow and thirdly $\bar{\omega}_k$ is the reaction rate. The first two terms are the fluxes for species in laminar and turbulence. The mass diffusion in laminar flow at ANSYS Fluent, by default, uses dilute approximation (Fick's Law). Another approximation uses Maxwell-Stefan equation for full multicomponent diffusion (ANSYS-Inc, 2016). For turbulence mass diffusion, ANSYS Fluent applies equation using variable of Schmidt number and the turbulence

viscosity. Further detail equations of the approach of mass diffusion by laminar and turbulent flow can be found in ANSYS Fluent theory guide chapter 7 (ANSYS-Inc, 2016).

The reaction rates $\overline{\dot{\omega}_k}$ are computed in ANSYS Fluent by one of the three models;

- Laminar finite-rate model,
- Eddy-dissipation model,
- Eddy-dissipation concept (EDC).

The laminar finite-rate ignores the turbulence fluctuation and the reaction rates are determined by Arrhenius kinetic expression. In contrast, the Eddy-dissipation model assumes the reaction rates to be controlled by the turbulence, so Arrhenius chemical kinetic calculations can be avoided. For EDC, the detailed Arrhenius chemical kinetics can be incorporated in turbulence flames. Those three models have been developed to describe chemistry using one single variable, namely mixture fraction, f . The mixture fraction models require statistical methods. To relate the mixture fraction interaction with the turbulence, a variable namely mixture fraction variance, f'^2 , is used (ANSYS-Inc, 2016). These generalized formulations for reaction models are suitable for a wide range of applications including laminar or turbulent reaction systems, combustion system with premixed, non-premixed or partially-premixed flames.

This study applies the mixture fraction sourced from non-premixed combustion model. This model uses Probability Density Functions (PDF) to describe the flow variables. The PDF can be assumed as the material fraction of the mixture spending in the vicinity at a time. In the non-premixed model, the highest mixing turbulence of the fuel and oxidizer, noted as the *flames*, controls the combustion. In the non-premixed model, flames are also called diffusion flames, as reacting species have to reach the stage of a molecular diffusion before reactioning (Poinsot, 2005). This phenomenon may be similar to the stage of combustion in the downdraft gasification.

Within the ANSYS Fluent, there is a template for the non-premixed combustion calculation, where a coal calculator is available which can be also used with other fuel sources such as biomass. This study has taken this option and incorporated it in the calculation. The biomass properties have been inputted to the coal calculator. The coal calculator provides the source term for reacting particles. This

tab can be inputted by the empirical fuel properties of the proximate and ultimate composition. By using these properties, the species mixtures are determined based on the chemical reactions with the oxidizer which is pre-selected under thermodynamic equilibrium conditions.

In the non-premixed combustion, fuel and oxidizer enter the reaction zone in distinct streams. The PDF approach relates three scalar variables of species fractions, density and temperatures (ANSYS-Inc, 2016). The mixture fraction, denoted by f (equation 6-14), is the local mass fraction of burnt and unburnt fuel stream in all species $i=1\dots N$. The approach also means that atomic elements are conserved in chemical reactions. Consecutively, the mixture fraction is a scalar quantity and the governing transport equation does not have a source term. Combustion is simplified into a mixing problem.

$$f_i = \frac{Z_i - Z_{i,ox}}{Z_{i,fuel} - Z_{i,ox}} \dots\dots\dots 6-13$$

where Z_i is the elemental mass fraction for element, i . The subscript ox denotes the value at the oxidizer stream inlet and the subscript fuel denotes the value at fuel stream inlet. The mixture fraction considers as a simple combustion system involving a fuel stream (F), an oxidant stream (O) and a product stream (P). At stoichiometric condition, it can be stated as follows:



whereas r is the air-to fuel ratio on mass basis, or the equivalence ratio ϕ as

$$\phi = \frac{(fuel/air)_{actual}}{(fuel/air)_{stoichiometric}} \dots\dots\dots 6-15$$

The mixture fraction under non-premixed combustion allows the computation at stoichiometric condition ($\phi = 1$), at fuel rich condition ($\phi > 1$) or fuel lean conditions ($\phi < 1$) (ANSYS-Inc, 2016).

The condition of flows can be either adiabatic or non-adiabatic. The non-adiabatic is applied to the system with one or more conditions as follows: with radiation, heat transfer through walls, heat transfer to/from discrete phase particles. As the particle combustion is sourced from the discrete phase particles, then the heat transfer is between continuous and discrete phase, hence the non-adiabatic conditions apply. At non-adiabatic condition, the local thermochemical energy is not only related to the mixture, f , but also to the enthalpy, H , or the heat loss. The system enthalpy

impacts the chemical equilibrium calculation, the temperature and species of the reacting flow. The logical model calculation for the system is shown in Fig 6.4 (ANSYS-Inc, 2016).

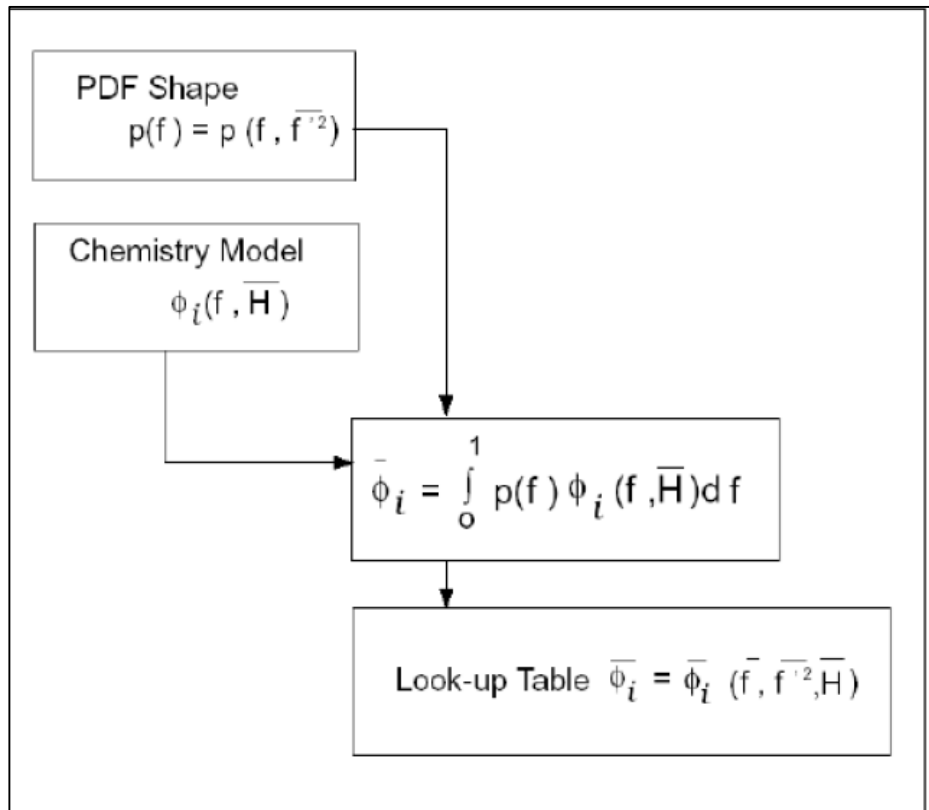


Figure 6.4: Chemistry models calculation based on Probability Density Function (PDF) ANSYS Theory Guide (ANSYS-Inc, 2016)

6.4.5. Particle combustion model

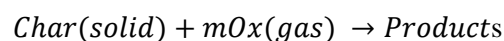
The particle interaction can be solved using two approaches: the Euler-Lagrange approach and the Euler-Euler approach. The first method is also known as ‘Discrete Phase’, while the second is ‘Multiphase’. This study will apply the first method, the Discrete Phase. The fluid phase is treated as a continuum by solving the Navier-Stokes equations, while the dispersed phase is solved by tracking a large number of particles, bubbles, or droplets through the calculated flow field. The dispersed phase can exchange momentum, mass, and energy with the fluid phase (ANSYS-Inc, 2016).

At first, a particle reaches a vaporization temperature. A particle remains in the devolatilization mode, when the mass of the particle is higher than the non-volatile mass. ANSYS Fluent provides 4 options of devolatilization models:

- Constant rate model: the devolatilization of material follows a linear rate constant value
- Single kinetic rate model: it is based on empirical kinetic data of first order escape of volatiles due to the effect of heat. An empirical value of activation energy (E_a) and pre-exponential factor (A) is required for the input data of the kinetic rate.
- Two competing rates model (Kobayashi model): this model controls the devolatilization at two different range temperatures. The two kinetic rates are required for the input data.
- The chemical percolation devolatilization model (CPD): this model was originally developed for coal and is not used in this study.

The pyrolysis behaviour of CGW pellets (Chapter 5) shows that the single stage reaction occurs for all developed pellets. Therefore, the single kinetic rate of devolatilization is adopted here instead of the constant rate or Kobayashi models. The empirical data of activation energy and pre-exponential factor of CGW pellets (Chapter 5) are inputted into the model to estimate their decomposition rate in this devolatilization stage.

After the volatile components of the particle have completely changed their phase, a surface reaction begins that consumes the combustible fraction until all the combustible components are consumed. In the discrete phase model (DPM), the surface combustion consumes the reactive content of the particle. The process is governed by stoichiometric requirement of the burnout char reaction, which is by the mass of available oxidant per mass of char. The types of oxidant and product species are specified by definition in the injection properties tab in the software.



ANSYS Fluent provides a choice of four heterogeneous surface reaction rate models for combusting particles:

- Diffusion-limited rate model: this is the default of the non-premix combustion model in ANSYS Fluent. It assumes that the surface reaction follows a rate determined by the diffusion of the gaseous oxidant to the surface of particles. It also assumes the constancy of the particle diameter. However, there is a decrease in density. This means that the particle mass is reduced and the particle becomes

more porous. To account for density reduction, shrink factor is introduced. This model does not require kinetic value of combustion particle.

- Kinetics/diffusion-limited rate model: It assumes that the surface reaction rate is determined either by kinetics or by diffusion. In this model, the diffusion rate and kinetic rate are weighted to yield a char combustion rate. The weighting factor is determined by the surface area, partial pressure of oxidant species in the gas surrounding particle and the kinetic rate. The kinetic rate incorporates the effects of chemical reaction on the internal surface (intrinsic reaction) and pore diffusion. This model requires the data of kinetic rate of combustion. To account for particle size reduction due to oxidation and other changes, shrink factor is also introduced.
- Intrinsic model: This model assumes the order of reaction is equal to unity. It also computes the diffusion rate coefficient, but the chemical rate is taken from intrinsic chemical and pore diffusion rate. Therefore, the char porosity, surface area of char particle, the fraction degree of char diameter to its burnout should be included in the input data. To account for particle size reduction due to oxidation and other changes, shrink factor is inputted.
- The multiphase surface reaction model: The model is based on oxidation studies of char particles, but it is also applicable to gas-solid reactions, not only to char oxidation reactions. The particle surface species constitute the reactive char mass of the particle, hence, if a particle surface species is depleted, the reactive char content of the particle is consumed. In turn, when a surface species is produced, it is added to the particle char mass.

Based on the kinetic behaviour of the CGW pellets combustion in the TGA tests (Chapter 4), the CGW100, CGW95 and CGW90 pellets have higher reaction rate (burning) at a lower temperature (~300°C). The TGA shows only a peak of high reaction occurring in a short time period. Based on this behaviour, it can be predicted that the particles may be combusted in the gasifier when reaching the temperature of 300°C close to the devolatilization temperature. The gas products are then assumed to be mainly generated from the extension of the oxidative pyrolysis reactions. No further high rate of conversion occurred to significantly influence the addition of the gas product. This fits to the Diffusion-limited model as this model does not require any further kinetics data in combustion zone. The reaction rate is the extension of the kinetics from the devolatilization step.

On the other hand, in the TGA behaviour of CGW85 and CGW80 pellets, two peaks were observed. The first was interpreted as pyrolysis and the second was assigned to the combustion. The appearances of double peaks were very clear at the highest heating rate. The second peak occurred also in relatively higher temperature than the first one, possibly indicating more surface reaction (intrinsic reaction). This second reaction had a distinct reaction rate. Hence, the appearance of two peaks (CGW85 and CGW80) fits much better to the Kinetic/diffusion-limited model than the Diffusion-limited model alone.

6.4.6. Input data and boundary condition

The particle combustion is defined by proximate and ultimate analyses of the pellet fuels. The chemical reaction is set to chemical equilibrium working under non-adiabatic conditions. The fuel temperature is defined as the devolatilization temperature. It is taken from the temperature data at about the starting point of the rate of devolatilization in the pyrolysis experiment, which was about 200°C. The oxidation temperature is taken as the temperature of the reaction peak from the TGA combustion experiment. In the material input, the particle density is specified as the apparent density of the pellet. The shrinkage coefficient is assumed to 0.6. This value is an approximation and refers to the experimental data of gasification empty fruit bunch (EFB) pellets in a downdraft gasifier (Erlich & Fransson, 2011). The ANSYS Fluent template uses a term of swelling coefficient which is about opposite to shrinkage.

The rate of fuel conversion in each devolatilization and combustion stage is determined as a single rate of conversion. The values of activation energy and pre-exponential factors are taken from previous TGA pyrolysis (Chapter 5) and TGA combustion (Chapter 4), respectively. The input properties data from previous chapters which were used in the simulations are provided in Table 6.2

Table 6.2: Input data of CGW properties in the model simulations

Pellets	CGW100	CGW95	CGW90	CGW85	CGW80
<i>Proximate analysis (wt. %, as received)</i>					
Moisture	7.9	9.0	5.7	5.6	8.4
Ash	14.6	9.0	13.9	11.4	11.4
Volatile	62.1	61.9	56.0	52.9	49.0
Fixed Carbon*	15.3	20.0	24.5	30.1	31.3
<i>Ultimate (wt. % as received)</i>					
Carbon	35.5	40.5	42.2	42.4	45.5
Hydrogen	4.4	4.6	4.2	4.1	3.8
Nitrogen	1.6	1.4	0.9	1.0	1.2
Sulfur	0.2	0.2	0.2	0.2	0.1
Phosphorus	0.1	0.0	0.0	0.0	0.0
Oxygen*	35.8	35.3	32.9	35.3	29.6
<i>Density</i>					
Aparent density, mean (kg/m ³)	1299	1238	1265	1230	1237
<i>Calorific value</i>					
HV, MJ/kg	14.0	15.9	16.9	17.6	18.2
<i>Thermo-kinetic properties</i>					
In combustion:					
Activation of Energy (kJ/mol)	203.7	173.2	173.8	176.0	169.8
Pre-exponential factor (1/s)	2.4E+16	4.9E+13	6.0E+13	3.8E+10	3.3E+09
In pyrolysis:					
Activation of Energy (kJ/mol)	130.5	132.2	113.7	107.9	106.7
Pre-exponential factor (1/s)	1.0E+07	3.80E+09	1.2E+07	2.7E+07	5.2E+06

In the boundary type of model, air and fuel are both defined as velocity (m/s). The air velocity is inputted from the boundary template, while fuel mass rate, as a discrete phase material, is defined from the injection template. As the pellet is cylindrical not spherical, the equivalent diameter is calculated considering the volume of pellet as follow (Erlich & Fransson, 2011):

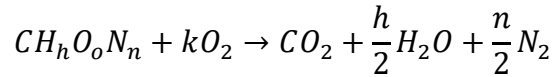
$$D_E = 2 \sqrt[3]{\frac{3}{4\pi} V_p} \dots\dots\dots 6-16$$

where D_E = particle diameter (m), V_p = average volume of particle (m³)

The calculation of mass to air fuel ratio is represented as the equivalence ratio (ER) of the proportion of air to fuel in gasification model (AF_{mod}) to the stoichiometric air-fuel ratio for a complete combustion (AF_{st}) (Erlich & Fransson, 2011).

$$ER = \frac{AF_{mod}}{AF_{st}} \dots\dots\dots 6-17$$

The (AF_{st}) can be calculated based on empirical formula of the fuel (Jaojaruek, 2014). The empirical formula of the fuel is derived from the ultimate analyses of the fuel.



Thus, the number of moles of oxygen required for a complete combustion is k :

$$k = \frac{h}{4} + 1 - \frac{o}{2} \dots\dots\dots 6-18$$

Where: k = the number of moles of oxygen for complete combustion

h = mole fraction of Hydrogen in fuel

O = mole fraction of Oxygen in fuel

If air is used to supply the oxygen, the mole ratio of air to oxygen is 4.76. Then, the stoichiometric air to fuel ratio (A/F_{st}) can be calculated as:

$$A/F_{st} = \frac{4.76 k (mw_{Ox})}{(mw_{fuel})} \dots\dots\dots 6-19$$

Where: A/F_{st} = stoichiometric air to fuel ratio

k = the number of moles of oxygen for complete combustion

mw_{Ox} = molecular weight of oxygen in air (g/mol)

mw_{fuel} = molecular weight of fuel (g/mol)

The reactor’s wall is assumed as stationary with no-slip condition. The wall temperatures of air pipe are set to certain constant values. It is adjusted so that the temperature at the air opening in the bed is close to the oxidation temperature (ANSYS-Inc, 2013). In the real situation, the air pipe is heated by the crawling produced gas before leaving the fuel bed. Table 6.3 summarizes the major characteristics of the current model under development

Table 6.3: Summary of model development parameters and assumptions for CGW pellets gasification

1. General	<ul style="list-style-type: none"> - Pressure based - Steady state - Axisymmetric - Gravitational effect
2. Radiation	P1: the reflection of incident radiation at the surface is isotropic with respect to an incident angle.
3. Turbulence	SST- $k\omega$ -intermittency: include the effect of shear stress transport, kinetic and its dissipation rate, and the change in viscosity
4. Reactions	Non-premix combustion – non adiabatic

5. Particle interaction	Euler-Lagrange (discrete phase) Particle devolatilization model: single kinetic rate Particle combustion: - Diffusion-limited rate for CGW100, CGW95, CGW90 - Kinetic/Diffusion-limited rate for CGW85, CGW80
6. Boundary conditions:	
- Air input	Simulated at air to fuel ratio 1.3 (v/m)
- Fuel input	0.0033 kg/s (12 kg/h) Equivalent particle diameter (D_E) = 0.013 m (pellet length = 0.035 m, dia= 0.007 m, uniform)
- Pressure outlet	Pressure min 249 Pascal and max 747 Pascal
- Air pipe wall	Stainless steel, thickness = 0.003 m
- Other walls (interior and exterior walls)	Stainless steel, thickness = 0.003 m

6.4.7. Numerical calculation

ANSYS FLUENT applies separate models for solving the partial differential equations of governing integral equations of the conservation of mass and momentum, energy and other scalars such as turbulence and chemical species. There are two approaches within a solver program of ANSYS Fluent: pressure-based and density-based. Pressure-based was formerly developed for low-speed incompressible flows, in contrast to the density-based approach which was used for high-speed compressible flows. Recently, both methods have been extended and reformulated to apply for a wide range of flows. Within the non-premix combustion model, the default of solver is to operate with the pressure-based model (ANSYS-Inc, 2013) .

Two pressure-based solver options are available in ANSYS Fluent: the segregated and coupled algorithms. In the coupled algorithm, the momentum and continuity equations are solved in a fewer steps than in the segregated algorithm (ANSYS-Inc, 2013). In the segregated algorithm, the convergence significantly improves and it reaches convergence faster. However, the segregated algorithm

requires higher memory, about 2 times of segregated algorithm. This model applies a coupled algorithm approach and to solve the equations a SIMPLE pressure-velocity coupling is used. The SIMPLE algorithm uses a relationship between velocity and pressure corrections to enforce mass conservation and to obtain the pressure field.

By default, ANSYS Fluent stores discrete values of the scalar parameters at the cell centres. The discretisation scheme is used to discretise the momentum equations for a scalar transport equation. The theory and user guide of ANSYS Fluent provides recommendation on how to use the various spatial discretisation schemes. In this model, the discretisation for the pressure applies PRESTO! (Pressure staggering option). The second order upwind is for other factors; except for the mixture variance was the first order upwind (ANSYS-Inc, 2016)

6.5. Results and discussions

6.5.1. Model validation through the previous experimental data on macadamia shell gasification

Due to the time limitation, model validation using the CGW pellets was not performed in this study. Instead, earlier experiment data of gasification on macadamia shell feed conducted in USQ in this GEK 10 kW type gasifier was used (Fig 6.5). Overall, the CFD model was developed for the specific design of 10 kW gasifier (Fig 6.3). The model can use a wide range of fuels which fuel property data would need to be inputted to the model by users. As this model provides dynamic fluid calculations as to effect of gasifier design platform, while the properties of fuels are the simulated values, then the model validation using macadamia shell experiments can be accepted as a basis for simulations of CGW pellets gasification performances.

Two thermocouples for the recording temperatures inside the bed were used. The first (T_{red}) was placed in the upper part of the concentric space, representing the combustion zone temperature, while the second (T_{bred}) was at the bottom side of concentric zone, representing the temperature of reduction. An online gas infrared analyzer was attached at the gas outlet to measure the concentrations of CO, CO₂ and total hydrocarbon (HC). These macadamia shell gasification experiment data were used to validate the development model.

Figure 6.5 shows the temperature data and the gas composition. The experiment reached a stable condition after 70 minutes of running time. The temperature at T_{red} (combustion zone) was about 1200-1250 K (927- 977°C) and the

T_{bred} (bottom reduction zone) was about 1000-1080 K (727-810°C). At a steady state operation, a gas with constant composition (in % v/v) was reached, containing about 9% CO₂ and 23% CO.

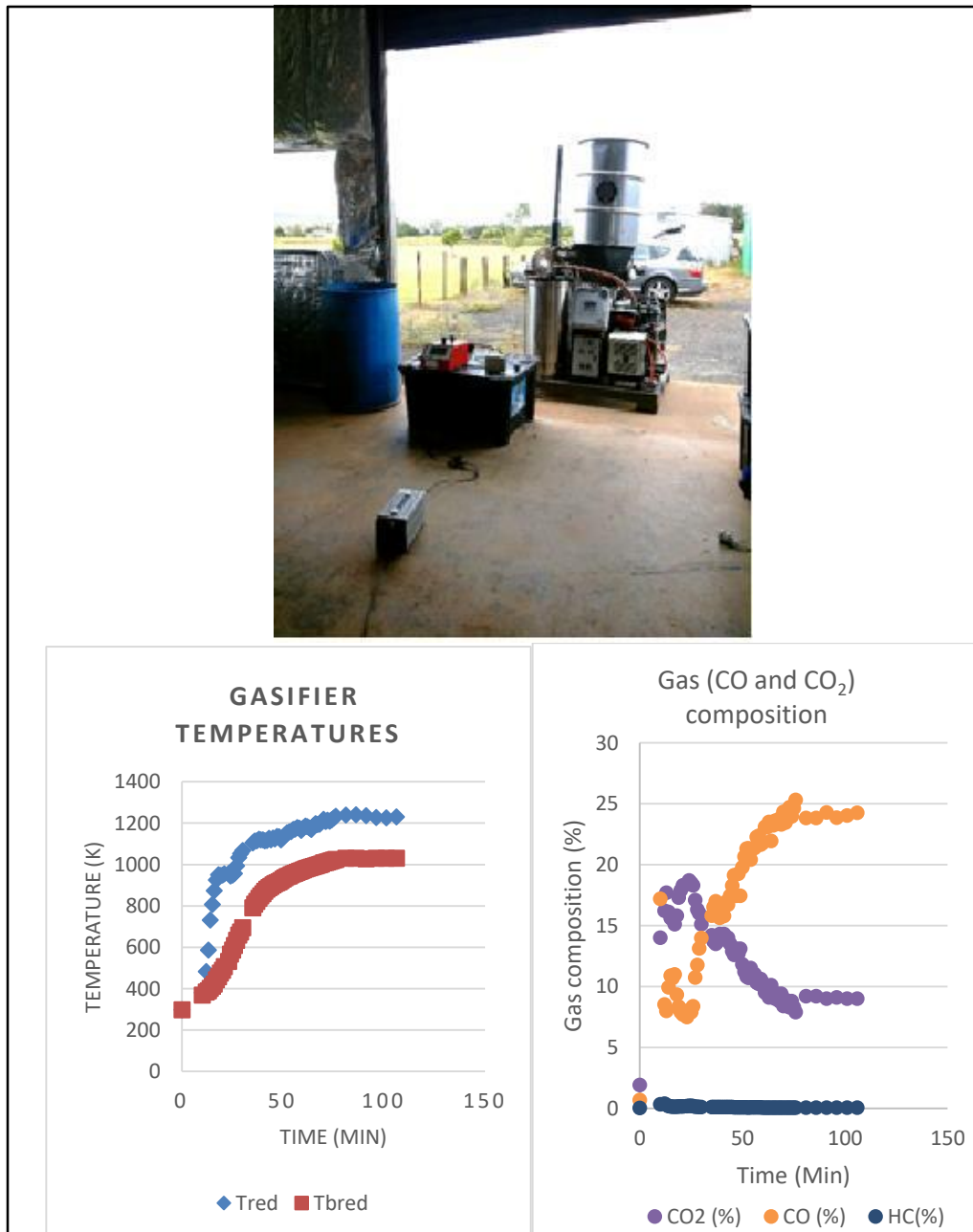


Figure 6.5: Experiment of macadamia shell gasification

To test this CFD model, data on composition, activation energy of TGA pyrolysis and combustion of macadamia shell from a previously published research (Vhathvarothai *et al.*, 2014b; Vhathvarothai *et al.*, 2014a) were used. With these data set, the model simulation applied air/fuel ratio 1.3 (v/m) corresponding to 25% of the stoichiometric full combustion ratio (ER =0.25).

Figure 6.6 shows the result of simulation in the form of vertical iso-surface within the reactor at $y=0.0015$ m. The iso-surface was constructed very close to the central symmetrical axis. The baseline of analyses (iso-surface line) is near a point of flame temperature of 1420 K. Table 6.4 shows the summary of the experimental data and the modeling result. The calculated temperature is very close to the experimental data. The average volumes for gas species are also relatively close to the experimental data. There are slight overestimations for the value of CO_2 and CH_4 and an underestimate for the CO. Unfortunately, the analyser was not set to separate and quantify the hydrogen content. Nevertheless, for the comparison purposes of the effect of fuel properties on the gasification performance, the accuracy of this model is very acceptable. The prediction of relatively high concentration of hydrogen still remains to be confirmed.

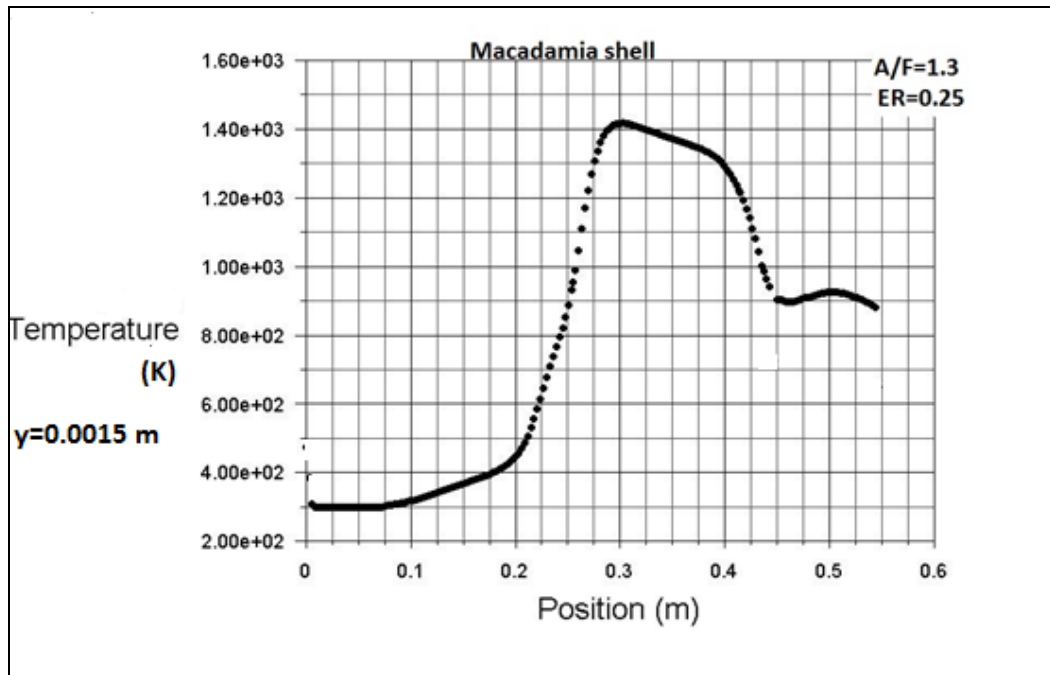


Figure 6.6: Iso-surface of the temperature of CFD model result for macadamia shell gasification

Table 6.4 Gasification of macadamia shell: modeling and experimental results

Results	Model	Experiment
<i>Temperature (K):</i>		
Combustion (upper concentric at x=0.25 to 0.3m)	900-1420	1250
Reduction (bottom reduction at x=0.425m)	1100	1080
<i>Species (% v/v):</i>		
CO ₂	10.2	9.4
CO	22.7	23.3
CH ₄	0.1	0.051
H ₂	16.5	NA

6.5.2. Predicted profiles of temperature, velocity, mass of carbon fraction, particle density and species fraction

Figure 6.7 shows simulation result of the example profile. At first, the fuel enters the pyrolysis zone. Next, it passes into the combustion zone. The area under the air inlet down to the neck of the concentric space is the combustion zone. Following that, it reaches the reduction/gasification zone. The area under the combustion zone is the reduction/gasification zone. Lastly, the particle leftovers (char and ash) pass down the grate, while the gas is exited through the pressure outlet.

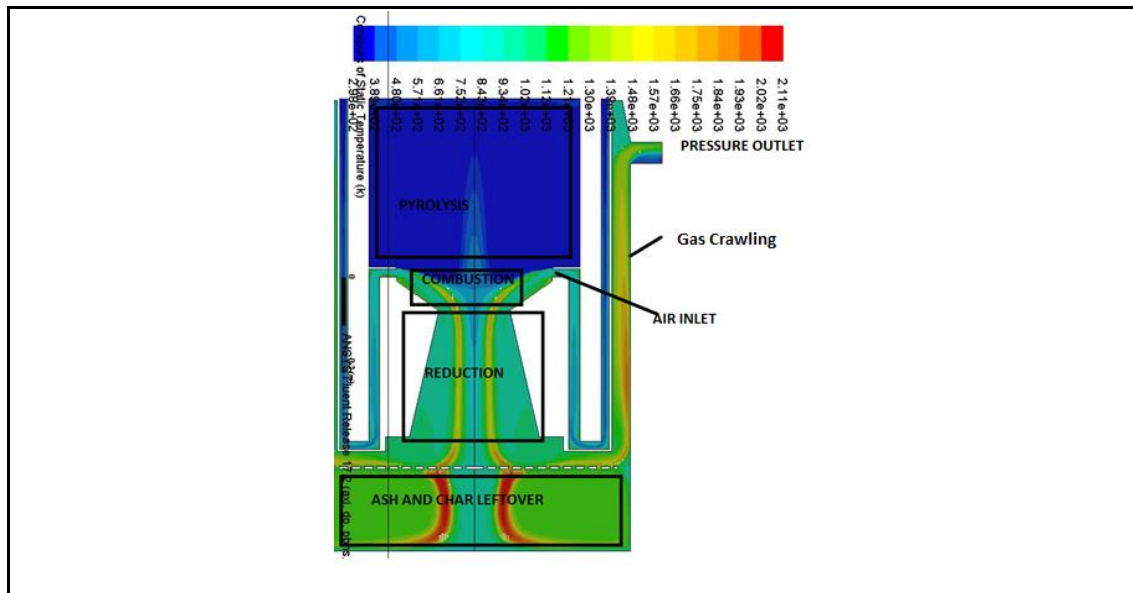


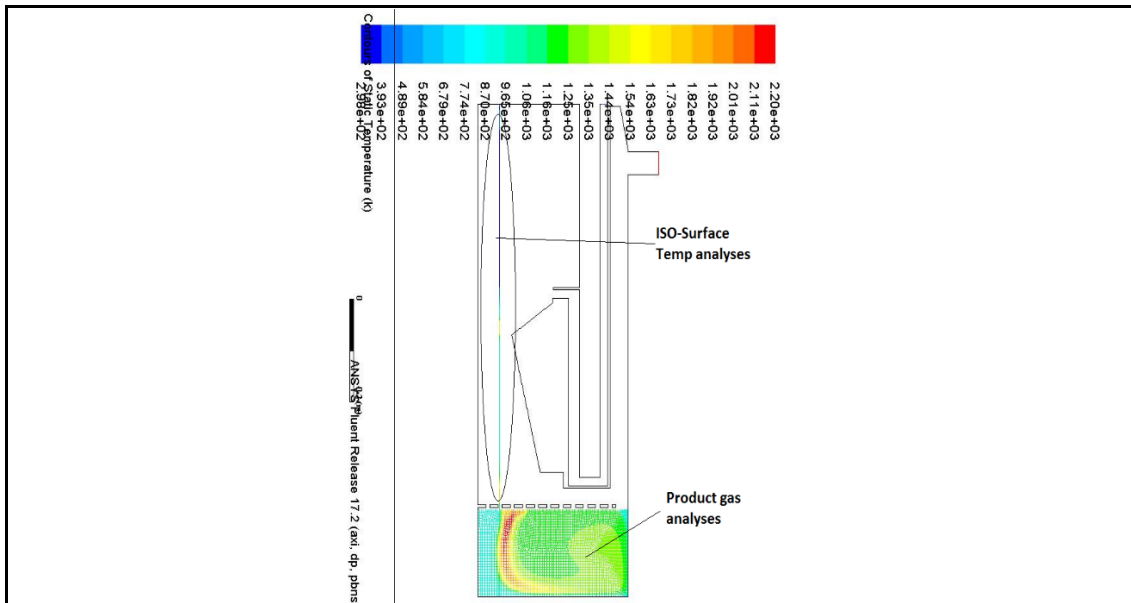
Figure 6.7: Model interpretation of temperature contours

The following paragraphs discuss the model interpretation and its limitations in analyzing the profiles of temperature, velocity, mass of carbon fraction, particle density and species fraction.

Temperature and velocity profiles

The developed model applies the non-premix combustion model for the source term of reacting particle. It firstly utilizes the point at the highest turbulence of mixture fuel-oxidizer to set the area of the diffusive flames. In this area, the mixture fraction values are also related to the hottest area. On contrary, the area with lowest turbulence would be also the coolest. Consequently, the longer the distance from the flame, the cooler the temperature (Fig 6.7).

A set of scalar numbers ranging from low to high ratio of fuel-oxidizer in the mixture is generated by the Probability Density Function (PDF) method. These numbers are then related to the particle temperature function. In the gasification, the lean mixture of fuel-oxidizer leads to the lean flame area. The scalar, then, controls a range of temperature profiles inside the bed. The model simulation was done in a half of the reactor; the vertical axis is the symmetrical axis. To analyze the temperature profile along the bed, an iso-surface line was constructed. This was to capture the temperature difference resulted from the model calculation based on a line inside the reactor (Fig 6.8).



*The simulation was done in a half of reactor geometry; the vertical axis was the symmetrical axis

Figure 6.8: Baseline of temperature analyses and surface zone of product gasses analyses

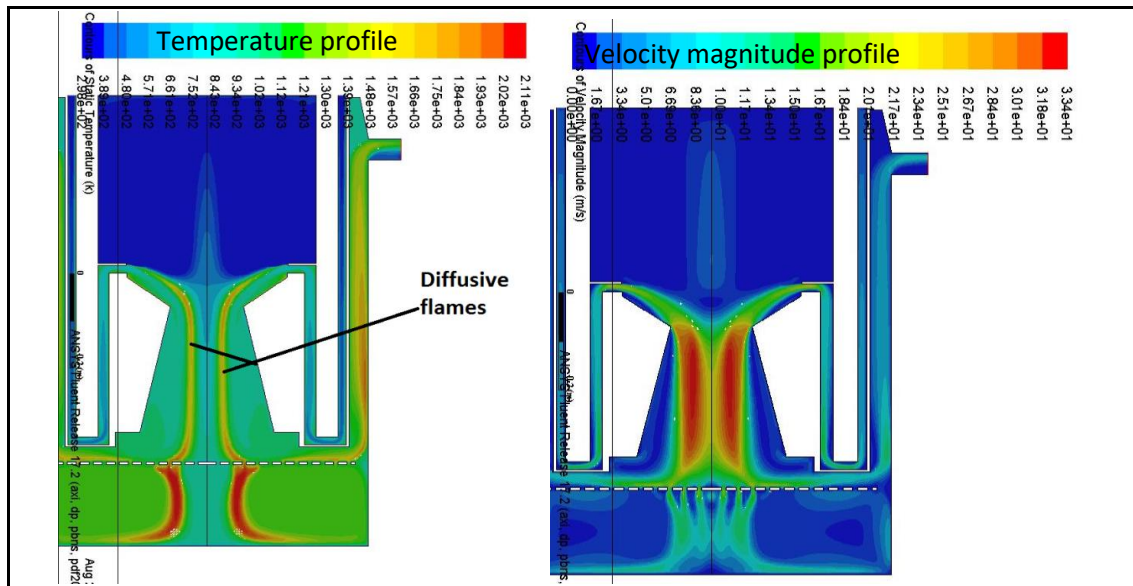


Figure 6.9: Temperature and velocity magnitude (right side) profiles

A case of temperature profile is shown in Figure 6.9 left side. The flame is shown as the dark yellow lines across the combustion and reduction zone. Because of these lean flames, the particles within the flame have varied in temperatures, though they are lying in the same designated area of combustion zone. From its iso-surface line, the flame temperature is predicted to be about 1700 K (~1400°C). The vicinity is found to be cooler at around 1000 K (~730°C). The pyrolysis area shows the temperature from 390-750 K (117- 470°C), similar to the onset of devolatilization temperature.

Following the temperature profile pattern, the fastest velocity particles (Fig 6.9 right side) occur in the middle zone of concentric area and the lowest at the devolatilization zone. This is reasonable, as the middle concentric area has a higher particle conversion through the combustion leading to higher velocity. The highest turbulence in the central part of concentric also influences different velocities of particles inside pyrolysis zone. The central area has particles with higher velocities than in the region near the wall. This is shown by a slightly brighter blue colour in the middle of pyrolysis region. This indicates that particles fed from the middle part of gasifier will drop drawn slightly faster than those in the nearer walls.

The limitation of this model is its inability to predict the temperatures in the middle area of char-ash leftover (area under the grate) and the area under the pressure outlet (Fig 6.9). In real situation, however, the gasifier has an automatic mechanical removal of char and ash. This model could not simulate this feature. In the model, it is possible that further reactions can occur under the grate as indicated by the flame lines

in the center of the char-ash leftover area. In turn, this would also impact onto the gas crawling area situated under the pressure outlet by significantly increasing the temperature. Further shortcoming of the current model is that due to predicted high turbulence in gas crawling space, continual combustion still exists, thus causing high temperature. In real situation this does not happen. Instead, the vacuum pump sucks out the gas products having moderate temperature $< 400^{\circ}\text{C}$; this is in contrary to model prediction of over 1000°C .

Mass fraction of carbon and density profiles

As described previously, this model applies the probability density function (PDF) which is dependent on a scalar parameter namely mixture fraction. This is the fraction of the unburnt fuel species to all the mixture species. At high turbulence, which also is referred to high temperature conditions, the mass of unburnt fuel would be lower than in the areas of low turbulence. The density of particles also follows the similar rule.

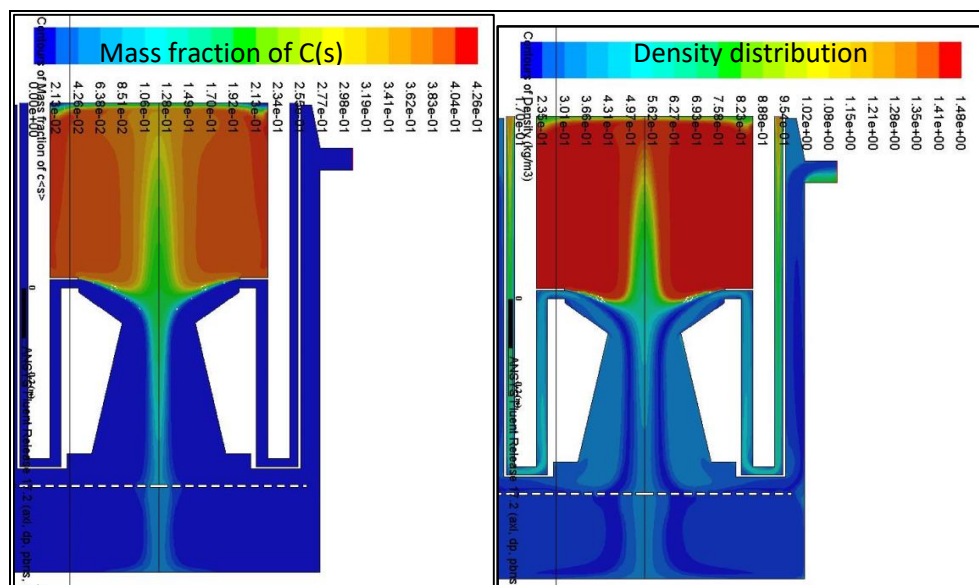


Figure 6.10: Mass fraction of C(s) and density distribution

Figure 6.10 shows the mass fraction of carbon (solid) and the density profiles from a simulation of CGW95 pellet gasification. It can be seen that the mass fraction of solid particles fulfills the pyrolysis zone. The highest unburnt carbon fraction is close to the wall of the pyrolysis zone. The mass fraction of unburnt carbon continuously drops when reaching the concentric space. This result is similar to the situation of coal gasification model in a downdraft type conducted by Patel *et al.* (2013) which also applied similar non-premix combustion model for the chemical

reactions. Janajreh and Al Shrah (2013) developed a CFD model for the same type of gasifier but with a bigger capacity. The developed model, however, applied species transport reactions. Despite using a different method of reactions modelling than this study, their work resulted in a similar trend for profile prediction of unburnt carbon. They reported the char concentration was significantly reduced right after the combustion zone, continually down to the bottom of gasifier.

Figure 6.10 also shows the particle density distribution vertically along the bed. It predicts that the density is the lowest in the flame and relates to the highest turbulence. The higher density particles might then be shifted closer to the wall. This would be in agreement with the reality that the design of concentric wall is expected to slow down the particle velocity, so that the reduction reaction could occur in this area.

Applying discrete phase model shows that the reduction zone is actually lying around the vicinity of the flame starting from the middle part of pyrolysis zone up to the bottom of concentric area. Similar to other previous studies (Janajreh & Al Shrah, 2013; Patel *et al.*, 2013) which use discrete phase model for downdraft gasifiers, the pyrolysis, combustion and reduction zones are certainly not layered based on the height of the gasifier but on the distance from the hottest area. This is the same conclusion as achieved in our model. These results are however in contrast with the outcome of the model developed by multiphase analyses (Murgia *et al.*, 2012).

Gas species profiles

In real condition, a vacuum pump with a variable pressure 1-3 mmH₂O is attached to the gas outlet for sucking out the product gas. This model applies an input pressure under the boundary condition of pressure outlet. The simulation results, however, show that it could not convey all the gasses out of the bed. In this model, the gasses are shown to be trapped under the grate (the ash and char leftover zone). Furthermore, the temperature inside the gas crawling (below the pressure outlet) is significantly higher than the real condition, so that the CO₂ gas appears inside the crawling area and might be from the extension of the combustion reaction. This is in contrast to the real condition in which further reactions would diminish here. Thus, this appears to be a limitation of this model. Therefore, an incident occurring in the area inside the crawling gas should not be considered as the proper/realistic model of the output. Instead, species gas fraction prediction is determined at the surface area

under the grate (Fig 6.8). This is based on the estimation that the products lying at and below the grate are predominantly those that have passed through the whole processes of pyrolysis, combustion and gasification at zones above it.

Figure 6.11 shows the contours of CO and CO₂ from a simulation result of CGW95 pellet gasification. It can be seen that a slightly higher CO₂ is detected in the area of pyrolysis, and become highest in the flame zone area. Meanwhile, CO is shown at first near the flash combustion zone and increases at the bottom of reduction zone. At the bottom of concentric zone, the mole or volume fraction of CO is at the maximum 19.8 % v/v, while the CO₂ is about 10% v/v. This prediction may be reasonable for the biomass downdraft gasification using air as the oxidant. Erlich and Fransson (2011) conducted an experiment of several biomass pellets gasification in the downdraft type using air to fuel ratio of 1.1-1.4. The average CO/CO₂ volume ratios were around 1-2.5.

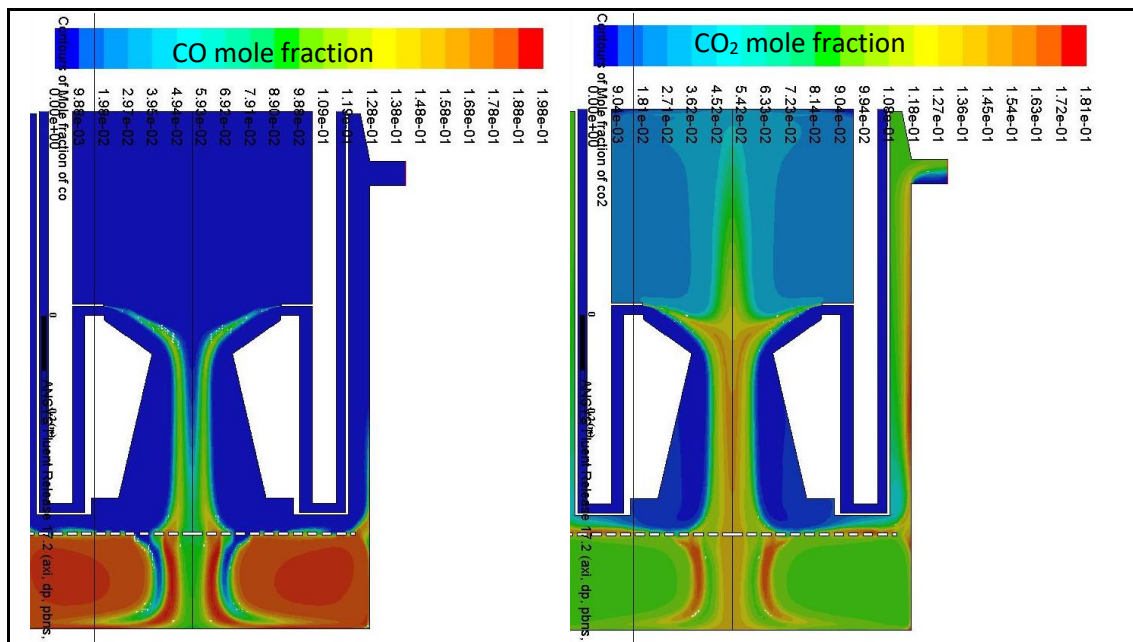


Figure 6.11: CO and CO₂ mole fraction profile

Figure 6.12 shows the contours of CH₄ and hydrogen. As a hydrocarbon gas, the CH₄ is produced more in pyrolysis zone, while the hydrogen is produced at higher temperature still. CH₄ reacts at those high temperature conditions with water producing CO, H₂ and CO₂. Thus, at the bottom of the gasifier (i.e. in the gas outlet also), it is expected to find relatively high CO and H₂ (Fig 6.13).

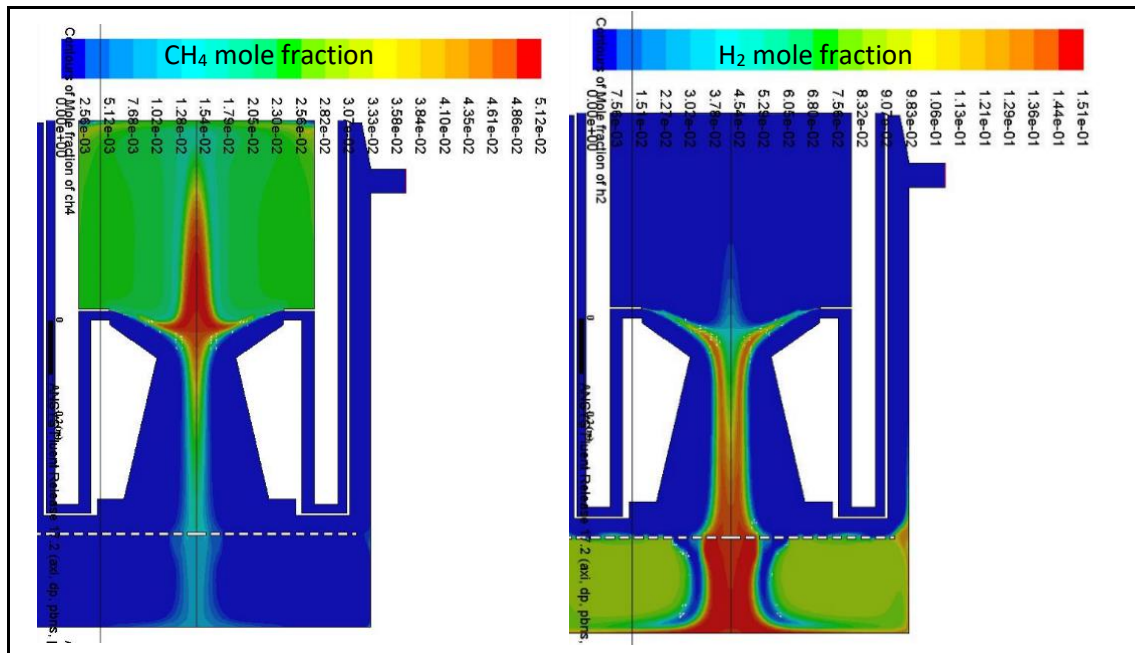


Figure 6.12: CH₄ and H₂ mole fraction profile

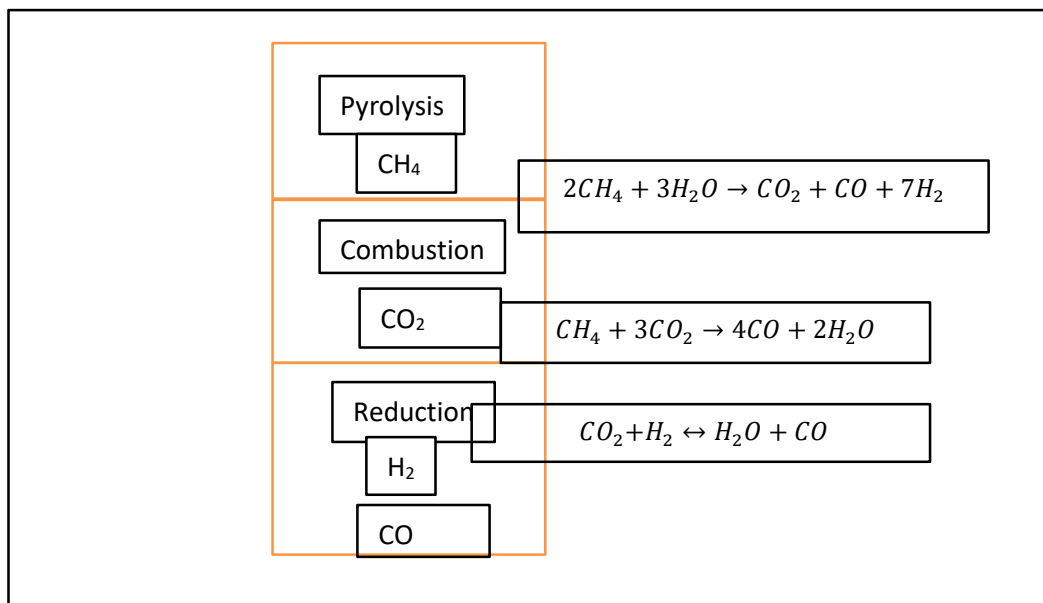


Figure 6.13: Model interpretation of reactions in each stage of gasification

This developed model which applies the PDF method is able to predict the production gas composition relatively close to the real situation, particularly for CO and CO₂ species. Applied for the same design as our gasifier, other studies (Janajreh & Al Shrah, 2013) used a different model: Species Transport Reaction model. In their model, the accuracy of prediction would depend on all species and their reaction rates as well as the mixing rate composition. Apart from taking data from other sources, the computing is still very time consuming and require extensive empirical data. The

reported result seems to predict a significant overestimation of CO (38.23% v/v) and underestimation of CO₂ (0.85% v/v) in comparison to the real condition. Furthermore, the reactions would only occur if the particle size is very small in comparison to the reactor volume. In the species transport model, the particle diameter for the discrete phase was set at 0.1 mm, while the experimental data related to 1-2 cm. In this developed non-premix combustion model, the particle diameter corresponds to a diameter of a spherical equivalent of actual fuel size.

6.5.3. Impact of different CGW pellets on gasification performance

The simulation of the CGW pellets gasification was done using this developed model for comparison of the gasification performance. Fig 6.14 shows the iso-surface analyses of the bed temperatures of the gasification CGW100 and CGW80 pellets. The other pellets profiles are provided in Appendix E. Table 6.5 shows the comparison of the combustion zone ($x=0.25-0.3$ m) temperatures and the bottom of reduction zone temperature ($x=0.425$ m). The simulations of the gasification was done using similar amount of air to fuel ratio which was 1.3.

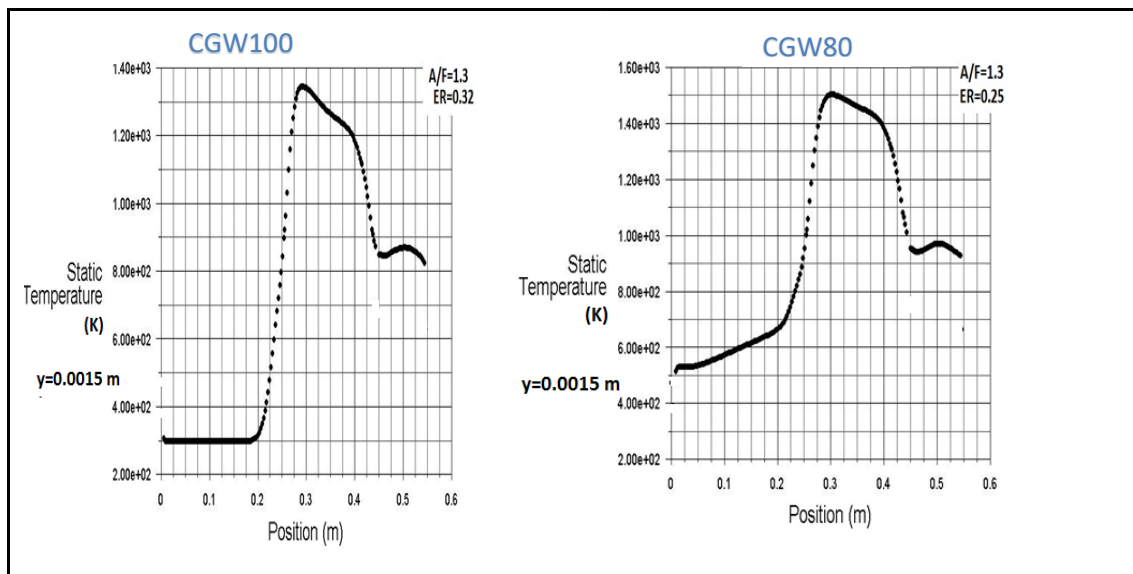


Figure 6.14: Iso-surface of the temperature profiles for CGW100 and CGW80 gasification

Table 6.5 CFD model generated results of combustion and reduction temperatures of gasification CGW Pellets at A/F=1.3

Type of pellet	Combustion temp. (K)	Reduction temp. (K)
CGW100	800-1450	1000
CGW95	800-1275	950
CGW90	850-1375	1050
CGW85	900-1500	1150
CGW80	900-1500	1100

It can be seen from the Table 6.5 that the higher carbon blends in the pellet increase the combustion and reduction temperatures. However, the CGW95 pellet gasification has a slightly lower temperature of combustion and reduction than those of CGW100. According to the previous chapters on combustion and pyrolysis behavior of the CGW pellet fuels, the CGW95 has the highest reaction rate both in combustion and pyrolysis. The initial oxidative pyrolysis reaction also occurs at a slightly lower temperature than for CGW100. The input data of kinetic properties of CGW95 pellet significantly affects the reduction temperature in gasification.

The prediction of average species fraction of produced gas is provided in Table 6.6. Theoretically, in all air gasification processes, the higher the carbon feed content, the higher is concentration carbon containing gasses (CO, CH₄, CO₂) as well. However, it can be seen that the predicted average composition of CGW95 gasification in respect to CO and CH₄ is higher than CGW90.

Table 6.6 also shows the predicted syngas heating value ranging from 3.9 to 5.1 MJ/m³. It was calculated as follows:

$$HV_{gas} = (Y_{CO} \times 13.1) + (Y_{CH_4} \times 37.1) + (Y_{H_2} \times 11.2) \dots\dots\dots 6-20$$

whereas: HV_{gas} : production gas lower heating value (MJ/m³)

Y : the mole fraction of the gas

The predicted heating value of CGW95 gas is higher than CGW90. Once more the synergy found in pyrolysis and combustion behavior of CGW95 could affect the gasification performance. It is demonstrated that the combustion and pyrolysis kinetic behavior will have an effect on modeling the gasification result.

Table 6.6: Prediction of species gas fraction (% volume)

Pellets	CO	CO ₂	H ₂	CH ₄	HV (MJ/m ³)	Production gas efficiency (%)
CGW100	16.5	13.1	15.9	0.2	4.19	47.7 -70.6
CGW95	19.8	11.6	14.2	0.2	4.40	44.4 - 69.4
CGW90	17.1	13.4	13.5	0.1	3.91	37.1 -58.0
CGW85	24.0	10.3	14.9	0.1	4.95	45.0-70.4
CGW80	25.4	9.7	14.7	0.1	5.10	44.9-70.2

The predicted production gas conversion efficiencies (Table 6.6) are based on the assumption of gas yield of about 1.6 – 2.5 m³/kg of fuel pellet. These reference values are based on experimental data of gasification of variety biomass pellets in a downdraft type gasifier at air to fuel ratio ranging from 1.1-1.4 (Erlich & Fransson, 2011). The production gas efficiencies were calculated as follow:

$$Eff_{gas} = \frac{HV_{gas} \times F_{gas}}{HV_{fuel}} \dots\dots\dots 6-21$$

- Where
- Eff_{gas} = production gas conversion efficiency (%)
 - HV_{gas} = production gas heating value (MJ/m³)
 - F_{gas} = production gas- fuel feed ratio (m³/kg)
 - HV_{fuel} = heating value of fuel (MJ/kg)

The production gas conversion efficiencies of the CGW pellets gasification are predicted to be about 37-75% using the range of gas-fuel ratios of 1.6-2.5 m³/kg fuel pellet (F_{gas}). These figures may require more experimental data on CGW pellets gasification. The hypothesis is that, most likely, the higher the biochar content in the pellet, the higher is the resulting producer gas-fuel ratio. Erlich and Fransson (2011) reported that the wood pellet, having higher carbon content, had higher dry gas-fuel ratio (2.0-2.5 m³/kg) in contrast to the non-woody pellets. Bagasse pellets gave yield 1.6-1.8 m³/kg and empty fruit bunch oil palm pellets gave 1.8-2.5 m³/kg.

Overall, this model can provide a reasonable and good prediction of CGW pellets gasification performances in the GEK 10 kW gasifier. The results are also close to the experimental gasification of hardwood pellets conducted by Brar *et al.* (2013). These authors gasified hardwood pellets using the same type of gasifier (GEK 10 kW)

and reported the combustion temperature about 1200°C (1473K). The CO content was approximately 21%, the CO₂, H₂ and CH₄ were 11 %, 16 % and 2 % respectively.

6.6. Summary and conclusion

This chapter has simulated the process of CGW pellets gasification in a pilot plant. A CFD model for a 10 kW gasifier capacity has been developed using ANSYS FLUENT 17.2 software. It is modeled in a 2D-axisymmetric plant applying a discrete phase particle model, with the reaction of non-premix combustion and the turbulence model of the SST-K ω -Intermittency factors. The non-premix combustion, by default, uses a simple method of the Probability Density Function (PDF) for determining the gas and temperature profiles.

The model has been validated using a set of previous experimental data for the gasification of macadamia shell. It has been shown that overall, the developed CFD model could provide a reasonable prediction of the profiles within the reactor, particularly the temperature profile. However, because it was not set to model the mechanism of char and ash removal as in the real situation, this has resulted in a considerable overestimate of the temperature profile inside the crawling gas and in a small area at the bottom grate where char and ash leftover are collected. In this model, the estimation of the gas product composition has been conducted by averaging the species fraction in the bottom grate area.

It has been shown that the developed CFD model is able to predict the gas composition close to the experimental data. The developed CFD model has also been applied to simulate the gasification of 5 types of CGW pellets (CGW100, CGW95, CGW90, CGW85, CGW80). The simulation employed the data on physical size, the proximate and ultimate properties of the fuel and the thermochemical behavior of combustion and pyrolysis resulting from the previous chapters.

The simulation results have shown that, in general, an increase of biochar in the pellet increases the reduction zone temperature. It also increases the CO content in the gas and its heating value. However and quite unexpectedly, at a 5% addition of biochar, the CGW95 yields a gas with higher CO content than that of CGW100 and CGW90. This contributes to the highest heating value of the product gas as compared to both CGW90 and CGW100 gas (Table 6.6). This is related to the input data from TGA behavior of CGW95 in combustion and pyrolysis experiments which indicate a

synergistic effect of biochar addition, yielding a blend of a higher conversion rate than in unblended pellet (CGW100) and 10% biochar pellet (CGW90).

The obtained gas heating values are in the range of 3.9 – 5.1 MJ/m³ (Table 6.5). Following this, the efficiency of product gas conversion has also been calculated assuming a variable of product gas-fuel ratio range of 1.6-2.5 m³/kg fuel (Erlich & Fransson, 2011). The conversion efficiencies are found to be ranging from 37%-70%, which may require additional confirmation. Possibly, the higher biochar content in the pellet has led to higher gas-fuel ratio.

In this study, the simulations of CGW pellets gasification has been conducted at a fixed air to fuel ratio. It is thus possible and even desirable to adjust this ratio to optimise the gas heating value. This may also lead to a need to modify the gasifier design, to allow the change of working pressure of the inlet air.

CHAPTER 7: Industry Impact of Converting Cotton Gin Waste into Thermochemical Energy

Abstract

This chapter evaluates the opportunity and impact of utilising the developed cotton gin waste pellets for energy production. Three simplified scenarios of energy productions from gasification of CGW100, CGW95 and CGW80 pellets are constructed and compared in a gin processing 35,000 lint bales per year. The energy input to produce pellets is estimated as 2-3 MJ/kg. The cost of production for the CGW pellets is AU\$101-AU\$128/tonne. The re-use of char from the gasification by-product could reduce the external purchasing cost of bio-char; otherwise this cost would significantly contribute to the pellet price. The costs of producing the pellets for covering the power and energy requirements of the gin are compared with the current expenditure of energy use. It is found that the CGW100 could replace 100% of the energy of drying and 64% of electricity consumption, while the CGW95 could cover all the drying energy and 81% of the electricity required to run the gin. The CGW80 could cover both of drying and electricity, yielding even a modest surplus of the pellet production at about 296 tonnes/year. The potential greenhouse gas emissions could also be reduced from 52.35 kg CO₂-e/bale to 16.28 for CGW100 and 8.59 for CGW95. The CGW80 case can achieve more GHG reduction credit from the remaining pellets sold into the market as an alternative to wood pellet fuel.

Keywords: cotton gin waste (CGW), fuel pellet, cost analyses, greenhouse gas emissions

7.1. Introduction

Australia is among the top 10 cotton producer countries. A postharvest method, namely the ginning process, is the first stage of processing the harvested materials. It separates the fiber (lint) from seed. In Australia, the separation in gin typically produces 35% of lint, 55% of cotton seed and the remaining 10% of cotton gin waste (Cotton-Australia, 2014). The lint is then further processed as an input material in the textile industry, while the cotton seeds are processed further in other factories to produce cotton seed oil. The oil is used in the food and chemical industries. The leftover of the ginning process is the cotton gin waste (CGW). It comprises of various parts of the cotton plant such as the leftover of lint (fibre), pods, stem, leaves and burs, together with a small amount of seed.

The lint is pressed in the form of bales. Each lint bale is weighted 227 kg (500 pound). A gin plant is often categorized from its ability to produce certain number of the lint bales. The baling press, a machine in the gin, is often the bottleneck in the ginning operation; the term of “capacity” often refers to this press machine’s capacity to produce a particular quantity of bales per hour (Ismail, 2009). Although some gins

can process up to 90 bales per hour, a survey reported that gins in Australia typically produce only between 24 to 60 bales/hour (Ismail, 2009). A medium size of cotton gin plant has an average capacity of processing 40 bales/hour lint and can potentially discharge about 2 tonnes/hour of CGW. That medium size of gin has yearly production of about 35,000 lint bales/year (Ismail, 2009).

The whole process is fully mechanised and energy extensive. It often requires a drying operation for obtaining a more uniform moisture content of lint. At present, most of the energy required for this operation is sourced from the natural gas or LPG. The next processes after drying are cleaning, ginning, packing and handling. The electricity required for running these machines is almost always sourced from the national electricity grid. Overall, the gas and electricity usage comprises approximately 39% and 61% respectively of the total energy required for producing a bale (Ismail, 2009). Unlike sugarcane industry which utilises its bagasse for electricity and steam generation, cotton gins are at the moment almost entirely dependent upon the external sources of energy. The potential of alternative energy production for self-usage is thus the reason for targeting the utilisation of CGW waste as a source of energy.

This chapter evaluates the opportunity and impact of utilising the cotton gin waste for energy production by calculating the costs of pellet productions and the economic/environmental benefits of using the pellets to power the gin. Selecting gasification for this end, three scenarios of energy productions from gasification of CGW100, CGW95 and CGW80 pellets are constructed and compared. Based on results reported in previous chapter, the CGW80 pellet produced the highest energy heating value in the gasification. The CGW95 pellet was chosen for a comparison as it produced the highest fuel conversion among other CGW based pellets. The CGW100 was necessarily included in this evaluation as a baseline of study. These constructed scenarios are compared with the current business as usual case in the gin operation.

7.2. Methods

Three scenarios of pellets production of CGW100, CGW85 and CGW80 in a gin are constructed. The gin is assumed to have an average processing capacity of 40 bales/hour or producing about 35,000 bales/year (Ismail, 2009). The pellets are assumed to be produced from the available CGW in the gin. In this study, the costs of producing pellets were first estimated. The pellets were then fed to a gasifier to provide

energy for drying the modules and electricity to power the machines in the gin. The energy produced from the pellets gasification was eventually used to replace the drying energy and electricity generation in the gin. If there are still remaining pellets, they are sold externally. The framework of the analyses is shown in Figure 7.1

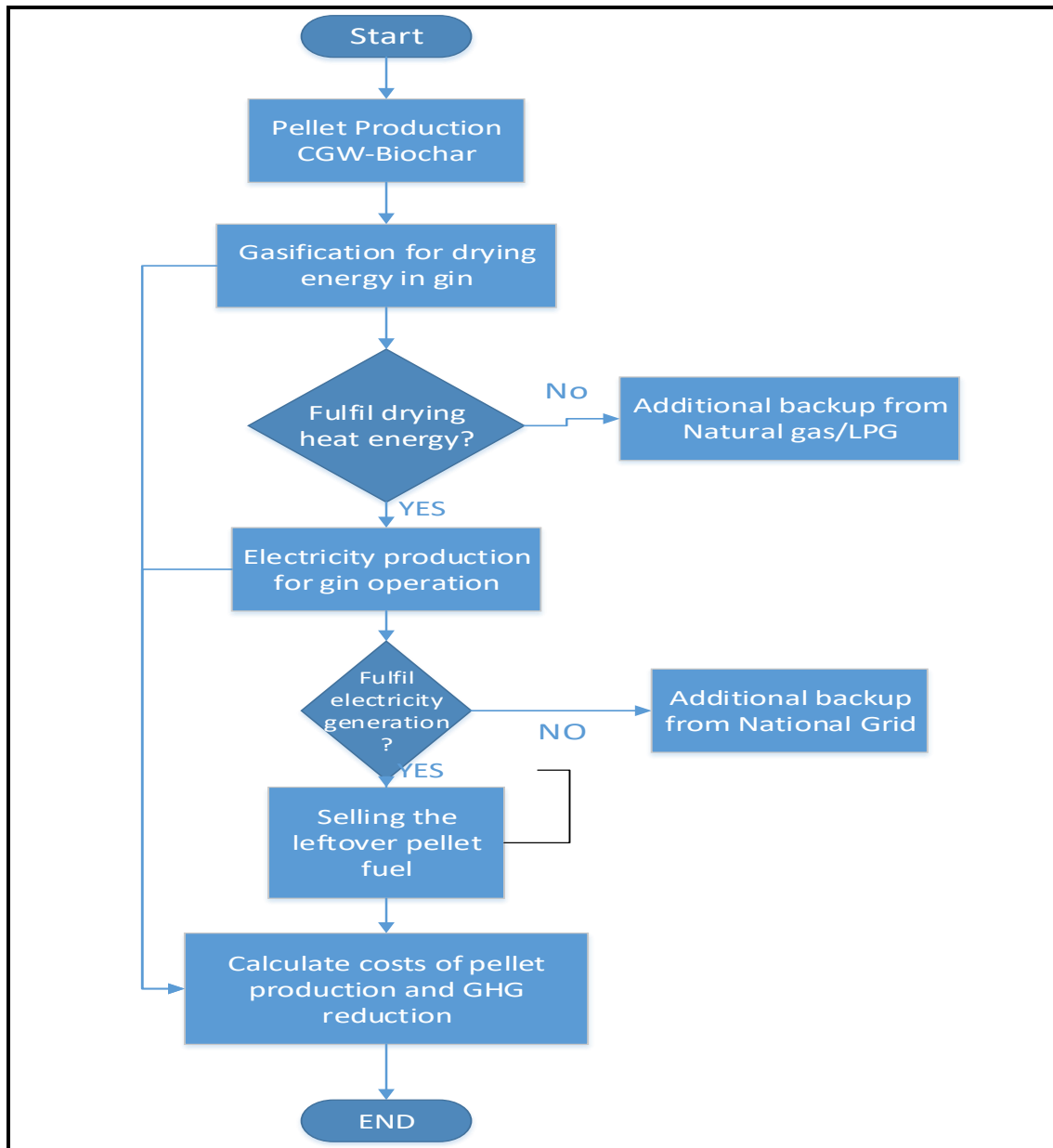


Figure 7.1: Scenarios constructed for re-utilizing CGW pellets as an energy source

The methods applied for evaluating CGW utilization as an energy source are as follows:

- Net energy analyses: calculating the energy input and energy gained in producing CGW100, CGW95 and CGW80 pellets. The input energy is calculated as follows:

$$I_p = E_C + E_b + E_m + E_p + E_d \dots\dots\dots 7-1$$

Where : I_p = input energy of pellet production (MJ/kg)

E_C = energy of size reduction (MJ/kg)

E_b = energy of biochar production (MJ/kg)

E_m = energy of mixing the CGW-biochar-binder (MJ/kg)

E_p = energy of pressing into pellet (MJ/kg)

E_d = energy of drying (MJ/kg)

The energy gained is the heating value of pellets (MJ/kg).

- Economic analyses: evaluating the costs of production of the CGW100, CGW95 and CGW80 pellets against the cost/price energy gained. Then, the CGW pellets are used to cover the energy of drying and electricity in the gin and compared it to the current business-as-usual (BAU) practice. It should be noted here that the investment cost for purchasing the gasifier and electricity generation are not included in the current analyses. The evaluation is simply based on the production costs of pellets to be fed into the gasifier to cover the drying energy and electricity and additional backup if required. The costs of pellet production and backup is then compared with the current energy expenditure.

$$C_p = \frac{(I_m \times f) + (P_c + BC_c + B_c + L_c)}{P_y} \dots\dots\dots 7-2$$

Where : C_p = cost of pellet production (\$/kg)

I_m = Investment cost of purchasing pellet mill (\$)

f = years operation factor (year⁻¹)

P_c = electricity cost to power chopper, mixer and pellet mill (\$/year)

BC_c = biochar cost (\$/year)

B_c = binder cost (\$/year)

L_c = labour cost (\$/year)

P_y = Pellet production (kg/year)

The current energy expenditure was calculated as follow:

$$E_{BAU} = (NG + EL) \times P_{yb} \dots\dots\dots 7-3$$

Where: E_{BAU} = current energy expenditure for bales production (\$/year)

NG = natural gas expenditure (\$/bale)

El = electricity expenditure (\$/bale)

P_{yb} = pellet production (bale/year)

Table 7.1 lists the main assumptions for this study. A gin having the capacity of processing 35,000 lint bales per year could discharge about 2,200 tonnes of cotton gin waste (Cotton-Australia, 2014). With the assumption that about 80% of the CGW is available and recoverable for energy conversion; then about 1,750 tonnes of CGW is available for conversion into the pellet material. As the CGW is a dry material, the weight of CGW100 pellet production could be roughly assumed the same, 1,750 tonnes. If the CGW95 or CGW80 pellet is selected, then 1,842 or 2,188 tonnes pellets per annum are assumed respectively.

Table 7.1: Assumptions for economic calculations

Pellet mill capacity	3.4	tonnes/hours
Electricity for running pellet mill	307	kWh
Bales production capacity	35,000	bales/year
CGW recoverable	0.05	tonnes/bale
Available CGW (ton/year)	1750	tonnes/year
Pellet machine operational time (hours/year)	CGW100	514.7
	CGW95	541.8
	CGW80	643.4
Investment cost (pellet mill)	419,000	\$/unit
electricity price	0.12	\$/kWh
Biochar price	150	\$/tonne
Starch price	200	\$/tonne
Starch (binder)	4%	weight
Labour cost	25	\$/hour

This study also assumes that a unit of pellet mill having a capacity of 3.4 tonnes/hour is used for pelleting the CGW. Based on available quantity of CGW converted into the pellet, the operational hours of pellet mill are found to be about 500-650 hours/year or about 3 months/year. This is due to the nature of seasonal operation of cotton gins. The cotton is usually planted in spring (September/October) and harvested in late March/early April in Australia. The ginning follows this. The biochar can be taken from the by-product of woody waste gasification. In this study, the biochar price was assumed as at \$150/tonne, obtained from the market price of wood waste in the form of chip (\$100/tonne). The associated price in the form of biochar is calculated using the conversion ratio of 65% of char yield from the fresh wood waste.

- Environmental analyses: calculating the net greenhouse gas emission (GHG) reduction from the utilization of CGW100, CGW95 and CGW80 pellets for self-energy production in the gin. To calculate GHG emission from the energy used in the BAU, the emission factors of the natural gas and electricity are used (Australian_Government, 2017).

$$GHG_{BAU} = Q * EF \dots\dots\dots 7-4$$

Where: GHG_{BAU} = greenhouse gas emission of current case (kg CO₂-e)

Q = fuel consumption in GJ or electricity used (kWh).

EF = emission factor (71.3 for natural gas and 1.04 for electricity)

The GHG emissions of the scenarios using CGW pellets to replace some portions of natural gas and electricity from the grid were calculated as follows:

$$GHG_{sc} = (f_d \times GHG_d) + (f_e \times GHG_e) \dots 7-5$$

Where: GHG_{sc} = greenhouse gas emission of scenario (kg CO₂-e)

f_d = percentage of drying using natural gas in scenario

GHG_d = GHG emission of drying in BAU case (kg CO₂-e)

f_e = percentage of electricity usage using external source in scenario

GHG_e = GHG emission of electricity using external resource/ national grid in BAU (kg CO₂-e)

7.3. Results and discussions

7.3.1. Net energy analyses

One of the main purposes of densification is to increase the energy density. The increase in energy density can significantly reduce the transportation and handling cost. However, the process requires an energy input. The comparison of energy consumption to the energy gained was already included in many pellet fuel production studies (Uslu *et al.*, 2008; Sultana *et al.*, 2010; Shahrukh *et al.*, 2016). The process of pellet production used in this study is as described in the Chapter 3 following the size reduction, mixing, pelleting and drying (Fig3.3).

The chopping is done for the purpose to reduce the size and to make the raw CGW more uniform in size. The chopping in this study was done using a table top high speed blender. On actual large scale production, this step may use a suitable sized speed grass chopper. An energy meter was attached to the blender to measure the

energy for chopping and found as much as 0.0658 kWh/kg or about 0.24 MJ/kg. Assuming a 40% energy efficiency of a plant size chopper, then the machine will consume 0.79 MJ/kg for chopping the raw CGW.

The biochar energy production was also accounted into the energy input production for the CGW95 and CGW80 pellet. The coconut shell biochar used in this study had calorific value of 23.36 MJ/kg. The energy input factor for biochar production firstly referred to the analyses of making a conventional woody biochar. It was reported the energy yield of biochar was about 79.8%, implying that the input energy was 20.2% (Bach & Skreiberg, 2016), or about 5.9 MJ/kg; that is an energy production of coconut shell biochar used in this study. This case required a high input energy because of the low conversion technology for carbonization. However, it is noted that the technology of biomass torrefaction is also being continuously improved. In particular, the hydro-char technology has been recently promoted, having a lower input energy for its production but having higher char energy content closer to coal (Liu *et al.*, 2014; Bach & Skreiberg, 2016). Uslu *et al.* (2008) calculated about 92% of the net energy gained from the torrefied biomass fuel. This means only 8% of the energy input was required for the process of torrefaction. If the assumption of 8% of biochar energy is used for its production, then the energy to produce the coconut shell biochar will be about 2.3 MJ/kg.

Mixing was done for the purpose to initially blend the gelatinised starch paste and water. Lately, the starch could also be functioned as the media for enzymatic process to soften the lignin. This study manually mixed the binder material. However, on a large scale, it may employ a windrow composting turner for mixing activity. Such machines have varied capacities and size. According to the study conducted by Levis and Barlaz (2013), such a machine may require an energy of 0.24 kWh/tonne of material mixed. Either a diesel engine or an electric power motor is often used to running the machine.

As stated previously in Chapter 3, this study used a small commercial pellet mill powered by electric motor of 7.5 kW. The manufacturer stated that the machine production capacity is 100 kg pellets/hour of wood pellet. Having different properties with wood, this study tried several times of re-feeding material resulted in of only about 20 kg/hour CGW pellets. The necessity of re-feeding the material was done 3-5 times to produce good, dense and dry pellets.

The pellets from the pellet mill typically had a moisture about 10-15% w.b. In a clear weather, they can be sun dried in an open condition. For a large operation, this option might be impractical and take a too long time, so they in reality are often dried using an artificial dryer. The energy needed for drying biomass is roughly about 2.3 MJ/kg moisture (Souza-Santos, 2010). The thermal dryer efficiency was assumed 60%. Therefore, for drying 15% moisture pellets down to 10% moisture content, an energy of 0.192 MJ/kg will be needed.

Table 7.2 shows the energy input-output analyses for producing the developed CGW pellets on large scale. Table 7.2 shows the no-biochar pellet (CGW100) consumed about 15.21% of the pellet energy content. This is compared with the 5% blended biochar (CGW95) which required 15% of its energy content. As already mentioned earlier, the total energy production of the blended biochar pellet was significantly influenced by the input energy of the biochar production. In this case, selecting the conventional technology of biochar production might require the input energy at about 5.9 MJ/kg of biochar, while the much more moderate improved torrefaction technology could reduce the energy for biochar production up to 2.3 MJ/kg of biochar. For CGW80, using the improved technique of biochar production would turn into a lower total energy input for the pellet production which is only about 13% of its energy content.

Table 7.2: Energy input-output analyses from pellet processing energy

	CGW100	CGW95	CGW80	
Energy input:				
Chopping the CGW	0.0658	0.06251	0.05264	kWh/kg pellet
	40	40	40	% efficiency Chopper
	0.59	0.56	0.47	MJ/kg pellet
bio-char production	n.a	0.09-0.24	0.37-0.94	MJ/kg pellet
Mixing	0.24	0.24	0.24	kWh/ton pellet
	0.000816	0.000816	0.000816	MJ/kg pellet
	60	60	60	% efficiency of mixer
	0.00136	0.00136	0.00136	MJ/kg pellet
Pelleting	20	20	20	kg/hour
	7.5	7.5	7.5	Kw
	0.38	0.38	0.38	kWh/kg pellet
	1.35	1.35	1.35	MJ/kg pellet
Drying	5	5	5	% reduction MC
	50	50	50	g/kg moisture
	2.3	2.3	2.3	kJ/g moisture
	60	60	60	% efficiency dryer
	0.1917	0.1917	0.1917	MJ/kg pellet
Total energy input	2.14	2.20-2.34	2.39-2.96	MJ/kg pellet
Pellet fuel Heating value	14.04	15.86	18.17	MJ/kg pellet
Energy for pellet production as % of its heating value	15.21	13.87-14.76	13.16-16.29	%

7.3.2 Economic analyses

7.3.2.1. Cost of pellets production

This section analyses the economic viability of utilizing the pellet fuel in the gin for covering the current energy needs of drying and electricity. The capital expenditures for energy conversions into heating energy or electricity generation were not included in the analyses. It only compared the CGW pellets energy prices to replace the current energy expenditure (business as usual case) in the gin. A gin having capacity of 35,000 lint bales per year was used as the baseline of the case study. A gin having maximum capacity of 90 bales per hour is often regarded as a typical medium size of gin in Australia. In reality, however, their average production capacities were reported only between 24 to 60 bales/hour (Ismail, 2009). The medium size gin produces about 40 bales/hour; producing 35,000 lint bales/year. Table 7.3 shows the estimated costs of CGW pellets production.

Table 7.3: Costs of CGW pellets production (in AU\$)

	CGW100	CGW95	CGW80
Pellet production capacity (ton/ye ar)	1750	1842	2188
Operational cost :			
Electricity (\$/year)	18,942	19,939	23,678
Bio-char (\$/year)	0	13,816	65,625
starch (\$/year)	14,000	14,737	17,500
Labour 8 persons (\$/year)	102,941	108,359	128,676
<i>Total operational cost</i>	135,883	156,851	235,479
<i>operational cost/prod (\$/ton)</i>	78	85	108
Investment cost/prod (\$/ton), 10 years	24	23	20
<i>Total production cost (\$/ton)</i>	102	108	128
<i>Pellet heating value (GJ/ton)</i>	14.0	15.9	18.2
<i>Comparable energy production cost (\$/GJ)</i>	7.2	6.8	7.0

Table 7.3 shows the costs of producing CGW100, CGW95 and CGW80 pellets were AU\$102, AU\$108 and AU\$128 per tonne respectively. For comparison, the selling price index of wood pellet in this year (2017) is about US\$110-150/tonne (AU\$132-180/tonne) and the world pellet market increases at about 10% annually (<http://www.pellet.org>).

Table 7.3 shows that the cost of CGW100 production is the lowest. However, because the heating value of this type of pellet is also low; it is actually found to be the most expensive for the given energy gained. The CGW80 has the highest energy content, comparable to wood pellet energy content. Nevertheless, the cost contribution from the biochar price is also significant. The CGW95 is the cheapest in terms of the production cost and the energy content benefit.

Sensitivity analyses is also performed in the current study to examine the effect of biochar price on the CGW-biochar pellets. In the previous analyses, it was calculated from the price of wood waste biomass with the conversion ratio into char. The char is produced from the gasification. As the char is also a commodity used for other purposes (activated carbon, soil amendment and other industrial materials), the price may be varied. This sensitivity analysis thus takes into account the current charcoal price from the market. The current bulk charcoal prices are varied from US\$175-US\$250/tonne or about AU\$230– AU\$330/tonne. The sensitivity analyses take the biochar prices of AU\$200/tonne, AU\$275/tonne and AU\$350/tonne (Table 7.4).

Table 7.4: Sensitivity analyses of production costs of CGW95 and CGW80 pellets based on the biochar price in the market (AU\$)

Biochar price, \$/tonne	200		275		350	
	CGW95	CGW80	CGW95	CGW80	CGW95	CGW80
Total cost of production (\$/ton)	110	137	114	152	115	157
Cost of production (\$/GJ comparable)	7.0	7.5	7.2	8.4	7.3	8.6

Table 7.4 indicates that the increase of biochar price of \$200-\$350/tonne would increase the production costs of CGW80 pellets to about \$137-\$157/tonne. In comparison, the production costs of CGW95 pellets would only be around \$110-\$115/tonne. The CGW80 pellet cost of production is more sensitive to the biochar price increase than that of the CGW95 pellet.

7.3.2.2. Economics of re-utilizing pellets to power the gin

In the following, this study would also assess the possible scenarios of re-utilizing the pellet for energy production in the gin. Table 7.5 shows the current expenditure of energy for ginning. Ismail (2009) reported that heat energy for drying and electricity required for running the gin was about 100 MJ and 156 MJ per bale respectively. The gin which has a production capacity of 35,000 bales per year would thus require about \$70,000/year for natural gas and/or \$280,000/year for the electricity usage to the national grid connection, respectively.

Table 7.5: Energy cost (AU\$) of current business-as-usual (BAU) at gin capacity 35000 bales/year

Energy for drying	100	MJ/bale
Electricity for ginning & handling	156	MJ/bale
Bale production capacity	35000	Bales/year
Energy need for drying (GJ/year)	3500	GJ/year
Electricity need for ginning & handling (GJ/year)	5474	GJ/year
Energy cost of current BAU:		
- Natural gas expenditure (@\$2/bale)	70,000	\$/year
- Electricity cost (@\$8/bale)	280,000	\$/year

Table 7.6 shows the scenarios of reutilizing the CGW pellet for the drying energy and electricity generation. It assumed the energy conversion efficiency of the gasification technology (to produce heat for drying) is 50%.

Table 7.6: Scenarios constructed for energy replacement at gin using CGW pellets

	CGW100	CGW95	CGW80
Pellet fuel required for drying with gas (conversion eff 50%) tonnes/year	499	441	385
Cost of pellets production for drying (\$/year)	50,650	47,620	48,850
Remaining pellet (tonnes/year)	1251	1401	1802
Pellet required for electricity (tonnes/year, conversion eff 20%)	1950	1726	1506
Pellet surplus (tonnes/year)	NA	NA	296
Recovered electricity generation from CGW pellet	64%	81%	100%
Cost of pellet production for electricity generation (\$/year)	127,133	151,131	191,018
Additional electricity expenditure to national grid (\$/year)	100,800	53,200	-
Total electricity cost (\$/year)	227,933	204,331	191,018
Benefit = BAU energy expenditure – scenario costs (\$/year)	71,417	98,049	147,642

Table 7.6 shows that the cheapest cost of pellets production to replace the energy of drying in the gin is for the CGW95 pellet. The remaining pellets are then used to produce electricity. The conversion efficiency of electricity generation was assumed 20% of the pellet heating value. For the CGW100 scenario, the remaining pellets could only cover 64% of the electricity needed. In comparison, the CGW95 could generate 81% of the electricity required. The CGW80 could fully cover the electricity required, even with a surplus in the pellet production of about 296 tonnes per year. All the scenarios could reduce the current business-as-usual (BAU) expenditure. The benefit gained is between \$71,000 and \$148,000 per annum, which is about 20%-40% of cost reduction from the current energy cost expenditure.

7.3.3 Greenhouse gas emission reduction

The GHG emission reduction was calculated and compared with the scenarios constructed emission of the BAU's one. Table 7.7 shows the comparison of potential greenhouse gas emission of the current use of energy and the scenario constructed from the replacement of energy using CGW pellet fuels. At the current situation, the GHG potential is about 52.35 kg CO₂-e/bale. By applying the scenarios for CGW100, CGW95 and CGW80, it could be found that the reduction could be ranging from 68.9%-100%.

Table 7.7: GHG emission reduction (% of BAU)

	BAU	CGW100	CGW95	CGW80
Drying (kg CO ₂ -e)	249550	0	0	0
Electricity (kg CO ₂ -e)	1582747	569788.8	300721.9	
Total emissions (kg CO₂-e)	1832297	569789	300722	0
Emissions (kg CO ₂ -e /bale)	52.35	16.28	8.59	
Emission reduction		68.9%	83.6%	100%

7.4 Summary and conclusion

The cotton gin waste for energy production in a gin has been evaluated. The case study was applied to a gin having a production capacity of 35,000 bales/year. The available amount of waste was about 1,750 tonnes per year. The scenarios for converting the CGW into the pellet fuel of CGW100 and the 5% bio-char blended in CGW pellet (CGW95) and the 20% bio-char blended in CGW pellet (CGW80) have been studied.

It has been found that the input-output energy analyses for producing the pellets results in energy range 2-3 MJ/kg. Though the CGW100 consumed the lowest energy input for its production, it has the highest energy input ratio due to its low heating value.

It has been shown that the biochar energy production adds a significant contribution to the input energy of making the pellet. The selection of char making technology could lead to either low or high input energy contribution to the pellet energy content. Applying the low technology of carbonization for char blended material would increase the energy input ratio to the calorific value gained in the pellet. Applying the conventional method of carbonization, the CGW80 could have slightly higher energy input ratio than the unblended biochar pellet (CGW100). The CGW95 had the lowest energy input ratio from its heating value.

The cost of production the CGW pellets is estimated to be AU\$101-AU\$128/tonne. This is comparable with the wood pellets having prices ranging from US\$110 to 150/tonne (AU\$132-180/tonne) at the moment. The blended biochar- CGW pellets could reach comparable heating values with the wood pellets. Generally, the higher the carbon content in the pellet, then the higher the energy content and cost. This shows a significant contribution of biochar price in the cost of pellet production. Comparing the overall energy content in the various blended pellets, it has been found that the unblended CGW pellet (CGW100) would be the most expensive one, at

AU\$7.24/GJ. The CGW95 was the cheapest one, AU\$6.8/GJ; while the CGW80 cost about AU\$7.0/GJ.

The scenarios constructed for replacing the external usage of energy in the gin with the CGW pellets energy have also been analysed. Currently, the gin used the energy from the natural gas and the national electricity grid. The 35000 bales gin production capacity is used as the baseline of the case study. The gin spends about \$70,000/year for the natural gas and \$280,000/year for the electricity. Based on available amount of cotton gin waste, the CGW100 scenario could replace the 100% energy of drying and 64% of electricity consumption, while the CGW95 could cover all the drying energy and 81% of the electricity required to run the gin. The CGW80 cover both of drying and electricity, yielding even a modest surplus of the pellet production at about 296 tonnes/year. The costs of producing the pellets for covering the power energy of the gin are compared with the current expenditure of energy. All the scenarios constructed could lower the price of energy about 20% for CGW100, 28% for CGW95 and 40% for CGW80.

It has also been found that the potential greenhouse gas emissions could also be reduced from 52.35 kg CO₂-e/bale to 16.28 for CGW100 and 8.59 for CGW95. The surplus pellets in CGW80 case can potentially achieve more GHG reduction from the remaining pellets sold into the market as an alternative to wood pellet fuel.

Finally, it is noted that the analysis presented in this chapter is a very simplistic analysis intended to only give a rough indication whether or not the technology presented is worthy of a more thorough investigation. A detailed engineering economic analyses would need to include the cost of installation and operation for the gasifier with a return on investment. This is mentioned as a recommendation for further research at the end of Chapter 8.

CHAPTER 8: Conclusions and Recommendations

8.1. General summary and conclusions

Upgrading non-woody biomass agricultural industrial waste into a good quality of solid fuel has been investigated in this research project. Focusing on cotton gin waste (CGW), which has low density and high ash content, this material has remained an underrated yet valuable resource and hence it has become the object of this study.

The upgrading of the heating values and lowering the ash content have been performed in this study by densification, blending the CGW with biochar and forming pellets. Instead of coal, which has been used in most published studies, this study applied renewably sourced biochar as the blending material. This study investigated in detail the necessary steps to achieve consistent quality pellets. This comprised of chopping, binding, pressing, and drying.

It has been demonstrated that densification of CGW alone is able to create pellets with acceptable density, uniformity and hardness. However, the heating value could only be significantly increased by addition of charcoal. The properties of the developed CGW pellets are summarized in Table 8.1.

The thermo-kinetic behavior of the pellets was significantly modified by the presence of increasing amount of biochar. However, the most outstanding effect was observed with only 5% biochar addition. It has been found that the CGW95 had the highest conversion rates both in combustion and pyrolysis. A further increase of biochar actually lowered the reactivity and the behavior was more dictated by the presence of biochar.

In combustion (Chapter 4), important differences have been found between low biochar (CGW95 and CGW90), and high biochar content (CGW85 and CGW80) pellets. The former group follows a single stage reaction pathway, starting and ending at lower temperatures. The latter group follows a multistage pathway, starting and ending at higher temperatures with wider gap between them.

Table 8.1: Summary of properties CGW pellets

Pellets	CGW100	CGW95	CGW90	CGW85	CGW80
<i>Proximate analysis (wt. %, as received)</i>					
Moisture	7.9	9.0	5.7	5.6	8.4
Ash	14.6	9.0	13.9	11.4	11.4
Volatile	62.1	61.9	56.0	52.9	49.0
Fixed Carbon*	15.3	20.0	24.5	30.1	31.3
<i>Ultimate (wt. % as received)</i>					
Carbon	35.5	40.5	42.2	42.4	45.5
Hydrogen	4.4	4.6	4.2	4.1	3.8
Nitrogen	1.6	1.4	0.9	1.0	1.2
Sulfur	0.2	0.2	0.2	0.2	0.1
Phosphorus	0.1	0.0	0.0	0.0	0.0
Oxygen*	35.8	35.3	32.9	35.3	29.6
<i>Ash analyses (wt. % in ash)</i>					
K	3.1	3.2	3.7	2.8	2.1
Ca	12.3	12.6	11.2	10.8	6.2
Mg	1.2	1.1	1.1	0.7	0.2
Na	0.6	0.8	0.8	0.6	0.4
Fe	0.6	0.7	0.7	0.4	0.4
Al	1.4	2.7	1.2	1.6	1.3
Si	2.8	3.3	2.7	4.0	3.5
<i>Size</i>					
Length, mean (mm)	35.99±4.39	36.01±2.98	36.62±4.14	37.08±3.66	37.78±3.18
Diameter, mean (mm)	7.47±0.13	7.60±0.09	7.59±0.12	7.54±0.10	7.57±0.10
Weight, mean (g)	2.05±0.28	2.02±0.17	2.09±0.27	2.15±0.22	2.10±0.19
<i>Density</i>					
Apparent density, mean (kg/m ³)	1299±71	1238±37	1265±30	1230±47	1237±42
Bulk density, mean (kg/m ³)	605	602	608	606	606
<i>Durability and Hardness</i>					
Single pellet drop test (%)	97.1±10.2	99.7±0.4	97.0±9.3	97.0±10	99.2±2.8
Hardness as compression test (N)	1639±392	1621±233	1833±273	1914±382	1950±237
<i>Calorific value**</i>					
HV, MJ/kg	14.0	15.9	16.9	17.6	18.2
Energy density, GJ/m ³	8.5	9.5	10.2	10.7	11.0
<i>Thermo-kinetic properties</i>					
In combustion:					
T-ignition (°C)	287	295	285	305	300
T-burnout (°C)	358	336	338	480	510
Activation of Energy (kJ/mol)	203.7	173.2	173.8	176.0	169.8
Pre-exponential factor (1/s)	2.4E+16	4.9E+13	6.0E+13	3.8E+10	3.3E+09
In pyrolysis:					
Activation of Energy (kJ/mol)	130.5	132.2	113.7	107.9	106.7
Pre-exponential factor (1/s)	1.0E+07	3.80E+09	1.2E+07	2.7E+07	5.2E+06

*by difference

**calculated (Demirbaş, 1997)

In pyrolysis (Chapter 5), the behavior of all pellets follow the single stage reaction model as supported by thermogravimetric analyses. This has not been reported previously in any available literatures investigating a small variation of biochar addition resulting in a different thermo-kinetics of non- woody biomass. However, this new finding needs to be confirmed as it will have important consequences to the design of an effective combustor or gasifier.

In gasification (Chapter 6), data obtained previously on pyrolysis and combustion were employed in a computer model of the gasification process. A CFD model which simulated the process in a GEK 10 kW gasifier was developed and tested using macadamia shells for which some data on composition and behaviour were already available in the published literature. The model was further validated by comparing predicted results with those from factual experiments on temperature profiles and gas compositions.

It has been found that the prediction on temperatures agreed well with experiments, except for in the lowest (ash) zone which was, unfortunately, not well covered in the model (no ash removal option); hence the predicted temperatures were much higher than actual values. Predicted values in CO and CO₂ were also in good agreement with the experiment. However, due to limitation of gas analyser capability, methane was actually included with other unspecified products as total hydrocarbons. The other main drawback of the available gas analyser was that it could not measure the hydrogen concentration.

The model predicted temperatures within the reduction zone, inside the reactor for CGW95, to be lower than those for other pellets. Furthermore, this model also predicted that higher biochar contents would primarily increase gas heating value with the exception of CGW95. The CGW95 gas, despite in lower biochar content, was predicted to have higher heating value than higher biochar CGW90. This indicated a possible synergism. The existence of a synergistic reaction between CGW and biochar may be supported in the previous finding of a lower mass in residual ash and char of thermogravimetric combustion and pyrolysis, respectively (Idris *et al.*, 2012). In this study, all the blends of biochar pellets showed synergistic effects in combustion, as evidenced by the lower ash content of empirical data than the calculation based on weighting factor one. In pyrolysis, only CGW95 pellets showed synergistic effects determined by slightly lower char yield of the empirical data than those of theoretical predictions based on weighting factor of individual conversions.

It has been found that 30% energy from CGW pellet gasification may be sufficient to cover the energy need of pellet production. The costs of energy in the ginning house can be reduced by 20-40% from the use of produced gas. The GHG emission is also lowered. Despite the cost of biochar blended pellets, the energy recovery via gasification has been found to be the highest for CGW80 out of other options. This study has proposed to use the CGW-biochar blend pellets in the gin to effectively replace the current energy consumption of using fossil fuel. Overall, it can be concluded that upgrading the non-woody biomass into pellet and applying it in a co-gasification could potentially provide an effective alternative fuel source to achieve agricultural energy self-sufficiency and off-grid operation.

8.2. Recommendations for further research

- 1) The established pelletisation of COBY system which this study has modified in the lab scale experiments could be further improved by focusing on the aging step to effectively loosen the hard structure of CGW.
- 2) While other studies are focusing on torrefied pellets, the densification of torrefied material with the blends of optimum amount of raw biomass could perhaps achieve other improvements from a possible synergism as well as a function of binder substitution. This study thus proposes another part of investigation to effectively produce the torrefied pellets.
- 3) Despite the results that biochar containing pellets emit much less volatiles than the pure CGW pellets, the issue of emission and deterioration of the pellets quality may be associated with self-combustion hazard. Hence, a quality standard covering the non-woody based pellets in respect to keeping quality, self-combustion should be set for the purpose of eliminating the possible fire hazard.
- 4) The design of industrial combustion and gasification relies on and is facilitated by suitable model. In particular, the developed CFD model which is quite good in predicting the gas and heating value in this study would need to be substantially extended to account for particularly solid emissions.
- 5) The economic analyses presented in this study have only estimated the costs of pellets production to replace the energy needs of drying and power of machines in the gin. Future analyses may also include the investment cost of installation and operation with a return on investment.

References

- Agbor, VB, Cicek, N, Sparling, R, Berlin, A & Levin, DB 2011, 'Biomass pretreatment: Fundamentals toward application', *Biotechnology Advances*, vol. 29, no. 6, pp. 675-85.
- André, RN, Pinto, F, Franco, C, Dias, M, Gulyurtlu, I, Matos, MAA & Cabrita, I 2005, 'Fluidised bed co-gasification of coal and olive oil industry wastes', *Fuel*, vol. 84, no. 12–13, pp. 1635-44.
- ANSYS-Inc 2013, *ANSYS FLUENT User's Guide Release 15.0 USA*.
- ANSYS-Inc 2016, *ANSYS Fluent Theory Guide*, Canonsburg, PA- USA, <<http://kncfd.ir/files/Ansys%20Fluent/ANSYS%2017%20Fluent%20Theory%20Guide.pdf>>.
- ANSYS_INC 2013, *ANSYS FLUENT Theory Guide Release 15.0, USA*.
- Antonopoulos, IS, Karagiannidis, A, Gkouletsos, A & Perkoulidis, G 2012, 'Modelling of a downdraft gasifier fed by agricultural residues', *Waste Management*, vol. 32, pp. 710-8.
- Ataei, A, Azimi, A, Kalhori, S, Abari, M & Radnezhad, H 2012, 'Performance analysis of a co-gasifier for organic waste in agriculture', *International Journal of Recycling of Organic Waste in Agriculture*, vol. 1, no. 1, pp. 1-10.
- Australian_Government, *National Greenhouse Accounts Factors 2017*, DotEa _Energy, <<http://www.environment.gov.au/climate-change/greenhouse-gas-measurement/publications/national-greenhouse-accounts-factors-july-2017>>.
- Babu, BV & Seth, PN 2006, 'Modeling and simulation of reduction zone of downdraft biomass gasifier : Effect of char reactivity factor', *Energy Conversion and Management*, vol. 47, pp. 2602-11.
- Bach, Q-V & Skreiberg, Ø 2016, 'Upgrading biomass fuels via wet torrefaction: A review and comparison with dry torrefaction', *Renewable and Sustainable Energy Reviews*, vol. 54, pp. 665-77.
- Bai, Y, Wang, Y, Zhu, S, Yan, L, Li, F & Xie, K 2014, 'Synergistic effect between CO₂ and H₂O on reactivity during coal chars gasification', *Fuel*, vol. 126, no. 0, pp. 1-7.
- Bain, RL 2004, 'An Introduction to Biomass Thermochemical Conversion', viewed 11 August 2017 <<https://www.nrel.gov/docs/gen/fy04/36831e.pdf>>.
- Barman, NS, Ghosh, S & De, S 2012, 'Gasification of biomass in a fixed bed downdraft gasifier - A realistic model including tar', *Resource Technology*, vol. 107, pp. 505-11.

- Baruah, D & Baruah, DC 2014, 'Modeling of biomass gasification: A review', *Renewable and Sustainable Energy Reviews*, vol. 39, pp. 806-15.
- Basu, P 2010, *Biomass Gasification and Pyrolysis: Practical Design and Theory*, Academic Press, US.
- Blaine, RL & Kissinger, HE 2012, 'Homer Kissinger and the Kissinger equation', *Thermochimica Acta*, vol. 540, pp. 1-6.
- Blasi, CD 2000, 'Dynamic behaviour of stratified downdraft gasifiers', *Chemical Engineering Science*, vol. 55, no. 15, pp. 2931-44.
- Brar, JS, Singh, K, wang, J & Kumar, S 2012, 'Cogasification of coal and biomass : A review', *International Journal of Forestry Research*, vol. 2012, pp. 1-10.
- Brar, JS, Singh, K, Zondlo, J & Wang, J 2013, 'Co-gasification of coal and hardwood pellets: Syngas composition, carbon efficiency and energy efficiency', *American Journal of Biomass and Bioenergy*, Columbia International Publishing, pp. 1385-8.
- Chandrasekaran, SR, Sharma, BK, Hopke, PK & Rajagopalan, N 2016, 'Combustion of Switchgrass in Biomass Home Heating Systems: Emissions and Ash Behavior', *Energy & Fuels*, vol. 30, no. 4, pp. 2958-67.
- Chen, G-y, Fang, M-x, Andries, J, Luo, Z-y, Spliethoff, H & Cen, K-f 2003, 'Kinetics study on biomass pyrolysis for fuel gas production', *Journal of Zhejiang University-SCIENCE A*, vol. 4, no. 4, pp. 441-7.
- Chen, G 2014, *Potential of producing bio-energy from cotton gin trash*, Personal communication, 8 August 2014.
- Chen, W-H & Wu, J-S 2009, 'An evaluation on rice husks and pulverized coal blends using a drop tube furnace and a thermogravimetric analyzer for application to a blast furnace', *Energy*, vol. 34, no. 10, pp. 1458-66.
- Coats, AW & Redfern, JP 1964, 'Kinetic parameters from thermogravimetric data [12]', *Nature*, vol. 201, no. 4914, pp. 68-9.
- Collot, A-G, Zhuo, Y, Dugwell, DR & Kandiyoti, R 2009, 'Co-pyrolysis and Co-gasification of coal and biomass in bench-scale fixed bed and fluidised bed reactors', *Fuel*, vol. 78, pp. 667-79.
- Cotton-Australia 2014, *Cotton Education Kit*, Cotton Australiaviewed 20 November 2014, <<http://cottonaustralia.com.au/cotton-classroom/education-kits>>.
- Damartzis, T, Vamvuka, D, Sfakiotakis, S & Zabaniotou, A 2011, 'Thermal degradation studies and kinetic modeling of cardoon (*Cynara cardunculus*) pyrolysis using thermogravimetric analysis (TGA)', *Bioresource Technology*, vol. 102, no. 10, pp. 6230-8.

- Demirbaş, A 1997, 'Calculation of higher heating values of biomass fuels', *Fuel*, vol. 76, no. 5, pp. 431-4.
- Duan, L, Duan, Y, Zhao, C & Anthony, EJ 2015, 'NO emission during co-firing coal and biomass in an oxy-fuel circulating fluidized bed combustor', *Fuel*, vol. 150, pp. 8-13.
- Duca, D, Riva, G, Foppa Pedretti, E & Toscano, G 2014, 'Wood pellet quality with respect to EN 14961-2 standard and certifications', *Fuel*, vol. 135, pp. 9-14.
- Emami-Taba, L, Irfan, MF, Daud, WMAW & Chakrabarti, MH 2013, 'Fuel blending effects on the co-gasification of coal and biomass - A review', *Biomass and Bioenergy*, vol. 57, pp. 249-63.
- Emami, S, Tabil, LG, Adapa, P, George, E, Tilay, A, Dalai, A, Drisdelle, M & Ketabi, L 2014, 'Effect of fuel additives on agricultural straw pellet quality', *International Journal of Agricultural & Biological Engineering*, vol. 7, no. 2, pp. 92-100.
- Erlich, C & Fransson, TH 2011, 'Downdraft gasification of pellets made of wood, palm-oil residues respective bagasse: Experimental study', *Applied Energy*, vol. 88, no. 3, pp. 899-908.
- Fermoso, J, Arias, B, Gil, MV, Plaza, MG, Pevida, C, Pis, JJ & Rubiera, F 2010, 'Co-gasification of different rank coals with biomass and petroleum coke in a high-pressure reactor for H₂-rich gas production', *Bioresource Technology*, vol. 101, no. 9, pp. 3230-5.
- Fernando, N & Narayana, M 2016, 'A comprehensive two dimensional Computational Fluid Dynamics model for an updraft biomass gasifier', *Renewable Energy*, vol. 99, pp. 698-710.
- Fryda, LE, Panopoulos, KD & Kakaras, E 2008, 'Agglomeration in fluidised bed gasification of biomass', *Powder Technology*, vol. 181, no. 3, pp. 307-20.
- Gabra, M, Pettersson, E, Backman, R & Kjellström, B 2001, 'Evaluation of cyclone gasifier performance for gasification of sugar cane residue—Part 1: gasification of bagasse', *Biomass and Bioenergy*, vol. 21, no. 5, pp. 351-69.
- Gai, C & Dong, Y 2012, 'Experimental study on non-woody biomass gasification in a downdraft gasifier', *International Journal of Hydrogen Energy*, vol. 37, pp. 4935 - 44.
- Gan, M, Lv, W, Fan, X, Chen, X, Ji, Z & Jiang, T 2017, 'Gasification Reaction Characteristics between Biochar and CO₂ as well as the Influence on Sintering Process', *Advances in Materials Science and Engineering*, vol. 2017, p. 8.
- Gerun, L, Paraschiv, M, Vîjeu, R, Bellettre, J, Tazerout, M, Gøbel, B & Henriksen, U 2008, 'Numerical investigation of the partial oxidation in a two-stage downdraft gasifier', *Fuel*, vol. 87, no. 7, pp. 1383-93.

Gil, MV, Casal, D, Pevida, C, Pis, JJ & Rubiera, F 2010, 'Thermal behaviour and kinetics of coal/biomass blends during co-combustion', *Bioresource Technology*, vol. 101, no. 14, pp. 5601-8.

Groves, J, Craig, J, LePori, WA & Anthony, RG 1979, 'Fluidized bed gasification of cotton gin waste', *Paper - American Society of Agricultural Engineers*.

Guo, F, Dong, Y, Dong, L & Guo, C 2014, 'Effect of design and operating parameters on the gasification process of biomass in a downdraft fixed bed', *International Journal of Hydrogen Energy*, vol. 39, pp. 5625-33.

Habibi, R 2013, 'Co-gasification of Biomass and Non-biomass Feedstoks', University of Calgary, Calgary, Alberta.

Hamawand, I, Sandell, G, Pittaway, P, Chakrabarty, S, Yusaf, T, Chen, G, Seneweera, S, Al-Lwayzy, S, Bennett, J & Hopf, J 2016, 'Bioenergy from Cotton Industry Wastes: A review and potential', *Renewable and Sustainable Energy Reviews*, vol. 66, pp. 435-48.

Higman, C & van der Burgt, M 2008, *Gasification*, Gulf Professional Publishing. Copyright Elsevier Inc. All right reserved.

Holt, GA 2014, *Questions about making pellet from cotton gin by product*, Personal communication, 4 September 2014.

Holt, GA, Blodgett, TL & Nakayama, FS 2006, 'Physical and combustion characteristics of pellet fuel from cotton gin by-products produced by select processing treatments', *Industrial Crops and Products*, vol. 24, no. 3, pp. 204-13.

Howaniec, N & Smoliński, A 2014, 'Effect of fuel blend composition on the efficiency of hydrogen-rich gas production in co-gasification of coal and biomass', *Fuel*, vol. 128, no. 0, pp. 442-50.

Huang, Y, Yin, X, Wu, C, Wang, C, Xie, J, Zhou, Z, Ma, L & Li, H 2009, 'Effects of metal catalysts on CO₂ gasification reactivity of biomass char', *Biotechnology Advances*, vol. 27, no. 5, pp. 568-72.

Idris, SS, Rahman, NA & Ismail, K 2012, 'Combustion characteristics of Malaysian oil palm biomass, sub-bituminous coal and their respective blends via thermogravimetric analysis (TGA)', *Bioresource Technology*, vol. 123, pp. 581-91.

Idris, SS, Rahman, NA, Ismail, K, Alias, AB, Rashid, ZA & Aris, MJ 2010, 'Investigation on thermochemical behaviour of low rank Malaysian coal, oil palm biomass and their blends during pyrolysis via thermogravimetric analysis (TGA)', *Bioresource Technology*, vol. 101, no. 12, pp. 4584-92.

IEA 2012, *In-depth country review*, International Energy Agency, <https://www.iea.org/countries/membercountries/australia/>.

- Iroba, KL, Tabil, LG, Sokhansanj, S & Meda, V 2014, 'Producing durable pellets from barley straw subjected to radio frequency-alkaline and steam explosion pretreatments', *International Journal of Agricultural & Biological Engineering*, vol. 7, no. 3, pp. 68-82.
- Ismail, SA 2009, 'Assessment of Energy Usage for Cotton Gins in australia', Master Thesis thesis, University of Southern Queensland.
- Ismail, TM & El-Salam, MA 2015, 'Numerical and experimental studies on updraft gasifier HTAG', *Renewable Energy*, vol. 78, pp. 484-97.
- ISO 2014, *ISO 17225-6 Solid biofuels-Fuel specifications and classes*, Part 6: Graded non-woody pellets, ISO 17225-6:2014 (E), ISO copyright office, Switzerland.
- Janajreh, I & Al Shrah, M 2013, 'Numerical and experimental investigation of downdraft gasification of wood chips', *Energy Conversion and Management*, vol. 65, no. 0, pp. 783-92.
- Jaojaruek, K 2014, 'Mathematical model to predict temperature profile and air-fuel equivalence ratio of a downdraft gasification process', *Energy Conversion and Management*, vol. 83, pp. 223-31.
- Jarungthammachote, S & Dutta, A 2007, 'Thermodynamic equilibrium model and second law analysis of a downdraft waste gasifier', *Energy*, vol. 32, no. 9, pp. 1660-9.
- Jeong, HJ, Park, SS & Hwang, J 2014, 'Co-gasification of coal–biomass blended char with CO₂ at temperatures of 900–1100°C', *Fuel*, vol. 116, no. 0, pp. 465-70.
- Jones, JM, Kubacki, M, Kubica, K, Ross, AB & Williams, A 2005, 'Devolatilisation characteristics of coal and biomass blends', *Journal of Analytical and Applied Pyrolysis*, vol. 74, no. 1–2, pp. 502-11.
- Jordan, CA & Akay, G 2012, 'Occurrence, composition and dew point of tars produced during gasification of fuel cane bagasse in a downdraft gasifier', *Biomass and Bioenergy*, vol. 42, pp. 51-8.
- Jordan, CA & Akay, G 2013, 'Effect of CaO on tar production and dew point depression during gasification of fuel cane bagasse in a novel downdraft gasifier', *Fuel Processing Technology*, vol. 106, pp. 654-60.
- Kastanaki, E & Vamvuka, D 2006, 'A comparative reactivity and kinetic study on the combustion of coal–biomass char blends', *Fuel*, vol. 85, no. 9, pp. 1186-93.
- Kaushal, P, Abedi, J & Mahinpey, N 2010, 'A comprehensive mathematical model for biomass gasification in a bubbling fluidized bed reactor', *Fuel*, vol. 89, no. 12, pp. 3650-61.

- Kumabe, K, Hanaoka, T, Fujimoto, S, Minowa, T & Sakanishi, K 2007, 'Co-gasification of woody biomass and coal with air and steam', *Fuel*, vol. 86, no. 5–6, pp. 684-9.
- Lahijani, P & Zainal, ZA 2011, 'Gasification of palm empty fruit bunch in a bubbling fluidized bed: A performance and agglomeration study', *Bioresource Technology*, vol. 102, no. 2, pp. 2068-76.
- Laidler, KJ 1987, *Chemical kinetics*, 3rd ed. edn, HarperCollins, New York.
- Lapuerta, Hernández, JJ, Pazo, A & López, J 2008, 'Gasification and co-gasification of biomass wastes: Effect of the biomass origin and the gasifier operating conditions', *Fuel Processing Technology*, vol. 89, no. 9, pp. 828-37.
- Lapuerta, M, Hernandez, JJ, Pazo, A & Lopez, J 2008, 'Gasification and co-gasification of biomass wastes : effect of the biomass origin and the gasifier operating condition ', *Fuel Processing Technology*, vol. 89, pp. 828 -37.
- Levis, JW & Barlaz, MA 2013, *Composting Process Model Documentatio*, November 2013, viewed 15 February 2017, <<http://www4.ncsu.edu/~jwlevis/Composting.pdf>>.
- Li, C, Yamamoto, Y, Suzuki, M, Hirabayashi, D & Suzuki, K 2009, 'Study on the combustion kinetic characteristics of biomass tar under catalysts', *Journal of Thermal Analysis and Calorimetry*, vol. 95, no. 3, pp. 991-7.
- Liu, Z, Quek, A & Balasubramanian, R 2014, 'Preparation and characterization of fuel pellets from woody biomass, agro-residues and their corresponding hydrochars', *Applied Energy*, vol. 113, pp. 1315-22.
- Lu, D, Tabil, LG, Wang, D, Wang, G & Emami, S 2014, 'Experimental trials to make wheat straw pellets with wood residue and binders', *Biomass and Bioenergy*, vol. 69, no. 0, pp. 287-96.
- Lu, J-J & Chen, W-H 2015, 'Investigation on the ignition and burnout temperatures of bamboo and sugarcane bagasse by thermogravimetric analysis', *Applied Energy*, vol. 160, pp. 49-57.
- Maglinao Jr, AL, Capareda, SC & Nam, H 2015, 'Fluidized bed gasification of high tonnage sorghum, cotton gin trash and beef cattle manure: Evaluation of synthesis gas production', *Energy Conversion and Management*, vol. 105, pp. 578-87.
- Mahapatra, AK, Harris, DL, Durham, DL, Lucas, S, Terrill, TH, Kouakou, B & Kannan, G 2010, 'Effects of moisture change on the physical and thermal properties of sericea lespedeza pellets', *International Agricultural Engineering Journal*, vol. 19, no. 3, pp. 23-9.
- Masmoudi, MA, Sahraoui, M, Grioui, N & Halouani, K 2014, '2-D Modeling of thermo-kinetics coupled with heat and mass transfer in the reduction zone of a fixed bed downdraft biomass gasifier', *Renewable Energy*, vol. 66, pp. 288-98.

Masnadi, MS, Habibi, R, Kopyscinski, J, Hill, JM, Bi, X, Lim, CJ, Ellis, N & Grace, JR 2014, 'Fuel characterization and co-pyrolysis kinetics of biomass and fossil fuels', *Fuel*, vol. 117, Part B, no. 0, pp. 1204-14.

McIntosh, S, Vancov, T, Palmer, J & Morris, S 2014, 'Ethanol production from cotton gin trash using optimised dilute acid pretreatment and whole slurry fermentation processes', *Bioresource Technology*, vol. 173, pp. 42-51.

Mendiburu, AZ, Jr, JAC, Zanzi, R & Coronado, CR 2014, 'Thermochemical equilibrium modeling of a biomass downdraft gasifier : Constrained and unconstrained non-stoichiometric models', *Energy*, vol. 71, pp. 624-37.

Mendiburu, AZ, Carvalho Jr, JA, Zanzi, R, Coronado, CR & Silveira, JL 2014, 'Thermochemical equilibrium modeling of a biomass downdraft gasifier: Constrained and unconstrained non-stoichiometric models', *Energy*, vol. 71, no. 0, pp. 624-37.

Mi, B, Liu, Z, Hu, W, Wei, P, Jiang, Z & Fei, B 2016, 'Investigating pyrolysis and combustion characteristics of torrefied bamboo, torrefied wood and their blends', *Bioresource Technology*, vol. 209, pp. 50-5.

Mineral-Council-of-Australia 2015, *Production and Resources*, Mineral Council of Australia, viewed 21 September 2015, <http://www.minerals.org.au/resources/coal/production_and_resources>.

Mohammed, MAA, Salmiaton, A, Wan Azlina, WAKG, Mohammad Amran, MS & Fakhru'l-Razi, A 2011, 'Air gasification of empty fruit bunch for hydrogen-rich gas production in a fluidized-bed reactor', *Energy Conversion and Management*, vol. 52, no. 2, pp. 1555-61.

Mohammed, MAA, Salmiaton, A, Wan Azlina, WAKG, Mohamad Amran, MS, Omar, R, Taufiq-Yap, YH & Fakhru'l-Razi, A 2012, 'Catalytic Gasification of Empty Fruit Bunch for Enhanced Production of Hydrogen Rich Fuel Gas', *Pertanika Journal of Science & Technology*, vol. 20, no. 1, pp. 139-49.

Murgia, S, Vascellari, M & Cau, G 2012, 'Comprehensive CFD model of an air-blown coal-fired updraft gasifier', *Fuel*, vol. 101, no. 0, pp. 129-38.

Muthuraman, M, Namioka, T & Yoshikawa, K 2010, 'Characteristics of co-combustion and kinetic study on hydrothermally treated municipal solid waste with different rank coals: A thermogravimetric analysis', *Applied Energy*, vol. 87, no. 1, pp. 141-8.

Nan, N, DeVallance, DB, Xie, X & Wang, J 2016, 'The effect of bio-carbon addition on the electrical, mechanical, and thermal properties of polyvinyl alcohol/biochar composites', *Journal of Composite Materials*, vol. 50, no. 9, pp. 1161-8.

Natarajan, E, Nordin, A & Rao, AN 1998, 'Overview of combustion and gasification of rice husk in fluidized bed reactors', *Biomass and Bioenergy*, vol. 14, no. 5, pp. 533-46.

Nemanova, V, Abedini, A, Liliedahl, T & Engvall, K 2014, 'Co-gasification of petroleum coke and biomass', *Fuel*, vol. 117, Part A, pp. 870-5.

Nunes, LJR, Matias, JCO & Catalão, JPS 2014, 'Mixed biomass pellets for thermal energy production: A review of combustion models', *Applied Energy*, vol. 127, pp. 135-40.

Onay, Oz, Bayram, E & Koc, kar, OM 2007, 'Copyrolysis of Seyitomer-Lignite and Safflower Seed: Influence of the Blending Ratio and Pyrolysis Temperature on Product Yields and Oil Characterization', *Energy & Fuels*, vol. 21, no. 5, pp. 3049-56.

Pan, YG, Velo, E, Roca, X, Manyà, JJ & Puigjaner, L 2000, 'Fluidized-bed co-gasification of residual biomass/poor coal blends for fuel gas production', *Fuel*, vol. 79, no. 11, pp. 1317-26.

Pan, YG, Velo, E, Roca, X, Manyà, JJ & Puigjaner, L 2000, 'Fluidized-bed co-gasification of residual biomass/poor coal blends for fuel gas production', *Fuel*, vol. 79, no. 11, pp. 1317-26.

Pandey, SN & Thejappa, N 1975, 'Study on relationship between oil, protein, and gossypol in cottonseed kernels', *Journal of the American Oil Chemists Society*, vol. 52, no. 8, pp. 312-5.

Patel, KD, Shah, NK & Patel, RN 2013, 'CFD Analysis of spatial distribution of various parameters in downdraft gasifier', *Procedia Engineering*, vol. 51, pp. 764-9.

Patra, TK & Sheth, PN 2015, 'Biomass gasification models for downdraft gasifier: A state-of-the-art review', *Renewable and Sustainable Energy Reviews*, vol. 50, pp. 583-93.

Pinto, F, Franco, C, André, RN, Tavares, C, Dias, M, Gulyurtlu, I & Cabrita, I 2003, 'Effect of experimental conditions on co-gasification of coal, biomass and plastics wastes with air/steam mixtures in a fluidized bed system', *Fuel*, vol. 82, no. 15-17, pp. 1967-76.

Poinsot, T 2005, *Theoretical and numerical combustion*, 2nd ed. edn, Edwards, Philadelphia.

Puig-Arnabat, M, Bruno, JC & Coronas, A 2010, 'Review and analysis of biomass gasification models', *Renewable and Sustainable Energy Reviews*, vol. 14, no. 9, pp. 2841-51.

Ramajo-Escalera, B, Espina, A, García, JR, Sosa-Arno, JH & Nebra, SA 2006, 'Model-free kinetics applied to sugarcane bagasse combustion', *Thermochimica Acta*, vol. 448, no. 2, pp. 111-6.

Raveendran, K, Ganesh, A & Khilar, KC 1995, 'Influence of mineral matter on biomass pyrolysis characteristics', *Fuel*, vol. 74, no. 12, pp. 1812-22.

Raveendran, K, Ganesh, A & Khilar, KC 1996, 'Pyrolysis characteristics of biomass and biomass components', *Fuel*, vol. 75, no. 8, pp. 987-98.

Reed, TB & Das, A 1988, *Handbook of Biomass Downdraft Gasifier Engine Systems*, SERI, Solar Energy Research Institute, Golden, Colorado, United States, <http://www.nrel.gov/docs/legosti/old/3022.pdf>.

Rizkiana, J, Guan, G, Widayatno, WB, Hao, X, Huang, W, Tsutsumi, A & Abudula, A 2014, 'Effect of biomass type on the performance of cogasification of low rank coal with biomass at relatively low temperatures', *Fuel*, vol. 134, no. 0, pp. 414-9.

Rodriguez Alonso, E, Dupont, C, Heux, L, Da Silva Perez, D, Commandre, J-M & Gourdon, C 2016, 'Study of solid chemical evolution in torrefaction of different biomasses through solid-state ¹³C cross-polarization/magic angle spinning NMR (nuclear magnetic resonance) and TGA (thermogravimetric analysis)', *Energy*, vol. 97, pp. 381-90.

Ruhul Kabir, M & Kumar, A 2012, 'Comparison of the energy and environmental performances of nine biomass/coal co-firing pathways', *Bioresource Technology*, vol. 124, pp. 394-405.

Sahoo, A & Ram, DK 2015, 'Gasifier performance and energy analysis for fluidized bed gasification of sugarcane bagasse', *Energy*, vol. 90, Part 2, pp. 1420-5.

Sahu, SG, Sarkar, P, Chakraborty, N & Adak, AK 2010, 'Thermogravimetric assessment of combustion characteristics of blends of a coal with different biomass chars', *Fuel Processing Technology*, vol. 91, no. 3, pp. 369-78.

Samy, SS 2013, 'Gasification of Raw and Torrefied Cotton Gin Wastes in an Auger System', *Applied Engineering in Agriculture, American Society of Agricultural and Biological Engineering*, vol. 29, no. 3, pp. 405-14.

Sarkar, M, Kumar, A, Shankar Tumuluru, J & Patil, KN 2014, 'Thermal devolatilization kinetics of switchgrass pretreated with torrefaction and densification', *Transactions of the ASABE*, vol. 57, no. 4, pp. 1199-210.

Serrano, C, Monedero, E, Lapuerta, M & Portero, H 2011, 'Effect of moisture content, particle size and pine addition on quality parameters of barley straw pellets', *Fuel Processing Technology*, vol. 92, no. 3, pp. 699-706.

Shahrukh, H, Oyedun, AO, Kumar, A, Ghiasi, B, Kumar, L & Sokhansanj, S 2016, 'Comparative net energy ratio analysis of pellet produced from steam pretreated biomass from agricultural residues and energy crops', *Biomass and Bioenergy*, vol. 90, pp. 50-9.

Sharma, AK 2008, 'Equilibrium and kinetic modeling of char reduction reactions in a downdraft gasifier', *Solar Energy*, vol. 82, pp. 918-28.

- Simone, M, Barontini, F, Nicolella, C & Tognotti, L 2013, 'Assessment of syngas composition variability in a pilot-scale downdraft biomass gasifier by an extended equilibrium model', *Bioresource Technology*, vol. 140, pp. 43-52.
- Sjöström, K, Chen, G, Yu, Q, Brage, C & Rosén, C 1999, 'Promoted reactivity of char in co-gasification of biomass and coal: synergies in the thermochemical process', *Fuel*, vol. 78, no. 10, pp. 1189-94.
- Song, Y, Feng, J, Ji, M, Ding, T, Qin, Y & Li, W 2013, 'Impact of biomass on energy and element utilization efficiency during co-gasification with coal', *Fuel Processing Technology*, vol. 115, no. 0, pp. 42-9.
- Souza-Santos, MLd 2010, *Solid Fuel Combustion and Gasification: Modeling, Simulation and Equipment Operations*, Second Edition edn, CRC Press Taylor and Francis Group, Boca Raton FL.
- Stelte, W 2011, 'Fuel Pellets from Biomass: Processing, Bonding, Raw Materials', Technical University of Denmark, Denmark.
- Strezov, V, Evans, TJ & Nelson, PF 2006, 'Carbonization of Biomass Fuels', in MD Brenes (ed.), *Biomass and Bioenergy: New Research*, Nova Science Publisher Inc., ch Chapter 4, pp. 91-123.
- Sultana, A, Kumar, A & Harfield, D 2010, 'Development of agri-pellet production cost and optimum size', *Bioresource Technology*, vol. 101, no. 14, pp. 5609-21.
- Tchapda, AH & Pisupati, SV 2014, 'A review of thermal co-conversion of coal and biomass/waste', *Energies*, vol. 7, pp. 1098-148.
- Tilay, A, Azargohar, R, Drisdelle, M, Dalai, A & Kozinski, J 2015, 'Canola meal moisture-resistant fuel pellets: Study on the effects of process variables and additives on the pellet quality and compression characteristics', *Industrial Crops and Products*, vol. 63, pp. 337-48.
- Toscano, G, Riva, G, Foppa Pedretti, E, Corinaldesi, F, Mengarelli, C & Duca, D 2013, 'Investigation on wood pellet quality and relationship between ash content and the most important chemical elements', *Biomass and Bioenergy*, vol. 56, pp. 317-22.
- Trache, D, Abdelaziz, A & Siouani, B 2017, 'A simple and linear isoconversional method to determine the pre-exponential factors and the mathematical reaction mechanism functions', *Journal of Thermal Analysis and Calorimetry*, vol. 128, no. 1, pp. 335-48.
- Urbanovici, E, Popescu, C & Segal, E 1999, 'Improved Iterative Version of the Coats-Redfern Method to Evaluate Non-Isothermal Kinetic Parameters', *Journal of Thermal Analysis and Calorimetry*, vol. 58, no. 3, pp. 683-700.
- Uslu, A, Faaij, APC & Bergman, PCA 2008, 'Pre-treatment technologies, and their effect on international bioenergy supply chain logistics. Techno-economic evaluation of torrefaction, fast pyrolysis and pelletisation', *Energy*, vol. 33, no. 8, pp. 1206-23.

Valero, A & Usón, S 2006, 'Oxy-co-gasification of coal and biomass in an integrated gasification combined cycle (IGCC) power plant', *Energy*, vol. 31, no. 10–11, pp. 1643-55.

Vhathvarothai, N, Ness, J & Yu, QJ 2014a, 'An investigation of thermal behaviour of biomass and coal during copyrolysis using thermogravimetric analysis', *International Journal of Energy Research*, vol. 38, no. 9, pp. 1145-54.

Vhathvarothai, N, Ness, J & Yu, J 2014b, 'An investigation of thermal behaviour of biomass and coal during co-combustion using thermogravimetric analysis (TGA)', *International Journal of Energy Research*, vol. 38, no. 6, pp. 804-12.

Vinterbäck, J 2004, 'Pellets 2002: the first world conference on pellets', *Biomass and Bioenergy*, vol. 27, no. 6, pp. 513-20.

Vyazovkin, S 2000, 'Computational aspects of kinetic analysis.: Part C. The ICTAC Kinetics Project — the light at the end of the tunnel?', *Thermochimica Acta*, vol. 355, no. 1–2, pp. 155-63.

Vyazovkin, S 2006, 'Model-free kinetics', *Journal of Thermal Analysis and Calorimetry*, vol. 83, no. 1, pp. 45-51.

Vyazovkin, S 2010, 'Thermal Analysis', *Analytical Chemistry*, vol. 82, no. 12, pp. 4936-49.

Wang, M, Tian, J, Roberts, DG, Chang, L & Xie, K 2015, 'Interactions between corncob and lignite during temperature-programmed co-pyrolysis', *Fuel*, vol. 142, no. 0, pp. 102-8.

Wang, Y & Yan, L 2008, 'Review CFD Studies on Biomass Thermochemical Conversion', *International Journal of Molecular Science*, vol. 9, pp. 1108-30.

Wei, J, Gong, Y, Guo, Q, Ding, L, Wang, F & Yu, G 2017, 'Physicochemical evolution during rice straw and coal co-pyrolysis and its effect on co-gasification reactivity', *Bioresource Technology*, vol. 227, pp. 345-52.

Wu, Y, Zhang, Q, Yang, W & Blasiak, W 2013, 'Two-Dimensional Computational Fluid Dynamics Simulation of Biomass Gasification in a Downdraft Fixed-Bed Gasifier with Highly Preheated Air and Steam', *Energy & Fuels*, vol. 27, no. 6, pp. 3274-82.

www.westbioenergy.org 2001, *Final Report and Gas Analysis for a Biomass Gasifier*, viewed 7 August 2014, <<http://www.westbioenergy.org/reports/55018a/55018a.htm>>.

Xie, J, Zhong, W, Jin, B, Shao, Y & Liu, H 2012, 'Simulation on gasification of forestry residues in fluidized beds by Eulerian–Lagrangian approach', *Bioresource Technology*, vol. 121, pp. 36-46.

- Xu, Q 2013, 'Investigation of Co-gasification Characteristic of Biomass and Coal in Fluidized Bed Gasifier', University of Canterbury, New Zealand.
- Xu, Q, Pang, S & Levi, T 2011, 'Reaction kinetics and producer gas compositions of steam gasification of coal and biomass blend chars, part 1: Experimental investigation', *Chemical Engineering Science*, vol. 66, no. 10, pp. 2141-8.
- Yi, Q, Qi, F, Cheng, G, Zhang, Y, Xiao, B, Hu, Z, Liu, S, Cai, H & Xu, S 2013, 'Thermogravimetric analysis of co-combustion of biomass and biochar', *Journal of Thermal Analysis and Calorimetry*, vol. 112, no. 3, pp. 1475-9.
- Yu, J, Paterson, N, Blamey, J & Millan, M 2017, 'Cellulose, xylan and lignin interactions during pyrolysis of lignocellulosic biomass', *Fuel*, vol. 191, pp. 140-9.
- Zainal, ZA, Ali, R, Lean, CH & Seetharamu, KN 2001, 'Prediction of performance of a downdraft gasifier using equilibrium modeling for different biomass materials', *Energy Conversion and Management*, vol. 42, no. 12, pp. 1499-515.
- Zhang, J-l, Guo, J, Wang, G-w, Xu, T, Chai, Y-f, Zheng, C-l & Xu, R-s 2016, 'Kinetics of petroleum coke/biomass blends during co-gasification', *International Journal of Minerals, Metallurgy, and Materials*, vol. 23, no. 9, pp. 1001-10.
- Zhang, Y, Hara, S, Kajitani, S & Ashizawa, M 2010, 'Modeling of catalytic gasification kinetics of coal char and carbon', *Fuel*, vol. 89, no. 1, pp. 152-7.
- Zhu, W, Song, W & Lin, W 2008, 'Catalytic gasification of char from co-pyrolysis of coal and biomass', *Fuel Processing Technology*, vol. 89, no. 9, pp. 890-6.

APPENDICES

Appendix A: Literature

Table A.1: Proximate and ultimate of fuels

Feedstock	Proximate (% as received)				Ultimate (% ash free)					High Heating value (MJ/kg)	Density (kg/m ³)	Reference
	FC	VM	M	Ash	C	H	O	N	S			
Non Woody												
Cotton gin waste	20.8	68.7	11.8	10.5	45.14	4.93	40.43	1.16	0.29	16.6	390	Samy (2013)
Sugar cane bagasse	31	65	9.4	3.6	49.4	6.3	43.9	0.3	0.07	18.9	68	Jordan and Akay (2012)
Oil palm empty fruit bunch	8.79	82.58	5.18	3.45	46.62	6.45	45.66	1.21	0.035	17.02	1422	Mohammed, M. A. A. <i>et al.</i> (2012)
Switchgrass	16.8	76.9	6.0	6.3	47.9	6.2	45.0	0.8	0.1	19.6	115.4	Masnadi <i>et al.</i> (2014) Mani <i>et al.</i> (2006)
Beef cattle manure	11.15	59.05	13.08	29.8	35.4	5.04	27.58	1.79	0.4	15.93	NA	Maglinao Jr <i>et al.</i> (2015)
Rice straw*	17.25	69.33	NA	13.42	41.78	4.63	36.57	0.7	0.08	16.28	75	Jenkins and Ebeling (1985)
Corncoobs*	18.54	80.10	NA	1.36	46.58	5.87	45.46	0.93	0.16	18.77	282	Jenkins and Ebeling (1985)
Rice hulls*	16.67	65.47	NA	17.86	40.96	4.3	35.86	0.4	0.02	16.14	70-145	Jenkins and Ebeling (1985)
Woody												
Sawdust*	16.27	82.45	NA	1.28	50.26	6.14	42.2	0.07	0.05	20.47	NA	Lapuerta, Magin <i>et al.</i> (2008)

Macadamia shells*	23.68	75.92	NA	0.40	54.41	4.99	39.69	0.36	0.01	21.01	680	Jenkins and Ebeling (1985)
Coconut shells*	21.38	77.82	NA	0.8	49.62	7.31	42.75	0.22	0.10	20.8	NA	Iqbalidin <i>et al.</i> (2013)
Redwood*	19.92	79.72	NA	0.36	50.64	5.98	42.88	0.05	0.03	20.72	481	Jenkins and Ebeling (1985)
Coal (examples)												Higman and van der Burgt (2008)
Lignite	27.8	24.9	36.9	10.4	71.0	4.3	23.2	1.1	0.4	26.7	641-865	
Sub-bituminous	43.6	34.7	10.5	11.2	76.4	5.6	14.9	1.7	1.4	31.8	650-900	
Bituminous	54.9	35.6	5.3	4.2	82.8	5.1	10.1	1.4	0.6	36.1	673-913	
Anthracite	81.8	7.7	4.5	6	91.8	3.6	2.5	1.4	0.7	36.2	800-929	
Bio-char												
Wood charcoal	67.5	18.7	6.1	7.7	77	4.2	11.5	0.3	0.6	30.3	200-400	Rasul (2001)
Coconut shells charcoal*	50.55	48.25	NA	1.2	64.87	4.66	29.54	0.84	0.09	30.75	450-600	Iqbalidin <i>et al.</i> (2013)

* Moisture free (dry fuel)

Table A.2: Studies on catalytic activities in gasification

Materials	Catalysts	Remarks	Reference
Empty fruit bunch oil palm (EFB)	<ul style="list-style-type: none"> - Malaysian dolomite (P1) - Malaysian dolomite (GML) - NaOH - NaCl - CaO - ZnO - NiO 	Adding dolomite at gasification temperature of 850°C significantly increased the H ₂ in Syngas composition. The catalytic reactions enhanced more occurrences of water shift reactions.	Mohammed, M. A. <i>et al.</i> (2012)
Cane bagasse pellet fuel	Granular CaO was mixed with pellet fuel.	The mixture of up to 6% granular CaO with the cane bagasse pellet fuel was fed into a downdraft gasifier bed. The tar content in syngas was reduced up to 80% and the syngas yield was increase 17-37%.	Jordan and Akay (2013)
Illionis 6 coal and switchgrass co-gasification	Switchgrass as source of potassium catalyst	Both switchgrass char and ash displayed catalytic activity in mixture with coal. At mixture ratio of 1:9 of coal: switchgrass ash and temperature at 895°C, gasification rate reached eight folds.	Brown <i>et al.</i> (2000)
Meat and bone meal (MBM) char and coal (anthracite and lignin) cogasification	Natural catalyst (Sodium and Calcium) from MBM	The co-gasification rate of anthracite-MBM at 950°C was 1.5 faster than individual materials.	Ren <i>et al.</i> (2011)
Biomass (Sawdust and Switchgrass) and coal (subbituminous and fluid coke) cogasification	Natural catalyst of potassium from the biomass	Potassium and aluminosilicates molar composition in the mixture had effect in the inhibition and catalytic activities in co-gasification.	(Masnadi <i>et al.</i> (2015))

Table A.3: Literature on the biomass pellet

Material	Method	Analyses	Reference
Cotton gin by product	<p>Treatments:</p> <ul style="list-style-type: none"> - Addition corn starch 4% (gelatinized) & 10% '(5% gelatinized + 1% dry) - Addition 5% corn starch (4% gelatinized + 1% dry), & 5% cotton seed oil <p>Machine:</p> <ul style="list-style-type: none"> - Lab scale extruder for mixing and making slurry before entering commercial pellet mill - Water was added when entering pellet mill for moisture content of 15% -20% 	<ul style="list-style-type: none"> • Bulk density (ASTME873) • Calorific value(D5865) • Ash(D1102) • Total sulphur(ASTMD4239) • Water soluble sodium(ASTME776) • Maximum pellet length (PFI) • Fines (PFI) • Proximate(Moisture, volatile, Fixed carbon) • Ultimate(C,H,N,O) 	Holt <i>et al.</i> (2006)
Pruning residues of <i>Olea europaea L</i>	<p>Using single pelleter. Treatments :</p> <ol style="list-style-type: none"> 1. pressure 2000, 3000, 4000, 5000 N 2. Temp 60, 90,120, 150°C 3. Biomass Moisture content 5,10,15,20% (w.b.) 4. Particle size 1 mm, 2 mm, 4 mm 	<ul style="list-style-type: none"> -Mass, dimensions & density - Durability: specific rigidity - <p>Statistical analysis: the response of treatments to density and modulus elasticity</p>	Carone <i>et al.</i> (2011)
<p>Wheat straw bonded with</p> <ul style="list-style-type: none"> - wood residues - pre-treated wood residues - glycerol - lignosulfonate - Bentonite <p>wood residue with glycerol</p>	<p>Methods:</p> <ol style="list-style-type: none"> 1. Binder treatment: <ul style="list-style-type: none"> • Single pelleting • 0% binder • 2% lignosulfonate • 2% bentonite • 5% glycerol • 10%,20%,30% wood residue • 10%,20% & 30% microwave pre-treated wood residue 	<ul style="list-style-type: none"> • Pellet density, dimension and relaxed density (14 days) • Specific energy consumption • Tensile strength • Higher heating value <p>Statistical analysis of the effect of binders on the physicochemical characteristics</p>	Lu <i>et al.</i> (2014)

Material	Method	Analyses	Reference
	10%,20%,30% microwave pre-treated wood residue with glycerol 5%		
Wheat straw bonded with - wood residues - pre-treated wood residues - glycerol - lignosulfonate - Bentonite - wood residue with glycerol	Methods: 1. Binder treatment: <ul style="list-style-type: none"> • Single pelleting • 0% binder • 2% lignosulfonate • 2% bentonite • 5% glycerol • 10%,20%,30% wood residue • 10%,20% & 30% microwave pre-treated wood residue • 10%,20%,30% microwave pre-treated wood residue with glycerol 5% • 9.5%-10% Moisture • Particle size: mean geometric 0.858 mm • Compressive press 4000 N, stop 60 second 	<ul style="list-style-type: none"> • Pellet density, dimension and relaxed density (14 days) • Specific energy consumption • Tensile strength • Higher heating value • Statistical analysis of the effect of binders on the physicochemical characteristics 	Lu <i>et al.</i> (2014)

Table A.4: Specification of non-woody pellets according to ISO 17225-6:2014(E)

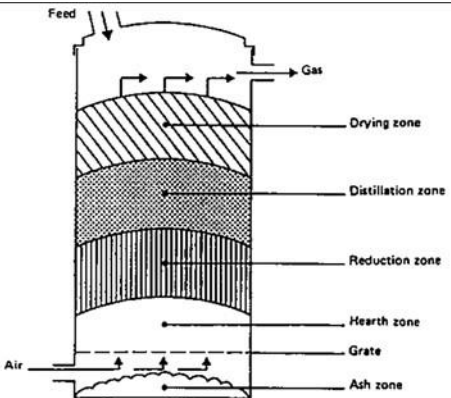
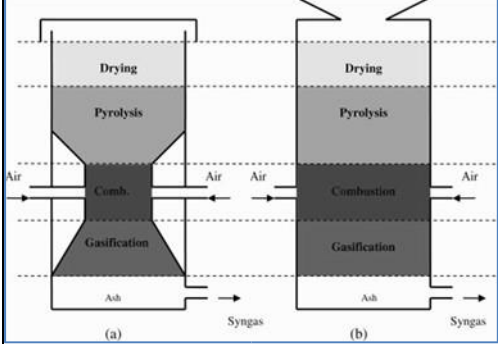
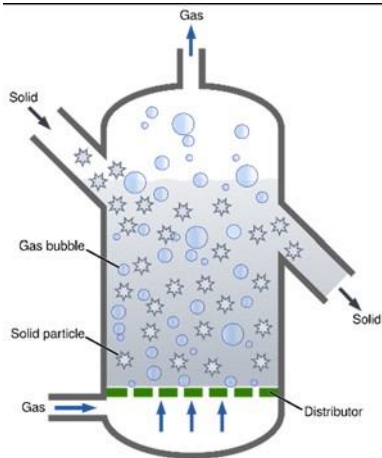
Specification of pellets produced from herbaceous biomass, fruit biomass, aquatic biomass and blends and mixtures

	Property class, Analyses method	Units	A	B
Normative	Origin and source ^a		Herbaceous biomass Fruit biomass Aquatic biomass Blends and mixtures	Herbaceous biomass Fruit biomass Aquatic biomass Blends and mixtures
	Diameter (D) ^b and Length (L) ^c	mm	D06 to D25, D ± 1: 3.15 < L ≤ 40 (from D06 to D10) 3.15 < L ≤ 50 (from D12 to D25)	D06 to D25, D ± 1: 3.15 < L ≤ 40 (from D06 to D10) 3.15 < L ≤ 50 (from D12 to D25)
	Moisture, M	w-% as received, wet basis	M12 ≤ 12	M15 ≤ 15
	Ash, A	w-% dry	A6.0 ≤ 6	A10 ≤ 10
	Mechanical durability, DU	w-% as received	DU97.5 ≥ 97.5	DU96.0 ≥ 96.0
	Fines, F ^d	w-% as received	F2.0 ≤ 2.0	F3.0 ≤ 3.0
	Additives ^e	w-% as received	≤ 5 Type and amount to be stated	≤ 5 Type and amount to be stated
	Net calorific value, Q	MJ/kg or kWh/kg as received	Q14.5 ≥ 14.5 or Q4.0 ≥ 4.0	Q14.5 ≥ 14.5 or Q4.0 ≥ 4.0
	Bulk density, BD	Kg/m ³ as received	BD600 ≥ 600	BD600 ≥ 600
	Nitrogen, N	w-% dry	N1.5 ≤ 1.5	N2.0 ≤ 2.0
	Sulfur, S	w-% dry	S0.20 ≤ 0.20	S0.30 ≤ 0.30
	Chlorine, Cl	w-% dry	Cl0.10 ≤ 0.10	Cl0.30 ≤ 0.30
	Arsenic, As	mg/kg dry	≤ 1	≤ 1
	Cadmium, Cd	mg/kg dry	≤ 0.5	≤ 0.5
	Chromium, Cr	mg/kg dry	≤ 50	≤ 50
	Copper, Cu	mg/kg dry	≤ 20	≤ 20
	Lead, Pb	mg/kg dry	≤ 10	≤ 10
	Mercury, Hg	mg/kg dry	≤ 0.1	≤ 0.1
	Nickel, Ni	mg/kg dry	≤ 10	≤ 10
Zinc, Zn	mg/kg dry	≤ 100	≤ 100	
Informative	Ash melting behavior	°C	Should be stated	Should be stated

^a To be stated the 4-digit classification (Table 1 ISO 17225-1). Blends and mixtures can include also woody biomass. If composition of blend is known the w-% can be used to specify blends ^b Selected size (e.g. D06, D08, D10, D12 or D25) of pellets to be stated ^c Amount of pellets longer than 40 mm can be 1% w-% (from D06 to D10). Maximum length shall be ≤ 45 mm for pellets from D06 to D10 ^d At factory gate in bulk transport (at the time of loading) and in small (up to 20 kg) and large sacks (at time of packing or when delivering to end-user) ^e Type of additives to aid production, delivery or combustion (e.g. pressing aids, slagging inhibitors or any other additives like starch, corn flour, potato flour, vegetable oil, lignin).

^f It is recommended that all characteristic temperatures (shrinkage starting temperature (SST), deformation temperature (DT), hemisphere temperature and flow temperature (FT) in oxidizing condition should be stated

Table A.5: Type of gasifier

Type	Sub Type	Main characteristics	
Fixed bed	Updraft	<ul style="list-style-type: none"> • Small to medium scale capacity (< 20 MW) • High tar and impurities • 700-900°C gasification temp • Small chunk of the fuel particle size 	
	Downdraft	<ul style="list-style-type: none"> • Small scale capacity (<5 MW) • Low tar • 700-900°C gasification temp • Small and uniform fuel particle size 	
Fluidised bed	Bubbling	<ul style="list-style-type: none"> • Medium to big scale (10-100 MW) • Medium tars • <900°C gasification tem • Small to fine fuel particle 	

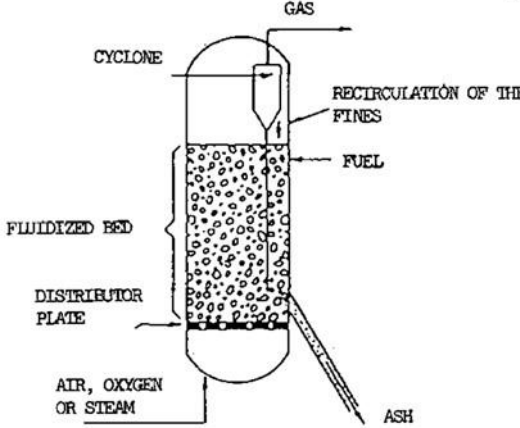
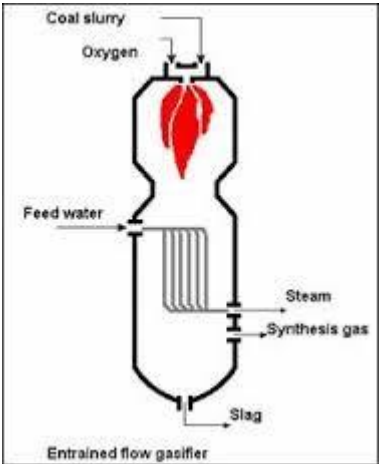
Type	Sub Type	Main characteristics	
	Circulating	<ul style="list-style-type: none"> • Medium to big scale (20-100 MW) • Medium tars • 1450°C gasification temperature • Small to fine fuel particle 	 <p>The diagram illustrates a circulating fluidized bed gasifier. At the bottom, a distributor plate allows the entry of 'AIR, OXYGEN OR STEAM'. Above this is the 'FLUIDIZED BED' where 'FUEL' is introduced. A 'CYCLONE' at the top separates the 'GAS' from the bed. 'RECIRCULATION OF THE FINES' is shown as a loop returning particles to the bed. 'ASH' is collected at the bottom right.</p>
Entrained bed		<ul style="list-style-type: none"> • Big scale (>100 MW) • Very low tar • 1450°C gasification temperature • Fuel particle in form of slurry 	 <p>The diagram shows an entrained flow gasifier. 'Coal slurry' and 'Oxygen' enter from the top. 'Feed water' enters from the side. 'Steam' and 'Synthesis gas' exit from the side. 'Slag' exits from the bottom. The entire unit is labeled 'Entrained flow gasifier'.</p>

Table A.6: Equilibrium models of gasification

No	Authors	Method	Type of gasifier	Objectives of studies
1	Zainal <i>et al.</i> (2001)	Stoichiometric equilibrium	Downdraft	<ul style="list-style-type: none"> • Prediction of syngas composition • Simulation using the effect of initial moisture content and temperatures
2	Babu and Seth (2006)	Stoichiometric equilibrium	Downdraft	<ul style="list-style-type: none"> □ Incorporated Char Reactivity Factor (CRF) for prediction of temperature and its syngas composition profile
3	Valero and Usón (2006)	Stoichiometric equilibrium	Entrained bed	<ul style="list-style-type: none"> • Study the gas composition of cogasification petroleum coke and 10% of several biomass using oxygen as oxidant • Simulation using variation of AF ratio and steam/fuel ratio for temperatures, efficiency and syngas compositions prediction
4	Jarungthammachote and Dutta (2007)	Stoichiometric equilibrium	Downdraft	<ul style="list-style-type: none"> • Determine the temperature of gasification at equilibrium condition • Modification of model using coefficient of correction to adjust methane composition
5	Antonopoulos <i>et al.</i> (2012)	Gibbs free energy	Downdraft	Determined the best temperature in reduction zone which has impact to the high gas heating value

No	Authors	Method	Type of gasifier	Objectives of studies
6	Barman <i>et al.</i> (2012)	Stoichiometric Equilibrium	Downdraft	<input type="checkbox"/> Prediction of syngas composition by including the tar in reactions.
7	Shabbar and Janajreh (2013)	Gibbs free energy	Universal	<ul style="list-style-type: none"> • Prediction of syngas composition using Bituminous coal proximate & ultimate • Simulation using air, air-steam, and solarsteam as oxidants

Table A.7: Kinetic models of gasification

No	Authors	Method	Type of gasifier	Objectives of studies
1	Blasi (2000)	Volumetric model 0-dimensional	Stratified downdraft	Prediction of gas composition and axial temperature profile Simulation described the effect of air to fuel ratio to the reaction rate in the reactor zones
2	Masmoudi <i>et al.</i> (2014)	Exponential Char Reactivity Factor 2-dimensional	Fixed bed downdraft (Reduction zones)	Prediction syngas compositions and temperature profiles at reduction zone both radially and longitudinally.
3	Kaushal <i>et al.</i> (2010)	Shrinking model One dimensional	Bubbling fluidized bed twophase(bubble and emulsion), two-zone (bottom dense bed and upper freeboard)	Prediction temperatures, solid remained and gas concentrations along the axis of reactor Simulation using wood pellet using air, oxygen, steam and mixed of oxygen and steam as oxidant
4	Xu <i>et al.</i> (2011)	Random pore model	universal	Prediction of syngas compositions and carbon consumption of the biomass at times of gasification progress for single biomass and coal gasification and mixed of biomass and coal co-gasification using steam as oxidant

Table A.8: Computational fluid dynamic models of gasification

No	Authors	Method	Type of gasifier	Objectives of studies
1	Gerun <i>et al.</i> (2008)	<ul style="list-style-type: none"> • 2D Axisymmetric • Discrete phase 	2 stage Downdraft	<ul style="list-style-type: none"> • To study the influence of air injection on tar cracking of steam and air as oxidant at the gasification stage • To investigate the detail of the partial oxidation zone which is crucial for tar cracking
2	Xie <i>et al.</i> (2012)	<ul style="list-style-type: none"> • 3D • Multiphase EulerianLagrangian 	Fluidized bed	<ul style="list-style-type: none"> • To predict the performance of fluidized bed biomass gasification • To simulate the effect of reactor temperature, ER and steam to biomass (wood chip) ratio on product gas composition and carbon conversion efficiency
3	Murgia <i>et al.</i> (2012)	<ul style="list-style-type: none"> • 2D planar • Euler-Euler Multiphase • Applied MFIX computer code 	Updraft	To simulate and evaluate the dynamics of the coal gasification process in updraft gasifier using air as oxidant
4	Patel <i>et al.</i> (2013)	<ul style="list-style-type: none"> • 2D planar • Non premixed combustion • Applied FLUENT software 	Downdraft	To investigate the flow pattern, temperature, turbulence and product gas composition of lignite gasification
5	Janajreh and Al Shrah (2013)	<ul style="list-style-type: none"> • 2D Axisymmetric • Discrete phase model • Applied ANSYS FLUENT 	Downdraft	To investigate the temperature distribution and evolution of the species inside the reactor in gasification of wood particle using air as oxidant
6	Wu <i>et al.</i> (2013)	<ul style="list-style-type: none"> • 2D planar • Euler-Euler Multiphase • Applied ANSYS FLUENT 	Downdraft	To study the gasification process in the downdraft configuration considering drying, pyrolysis, combustion and gasification reactions of wood pellet
7	ContrerasAndrade <i>et al.</i> (2014)	<ul style="list-style-type: none"> • 2D Axisymmetric • Eulerian multiphase • Applied ANSYS FLUENT 	Downdraft	To study the temperature, syngas composition and flow pattern inside the reactors using wood charcoal as feedstock and air as oxidant

Appendix B: Pellet size

B.1. Raw data of pellet size before and after storage

Table B.1: Pellet size measurement

Storage	Treatment	Length (mm)	Diameter (mm)	Individual weight (g)	Apparent density (kg/m ³)
0	0	37	7.3	2.02	1305.07
0	0	33.4	7.3	2.01	1438.58
0	0	37.7	7.4	2.03	1252.63
0	0	32.5	7.6	1.85	1255.43
0	0	29.6	7.8	1.69	1195.46
0	0	33.2	7.6	2.12	1408.32
0	0	37.8	7.4	2.22	1366.24
0	0	34.6	7.4	1.9	1277.45
0	0	40.4	7.5	2.15	1205.22
0	0	41.7	7.5	2.44	1325.14
0	0	39.6	7.6	2.19	1219.7
0	0	37.6	7.4	2.22	1373.51
0	0	30.7	7.6	1.78	1278.75
0	0	34.8	7.7	2.02	1247.16
0	0	42.2	7.6	2.69	1405.86
0	0	33.1	7.7	1.91	1239.81
0	0	39.6	7.6	2.43	1353.36
0	0	34.8	7.5	1.85	1203.93
0	0	38.2	7.6	2.35	1356.77
0	0	31.8	7.5	1.84	1310.38
0	0	34	7.5	2.08	1385.45
0	0	36.3	7.5	1.96	1222.81
0	0	36.2	7.4	2.04	1310.96
0	0	38	7.5	2.18	1299.21
0	0	40.6	7.6	2.34	1271.14
0	0	40.5	7.3	2.07	1221.8
0	0	31.7	7.7	1.63	1104.78
0	0	38.8	7.5	2.31	1348.3
0	0	37.2	7.4	2.06	1288.22
0	0	34.1	7.5	2.02	1341.54
0	0	34.6	7.4	2.04	1371.58
0	0	38.9	7.5	2.1	1222.58
0	0	34.9	7.5	2.09	1356.22
0	0	38.3	7.4	2.23	1354.48
0	0	36.9	7.4	2.1	1323.91
0	0	41.4	7.4	2.44	1371.06

Storage	Treatment	Length (mm)	Diameter (mm)	Individual weight (g)	Apparent density (kg/m ³)
0	0	30.8	7.3	1.73	1342.7
0	0	35.1	7.6	2.23	1401.2
0	0	30.9	7.9	1.81	1195.63
0	0	33.6	7.4	1.89	1308.55
0	0	30.7	7.7	1.64	1147.77
0	0	31.7	7.4	1.74	1276.9
0	0	30	7.4	1.73	1341.5
0	0	31.9	7.4	1.87	1363.7
0	0	36.6	7.4	1.86	1182.22
0	0	32.2	7.5	1.63	1146.41
0	0	30.7	7.5	1.75	1290.94
0	0	26.6	7.4	1.53	1338.06
0	0	30.9	7.6	1.65	1177.68
0	0	26.8	7.6	1.46	1201.49
0	5	31.2	7.5	1.66	1204.93
0	5	34.4	7.6	1.96	1256.61
0	5	37.2	7.6	2.14	1268.74
0	5	36.3	7.9	2.11	1186.46
0	5	38.7	7.7	2.27	1260.27
0	5	38.2	7.6	2.13	1229.76
0	5	38	7.6	2.12	1230.43
0	5	38	7.7	2.02	1142.13
0	5	32.1	7.6	1.87	1284.81
0	5	39.7	7.6	2.23	1238.85
0	5	35.9	7.7	2.01	1202.96
0	5	33.7	7.6	1.8	1178
0	5	38	7.8	2.25	1239.77
0	5	36.9	7.6	2.1	1255.15
0	5	36.7	7.6	2.03	1219.93
0	5	30.6	7.6	1.75	1261.3
0	5	32.6	7.4	1.81	1291.6
0	5	31.5	7.7	1.82	1241.39
0	5	35.4	7.6	2.06	1283.42
0	5	29.8	7.5	1.65	1253.94
0	5	34.5	7.7	1.96	1220.64
0	5	37.7	7.4	2.17	1339.01
0	5	32.1	7.7	1.81	1211.5
0	5	35.4	7.5	1.9	1215.51
0	5	35.3	7.6	1.95	1218.32
0	5	37.5	7.6	2.23	1311.53

Storage	Treatment	Length (mm)	Diameter (mm)	Individual weight (g)	Apparent density (kg/m ³)
0	5	33.1	7.6	1.83	1219.34
0	5	34.8	7.7	1.96	1210.11
0	5	38	7.5	2	1191.94
0	5	34.8	7.6	1.99	1261.18
0	5	32.2	7.6	1.9	1301.37
0	5	41.5	7.6	2.27	1206.37
0	5	32.8	7.8	1.84	1174.59
0	5	41.5	7.6	2.35	1248.89
0	5	31.5	7.6	1.77	1239.27
0	5	37.4	7.7	2.23	1281.1
0	5	29.3	7.6	1.63	1226.94
0	5	31.1	7.5	1.62	1179.68
0	5	32.9	7.5	1.79	1232.15
0	5	38.9	7.5	2.22	1292.44
0	5	33.8	7.8	1.92	1189.39
0	5	38.4	7.7	2.23	1247.74
0	5	37	7.6	2.06	1227.92
0	5	29.6	7.6	1.66	1236.86
0	5	32.5	7.7	1.95	1289.14
0	5	32.2	7.6	1.81	1239.73
0	5	34.7	7.7	1.87	1157.87
0	5	30.2	7.6	1.74	1270.71
0	5	29.6	7.5	1.61	1231.81
0	5	24.7	7.5	1.41	1292.8
0	10	38.9	7.5	2.22	1292.44
0	10	39.8	7.5	2.22	1263.22
0	10	29.9	7.5	1.82	1378.5
0	10	34.7	7.6	1.94	1233.04
0	10	35.1	7.6	2.02	1269.25
0	10	42	7.5	2.35	1267.15
0	10	40.5	7.5	2.47	1381.18
0	10	33	7.6	1.9	1269.82
0	10	36.7	7.6	2.17	1304.06
0	10	37.6	7.7	2.23	1274.28
0	10	36.7	7.6	2.11	1268
0	10	36.8	7.7	2.21	1290.31
0	10	35.8	7.6	2.26	1392.29
0	10	33	7.5	1.94	1331.36
0	10	34.7	7.5	2.07	1350.98
0	10	39.4	7.5	2.32	1333.52

Storage	Treatment	Length (mm)	Diameter (mm)	Individual weight (g)	Apparent density (kg/m ³)
0	10	39.7	7.6	2.27	1261.07
0	10	28.8	7.7	1.71	1275.71
0	10	41.8	7.5	2.39	1294.88
0	10	34.7	7.7	2.14	1325.05
0	10	41.5	7.5	2.32	1266.04
0	10	42.1	7.5	2.48	1334.07
0	10	34.2	7.3	1.68	1174.27
0	10	35.5	7.3	2.04	1373.68
0	10	37.8	7.6	2.27	1324.46
0	10	36.6	7.6	2.23	1343.78
0	10	32.1	7.6	1.89	1298.55
0	10	40.3	7.5	2.27	1275.64
0	10	39.2	7.6	2.36	1327.79
0	10	37	7.5	2.15	1315.97
0	10	40.2	7.6	2.34	1283.79
0	10	39.5	7.6	2.37	1323.29
0	10	37.6	7.5	2.29	1379.29
0	10	37.6	7.5	2.22	1337.13
0	10	36	7.8	2.19	1273.75
0	10	40	7.5	2.33	1319.18
0	10	40.5	7.6	2.38	1296.06
0	10	35.1	7.8	2.23	1330.27
0	10	29.7	7.5	1.62	1235.28
0	10	39.7	7.6	2.36	1311.07
0	10	35.3	7.6	2.05	1280.8
0	10	40.6	7.7	2.43	1285.96
0	10	30.4	7.6	1.75	1269.6
0	10	31.3	7.8	1.96	1311.15
0	10	38.6	7.4	2.17	1307.79
0	10	31.9	7.5	1.94	1377.27
0	10	36.8	7.6	2.2	1318.49
0	10	30.4	7.6	1.7	1233.33
0	10	32	7.8	1.9	1243.21
0	10	34.4	7.4	2.23	1508.04
0	15	36.5	7.5	2.05	1271.95
0	15	40.2	7.4	2.35	1359.91
0	15	40.6	7.6	2.35	1276.57
0	15	34.8	7.4	1.88	1256.74
0	15	40	7.6	2.34	1290.21
0	15	33.3	7.5	1.87	1271.76

Storage	Treatment	Length (mm)	Diameter (mm)	Individual weight (g)	Apparent density (kg/m ³)
0	15	38.9	7.8	2.3	1238
0	15	39.4	7.4	2.25	1328.47
0	15	40.6	7.4	2.49	1426.72
0	15	38.5	7.8	2.39	1299.81
0	15	40.5	7.4	2.35	1349.83
0	15	36.6	7.5	2.11	1305.6
0	15	29.5	7.5	1.76	1351.13
0	15	36	7.6	2.19	1341.67
0	15	39.1	7.5	2.26	1309
0	15	32.9	7.6	2.04	1367.53
0	15	37.7	7.3	2.14	1356.93
0	15	34.6	7.4	2.07	1391.75
0	15	34.5	7.6	2.05	1310.5
0	15	40.9	7.4	2.46	1399.2
0	15	36.9	7.5	2.21	1356.36
0	15	36.3	7.6	2.17	1318.43
0	15	32.9	7.5	1.8	1239.04
0	15	28.4	7.5	1.71	1363.6
0	15	33.7	7.6	2	1308.89
0	15	33.3	7.5	2.06	1400.98
0	15	43.1	7.9	2.53	1198.17
0	15	39.3	7.6	2.22	1245.84
0	15	33.4	7.3	1.93	1381.32
0	15	42.3	7.4	2.49	1369.39
0	15	42.9	7.7	2.68	1342.23
0	15	39.3	7.5	2.29	1319.63
0	15	39.3	7.7	2.26	1235.56
0	15	37.6	7.6	2.02	1184.86
0	15	36.2	7.5	2.1	1313.77
0	15	40.6	7.5	2.41	1344.31
0	15	33.9	7.4	1.9	1303.83
0	15	35	7.5	2.06	1332.93
0	15	35.8	7.6	2.18	1343
0	15	30.2	7.4	1.82	1401.95
0	15	36.6	7.5	2.22	1373.66
0	15	29.6	7.4	1.71	1343.91
0	15	27.9	7.7	1.48	1139.74
0	15	26.6	7.6	1.46	1210.53
0	15	42.1	7.6	2.48	1299.19
0	15	41.1	7.6	2.39	1282.51

Storage	Treatment	Length (mm)	Diameter (mm)	Individual weight (g)	Apparent density (kg/m ³)
0	15	36.9	7.6	2.18	1302.97
0	15	35.8	7.4	2.15	1397.08
0	15	23.3	7.5	1.25	1214.96
0	15	37.3	7.4	2.22	1384.56
0	20	42.7	7.7	2.74	1189.13
0	20	38.9	7.9	2.47	1199.71
0	20	41.5	7.9	2.58	1230.59
0	20	32.1	7.9	1.96	1197.64
0	20	33.6	7.8	2.16	1278.32
0	20	32.6	7.6	1.97	1219.93
0	20	37.3	8.1	2.45	1213.6
0	20	36.1	7.9	2.31	1228.64
0	20	34.2	7.7	2.11	1184.73
0	20	47.3	7.8	3.12	1206.66
0	20	37.9	8	2.62	1278.85
0	20	37.6	8	2.27	1254.46
0	20	42.9	7.8	2.71	1210.74
0	20	40.7	7.7	2.51	1276.69
0	20	38.2	8.1	2.54	1177.3
0	20	38.6	7.8	2.27	1370.81
0	20	39.2	7.7	2.47	1201.12
0	20	34.4	7.6	2.15	1258.81
0	20	31.7	7.8	2.03	1170.25
0	20	44.9	7.8	2.93	1252.8
0	20	34.1	7.8	2.19	1213.22
0	20	39.5	7.8	2.5	1280.19
0	20	38.4	8	2.44	1210.32
0	20	34.1	8	2.14	1196.74
0	20	40.6	7.7	2.44	1239.87
0	20	38.6	7.8	2.34	1258.16
0	20	36.7	8.2	2.51	1242.74
0	20	35.8	7.9	2.19	1274.63
0	20	32.4	7.9	2.04	1263
0	20	25.3	7.9	1.63	1302.49
0	20	24.3	8	1.63	1187.09
0	20	19.3	7.8	1.25	1182.32
0	20	38.2	7.6	2.16	1289.75
0	20	42.7	7.7	2.4	1206.73
0	20	39.6	7.5	2.17	1199.04
0	20	35.5	7.5	1.84	1218.08

Storage	Treatment	Length (mm)	Diameter (mm)	Individual weight (g)	Apparent density (kg/m ³)
0	20	40	7.5	2.06	1311.45
0	20	40.4	7.7	2.12	1256.84
0	20	38.6	7.7	2.15	1271.14
0	20	30.4	7.5	1.59	1280.23
0	20	35.5	7.4	1.8	1217.63
0	20	35.8	7.7	1.98	1223.4
0	20	36.7	7.7	2.08	1280.47
0	20	32.6	7.7	1.77	1196.72
0	20	37.2	7.7	2.05	1225.27
0	20	29.5	7.7	1.64	1262.74
0	20	29.6	7.7	1.74	1254.95
0	20	29	7.7	1.48	1290.36
0	20	27.4	7.6	1.4	1217.73
0	20	28.3	7.5	1.58	1202.61
1	0	43.1	7.5	2.36	1240.06
1	0	41.1	7.5	2.46	1355.5
1	0	41.1	7.4	2.43	1375.41
1	0	38.8	7.5	2.36	1377.49
1	0	41.3	7.4	2.43	1368.75
1	0	34	7.4	2	1368.42
1	0	37	7.4	2.1	1320.34
1	0	41.1	7.4	2.51	1420.69
1	0	34.6	7.6	2	1274.84
1	0	36.2	7.5	2.06	1288.74
1	0	36.3	7.5	1.98	1235.28
1	0	32.4	7.5	1.73	1209.23
1	0	33.8	7.3	1.94	1372.05
1	0	30.4	7.4	1.69	1293.24
1	0	38.4	7.8	2.36	1286.83
1	0	43.9	7.7	2.5	1223.56
1	0	32.2	7.5	1.76	1237.84
1	0	35.6	7.5	2.18	1386.8
1	0	37.3	7.7	2.17	1249.97
1	0	39.4	7.6	2.19	1225.89
1	0	32.7	7.4	1.96	1394.36
1	0	33.6	7.7	1.89	1208.57
1	0	32.2	7.4	1.7	1228.17
1	0	42.4	7.4	2.28	1250.94
1	0	28.6	7.6	1.71	1318.66
1	0	36.6	7.5	2.17	1342.72

Storage	Treatment	Length (mm)	Diameter (mm)	Individual weight (g)	Apparent density (kg/m ³)
1	0	29.7	7.4	1.7	1331.56
1	0	39.2	7.3	1.93	1176.94
1	0	31.5	7.3	1.71	1297.69
1	0	36	7.7	2.11	1259.3
1	0	37	7.7	2.08	1207.84
1	0	35.7	7.5	2.22	1408.29
1	0	36.2	7.5	2.09	1307.51
1	0	33.7	7.5	1.85	1243.22
1	0	38.7	7.5	2.29	1340.08
1	0	33.9	7.4	1.98	1358.73
1	0	41.7	7.3	2.38	1364.35
1	0	40.4	7.4	2.41	1387.72
1	0	35.5	7.4	1.97	1290.94
1	0	30.7	7.3	1.64	1277
1	0	41.8	7.5	2.31	1251.54
1	0	29.6	7.5	1.54	1178.25
1	0	34.1	7.2	1.96	1412.43
1	0	35.8	7.3	2.14	1428.94
1	0	42.7	7.5	2.53	1341.84
1	0	33.4	7.5	1.88	1274.73
1	0	41.8	7.3	2.12	1212.4
1	0	28.2	7.6	1.5	1173.13
1	0	26.7	7.4	1.5	1306.91
1	0	31.3	7.5	1.78	1287.9
1	5	39.4	7.6	2.17	1214.69
1	5	42.2	7.8	2.44	1210.65
1	5	38.6	7.7	2.21	1230.14
1	5	37.2	7.7	2.1	1212.9
1	5	35.8	7.5	2	1265.19
1	5	35.2	7.4	1.98	1308.55
1	5	40.6	7.6	2.24	1216.82
1	5	36.5	7.6	2.02	1220.57
1	5	41.3	7.5	2.35	1288.62
1	5	37.7	7.6	2.12	1240.22
1	5	31.5	7.8	1.96	1302.83
1	5	35.1	7.6	1.9	1193.85
1	5	38.9	7.6	2.17	1230.31
1	5	37.6	7.5	2.18	1313.04
1	5	34.3	7.6	1.95	1253.84
1	5	34.6	7.6	1.97	1255.72

Storage	Treatment	Length (mm)	Diameter (mm)	Individual weight (g)	Apparent density (kg/m ³)
1	5	36.9	7.5	2.09	1282.71
1	5	33	7.6	1.88	1256.46
1	5	34.1	7.6	1.99	1287.07
1	5	40.2	7.5	2.22	1250.65
1	5	39.8	7.6	2.22	1230.19
1	5	39.9	7.6	2.21	1221.58
1	5	39.4	7.6	2.2	1231.49
1	5	37.7	7.7	2.17	1236.71
1	5	35.8	7.6	1.99	1225.95
1	5	32	7.6	1.75	1206.12
1	5	35.3	7.8	2.03	1204.1
1	5	40.8	7.6	2.29	1237.88
1	5	32.3	7.7	1.68	1117.52
1	5	35.6	7.6	1.92	1189.47
1	5	37.5	7.5	2.04	1231.99
1	5	35.6	7.6	2	1239.03
1	5	33.4	7.7	1.87	1202.94
1	5	35.1	7.5	1.96	1264.61
1	5	36.1	7.5	1.98	1242.13
1	5	35.9	7.6	1.97	1210.25
1	5	36.1	7.7	2.05	1220.1
1	5	35.6	7.6	2.02	1251.42
1	5	39	7.5	2.14	1242.67
1	5	32.4	7.6	1.78	1211.65
1	5	36	7.6	2.07	1268.15
1	5	35.9	7.7	2.05	1226.9
1	5	36.1	7.6	2.08	1270.75
1	5	33	7.4	1.82	1282.99
1	5	28.5	7.6	1.61	1245.9
1	5	33.3	7.5	1.85	1258.16
1	5	33.6	7.8	1.98	1233.86
1	5	35.6	7.7	1.9	1146.71
1	5	32.4	7.5	1.8	1258.16
1	5	30.2	7.5	1.7	1274.82
1	10	35.8	7.8	1.89	1105.4
1	10	37.2	7.8	2.18	1227.03
1	10	39.4	7.6	2.34	1309.85
1	10	37.9	7.6	1.99	1158.02
1	10	39.1	7.8	2	1071.01
1	10	36.8	7.6	2.24	1342.47

Storage	Treatment	Length (mm)	Diameter (mm)	Individual weight (g)	Apparent density (kg/m ³)
1	10	38.6	7.5	2.17	1273.15
1	10	36.2	7.7	2.19	1299.82
1	10	36.7	7.7	2	1170.88
1	10	37.2	7.6	2.22	1316.17
1	10	29.5	7.7	1.52	1107.06
1	10	40.5	7.7	2.38	1262.61
1	10	38.5	7.6	2.21	1266
1	10	34.4	7.4	1.68	1136.1
1	10	39.8	7.7	2.11	1139.06
1	10	37.3	7.7	2.03	1169.33
1	10	34.8	7.8	2.12	1275.55
1	10	40.3	7.2	1.94	1182.94
1	10	28.9	7.6	2.2	1678.91
1	10	34	7.7	2.05	1295.46
1	10	40.1	7.6	2.33	1281.49
1	10	38.7	7.6	2.16	1230.97
1	10	35.3	7.6	2.04	1274.56
1	10	37.3	7.5	1.82	1105.02
1	10	24.3	7.4	1.18	1129.65
1	10	36.3	7.5	2.04	1272.72
1	10	40.7	7.6	2.34	1268.02
1	10	32.1	7.7	2.28	1526.08
1	10	40.4	7.6	2.47	1348.4
1	10	34.4	7.6	1.92	1230.97
1	10	42.5	7.5	2.31	1230.92
1	10	38.5	7.6	1.93	1105.6
1	10	30.3	7.4	2.4	1842.62
1	10	39.7	7.7	2.33	1261
1	10	30.3	7.6	1.72	1251.96
1	10	39.7	7.5	2.28	1300.63
1	10	39.6	7.5	2.32	1326.79
1	10	41.3	7.6	2.42	1292.32
1	10	23.6	7.4	1.27	1251.87
1	10	38.1	7.7	2.25	1268.84
1	10	33	7.5	1.8	1235.28
1	10	41.1	7.5	2.31	1272.85
1	10	37.2	7.6	2.16	1280.6
1	10	35.5	7.6	2	1242.52
1	10	38.4	7.7	2.23	1247.74
1	10	39.5	7.5	2.23	1278.54

Storage	Treatment	Length (mm)	Diameter (mm)	Individual weight (g)	Apparent density (kg/m ³)
1	10	33.1	7.6	1.94	1292.64
1	10	36.7	7.7	2.2	1282.11
1	10	39.8	7.5	2.21	1257.53
1	10	40.4	7.5	2.28	1278.09
1	15	42.6	7.4	2.66	1452.58
1	15	39.8	7.4	2.21	1291.74
1	15	36.3	7.6	2.16	1312.35
1	15	42.3	7.4	2.33	1281.39
1	15	38	7.6	2.03	1178.19
1	15	35.9	7.7	2.17	1298.72
1	15	36.8	7.6	2.1	1258.56
1	15	41.3	7.5	2.37	1299.59
1	15	39.6	7.6	2.29	1275.39
1	15	41.6	7.7	2.53	1306.7
1	15	33.9	7.5	2	1336.1
1	15	36.3	7.5	1.98	1235.28
1	15	32.2	7.5	1.79	1258.94
1	15	39.3	7.5	2.21	1273.53
1	15	27	7.7	1.56	1241.39
1	15	36.3	7.7	2.15	1272.57
1	15	39.5	7.5	2.25	1290.01
1	15	42.6	7.6	2.46	1273.59
1	15	39.1	7.7	2.27	1247.38
1	15	40.1	7.7	2.34	1253.78
1	15	40.8	7.4	2.44	1391.22
1	15	35	7.5	2.12	1371.75
1	15	35.9	7.7	2.18	1304.7
1	15	34.6	7.5	2.03	1328.7
1	15	36.5	7.5	2.19	1358.81
1	15	42.5	7.5	2.48	1321.51
1	15	39.5	7.5	2.39	1370.28
1	15	33.7	7.6	2.04	1335.07
1	15	42.4	7.6	2.46	1279.59
1	15	40.6	7.5	2.34	1305.26
1	15	32.5	7.5	1.86	1296.1
1	15	32.8	7.5	1.91	1318.76
1	15	35.3	7.5	2.06	1321.6
1	15	38.4	7.6	2.12	1217.61
1	15	39.4	7.5	2.28	1310.53
1	15	41.4	7.4	2.33	1309.25

Storage	Treatment	Length (mm)	Diameter (mm)	Individual weight (g)	Apparent density (kg/m ³)
1	15	37.5	7.4	2.15	1333.75
1	15	30.3	7.5	1.71	1278.09
1	15	32.9	7.6	2.03	1360.83
1	15	37	7.5	2.18	1334.33
1	15	36.1	7.4	2.03	1308.14
1	15	30.8	7.5	1.81	1330.87
1	15	35.4	7.5	2.07	1324.26
1	15	38.2	7.8	2.36	1293.57
1	15	36.8	7.5	2.09	1286.19
1	15	36.3	7.7	2.09	1237.05
1	15	33.7	7.4	1.89	1304.66
1	15	40.6	7.5	2.33	1299.68
1	15	30.9	7.5	1.77	1297.25
1	15	35.9	7.7	2.04	1220.91
1	20	43.4	7.6	2.34	1189.13
1	20	39.4	7.7	2.2	1199.71
1	20	41.4	7.6	2.31	1230.59
1	20	37.1	7.4	1.91	1197.64
1	20	40.4	7.4	2.22	1278.32
1	20	36.7	7.6	2.03	1219.93
1	20	37.8	7.6	2.08	1213.6
1	20	34.1	7.5	1.85	1228.64
1	20	43.3	7.8	2.45	1184.73
1	20	38.2	7.6	2.09	1206.66
1	20	40.7	7.6	2.36	1278.85
1	20	40.8	7.5	2.26	1254.46
1	20	43.3	7.7	2.44	1210.74
1	20	35.3	7.5	1.99	1276.69
1	20	36.5	7.7	2	1177.3
1	20	36.2	7.6	2.25	1370.81
1	20	33.7	7.4	1.74	1201.12
1	20	43.1	7.6	2.46	1258.81
1	20	39.2	7.6	2.08	1170.25
1	20	37.6	7.5	2.08	1252.8
1	20	36.4	7.5	1.95	1213.22
1	20	34.8	7.6	2.02	1280.19
1	20	41	7.6	2.25	1210.32
1	20	42.2	7.5	2.23	1196.74
1	20	38.6	7.6	2.17	1239.87
1	20	39.6	7.5	2.2	1258.16

Storage	Treatment	Length (mm)	Diameter (mm)	Individual weight (g)	Apparent density (kg/m ³)
1	20	35.9	7.5	1.97	1242.74
1	20	38.2	7.5	2.15	1274.63
1	20	41.6	7.5	2.32	1263
1	20	38.6	7.5	2.22	1302.49
1	20	35.3	7.6	1.9	1187.09
1	20	38.8	7.6	2.08	1182.32
1	20	34.2	7.6	2	1289.75
1	20	29.2	7.7	1.64	1206.73
1	20	35.5	7.6	1.93	1199.04
1	20	38.3	7.5	2.06	1218.08
1	20	37.3	7.5	2.16	1311.45
1	20	38.2	7.5	2.12	1256.84
1	20	40.6	7.6	2.34	1271.14
1	20	38.6	7.7	2.3	1280.23
1	20	36.3	7.4	1.9	1217.63
1	20	39.3	7.6	2.18	1223.4
1	20	34.7	7.4	1.91	1280.47
1	20	35.2	7.6	1.91	1196.72
1	20	39.6	7.6	2.2	1225.27
1	20	32.5	7.8	1.96	1262.74
1	20	35.5	7.6	2.02	1254.95
1	20	35.3	7.7	2.12	1290.36
1	20	30.5	7.5	1.64	1217.73
1	20	39	7.8	2.24	1202.61

Storage 0= Data of pellet measurement before storage

Storage 1= Data of pellet measurement after 14 days storage for stabilisation

Treatment = the number 0-20 represents the biochar weight percentage in the pellet

B.2. Independent T-Test of pellet size before and after storage (stabilization)

T-Test Treatment=0%

Group Statistics

	storage	N	Mean	Std. Deviation	Std. Error Mean
Diameter	before	50	7.5040	.13087	.01851
	After	50	7.4720	.12784	.01808
app_density	before	50	1290.5512	78.66018	11.12423
	After	50	1299.4718	70.73530	10.00348
Weight	before	50	1.9984	.26235	.03710
	After	50	2.0508	.28496	.04030
Length	before	50	35.0240	3.88238	.54905
	After	50	35.9880	4.39214	.62114

Independent Samples Test

		Levene's Test for Equality of Variances		t-test for Equality of Means						
		F	Sig.	t	df	Sig. (2tailed)	Mean Difference	Std. Error Difference	95% Confidence Interval of the Difference	
									Lower	Upper
Diameter	Equal variances assumed	.014	.905	1.237	98	.219	.03200	.02587	-.01934	.08334
	Equal variances not assumed			1.237	97.94	.219	.03200	.02587	-.01934	.08334

App density	Equal variances assumed	.554	.458	-.596	98	.552	-8.92060	14.96055	-38.609	20.76813
	Equal variances not assumed			-.596	96.91	.552	-8.92060	14.96055	-38.613	20.77228
Weight	Equal variances assumed	.720	.398	-.957	98	.341	-.05240	.05478	-.16110	.05630
	Equal variances not assumed			-.957	97.33	.341	-.05240	.05478	-.16111	.05631
Length	Equal variances assumed	.585	.446	-1.163	98	.248	-.96400	.82902	-2.6091	.68116
	Equal variances not assumed			-1.163	96.54	.248	-.96400	.82902	-2.6094	.68147

T-Test Treatment=5%

Group Statistics

	storage	N	Mean	Std. Deviation	Std. Error Mean
Diameter	before	50	7.6140	.09899	.01400
	After	50	7.6000	.09476	.01340
app_density	before	50	1237.9260	41.10212	5.81272
	After	50	1238.3806	36.85941	5.21271
Weight	before	50	1.9494	.21385	.03024
	After	50	2.0214	.17306	.02447
Length	before	50	34.5980	3.51246	.49674
	After	50	36.0120	2.97586	.42085

Independent Samples Test

	Levene's Test for Equality of Variances		t-test for Equality of Means						
	F	Sig.	t	df	Sig. (2tailed)	Mean Difference	Std. Error Difference	95% Confidence Interval of the Difference	
								Lower	Upper
Diameter									
Equal variances assumed	.308	.580	.722	98	.472	.01400	.01938	-.02446	.05246
Equal variances not assumed			.722	97.813	.472	.01400	.01938	-.02446	.05246

app_density	Equal variances assumed	.933	.336	-.058	98	.954	-.45460	7.80769	-15.948	15.0395
	Equal variances not assumed			-.058	96.859	.954	-.45460	7.80769	-15.950	15.04179
Weight	Equal variances assumed	3.160	.079	-1.85	98	.067	-.07200	.03891	-.14921	.00521
	Equal variances not assumed			-1.85	93.917	.067	-.07200	.03891	-.14925	.00525
Length	Equal variances assumed	2.505	.117	-2.17	98	.032	-1.41400	.65105	-2.7059	-.12202
	Equal variances not assumed			-2.17	95.425	.032	-1.41400	.65105	-2.7064	-.12158

T-Test Treatment =10%

Group Statistics

	storage	N	Mean	Std. Deviation	Std. Error Mean
Diameter	before	50	7.5700	.11112	.01571
	After	50	7.5940	.12022	.01700
app_density	before	50	1306.3022	53.21724	7.52605
	After	50	1265.1030	130.46966	18.45120
Weight	before	50	2.1422	.22125	.03129
	After	50	2.0926	.27089	.03831
Length	before	50	36.4700	3.60913	.51041
	After	50	36.6160	4.13647	.58498

Independent Samples Test

		Levene's Test for Equality of Variances		t-test for Equality of Means						
		F	Sig.	t	df	Sig. (2tailed)	Mean Difference	Std. Error Difference	95% Confidence Interval of the Difference	
									Lower	Upper
Diameter	Equal variances assumed	.029	.866	-1.037	98	.302	-.02400	.02315	-.06994	.02194
	Equal variances not assumed			-1.037	97.398	.302	-.02400	.02315	-.06995	.02195
app_density	Equal variances assumed	4.752	.032	2.067	98	.041	41.1992	19.927	1.65458	80.7438

	Equal variances not assumed			2.067	64.865	.043	41.1992	19.927	1.40053	80.9978
Weight	Equal variances assumed	.558	.457	1.003	98	.318	.04960	.04946	-.04856	.14776
	Equal variances not assumed			1.003	94.242	.319	.04960	.04946	-.04861	.14781
Length	Equal variances assumed	.061	.805	-.188	98	.851	-.14600	.77635	-1.68665	1.39465
	Equal variances not assumed			-.188	96.232	.851	-.14600	.77635	-1.68700	1.39500

T-Test Treatment=15%

Group Statistics

	storage	N	Mean	Std. Deviation	Std. Error Mean
Diameter	before	50	7.5260	.12586	.01780
	After	50	7.5440	.10333	.01461
app_density	before	50	1315.1296	63.34141	8.95783
	After	50	1299.7620	47.39621	6.70284
Weight	before	50	2.1216	.29013	.04103
	After	50	2.1528	.22500	.03182
Length	before	50	36.2540	4.43618	.62737
	After	50	37.0840	3.66357	.51811

Independent Samples Test

		Levene's Test for Equality of Variances		t-test for Equality of Means						
		F	Sig.	t	df	Sig. (2tailed)	Mean Difference	Std. Error Difference	95% Confidence Interval of the Difference	
									Lower	Upper
Diameter	Equal variances assumed	.905	.344	-.782	98	.436	-.01800	.02303	-.0637	.02770
	Equal variances not assumed			-.782	94.421	.436	-.01800	.02303	-.0637	.02772
app_density	Equal variances assumed	5.015	.027	1.374	98	.173	15.3676	11.187	-6.834	37.56976

	Equal variances not assumed			1.374	90.774	.173	15.3676	11.187	-6.856	37.59187
Weight	Equal variances assumed	2.009	.160	-.601	98	.549	-.03120	.05192	-.1342	.07184
	Equal variances not assumed			-.601	92.283	.549	-.03120	.05192	-.1343	.07192
Length	Equal variances assumed	.928	.338	-1.020	98	.310	-.83000	.81365	-2.444	.78467
	Equal variances not assumed			-1.020	94.618	.310	-.83000	.81365	-2.445	.78539

T-Test Treatment=20%

Group Statistics

	storage	N	Mean	Std. Deviation	Std. Error Mean
Diameter	before	50	7.7700	.17409	.02462
	After	50	7.5740	.10063	.01423
app_density	before	50	1237.1338	41.64421	5.88938
	After	50	1237.1338	41.64421	5.88938
Weight	before	50	2.1536	.39670	.05610
	After	50	2.1046	.19223	.02719
Length	before	50	35.7700	5.45221	.77106
	After	50	37.7800	3.17786	.44942

Independent Samples Test

		Levene's Test for Equality of Variances		t-test for Equality of Means						
		F	Sig.	t	df	Sig. (2tailed)	Mean Difference	Std. Error Difference	95% Confidence Interval of the Difference	
									Lower	Upper
Diameter	Equal variances assumed	11.841	.001	6.892	98	.000	.19600	.02844	.13957	.25243
	Equal variances not assumed			6.892	78.457	.000	.19600	.02844	.13939	.25261
app_density	Equal variances assumed	.000	1.000	.000	98	1.000	.00000	8.32884	-16.528	16.5283

	Equal variances not assumed			.000	98.000	1.000	.00000	8.32884	-16.528	16.5283
Weight	Equal variances assumed	15.352	.000	.786	98	.434	.04900	.06234	-.07471	.17271
	Equal variances not assumed			.786	70.809	.434	.04900	.06234	-.07531	.17331
Length	Equal variances assumed	9.327	.003	-2.25	98	.027	-2.01000	.89247	-3.7810	-.23892
	Equal variances not assumed			-2.25	78.848	.027	-2.01000	.89247	-3.7864	-.23352

B.3. One way ANOVA TEST and POSTHOC test of effect biochar blends treatment in pellet size

ANOVA

		Sum of Squares	df	Mean Square	F	Sig.
Length	Between Groups	115.056	4	28.764	2.091	.083
	Within Groups	3370.100	245	13.756		
	Total	3485.156	249			
Diameter	Between Groups	.545	4	.136	11.246	.000
	Within Groups	2.968	245	.012		
	Total	3.513	249			
Weight	Between Groups	.513	4	.128	2.355	.054
	Within Groups	13.333	245	.054		
	Total	13.846	249			
App_density	Between Groups	191885.909	4	47971.477	8.765	.000
	Within Groups	1340888.541	245	5473.014		
	Total	1532774.450	249			

Multiple Comparisons

LSD

Dependent Variable	(J)	(I)	Mean Difference (I-J)	Std. Error	Sig.	95% Confidence Interval	
						Lower Bound	Upper Bound
Length	0 percent biochar	5 percent biochar	-.02400	.74177	.974	-1.4851	1.4371
		10 percent biochar	-.62800	.74177	.398	-2.0891	.8331
		15 percent biochar	-1.09600	.74177	.141	-2.5571	.3651

	20 percent biochar	-1.79200*	.74177	.016	-3.2531	-.3309
5 percent biochar	0 percent biochar	.02400	.74177	.974	-1.4371	1.4851
	10 percent biochar	-.60400	.74177	.416	-2.0651	.8571
	15 percent biochar	-1.07200	.74177	.150	-2.5331	.3891

	20 percent biochar	-1.76800*	.74177	.018	-3.2291	-.3069
10 percent biochar	0 percent biochar	.62800	.74177	.398	-.8331	2.0891
	5 percent biochar	.60400	.74177	.416	-.8571	2.0651
	15 percent biochar	-.46800	.74177	.529	-1.9291	.9931
15 percent biochar	20 percent biochar	-1.16400	.74177	.118	-2.6251	.2971
	0 percent biochar	1.09600	.74177	.141	-.3651	2.5571
	5 percent biochar	1.07200	.74177	.150	-.3891	2.5331
	10 percent biochar	.46800	.74177	.529	-.9931	1.9291
	20 percent biochar	-.69600	.74177	.349	-2.1571	.7651
20 percent biochar	0 percent biochar	1.79200*	.74177	.016	.3309	3.2531

		5 percent biochar	1.76800*	.74177	.018	.3069	3.2291	
		10 percent biochar	1.16400	.74177	.118	-.2971	2.6251	
		15 percent biochar	.69600	.74177	.349	-.7651	2.1571	
Diameter	0 percent biochar	5 percent biochar	-.12800*	.02201	.000	-.1714	-.0846	
		10 percent biochar	-.12200*	.02201	.000	-.1654	-.0786	
		15 percent biochar	-.07200*	.02201	.001	-.1154	-.0286	
		20 percent biochar	-.10200*	.02201	.000	-.1454	-.0586	
	5 percent biochar	0 percent biochar	.12800*	.02201	.000	.0846	.1714	
		10 percent biochar	.00600	.02201	.785	-.0374	.0494	
		15 percent biochar	.05600*	.02201	.012	.0126	.0994	
			20 percent biochar	.02600	.02201	.239	-.0174	.0694
	10 percent biochar	0 percent biochar	.12200*	.02201	.000	.0786	.1654	
		5 percent biochar	-.00600	.02201	.785	-.0494	.0374	
15 percent biochar		.05000*	.02201	.024	.0066	.0934		
20 percent biochar		.02000	.02201	.365	-.0234	.0634		

15 percent biochar	0 percent biochar	.07200*	.02201	.001	.0286	.1154	
	5 percent biochar	-.05600*	.02201	.012	-.0994	-.0126	
	10 percent biochar	-.05000*	.02201	.024	-.0934	-.0066	
	20 percent biochar	-.03000	.02201	.174	-.0734	.0134	
20 percent biochar	0 percent biochar	.10200*	.02201	.000	.0586	.1454	
	5 percent biochar	-.02600	.02201	.239	-.0694	.0174	
	10 percent biochar	-.02000	.02201	.365	-.0634	.0234	
	15 percent biochar	.03000	.02201	.174	-.0134	.0734	
Weight	0 percent biochar	5 percent biochar	.02940	.04666	.529	-.0625	.1213
		10 percent biochar	-.04180	.04666	.371	-.1337	.0501
		15 percent biochar	-.10200*	.04666	.030	-.1939	-.0101
		20 percent biochar	-.05380	.04666	.250	-.1457	.0381
		5 percent biochar	-.02940	.04666	.529	-.1213	.0625
5 percent biochar	0 percent biochar	-.02940	.04666	.529	-.1213	.0625	
	10 percent biochar	-.07120	.04666	.128	-.1631	.0207	
	15 percent biochar	-.13140*	.04666	.005	-.2233	-.0395	
	20 percent biochar	-.08320	.04666	.076	-.1751	.0087	

10 percent biochar	0 percent biochar	.04180	.04666	.371	-.0501	.1337
	5 percent biochar	.07120	.04666	.128	-.0207	.1631
	15 percent biochar	-.06020	.04666	.198	-.1521	.0317
	20 percent biochar	-.01200	.04666	.797	-.1039	.0799
15 percent biochar	0 percent biochar	.10200*	.04666	.030	.0101	.1939
	5 percent biochar	.13140*	.04666	.005	.0395	.2233
	10 percent biochar	.06020	.04666	.198	-.0317	.1521
	20 percent biochar	.04820	.04666	.303	-.0437	.1401
20 percent biochar	0 percent biochar	.05380	.04666	.250	-.0381	.1457
	5 percent biochar	.08320	.04666	.076	-.0087	.1751
	10 percent biochar	.01200	.04666	.797	-.0799	.1039
	15 percent biochar	-.04820	.04666	.303	-.1401	.0437
App_density	0 percent biochar	61.09120*	14.79596	.000	31.9477	90.2347
	5 percent biochar					
	10 percent biochar					
	15 percent biochar	-.29020	14.79596	.984	-29.4337	28.8533

		20 percent biochar	62.33800*	14.79596	.000	33.1945	91.4815
	5 percent biochar	0 percent biochar	-61.09120*	14.79596	.000	-90.2347	-31.9477
		10 percent biochar	-26.72240	14.79596	.072	-55.8659	2.4211
		15 percent biochar	-61.38140*	14.79596	.000	-90.5249	-32.2379
		20 percent biochar	1.24680	14.79596	.933	-27.8967	30.3903
	10 percent biochar	0 percent biochar	-34.36880*	14.79596	.021	-63.5123	-5.2253
		5 percent biochar	26.72240	14.79596	.072	-2.4211	55.8659
		15 percent biochar	-34.65900*	14.79596	.020	-63.8025	-5.5155
	15 percent biochar	20 percent biochar	27.96920	14.79596	.060	-1.1743	57.1127
		0 percent biochar	.29020	14.79596	.984	-28.8533	29.4337
		5 percent biochar	61.38140*	14.79596	.000	32.2379	90.5249
	20 percent biochar	10 percent biochar	34.65900*	14.79596	.020	5.5155	63.8025
		20 percent biochar	62.62820*	14.79596	.000	33.4847	91.7717
		0 percent biochar	-62.33800*	14.79596	.000	-91.4815	-33.1945
		5 percent biochar	-1.24680	14.79596	.933	-30.3903	27.8967

10 percent biochar	-27.96920	14.79596	.060	-57.1127	1.1743
15 percent biochar	-62.62820*	14.79596	.000	-91.7717	-33.4847

*. The mean difference is significant at the 0.05 level.

DUNCAN POSTHOC TEST

Length Duncan^a

Treatment	N	Subset for alpha = 0.05	
		1	2
0 percent biochar	50	35.9880	
5 percent biochar	50	36.0120	
10 percent biochar	50	36.6160	36.6160
15 percent biochar	50	37.0840	37.0840
20 percent biochar	50		37.7800
Sig.		.182	.140

Means for groups in homogeneous subsets are displayed. a. Uses Harmonic Mean Sample Size = 50.000.

Diameter Duncan^a

Treatment	N	Subset for alpha = 0.05		
		1	2	3
0 percent biochar	50	7.4720		
15 percent biochar	50		7.5440	
20 percent biochar	50		7.5740	7.5740
10 percent biochar	50			7.5940
5 percent biochar	50			7.6000
Sig.		1.000	.174	.269

Means for groups in homogeneous subsets are displayed. a. Uses Harmonic Mean Sample Size = 50.000.

Weight Duncan^a

Treatment	N	Subset for alpha = 0.05	
		1	2
5 percent biochar	50	2.0214	
0 percent biochar	50	2.0508	
10 percent biochar	50	2.0926	2.0926
20 percent biochar	50	2.1046	2.1046
15 percent biochar	50		2.1528
Sig.		.105	.227

Means for groups in homogeneous subsets are displayed. a. Uses Harmonic Mean Sample Size = 50.000.

Apparent density Duncan^a

Treatment	N	Subset for alpha = 0.05	
		1	2
20 percent biochar	50	1237.1338	
5 percent biochar	50	1238.3806	
10 percent biochar	50	1265.1030	
0 percent biochar	50		1299.4718
15 percent biochar	50		1299.7620
Sig.		.075	.984

Means for groups in homogeneous subsets are displayed. a. Uses Harmonic Mean Sample Size = 50.000.

Appendix C: Drop Test

C.1. Raw data of Drop Test

Table C.1: Data of Drop Test

Treatment	Pellet initial weight	Pellet weight after dropped	durability
0	2.28	2.28	100
0	2.05	2.05	100
0	2.21	2.19	99.1
0	2.5	2.49	99.6
0	2.41	2.4	99.6
0	1.61	1.6	99.4
0	2.1	2.1	100
0	2.15	2.12	98.6
0	2.64	2.63	99.6
0	2.2	2.2	100
0	1.63	1.63	100
0	1.08	1.05	97.2
0	1.9	1.89	99.5
0	2.61	2.6	99.6
0	1.75	0.99	56.6
0	2.39	2.39	100
0	1.73	1.73	100
0	2.16	1.21	56
0	2.31	2.31	100
0	1.89	1.88	99.5
0	2.52	2.5	99.2
0	1.52	1.52	100
0	2.4	2.4	100
0	2.65	2.65	100
0	2.25	2.24	99.6
0	2.3	2.29	99.6
0	1.99	1.19	59.8
0	2.3	2.3	100
0	1.6	1.6	100
0	1.68	1.68	100
0	2.15	2.15	100
0	1.98	1.98	100
0	1.1	1.1	100
0	2.17	2.17	100
0	2.34	2.34	100
0	2.4	2.4	100
0	2.39	2.38	99.6

Treatment	Pellet initial weight	Pellet weight after dropped	durability
0	1.94	1.94	100
0	2.18	2.17	99.5
0	1.73	1.72	99.4
0	2.16	2.15	99.5
0	2.18	2.18	100
0	2.25	2.25	100
0	2.46	2.44	99.2
0	2.52	2.51	99.6
0	2.04	2.03	99.5
0	2.12	2.1	99.1
0	1.81	1.81	100
0	1.31	1.31	100
0	1.51	1.5	99.3
5	2.19	2.18	99.54
5	1.88	1.88	100
5	2.28	2.28	100
5	1.93	1.93	100
5	1.78	1.77	99.44
5	2.04	2.04	100
5	1.82	1.82	100
5	1.87	1.85	98.93
5	2.05	2.05	100
5	2.04	2.04	100
5	2.06	2.06	100
5	2.33	2.33	100
5	1.5	1.5	100
5	1.68	1.68	100
5	2.22	2.21	99.55
5	2.15	2.15	100
5	2.32	2.32	100
5	2.07	2.04	98.55
5	2.05	2.03	99.02
5	2.15	2.14	99.53
5	1.79	1.79	100
5	2.25	2.25	100
5	1.58	1.58	100
5	1.68	1.68	100
5	2.17	2.17	100
5	1.81	1.8	99.45
5	2.03	2.02	99.51

Treatment	Pellet initial weight	Pellet weight after dropped	durability
5	1.87	1.85	98.93
5	2.06	2.05	99.51
5	2.25	2.23	99.11
5	2.19	2.17	99.09
5	2.19	2.18	99.54
5	2.2	2.2	100
5	2.08	2.07	99.52
5	1.7	1.69	99.41
5	1.71	1.7	99.42
5	1.99	1.99	100
5	1.92	1.91	99.48
5	2.44	2.44	100
5	1.64	1.64	100
5	2.03	2.03	100
5	1.64	1.64	100
5	2	2	100
5	1.45	1.45	100
5	1.59	1.59	100
5	1.95	1.92	98.46
5	1.85	1.83	98.92
5	2.1	2.1	100
5	2.27	2.27	100
5	2.02	2.02	100
10	2.54	2.54	100
10	2.42	2.42	100
10	1.98	1.95	98.5
10	2.25	2.24	99.6
10	2.01	2.01	100
10	2.44	2.44	100
10	2.45	2.45	100
10	1.8	1.8	100
10	2.18	1.68	77.1
10	1.91	1.9	99.5
10	1.68	1.68	100
10	2.27	1.38	60.8
10	2	2	100
10	2.41	2.4	99.6
10	2.06	2.06	100
10	2.29	2.29	100
10	1.98	1.98	100

Treatment	Pellet initial weight	Pellet weight after dropped	durability
10	2.44	2.44	100
10	1.68	1.66	98.8
10	2.04	1.29	63.2
10	2.12	2.12	100
10	2.4	2.4	100
10	2.48	2.48	100
10	2.35	2.35	100
10	2.1	2.1	100
10	2.46	1.58	64.2
10	2.25	2.25	100
10	2.22	2.21	99.5
10	2.34	2.34	100
10	1.79	1.78	99.4
10	2.5	2.5	100
10	2.32	2.32	100
10	2.42	2.42	100
10	2.39	2.37	99.2
10	2.4	2.38	99.2
10	2.42	2.42	100
10	1.88	1.86	98.9
10	2.34	2.34	100
10	2.38	2.37	99.6
10	1.98	1.96	99
10	2.17	2.14	98.6
10	2.09	2.08	99.5
10	2.62	2.62	100
10	2.21	2.21	100
10	2.42	2.4	99.2
10	2.39	2.38	99.6
10	1.93	1.93	99
10	2.64	2.64	100
10	2.39	2.38	99.6
10	2.37	2.35	99.2
15	2.23	2.23	100
15	2.49	2.49	100
15	2.36	2.36	100
15	2.03	2.03	100
15	2.21	2.21	100
15	2.24	2.24	100
15	2.2	1.31	59.55

Treatment	Pellet initial weight	Pellet weight after dropped	durability
15	2.38	2.37	99.58
15	2.47	2.47	100
15	1.92	1.92	100
15	2.34	2.34	100
15	2.16	2.16	100
15	2.54	2.54	100
15	2.08	2.07	99.52
15	2.22	2.11	95.05
15	1.8	1.8	100
15	1.88	1.88	100
15	2.17	2.16	99.54
15	2.2	2.2	100
15	2.34	2.33	99.57
15	1.94	1.93	99.48
15	1.91	1.89	98.95
15	2.31	2.3	99.57
15	2.2	2.2	100
15	2.21	2.2	99.55
15	2.2	2.19	99.55
15	2.03	2.03	100
15	2.24	2.24	100
15	2.5	2.5	100
15	1.54	1.52	98.7
15	2.08	2.07	99.52
15	2.5	1.39	55.6
15	2.17	2.16	99.54
15	2.15	2.15	100
15	1.95	1.94	99.49
15	2.01	2.01	100
15	2.28	2.28	100
15	1.72	1.72	100
15	2.33	2.31	99.14
15	1.79	1.25	69.83
15	2.26	2.25	99.56
15	2.42	2.42	100
15	2.45	2.45	100
15	1.91	1.91	100
15	2.3	2.3	100
15	2.35	2.35	100
15	2.29	2.29	100

Treatment	Pellet initial weight	Pellet weight after dropped	durability
15	2.57	2.06	80.16
15	2.25	2.25	100
15	1.85	1.85	100
20	2.42	2.42	100
20	1.69	1.68	99.41
20	2.17	2.17	100
20	2.33	1.96	84.12
20	2.51	2.51	100
20	1.91	1.91	100
20	2.39	2.37	99.16
20	1.65	1.65	100
20	1.88	1.88	100
20	2.48	2.18	87.9
20	2.13	2.11	99.06
20	2.04	2.04	100
20	2.07	2.06	99.52
20	2.15	2.15	100
20	1.78	1.78	100
20	1.71	1.71	100
20	1.83	1.82	99.45
20	2	2	100
20	1.96	1.96	100
20	1.95	1.95	100
20	2.21	2.2	99.55
20	1.88	1.88	100
20	2.46	2.46	100
20	2.2	2.2	100
20	2.27	2.26	99.56
20	2.17	2.17	100
20	1.98	1.98	100
20	2.29	2.29	100
20	1.87	1.87	100
20	1.97	1.96	99.49
20	2.15	2.15	100
20	2.15	2.15	100
20	2.09	2.08	99.52
20	1.68	1.66	98.81
20	2.25	2.25	100
20	2.21	2.21	100
20	2.13	2.13	100

Treatment	Pellet initial weight	Pellet weight after dropped	durability
20	1.64	1.63	99.39
20	1.62	1.6	98.77
20	2.18	2.18	100
20	1.72	1.71	99.42
20	1.78	1.78	100
20	2.2	2.19	99.55
20	2	2	100
20	1.93	1.93	100
20	2.04	2.04	100
20	2.22	2.22	100
20	2.19	2.17	99.09
20	2.34	2.34	100
20	1.88	1.88	100

Treatment = the number 0-20 represents the biochar weight percentage in the pellet

C.2. One-way ANOVA TEST and POSTHOC Test of effect biochar blends treatment in the drop test (durability)

ANOVA

durability

	Sum of Squares	df	Mean Square	F	Sig.
Between Groups	352.546	4	88.137	1.521	.197
Within Groups	14196.383	245	57.944		
Total	14548.929	249			

Post Hoc Tests

Multiple Comparisons

Dependent Variable: durability

(I) mixture	(J) mixture	Mean Difference (I-J)	Std. Error	Sig.	95% Confidence Interval	
					Lower Bound	Upper Bound
LSD 0	5	-2.55420	1.52242	.095	-5.5529	.4445
	10	.12800	1.52242	.933	-2.8707	3.1267
	15	.11500	1.52242	.940	-2.8837	3.1137
	20	-2.09140	1.52242	.171	-5.0901	.9073
5	0	2.55420	1.52242	.095	-.4445	5.5529
	10	2.68220	1.52242	.079	-.3165	5.6809
	15	2.66920	1.52242	.081	-.3295	5.6679
	20	.46280	1.52242	.761	-2.5359	3.4615
10	0	-.12800	1.52242	.933	-3.1267	2.8707
	5	-2.68220	1.52242	.079	-5.6809	.3165
	15	-.01300	1.52242	.993	-3.0117	2.9857
	20	-2.21940	1.52242	.146	-5.2181	.7793
15	0	-.11500	1.52242	.940	-3.1137	2.8837
	5	-2.66920	1.52242	.081	-5.6679	.3295
	10	.01300	1.52242	.993	-2.9857	3.0117
	20	-2.20640	1.52242	.149	-5.2051	.7923
20	0	2.09140	1.52242	.171	-.9073	5.0901
	5	-.46280	1.52242	.761	-3.4615	2.5359
	10	2.21940	1.52242	.146	-.7793	5.2181
	15	2.20640	1.52242	.149	-.7923	5.2051

durability

		Subset for alpha = 0.05
mixture	N	1
Duncan ^a	50	97.0160
10	50	97.0290
15	50	97.1440
0	50	99.2354
20	50	99.6982
5	50	.119
Sig.		

Means for groups in homogeneous subsets are displayed.

a. Uses Harmonic Mean Sample Size = 50.000.

Appendix D: Hardness Test

D.1. Raw data of Hardness Test

Table D.1: Database of Hardness Test

Treatment	Max load (N)	Pellet length (mm)
0	1175	30.80
0	1317	31.60
0	2103	32.10
0	2013	34.90
0	1854	32.00
0	1692	33.90
0	1113	33.20
0	2200	33.60
0	1397	29.90
0	1524	26.80
5	1397	31.90
5	1528	34.30
5	1554	35.70
5	1367	31.50
5	1654	33.50
5	1292	32.30
5	1724	33.00
5	1904	33.40

Treatment	Max load (N)	Pellet length (mm)
5	1830	31.20
5	1964	32.10
10	1806	31.80
10	1642	32.60
10	1645	35.50
10	1886	32.20
10	1946	34.90
10	2463	34.30
10	1510	35.40
10	1648	34.90
10	1746	29.80
10	2035	35.00
15	1846	33.50
15	2465	36.20
15	1049	28.90
15	1714	34.60
15	1828	31.50
15	2228	31.60
15	2190	35.00
15	1922	32.50
15	2078	35.40

Treatment	Max load (N)	Pellet length (mm)
15	1822	27.40
20	2115	35.80
20	1938	31.50
20	1832	30.30
20	1906	30.50
20	2100	35.80
20	1810	34.00
20	1900	34.10
20	1680	32.50
20	1726	33.40
20	2493	26.60

D.2. One way ANOVA TEST and POSTHOC Test of effect biochar blends treatment in the hardness test

Descriptives

Max_load

	N	Mean	Std. Deviation	Std. Error	95% Confidence Interval for Mean		Minimum	Maximum
					Lower Bound	Upper Bound		
80	10	1950.00	237.055	74.963	1780.42	2119.58	1680	2493
85	10	1914.20	382.106	120.832	1640.86	2187.54	1049	2465
90	10	1832.70	273.244	86.407	1637.23	2028.17	1510	2463
95	10	1621.40	233.140	73.725	1454.62	1788.18	1292	1964
100	10	1638.80	392.481	124.113	1358.04	1919.56	1113	2200
Total	50	1791.42	329.148	46.549	1697.88	1884.96	1049	2493

ANOVA

Max_load

	Sum of Squares	df	Mean Square	F	Sig.
Between Groups	941262.480	4	235315.620	2.425	.062
Within Groups	4367311.700	45	97051.371		
Total	5308574.180	49			

Post Hoc Tests

Multiple Comparisons

Dependent Variable: Max_load

	(I) Treatment	(J) Treatment	Mean Difference (I- J)	Std. Error	Sig.	95% Confidence Interval	
						Lower Bound	Upper Bound
LSD 80	85	85	35.800	139.321	.798	-244.81	316.41
		90	117.300	139.321	.404	-163.31	397.91
		95	328.600*	139.321	.023	47.99	609.21
		100	311.200*	139.321	.031	30.59	591.81
	85	80	-35.800	139.321	.798	-316.41	244.81
		90	81.500	139.321	.561	-199.11	362.11
		95	292.800*	139.321	.041	12.19	573.41
		100	275.400	139.321	.054	-5.21	556.01
90	80	80	-117.300	139.321	.404	-397.91	163.31
		85	-81.500	139.321	.561	-362.11	199.11
		95	211.300	139.321	.136	-69.31	491.91
		100	193.900	139.321	.171	-86.71	474.51
	95	80	-328.600*	139.321	.023	-609.21	-47.99
		85	-292.800*	139.321	.041	-573.41	-12.19
		90	-211.300	139.321	.136	-491.91	69.31
		100	-17.400	139.321	.901	-298.01	263.21
	100	80	-311.200*	139.321	.031	-591.81	-30.59
		85	-275.400	139.321	.054	-556.01	5.21
		90	-193.900	139.321	.171	-474.51	86.71
		95	17.400	139.321	.901	-263.21	298.01

*. The mean difference is significant at the 0.05 level.

Homogeneous Subsets

Max_load				
	Treatment	N	Subset for alpha = 0.05	
			1	2
Duncan ^a	95	10	1621.40	
	100	10	1638.80	
	90	10	1832.70	1832.70
	85	10	1914.20	1914.20
	80	10		1950.00
	Sig.		.060	.434

Means for groups in homogeneous subsets are displayed. a. Uses Harmonic Mean Sample Size = 10.000.

Appendix E: Iso-surface of temperature profiles for CGW pellets gasification A/F=1.3

